AD 727653

AD

USAAVLABS TECHNICAL REPORT 70-60

THE AERODYNAMIC AND AEROELASTIC CHARACTERISTICS OF A FULL-SCALE ROTOR OPERATING AT VERY HIGH ADVANCE RATIOS AND DURING START/STOP OPERATION

By

Andrew R. Trenka

May 1971

EUSTIS DIRECTORATE
U. S. ARMY AIR MOBILITY RESEARCH AND DEVELOPMENT LABORATORY
FORT EUSTIS, VIRGINIA

184

DISCLAIMERS

The findings in this report are not to be construed as an official Department of the Army position unless so designated by other authorized documents.

When Government drawings, specifications, or other data are used for any purpose other than in connection with a definitely related Government procurement operation, the United States Government thereby incurs no responsibility nor any obligation whatsoever; and the fact that the Government may have formulated, furnished, or in any way supplied the said drawings, specifications, or other data is not to be regarded by implication or otherwise as in any manner licensing the holder or any other person or corporation, or conveying any rights or permission, to manufacture, use, or sell any patented invention tha. may in any way be related thereto.

DISPOSITION INSTRUCTIONS

Destroy this report when no longer needed. Do not return it to the originator.

DOCUMENT CONTROL DATA - R & D

(Security classification of title, body of abstract and indexing annotation must be entered when the overall report is classified)

1. ORIGINATING ACTIVITY (Corporate author)	2a. REPORT SECURITY CLASSIFICATION
Cornell Aeronautical Laboratory, Inc. Buffalo, New York	Unclassified
	2b. GROUP

3. REPORT TITLE THE AERODYNAMIC AND AEROELASTIC CHARACTERISTICS OF A FULL-SCALE ROTOR OPERATING AT VERY HIGH ADVANCE RATIOS AND DURING START/STOP OPERATION, ~~VOLUME I - DISCUSSION OF RESULTS~~

4. DESCRIPTIVE NOTES (Type of report and inclusive dates)
Final Report

5. AUTHOR(S) (First name, middle initial, last name)
Andrew R. Trenka

6. REPORT DATE	7a. TOTAL NO. OF PAGES	7b. NO. OF REFS
May 1971	178	11

8a. CONTRACT OR GRANT NO. DAAJ02-68-C-0017	9a. ORIGINATOR'S REPORT NUMBER(S)
b. PROJECT NO.	USAAVLABS Technical Report 70-60
c. Task 1F162204A13902	9b. OTHER REPORT NO(S) (Any other numbers that may be assigned this report)
d.	BB-2595-S-1

10. DISTRIBUTION STATEMENT

Approved for public release; distribution unlimited.

11. SUPPLEMENTARY NOTES	12. SPONSORING MILITARY ACTIVITY Eustis Directorate U.S. Army Air Mobility R&D Laboratory Fort Eustis, Virginia

13. ABSTRACT

The purpose of this program was to study the aerodynamic and aeroelastic behavior of a rigid two-bladed rotor system operating at steady-state advance ratios up to approximately 15. Also to be investigated was the operation of this rotor during periods of acceleration and deceleration which were representative of the starting/stopping sequence of a stowable rotor. The objective of the program was accomplished by conducting wind tunnel tests in the NASA-Ames 40- x 80-Foot Wind Tunnel on a full-scale rotor. Hub forces and moments, blade pressure distributions (chordwise and spanwise), and blade flatwise, chordwise and torsional moments were measured. The experimental results were used to correlate with existing theory. ~~The results of the program are presented~~ in a two-volume report. Volume I contains a complete description of the test apparatus, testing technique and a discussion of the results. Volume II constitutes a data report which presents the experimentally obtained time (azimuthal) histories of the loads, moments and pressures.

It was found that for steady-state operation of the rotor at very high advance ratios, autorotation was encountered with an increase of collective or shaft angle above a given value. The mean values of the shaft loads and moments were found to be relatively insensitive to variation in blade collective or shaft angle; however, the oscillatory loads and moments were affected considerably. It was found that the shaft angle and the sine component of the blade cyclic angle are interchangeable at very high advance ratio operation.

The start/stop tests indicated no unusual aerodynamic or structural response phenomenon for the rotor tested.

DD , FORM 1473   REPLACES DD FORM 1473, 1 JAN 64, WHICH IS OBSOLETE FOR ARMY USE.

14. KEY WORDS	LINK A		LINK B		LINK C	
	ROLE	WT	ROLE	WT	ROLE	WT
Aerodynamic						
Aeroelastic						
Pressures						
Experimental						
Stowable-rotor						
Helicopter						
Rotor						

This report has been reviewed by the Eustis Directorate, U. S. Army Air Mobility Research and Development Laboratory, and is considered to be technically sound. The report is published for the dissemination of information and the stimulation of research.

The technical monitor for this contract was Mr. William E. Nettles, Aeromechanics Division.

Task 1F162204A13902
Contract DAAJ02-68-C-0017
USAAVLABS Technical Report 70-60
May 1971

THE AERODYNAMIC AND AEROELASTIC CHARACTERISTICS
OF A FULL-SCALE ROTOR OPERATING AT VERY HIGH
ADVANCE RATIOS AND DURING START/STOP OPERATION

Final Report

Cornell Aeronautical Laboratory, Inc. Report No. BB-2595-S-1

By

Andrew R. Trenka

Prepared by

Cornell Aeronautical Laboratory, Inc.
Buffalo, New York

for

EUSTIS DIRECTORATE
U. S. ARMY
AIR MOBILITY RESEARCH AND DEVELOPMENT LABORATORY
FORT EUSTIS, VIRGINIA

SUMMARY

The purpose of this program was to study the aerodynamic and aeroelastic behavior of a rigid two-bladed rotor system operating at steady-state advance ratios up to approximately 15. Also to be investigated was the operation of this rotor during periods of acceleration and deceleration which were representative of the starting/stopping sequence of a stowable rotor. The objective of the program was accomplished by conducting wind tunnel tests in the NASA-Ames 40- x 80-Foot Wind Tunnel on a full-scale rotor. Hub forces and moments, blade pressure distributions (chordwise and spanwise), and blade flatwise, chordwise and torsional moments were measured. The experimental results were used to correlate with existing theory.

It was found that for steady-state operation of the rotor at very high advance ratios, autorotation was encountered with an increase of collective or shaft angle above a given value. The mean values of the shaft loads and moments were found to be relatively insensitive to variation in blade collective or shaft angle; however, the oscillatory loads and moments were affected considerably. It was found that the shaft angle and the sine component of the blade cyclic angle are interchangeable at very high advance ratio operation.

The start/stop tests indicated no unusual aerodynamic or structural response phenomenon for the rotor tested.

FOREWORD

This report presents the results of the research program entitled "The Aerodynamic and Aeroelastic Characteristics of a Full-Scale Rotor Operating at Very High Advance Ratios and During Start and Stop Operation". It describes the objectives of the program and presents the data analysis and discussion of the results and correlation of the experimental and theoretical data.

TABLE OF CONTENTS

TABLE OF CONTENTS (Cont'd)

LIST OF ILLUSTRATIONS

LIST OF ILLUSTRATIONS (Cont'd)

LIST OF TABLES

LIST OF SYMBOLS

Ω	OMEGA	rotor speed, rpm
V_f	VF	freestream velocity, fps
α_S	ALPHS	shaft angle relative to vertical, degrees
θ_R	THETR	collective angle of attack of blade root, degrees
θ_{1C}	THETIC	cosine component of cyclic blade angle of attack, degrees
θ_{1S}	THETIS	sine component of cyclic blade angle of attack, degrees
μ		rotor tip advance ratio
R		rotor radius, ft
ψ		azimuthal position of reference blade, degrees

INTRODUCTION

The ever-present demand for increased speed capability of VTOL-type aircraft has been a prime mover in advancing the state of the art of VTOL technology. The most recent advances have been made with compound-type helicopters in which the lifting and propulsive role of the rotor is augmented by other lifting and propulsive devices. In these aircraft, the rotor is slowed and unloaded as the auxiliary lifting and propulsive units take on the principal lift and propulsion functions. It is reasonable to anticipate that, in the foreseeable future, the quest for higher and more efficient cruise speeds will lead to the design of a compound aircraft which will be capable of stopping its rotor (perhaps stowing it) and operating as a conventional fixed-wing aircraft. The operating conditions experienced by such a rotor would necessarily be very unusual. The rotor would be operating in regimes in which there is very little known about the aerodynamic behavior of the rotor blades. Hence, the aeroelastic response of such a rotor is, likewise, unknown at this time.

The purpose of this program was to study the aerodynamic and aeroelastic behavior of such a rotor system operating at steady-state advance ratios up to approximately 15. Also investigated during this study was the operation of such a rotor during periods of acceleration and deceleration which would be representative of the starting and stopping sequence. The objective of the program was accomplished by conducting wind-tunnel tests in the NASA-Ames 40-Foot by 80-Foot Wind Tunnel on a full-sized rotor. Hub forces and moments, blade pressure distributions (chordwise and spanwise), and blade flatwise, chordwise and torsional moments were measured. The experimental results were also used to correlate with theoretical results obtained from theories previously developed by Cornell Aeronautical Laboratory, Inc. (CAL) under U. S. Army sponsorship.

This report contains a complete description of the test apparatus, calibration and testing techniques; detailed analyses of selected experimental results; discussion of the correlation between theoretically predicted values and experimentally obtained values; and, finally, the major conclusions of the program.

DESCRIPTION OF TEST SYSTEM

Presented in Figure 1 is a photograph of the test rotor mounted in the NASA-Ames 40-Foot by 80-Foot Wind Tunnel. Figure 2 is a graphical description of that model system. The rotor test module included a mounting frame, a rotor pylon, a drive system and an aerodynamic fairing. The module was designed so that it could be mounted on the primary support system in the NASA-Ames 40-Foot by 80-Foot Wind Tunnel. The module was supported in the tunnel by two fixed struts and a gimbal-mounted tail strut. These were attached to the test module through ball and socket joints. The tail strut was extended or retracted by an electrically driven jack screw to provide the desired rotor shaft angle of attack. A detailed description of the NASA-Ames Wind Tunnel is given in Reference 1.

The test module frame supported the pylon, the speed increaser gearbox, and the drive motor as shown in Figure 2. The pylon installation consisted of a UH-1B transmission and mast assembly and modified rotor controls. The mounting arrangements and suspension configuration were the same as those of the corresponding helicopter installation. Except for the control input linkages, the basic control geometry was the same as that of the helicopter installation (see Figure 3). The rotor drive system consisted of a UH-1B transmission, a speed increaser gearbox, and an electric drive motor. The drive motor was provided by NASA-Ames and was rated for 1,500 horsepower at 3,000 rpm. To provide the proper power and speed match between the drive motor and helicopter transmission, a 1.085 to 1 ratio gear set was introduced between the electric drive motor and the transmission. The transmission provided a 1 to 0.0491 speed reduction to the shaft of the rotor. A brake assembly was mounted to the transmission. This brake assembly was used during the start/stop and stopped tests. The test rotor was a rigid configuration of the normally semirigid two-bladed UH-1A underslung hub. The rotor blades used in this program were the same ones used in the programs reported in References 2 and 3.

A split cone installed around the rotor shaft against the rotor flapping stops was employed to provide a positive lockout of blade flapping. The basic data for the rotor blades is summarized below:

Airfoil designation	NACA 0015
Chord	1.26 feet
Diameter	43.75 feet
Geometric twist	-11.9 degrees
Disk area	1,503 square feet
Solidity	0.0369

One of the rotor blades was termed the reference blade and was extensively instrumented with pressure measuring devices and strain (moment) measuring devices. The second blade was instrumented for

2

strains (moments) only at two stations. Figure 4 illustrates the blade
planform and indicates the location on the reference blade of the strain
gages used to measure the blade moments and differential pressures.
The blade moments measured were: blade flapwise bending moments,
blade edgewise bending moments, and blade torsional moments. Table
I presents the pressure transducer locations as well as the range of
differential pressure for each pressure transducer. For further dis-
cussion and description of the test module and blades, see Appendix I.

Figure 5 is a schematic of the mast and yoke indicating the
location of the moment gages. Yoke flatwise and chordwise bending
moments were measured. Mast bending moments were measured at
two positions on the mast. One, at 16.35 inches below the yoke assem-
bly, was referred to as the upper mast station. The second position,
at 46.75 inches below the yoke assembly, was referred to as the lower
mast station. Two components of the mast bending were measured at
each station. The component of the mast bending moment which pro-
duced motion parallel to the span of the rotor blades was referred to as
the parallel mast bending moment. The mast bending moment which
produced motion of the mast perpendicular to the span of the blades was
referred to as the perpendicular mast bending moment. The location of
the mast torque gage was 24.63 inches below the yoke assembly.

Presented in Figure 6 is a pictorial drawing indicating the
sign convention for the measured loads, moments and pressures. Note
also the table of additional measured loads not shown in the pictorials.

A slipring assembly mounted at the top and coincident with
the centerline of the shaft transferred the blade signals from the
rotating frame to the fixed frame. From this point the signals were
fed into the conditioning, amplifying and recording equipment. Figure 7
is a block diagram describing the electrical recording system. Shown
are the blade signals and pod signals passing through the slipring
assembly and into the signal conditioning equipment. Note that a portion
of the pod signals indicated by the dashed box B pass directly to the
signal conditioning equipment since they were already in the fixed frame.
Note also that some of the pod signals were also displayed directly on the
control module which controlled the test rig. All of the signals coming
into the signal conditioning equipment were passed on to the recording
devices which were remotely actuated by the master control panel. The
primary recording devices consisted of two 50-channel oscillographs.
One oscillograph recorded all of the blade and mast strain (moment and
load) signals. The second oscillograph recorded all the pressure
signals. To provide for on-line monitoring of critical signals, a vis-
corder, three oscilloscopes and an automatic counter were employed.
The viscorder displayed all of the mast and control signals as well as
four of the critical blade signals. The oscilloscopes displayed the two

mast parallel bending moments (upper and lower) and the yoke flatwise bending moment. The maximum allowable oscillatory peak-to-peak values of each of these parameters were marked distinctly on the face of the oscilloscopes. These oscilloscopes were continuously monitored for overload conditions. An automatic counter was incorporated which was triggered by the yoke bending moment whenever a value of 30,000 inch-pounds was exceeded. Thus, a continuous count of the number of cycles above a maximum allowable was kept. For further description of the data recording equipment, see Appendix II.

DESCRIPTION OF CALIBRATION AND
DATA REDUCTION PROCEDURES

Extensive calibrations were conducted on all of the data gathering instrumentation as well as the data recording equipment. The pressure transducers, as well as the blade strain gages, were calibrated several times using different incremental loads. The purpose of these tests was not only to determine the calibration constants associated with the pressure transducers and the moment gages but also to determine the maximum sensitivity which could be obtained. Also obtained was an evaluation of the associated errors and repeatability involved in the measurements. The calibration of the pressure transducers consisted of the application of known static pressures applied to each transducer. Calibration of the moment gages was accomplished by applying known loads at prespecified positions along the span of the blade.

Tests of the data recording equipment were also conducted. These tests provided information relative to the behavior of the linearity, zero shift, repeatability and dynamic response characteristics of the system. Certain of these calibrations were repeated just prior to tunnel entry. They were also repeated at intervals through the test period as well as at the conclusion of the test period. The results from all these calibrations were used to determine the overall accuracy of the measurements made. For a more complete description of the calibrations which were conducted, as well as the calibration results, see Appendix III.

As a result of these calibrations, the errors estimated for each of the parameters measured and presented in this report are listed below:

Flatwise bending moment	$\pm$ 20 foot-pounds
Edgewise bending moment	$\pm$ 40 foot-pounds
Torsional moment	$\pm$ 10 foot-pounds
Mast bending moment	$\pm$ 50 foot-pounds
Shaft torque	$\pm$ 20 foot-pounds
Axial loads	$\pm$ 20 pounds
θ_R (Root collective angle)	$\pm$ 0.10 degree
θ_{1c} and θ_{1s} (Cosine and sine cyclic angle)	$\pm$ 0.10 degree
α_s (Shaft angle)	$\pm$ 0.02 degree
Ω (Rotor speed)	$\pm$ 0.05 rpm
Differential pressure	$\pm$ 0.03 psi

The experimental data generated during the test phase of this program were collected in analog form on the two oscillographs. These analog signals were transcribed into a digital format, and the digitized data were operated on by a digital program, which converted the data to loads, moments and pressures at each of the digitized points. These loads, moments and pressures were harmonically analyzed. Each analog signal was read at 20 equally spaced intervals over one revolution of the rotor. It was thus possible to obtain for each analog signal the steady component plus the sine and cosine components of the first nine harmonics.

For a given test point the entire data record taken was surveyed for such features as repeatability from one rotor revolution to the next, unusually large loads in some particular signal, or any other anomalous behavior of the traces. A single, typical rotor revolution interval was then selected and each of the signal traces read.

PHILOSOPHY OF THE TEST PROCEDURE AND
PRESENTATION OF THE DATA

As noted previously, it was the objective of this program to investigate the aerodynamic and aeroelastic behavior of a rotor operating at very high advance ratios in starting and stopping conditions. The data collected were to be used in the correlation of experiment and existing theory as well as to contribute to the building up of a body of accurate experimental data to aid in the design of stowable rotors. These tests were also to provide a preview of problems which might be encountered by a rotor operating in a start/stop configuration. It was desired to collect a sufficient amount of data to aid in delineating the load and moment distributions and their trends as parameters were varied over the flight regimes in which stoppable/stowable rotors were likely to operate. The range of test parameters was chosen so as to be compatible with the available tunnel testing time, the financial restraints on the program, and finally, and perhaps most important, the concern for the fatigue life of the blade. This latter consideration resulted in a test envelope which was limited by the rotor speed. The rotor speed limitation was 70 rpm. At this speed, it was estimated that the loss of one of the rotor blades due to a fatigue failure would produce a rotating unbalance which would not be large enough to damage irreparably the 40-Foot x 80-Foot Wind Tunnel balance system. At higher rotational speeds, however, serious damage to the wind tunnel balance might be sustained in the event of loss of the blade. Furthermore, the reduced operating speed virtually eliminated the possibility that any portion of a fractured blade would penetrate the tunnel test section.

In addition to the rotor speed limitation, the following operating limits were imposed on the oscillating loads:

Upper mast bending moment	±	3300 foot-pounds
Lower mast bending moment	±	7300 foot-pounds
Yoke flapwise moment	±	4500 foot-pounds
Blade bending moment at 28% span	±	7300 foot-pounds

Operation at any one of these levels was not to exceed 100,000 cycles.

Because of the unknown character of the rotor aerodynamic behavior in these flight ranges and because of the inherent dangers due to blade or component failure, the following mode of testing was followed. The test procedure required the determination of the rotor trim conditions. For the purposes of these tests, "rotor trim conditions" were defined to mean minimum shaft moments. These trim conditions were first estimated from an analytical model developed under Contract DAAJ02-67-C-0096.

7

Using the estimated control conditions as a starting point, the actual trim conditions during the test were determined. Variations in the rotor control settings were then made from these trim conditions in a systematic fashion until one of the following limits was encountered:

1. Total stress limitations on critical components were reached.

2. Rotor instabilities were encountered.

3. Oscillatory stresses that seriously degraded the expected life limits on critical components were encountered.

A priority for the test data to be collected was established. Priority 1 data points consisted of steady-state operation of the rotor at advance ratios (μ) from 0.25 to approximately 15. Since considerable data have been collected for rotor operation at advance ratios less than 0.45 in previous tests (see References 2, 5, 6 and 7), the major emphasis was placed upon collecting data at the high advance ratios, i.e., μ greater than 0.5. The principal parameter variations at a given advance ratio were blade collective, blade cyclic and combinations thereof. Less emphasis was placed upon the variation of shaft angle because it was felt that typical stowable rotor operation would be with rotor shaft angle nominally at zero degrees. All Priority 1 points were collected before the initiation of tests on Priority 2 data.

Priority 2 data consisted of data collected during starting and stopping of the rotor. Initially, these start/stop sequences were conducted from the trim condition of the rotor operating at its lowest attainable rotor speed (i.e., about 5 rpm). Repeated tests were run with increasing rotor speed until enough data had been obtained to indicate that no serious difficulties would be encountered. Acceleration tests were similarly conducted.

A typical start-up procedure is presented in detail below:

1. With the wind tunnel off, the rotor blades were set with the reference blade at $\psi = 0$ (downstream), the shaft angle and the cyclic blade angle set at zero degrees, and with the collective angle set to give the minimum shaft moments for the desired steady-state rotor speed.

2. The rotor blade brake was applied.

3. All of the electrical equipment was put in a stand-by condition.

4. The wind tunnel was brought up to speed.

8

5. The recording equipment was actuated, power was applied to the electric motor, and the blade brake was released. Rotor speed was brought up as rapidly as possible to the prescribed steady-state value.

The stopping tests were similarly conducted. With the rotor operating in a steady-state condition and the recording equipment on, the power to the electric motor was removed and the brake applied. Tests were conducted using different levels of applied brake pressure to determine if any significant changes in the rotor loading or response characteristics could be observed with different rotor decelerations.

The rotor start/stop tests were also conducted for several different values of shaft angles as well as collective and cyclic values.

Priority 3 tests consisted of collecting data on the stopped rotor at several different azimuthal positions. These tests had the lowest priority and the least data was collected.

Presented in Figure 8, on a plot of rotor tip speed vs. tunnel velocity, are the indicated test points at which experimental data was collected. Each test point represents numerous test configurations. Presented in Table II are these test configurations in terms of their nominal values of rotor speed, tunnel velocity, shaft angle, blade root collective and cyclic values as well as values of the nominal tip advance ratio. Also noted in the far left-hand column--denoted case number-- is a sequence of numbers representing the run and point designation. These numbers refer to the actual sequence in which the data were collected during the test program. The data have been arranged in terms of increasing tunnel velocity and increasing rotor speed. At each advance ratio, that is, combination of rotor speed and tunnel velocity, the ranges of blade root collective, blade cyclic, and shaft angle are presented.

The starting/stopping test configurations which were investigated are presented in Table III. The format of Table III is nominally the same as that of Table II.

The stopped-rotor configurations which were tested are presented in Table IV. The format is similar to that of Tables II and III with the exception of the column denoted rotor speed. In its place is presented the angular position of the reference blade.

9

The scope of this program did not permit a detailed analysis of all of the data. Reported herein are the results of all of the start/stop tests, all of the stopped rotor tests, but only selected results obtained with the rotor operating at constant speed.

DISCUSSION OF RESULTS

The results will be discussed in three sections. The first section will discuss the results obtained during steady-state operation of the rotor at advance ratios from approximately 0.5 to 15. Included in this discussion will be the results of the correlation of theory and experiment. The second section will consist of data collected from the tests during which the rotor was operating under starting and stopping conditions. Presented in this section will be a discussion of the attempts to correlate the data. Finally, the third section will consist of data collected during the stopped-rotor tests--that is, with the rotor stopped at various azimuthal positions.

DISCUSSION OF HIGH-ADVANCE-RATIO RESULTS

The discussions in this section will be concerned initially with some typical experimental results and secondarily with the results of the correlation effort conducted for this study. The data will be presented in several different forms; namely, as (1) plots of the mean values of various loads and moments and pressures vs. the blade collective angles and shaft angles for various combinations of the free-stream velocity and rotor speed, and (2) for selected cases, the time histories of the total values (mean plus oscillatory) of the various measured test parameters. Also presented here (and briefly discussed) is one case for which the azimuthal variations of all of the data collected for one rotor operating condition are plotted (see Figure 9).

The results obtained from the rotor operating in a steady-state configuration are presented in Figure 9. The azimuthal variation of the flatwise, edgewise, and torsional bending moments on the blade; the moments measured on the mast and yoke; and the axial loads measured in the drag brace, pitch links and boost tubes are shown. Also presented are the azimuthal variation of the various control settings and the differential pressures measured at the various span and chordwise stations. The nominal advance ratio for the subject case is 0.50.

The 1-per-rev variation expected in the flatwise bending is readily discernible in the figure. In particular, note the higher frequency response experienced by the flatwise bending moment gages outboard of the 45% span. This characteristic is also readily identifiable in the differential pressure measurements made at the 85 percent and outboard pressure transducer locations. Attention is drawn to this point merely to illustrate that bending moment behavior was identifiable in the differential pressure measurements.

11

Presented in Figure 10 are plots of selected mean values of the blade and mast moments measured for the rotor operating at approximately 141 ft/sec and at rotor speeds of approximately 71 rpm (this corresponds to an advance ratio of 0. 87). The results of the variation of the root collective angle on the mean values of the blade and mast moments are presented. The mean flatwise and edgewise bending moment distributions are presented for each value of the blade collective in Figure 10(a). The remaining quantities are presented as plots of the mean value vs. the collective angle in Figure 10(b).

When interpreting the flatwise bending moment data, it must be kept in mind that the moment was generated by three load distributions. One contribution to the moment was generated by the weight distribution of the blade; the second contribution was generated by the effect of the centrifugal loads; and finally, the third portion of the flatwise bending moment was generated by the aerodynamic loads. The contribution to the flatwise bending moments due to the blade weight distribution is known and is presented in Appendix III. However, the contribution generated by the centrifugal forces cannot be determined readily since the value of the centrifugal moment depends upon the bent shape of the blade and hence upon the aerodynamic loads. Thus, it is possible for the centrifugal moment to contribute positive or negative values of the bending moment at a given station depending upon the aerodynamic loading on the blades. For instance, consider the case where the blade is carrying an aerodynamic load just sufficient to counteract the distributed weight of the blade. For this configuration, the centrifugal moment contribution at each spanwise station will be negative due to the three degrees of coning which this rotor system had. Now consider the case where the rotor blade is carrying a considerable negative load, as, for instance, in the case of root collective equal to six degrees as shown in Figure 10. Here it is conjectured that the blade tip is bent such that it is very nearly in the plane of rotation or slightly below it. Hence, the centrifugal load generated by this portion of the blade will be contributing positive moments to blade stations which lie above the plane of rotation. Thus, conclusions drawn from these data relative to the behavior of the aerodynamic moments with collective blade angle must be qualified by these considerations.

In any event, the variation, with the root collective angle, of the distribution of the mean flatwise bending moments is relatively smooth and shows no unusual characteristics (Figure 10a). The mean edgewise bending moment distribution indicates that for all values of the collective angle at this advance ratio, the blade was experiencing a mean positive edgewise force (chord force) about the azimuth, i. e., the rotor was drawing power. This was substantiated by the plot of the mean value of the shaft torque versus the collective angle. The positive value of torque at Θ_R = 9. 2 degrees in Figure 10b is questionable. Plots of the azimuthal variation of the shaft torque indicated that a very large torque oscillation occurred for this case. However, a check of the original oscillograph records indicated no corresponding large oscillations. It was

12

subsequently found that the transcribed data were in error at several azimuthal points. Thus, not only is the time history of the shaft torque questionable, but the mean value for this particular case is also questionable. This type of error occurred for several cases. It is believed that this problem was caused by a malfunction of the data transcribing equipment. It was noted for live signals in four different cases. Insufficient time prevented correction of these cases. The cases, presented in Volume II, are noted here along with the questionable quantities: Figure 9 (Run 2.19)-torque; Figure 24 (Run 7.11)-parallel mast bending, upper; Figure 57 (Run 7.25)-parallel mast bending, upper; Figure 77 (Run 8.3)-torque and parallel mast bending, upper.

Presented in Figures 11 and 12 are the corresponding plots of the mean values of the blade and mast bending data for the same velocity (140 ft/sec) but with the steady-state rotor speeds being 51 rpm and 7 rpm, respectively. The corresponding advance ratios for these two cases are 1.20 and 8.69 based upon the nominal values of freestream velocity and rotor speed. With the exception of the flatwise and edgewise bending moment distribution shapes, no significant changes in the mean loads are noted for these advance ratios. The change in the character of the distribution of the flatwise bending moments is attributed largely to the decreased effect of the centrifugal stiffening on the blades as the rotor speed was reduced. This is quite evident in the comparison of the flatwise moments for θ_R = 7.5 degrees in Figures 10, 11 and 12. Here it is observed that for the same freestream velocity and θ_R, a decrease in rotor speed results in an increase in the mean flatwise moment. It is suggested that this is due to the decreased negative centrifugal moment.

The positive value of shaft torque indicated at 6.3 degrees in Figure 11 is believed to be an error. Again, the error is attributed to transcription. The positive value indicated at 9.1 degrees is probably not an error and indicates that for this collective setting, the rotor was operating in an autorotative state, i.e., extracting energy from the air. This conjecture appears to be substantiated by the yoke chordwise bending moment data, which indicate a small negative value (i.e., negative bending moment indicates compression in the leading edge of the blade and hence corresponds to a negative chord force). The increasingly positive value of the mean shaft torque with increasing collective angle is believed to be due to the relatively large reverse flow region existing for this advance ratio. Shown in Figure 13 are regions of the rotor disk which experience reverse flow for various advance ratios. As can be seen for the case in hand (μ = 1.22), the blade is in a region of reverse flow for approximately one quarter of the time that it is operating on the retreating side. Now, with the sharp trailing edge of the blade acting as the leading edge, a positive increase of the collective angle represents an increased negative angle of attack of the blade over this portion of the rotor disk and, hence, an increased negative lift (i.e., acting downward). This increased negative lift with its corresponding induced drag coupled with the profile drag gives rise to a torque which tends to accelerate the rotor over this portion of the disk. Thus, as the collective angle of attack is increased, the magnitude of the

torque over this portion of the disk is increased. Further, with the trailing edge of the airfoil leading into the wind, it might be anticipated that airfoil stall with its correspondingly large increase in drag would be encountered at a lower value of the collective angle than might be expected on the advancing side. Thus, it might be expected that for a rotor operating at this advance ratio range (or for any advance ratio where a large portion of the retreating half of the disk experiences reverse flow), an increase of the collective angle will tend to cause the rotor to operate in an autorotative state. Furthermore, one might expect that as the advance ratio was increased for a fixed collective, the rotor would tend toward an autorotative operating condition also. These conjectures appear to be substantiated by the shaft torque vs. collective angle plots in Figures 11 and 12. Observe, first, that as the advance ratio is increased, the shaft torque is increased from negative to positive values for the range of collective angles tested and second, that at a fixed advance ratio, an increase in θ_R caused a corresponding increase (in positive direction) of the torque. As can be seen from Figure 13, for an advance ratio of 8.7, the blade operating on the retreating side was almost entirely in a region of reverse flow.

As further evidence to support these conjectures as well as to provide an indication of the azimuthal variations of certain of the loads measured at the various collective settings, selected moments are presented in Figure 14. Presented are the azimuthal variation of the shaft torque, parallel mast bending (upper), edgewise and flatwise bending moments at the 60 and 65 percent span stations, respectively, and the torsional moments at the 50 percent span. The advance ratio was 1.20 (V_f = 141 ft/sec, Ω = 51 rpm). For a collective angle of approximately 7.5 degrees, the torque is clearly negative for approximately the first 60 degrees of the rotor revolution, after which point the torque rises almost to zero and remains nearly zero until approximately 160 degrees after which point it becomes increasingly negative. It is noted that over the range 60 degrees to approximately 160 degrees, the retreating blade is operating in a reverse flow region and hence it can be inferred that the drag generated over the retreating blade approximately equals the drag generated on the advancing blade. With the collective angle increased to 9.1 degrees, it is observed that a large positive torque results over this region (60° to 160°); with the collective angle reduced to 5.8 degrees, the torque assumes a very large negative value. Thus the arguments made previously appear to be substantiated. It should be noted here that by similar arguments, it can be inferred that for advance ratios of approximately 1.0 and greater, autorotation will be encountered for very low ($\theta_R <$ 5.8) collective angles also. For this latter situation, however, the advancing blade will generate the accelerating torque.

While the variation of the mean mast bending moments was not large for variations in collective angle, this was not the case for the oscillatory components of these moments as indicated in Figure 14. The corresponding oscillatory loads experienced were quite large and reached peak values on the order of $\pm$ 4,000 foot-pounds. The variations occurred at 1-per rev and indicate that the rotor was subjected to very large pitching and rolling moments (in the fixed frame). The amplitude of these 1-per-rev

14

variations increased with increased collective angle.

Superimposed on the 1-per-rev flatwise bending response at 65 percent span can be seen a large 2-per-rev signal. The results presented for the 65 percent span are typical for all other stations. This 2 per rev response was identifiable with the 2-per-rev resonance indicated on the main rotor natural frequency plot in Figure 58.

Consider the case of the rotor operating at a velocity of approximately 78 ft/sec and a rotor speed of 71 rpm. This corresponds to an advance ratio of 0.5. Presented in Figure 15 are the plotted variations of the mean values of the blade and mast bending moments and in Figure 16 certain of the corresponding azimuthal variations of these data. The most significant change to note relative to the data collected at $\mu = 1.20$ is the behavior of the mean shaft torque with increasing collective angle. Here, for $\mu = 0.5$, the shaft torque became increasingly negative as the collective angle was increased.

Presented in Figure 17 are the mean values of the blade and mast bending moments obtained for a variation of the shaft angle at an advance ratio of approximately 0.74 (V_f = 121 ft/sec and Ω = 71 rpm). Generally, the mean values at this advance ratio show little sensitivity to changes in shaft angle. Of particular interest is the behavior of the torque with variations in shaft angle. A minimum in the shaft torque occurs at approximately -0.5 degree. The shaft torque increases on either side of the shaft angle at which the minimum torque occurs. Note that if this trend maintains itself as the shaft angle is increased or decreased, autorotation will occur at relatively small shaft angles (i.e., approximately ±3 degrees).

Presented in Figure 18 are the effects on the mean loads and moments of a variation in shaft angle at a considerably higher advance ratio of 13. Presented in Figure 19 are the corresponding azimuthal variations of several of these quantities. Note the large change in the mean flatwise and edgewise bending moments distributions as the shaft angle is varied from -4 degrees to a +4 degrees. This variation in the flatwise bending moment is believed to be directly attributable to the effect of the reverse flow region. Briefly, with θ_R fixed, the effect of a positive shaft inclination is to increase the angle of attack on the advancing side of the disk while decreasing it on the retreating side. Thus, positive bending moments on the advancing side of the disk become larger while the negative moments on the retreating side become less negative, and hence the mean bending moments increase. A similar argument holds for negative shaft angles.

Clearly discernible in the azimuthal variations of the edgewise bending moments and the torsional moments are 2-per-rev responses. The torsional moment variation can be explained by considering the case for α_s = +3.92 degrees. As the blade moves through $\psi = 0$ to $\psi = 180$ degrees, the aerodynamic load acting ahead of the blade elastic axis would be expected to increase as would the corresponding torsional moment

15

produced. As the blade moves into the retreating side of the disk, the effect of the shaft inclination would be to reduce the negative angle of attack experienced by the blade in the reverse flow region, thereby reducing the corresponding negative aerodynamic load. However, the approximate location of the effective aerodynamic load on the retreating side of the blade is probably close to the 3/4 chord, and hence a larger moment arm is effected than existed on the advancing side. Thus, the torsional moments are brought back up to approximately the same level as on the advancing side.

The 2-per-rev edgewise bending moment for the same case is not as readily explainable.

Presented in Figures 20 and 21 are the results obtained at an advance ratio of 13 for a variation of the blade collective angle. The behavior of the mean values is much the same as discussed previously for V_f = 141 fps and Ω = 7.1 rpm.

Heuristic arguments, such as those presented earlier in this report to explain the effects of certain parameter variations, led to the conclusion that for high-advance-ratio operation ($\mu > 1.0$), the effect of shaft angle and blade sine component of cyclic variation would be similar. Further, the higher the advance ratio, the closer the similarity. To check this reasoning several cases were compared where the corresponding test parameters were similar. A typical comparison is presented in Figure 22. Even though the cases are not precisely comparable, the similarity in the azimuthal variation of the loads is good. The agreement between the pressure variations for these two cases is also very good. Hence, it is concluded that for high-advance-ratio operation the effects of shaft angle and blade sine component of cyclic variation are interchangeable.

Several attempts were made to correlate the steady-state experimental results (loads, moments and pressure distributions) with the theoretically predicted airloads computed by the program given in Reference 9. The approach of Reference 9 (referred to hereafter as transmitted shear program - TSP) was based upon Reference 10. The analysis of Reference 10 (referred to hereafter as blade loads program - BLP) represents each blade section as a chordwise distribution of bound vorticity. The distribution is then approximated by a Glauert series, and the coefficients are determined by satisfying the boundary conditions at a discrete number of chordwise stations. The blade wake is modeled as a mesh of straight-line vortex elements. Positioning of the wake is predetermined. The elastic characteristics of the blade are accounted for as well as the corresponding blade deflections in determining the aerodynamic loads. The two principal reasons for correlating with the TSP theory rather than BLP were: (1) the digital program associated with TSP was in an operating condition at the time of the initiation of this program, and (2) the TSP theory included the pitch, torsion, and inplane degrees of freedom as well as the significant mass. elastic and geometric coupling terms between all the degrees of freedom which were

16

not included in the BLP digital program.

Three cases were selected for theoretical computation and correlation. They were: (1) V_f = 80 fps, Ω = 71 rpm, θ_R = 5 degrees (this corresponds to an advance ratio of approximately 0.5); (2) V_f = 120 ft/sec, Ω = 70 rpm, θ_R = 7.5 degrees, shaft angle equal approximately -4 degrees (this corresponds to an advance ratio of approximately 13); (3) V_f = 120 ft/sec, Ω = 71 rpm, θ_R = 7.5 degrees, and the shaft angle equal approximately -2 degrees (this corresponds to an advance ratio of 0.74). These three cases were selected because they would provide a check on the theory over the entire range of advance ratios tested. The first case was selected because it provided the lowest advance ratio of all the points tested and it was believed that correlation with the theory should be best at this point. The latter two cases were selected because they provided an axial component of the freestream through the rotor due to shaft inclination. This axial component would provide the mechanism by which the blade wake would be removed from the rotor plane, thereby minimizing computational difficulties in the digital program which occur when the wake lies very close to the plane of the rotor. The results obtained for the advance ratio cases 0.74 and 13 are presented in Figures 23 and 24, respectively. Presented in these figures are the azimuthal variations of the theoretical and experimental values to be compared. The results for the case of advance ratio equal to 0.5 were not presented because no converged solutions could be obtained. In particular, it was found that the motions of the blade did not converge to reasonable values. It is believed that this may be due to the fact that the Glauert coefficients were not being properly limited in the digital program. The expression for the lift at a given blade segment as presented in Reference 9 is presented here:

$$\mathscr{L} = C_{L_\alpha} b\rho \, V_f \left(A_0 + \frac{1}{2} A_1 \right) + \pi b^2 \rho \frac{\partial}{\partial t}\left(3A_0 + A_1 + \frac{1}{2} A_2 \right)$$

where

b	=	blade semichord
ρ	=	freestream air density
V_f	=	freestream velocity
C_{L_α}	=	local lift curve slope
A_0, A_1, A_2	=	coefficients of the Glauert series representing the bound vorticity distribution

17

It is conjectured that for those cases where a wake vortex element lies very close to a collocation station (point on the blade surface at which the boundary conditions are satisifed) at some azimuthal position, the computed values of one or more of the Glauert coefficients may become extremely large. Hence, because of the manner in which the time rate of change term of the Glauert coefficient is evaluated (that is, by curve fit through points at discrete, equally spaced intervals), very large values of their time rate of change might be computed. Thus, the corresponding lift could become extremely large. Despite all of the various limiting schemes built into the program to prevent such an occurrence, indications are that this did occur for the case in question.

As evident from the comparisons in the figures, the agreement between the theory and the experiment was poor for both cases for which converged solutions were obtained.

Even for these converged solution cases, it was observed that the computed induced velocities over the entire rotor disc were limited to their maximum allowable values. This maximum value was predetermined arbitrarily and is employed in the program to circumvent the computational difficulties which arise when a wake vortex element lies close to a collocation point at which the blade boundary conditions are being satisfied. Because of this limitation, the true effects of the wake could not properly be assessed for those cases analyzed. Whether these wake effects were significant to the computed rotor loads is not known.

While the reasons for the lack of agreement between the theory and experiment for these two cases is not definitely known, numerous possibilities exist: first, the possibility that computational errors may exist in the program which did not become apparent until the very unusual cases attempted herein were run; second, the possibility that the effects described above which led to the unconverged solution for $\mu = 0.5$ might be occurring for the remaining cases and thereby account for the lack of agreement. Last, and most probable, is the fact that the rotor operating conditions of these tests represents a basic departure from the theoretical model used in TSP and BLP.

One of the fundamental assumptions being violated in the mathematical model is the assumption that an adequate description of the wake is known under these flow circumstances. In addition to the question of the wake location is the question associated with the character of the wake shed from a blade which has a bound vorticity distribution which changes sign across the span.

Further, since the major portion of the rotor is in a reverse flow region, the question of the behavior of the airfoil with its sharp trailing edge now acting as the leading edge becomes extremely important.

Finally, the assumption made in TSP and BLP that the interference effects from the fuselage (pod in this case) are small is not necessarily valid for the cases under consideration. Thus, any one or

combination of the above may account for the lack of correlation.

DISCUSSION OF STARTING/STOPPING SEQUENCES

The start/stop cases listed in Table III were studied in order to determine: which cases should be reduced; whether the entire record should be reduced for the entire stopping/starting period; and whether all traces should be reduced. The problem of data reduction was a formidable one since the shortest stopping period (from 70 rpm) was 24 seconds, while the shortest start-up time was approximately 60 seconds. To reduce with fine resolution from the beginning to the end, all of the traces for all of the cases, would have required an inordinate effort (that is, approximately 500,000 bits of information would have had to have been read). However, from inspection of the records, it appeared that no significant difficulties or unusual behavior of the blade response or loadings were encountered during any of the starting/stopping sequences. This proved true for all the cases inspected. Hence, only one start case and one stop case were selected in order to provide typical detailed results. However, the remaining start/stop records were analyzed to obtain characteristic times, accelerations and peak amplitudes measured during the maneuver.

For both the start/stop cases, three major time intervals were inspected and reduced. For stopping cases, the first ten seconds after application of the rotor blade brake was read in increments of 0.05 seconds. The second time period read for the stopping case was the three seconds during which the rotor speed passed through one half of its steady state operating speed. This interval was also read in time increments of 0.05 second. The final time period reduced was that which encompassed the final seconds of the rotor stopping. Since the rotor high frequency oscillatory responses were almost completely attenuated by this time, this final period was read in time increments of 0.10 second. The time increments in each period were selected so as to provide an indication of the highest significant frequency present in the traces.

The start-up cases were read similarly. The first 13 seconds after application of power to the rotor were read as follows: For the time period 0 to 8 seconds, the time increments at which readings were taken were 0.5 second; for the time period from 8 to 10 seconds, the time increments were 0.10 second; and for the 10 to 13 second time period, the time increments were 0.05 second. Readings were again taken over the time period during which the rotor achieved one half of its steady state operating speed; the time increments were 0.05 second. Finally, the data from the last seconds before the rotor achieved steady state operating speed were read in increments of 0.05 second.

Of the moment data, only selected blade and mast moments (blade flatwise and edgewise moments, lower mast parallel and perpendicular, bending and mast torque) were reduced for these cases. Of the pressure data, only the pressure at the 85 percent span were analyzed.

19

The results for the starting case are presented in Figure 25. The results for the stopping case are presented in Figure 26.

Presented in these figures are the analog signals reconstructed from the digitized data. The choppy appearance is due to the fact that the time increments were 0.05 second and larger. Even though the values of the loads experienced are accurately shown only at specific points on the graphs, it is felt that the major characteristics of the frequency and amplitude are preserved in the figures. For a typical example of the actual traces, see Figure 27.

The remaining start/stop records were studied to obtain such information as, the total time to start or stop, and the acceleration or deceleration. Also noted for selected traces were: (1) the steady-state amplitude, (2) the amplitude and the time at which the rotor reached one-half its steady-state rotor speed, (3) the time required to reach one-half the steady-state amplitude, and (4) the time and magnitude of the maximum amplitude reached for each trace during the start or stop sequence. Presented in Figures 28 through 33 are typical results of these analyses.

The start-up shown in Figure 25 took approximately 62 seconds. The conditions at time $t = 0$ were: the freestream velocity was 140.6 feet per second; the blade root collective was at 7.35 degrees, and the shaft angle and cyclic angles were set at zero. The reference blade was at $\psi = 0$ (i.e., downstream).

As noted in the figure, it took approximately 9.3 seconds for the first rotor revolution. The second rotor revolution occurred at approximately 13.3 seconds. The time history of each successive rotor revolution is shown in Figure 28(a). The rotor speed is given by the rate of change of the curve shown. The rotor acceleration is correspondingly given by the second derivative of the curve shown. It was determined that the acceleration achieved for this case was very nearly constant. Indicated in the figure are the times required to reach one-half of the rotor steady-state operating speed and the time required to reach the rotor steady-state operating speed. Also noted are the rotor speeds at each of these instants of time. Note that at $t = 33$ seconds, $\Omega \approx 37$ rpm, while at $t = 61.7$ seconds, $\Omega \approx 72$ rpm, which indicates a nearly linear variation of Ω with time, i.e., a constant acceleration. Shown also in this figure (Figure 28(b)) is the corresponding information for a rotor start-up at 120 fps. The acceleration of the rotor, though less than the 140 fps start-up, was again approximately constant.

The flatwise bending moments for the 140 fps start-up in the vicinity of $t = 0$ were nominally zero from the blade tip to approximately 50 percent span (Figure 25). Inboard of this spanwise station, the flatwise bending moments were clearly positive, indicating a positive loading on the blade. The corresponding edgewise bending moments were also nominally zero around the time of start-up of the rotor. The parallel mast bending and perpendicular bending moments indicate relatively

20

large negative values. The observed negative parallel bending moment value at $\psi = 0$ is believed to be generated by the larger positive aerodynamic loading of the forward blade relative to the aft positioned reference blade. A larger aerodynamic load is believed to exist on the forward blade for two reasons: (1) the interference effects due to the rotor module are much less on the forward blade than on the aft blade, and (2) the three degrees of hub coning is sufficient to overcome the deflection of the tip due to the blade weight and hence presents the blade as effectively a low-aspect-ratio wing at positive angle of attack relative to the freestream. Both of these reasons tend to infer a lower blade loading on the reference or aft blade. As the rotor traverses through its first revolution, the blade loadings behave as might be expected. For example, we see the flatwise bending moment at 15 percent span increase to its maximum value at approximately five seconds which corresponds roughly to the reference blade now being at $\psi = 180$ degrees (i.e., into the wind). Corresponding to this increase in the flatwise bending moment, we see the parallel mast bending increase from a negative value to a corresponding positive value in the same time period. (Recall that positive parallel mast bending corresponds to a positive load on the reference blade.)

Toward the end of the second rotor revolution, a response in the flatwise bending moment at approximately 54 cpm was observed. It persisted until approximately the third rotor revolution, after which point it was not clearly discernible. Variations in the differential pressure at this frequency were also noted. The source of the excitation was not readily identifiable. However, the following explanation might be conjectured. The rotor frequency plot presented in Appendix III, Figure 58, was computed with the assumptions that the pylon and mast assembly was rigid (i.e., no inplane hub motion was allowed) and that no edgewise-flatwise coupling existed. Hence, the first uncoupled, symmetric flatwise bending mode was calculated to be approximately 80 cpm. Calculations were then made which included edgewise coupling but still ignored the mast flexibility. The natural frequency of the first symmetric flatwise bending mode was found to be approximately 63 cpm at zero rotor speed. The rotor speed at the end of the second revolution was approximately 10 rpm. Hence, it is conjectured that the sixth harmonic of the rotor rpm could have provided the excitation. Its symmetric characteristic was substantiated by the fact that no response at this frequency was noted in the mast parallel bending signals.

As the rotor speed increased, another significant response in the flatwise bending moment was observed. The frequency of the response was at approximately 540 cpm (9 cps) and is believed to correspond to the third flatwise bending mode of the blade (see Figure 58). The maximum amplitude of this response seemed to occur between rotor speeds of 60 and 70 rpm. It is clearly identifiable in the trace for the 65 percent flatwise bending.

A blade response that is not as apparent on the plots presented

in Figure 25 was noted on the oscillograph records. Its character was somewhat attenuated in the transcribed data plots because of the selected time intervals at which the readings were made. This response was noted in the perpendicular mast bending at approximately 420 cpm (7 cps). It was also observed in the edgewise bending moment traces. It corresponds approximately to the calculated first symmetric edgewise bending mode. This response appeared very early in the start-up sequence and was particularly apparent in the perpendicular mast bending moment. It can best be seen in the response of the 60 percent span edgewise bending moment presented in Figure 25.

The torsional response of the rotor shaft is shown in the torque vs. time plot. This plot actually represents the angular displacement time history of the shaft. While the detailed behavior of the shaft response depended upon (1) the time history of the applied torque (which was not kept constant throughout the start sequence), (2) the elastic characteristics of the rotor blades, shaft, transmission, etc., and (3) the resultant aerodynamic torque, it is suggested that the principal character of the shaft response is explained by considering the response of the following system:
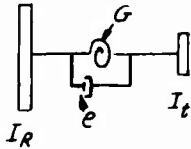
Let I_R represent the rigid body inertia of the rotor system and I_T the rigid body inertia of the transmission and motor. The shaft torsional flexibility is given by G and the damping in the system by C. The response of this system to a step input of torque is shown below.
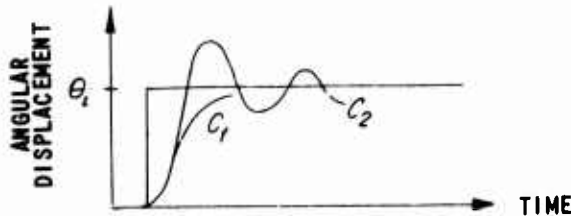
The step input of torque to I_T results in an angular deflection of θ_i . The manner in which I_R reaches this value depends upon the ratio of the inertias, the shaft stiffness, and the damping of the system. For a highly damped system, the shaft angular displacements are shown by the curve labeled C_1 . As the damping is decreased, the response tends to overshoot the steady value θ_i as depicted by the curve labeled C_1.

This characteristic overshoot is observed in the torque signal as it rises to its maximum value at t = 8.5 seconds and then rapidly falls off. The successive peaks at t = 10 seconds and 11.5 seconds, etc., are conjectured to represent oscillatory character of the

22

system inertias (rotor and transmission) on the flexible mast.

The oscillatory peaks at t = 1 to 4 seconds and again shown from t = 33 to 35 seconds correspond to a torsional response of the shaft at approximately 60 cpm (1 cps). It was damped out as the rotor reached steady operation. The source of this excitation was not obvious and no conjecture was made. A similar excitation was observed during the stopping sequence.

To indicate the behavior of the differential pressures during start-up, the results obtained from the 85 percent span station are also presented.

The amplitude ratios (peak-to-peak amplitude at a given time divided by the peak-to-peak amplitude at steady-state rotor operation) for several of the more critical bending traces (flatwise bending at 15 percent span, lower parallel and perpendicular mast bending) are shown in Figure 29. Also presented is a time history of the mast torque amplitude ratio. Indicated on the plots by the symbols are (1) the amplitude ratio at the instant of time at which the rotor speed attained one-half the steady-state rotor speed, (2) the maximum amplitude ratio achieved, (3) the time required to reach one-half steady-state rotor amplitude, and finally (4) the time required to reach the steady-state rotor operating speed. Part (a) of the figure presents the results for a start-up at 120 ft/sec, and (b) presents results observed at a start-up of 140 ft/sec and corresponds to the detailed results presented in Figure 25. The start-up acceleration for the 120 ft/sec case is shown in Figure 28(a) and, as noted previously, was less than that for the 140 ft/sec start-up case, but still approximately constant. As can be seen from the time histories of the amplitude ratios, no startling behavior of the critical rotor amplitude ratios was observed during the start-ups. This was typical of all of the start-ups attempted during these rotor tests.

Typical time histories of data collected from a rotor being stopped from approximately 70 rpm in a freestream velocity of approximately 140 ft/sec are presented in Figure 26. The blade root collective setting was approximately 7.4 degrees with shaft and cyclic angles set equal to zero. The same data presented in the start-up case are presented for the stopping case. Again, three principal time periods are presented: the first 10 seconds of the rotor operation after application of the brake, the time period which included the rotor reaching one-half steady-state rpm, and finally, the time period encompassing the final stopping of the rotor. Each trace was read at time increments of 0.05 second for the initial 10-second time period as well as for the time period encompassing the rotor operating at one-half its steady-state rotor operating speed. The last 2 seconds of the rotor stopping were read in time increments of 0.10 second.

The same general characteristics of the rotor behavior were noted on stopping the rotor as previously noted on starting up. In particular, note the 65 percent span flatwise bending moment. A clearly

23

identifiable buildup in the flatwise bending moment response at approximately 540 cpm (9cps) is evident. Since the rotor was operating for these tests very near a flatwise resonant point with the 7-pre-rev input, the large response generated at this frequency upon application of the brake is not unexpected. Further, the response disappeared very quickly after the rotor passed through the resonant point. Note that as the rotor slowed down, the oscillatory response in the edgewise bending moment tended to increase. Further, the mean value of the edgewise bending moment tended to move from a positive value to an increasingly negative value. The oscillatory edgewise bending moments occurred predominantly at 60 cpm (1.1 cps) throughout the entire stopping time.

The mast parallel bending moment showed a similar tendency. That is, the oscillatory amplitude appeared to grow as the rotor slowed down. The mean value, however, did not seem to change significantly from its steady-state value. If anything, it appeared to tend to zero.

The rotor mast torque showed surprisingly large values of oscillatory response during the stopping of the rotor. A peak amplitude of approximately 2,000 foot-pounds was reached. The behavior of the mean value of the torque curve shown in Figure 26 is as might be expected. However, the source of the large oscillatory amplitudes observed in the torque response is not known. It is observed, however, that these oscillations occur at approximately 1.1 cycles per second throughout the entire stopping sequence. This frequency corresponds to the observed edgewise bending moment response. If the edgewise response of the blade (as noted above) were antisymmetric in character, it could be reflected in the torque response. However, no mechanism could be readily found which clearly accounted for the source of excitation since no known edgewise resonances occur at this frequency.

The time histories of the differential pressure at the 85 percent span are also presented. Note that none of the very high frequency oscillations observed in moment signals are observed in pressure signals. Also note that the characteristic shape of pressures at each transducer location is very similar and maintains its character with time.

Presented in Figures 30 and 31 are the time histories of the number of rotor revolutions from the time of brake application until the time the rotor was deemed to be stopped. Stops from 70 rpm were made at three different tunnel velocities: 120, 140 and 158 ft/sec. Stops were also made from 70 rpm at a tunnel velocity of 140 ft/sec employing three different brake pressures: 150 psi, 200 psi and 225 psi. As can be seen in Figure 31, the difference in the deceleration of the rotor for the 200 and 225 psi applied brake pressure cases is virtually negligible. The deceleration for the 150-psi applied brake pressure was less than for the two previous cases. The results in terms of the oscillatory amplitude ratio, however, are not appreciably different, as can be seen in Figure 32. The major differences occur in the time at which the maximum amplitudes were observed. The magnitude of the maximum amplitude

24

ratios remains approximately the same for all cases.

Presented in Figure 33 are the results observed during stops from 70 rpm at several freestream velocities with the same applied brake pressure. Again, no significant trends could be established with stopping from the different velocities. The differences in the maximum oscillatory amplitude ratios observed and the times at which these peaks were obtained differed from case to case. Thus, the effect of airspeed on the stops was not clearly discernible. The noted differences could be attributable to slight differences in the initial rotor speed from which the stop was begun as well as to the azimuthal location of the blade at the time of brake application. Generally, it was noted that as the length of time required to stop the rotor was increased, the peak oscillatory amplitudes observed also increased. The differences between the oscillatory loads for the different stopping conditions were not appreciable. All had approximately the same characteristics. Further, at no time for any of the start or stop cases were maximum oscillatory loads encountered which exceeded approximately twice the steady-state oscillatory loads.

Attempts were made to correlate the stopping and starting experimental data obtained in these tests with the theory developed under USAAVLABS Contract No. DA 44-177-AMC-77(T) and reported in Reference 8. These efforts were singularly unsuccessful. Analysis was attempted for one start case and one stop case. For both of these cases, computational instabilities were encountered which could not be circumvented within the framework of the present effort.

DISCUSSION OF STOPPED-ROTOR RESULTS

Results of the Priority three tests are discussed in this section. These data constitute information taken while the rotor was stopped at various azimuthal positions in a freestream velocity of approximately 160 ft/sec. The tests were conducted to provide a partial check of the current data with those data obtained in Reference 3 as well as to supplement the data of Reference 3. Of particular interest was the verification of the pressure distributions measured during the previous test program.

While the rotor blades used in the two tests were the same, there were some differences between the tests reported in Reference 3 and those reported here. These differences were: (a) the rotor used in the current test had three degrees of coning whereas the rotor used in Reference 3 had no coning, (b) the rotor configuration of Reference 3 provided for independent collective settings of the two blades, (c) the test configuration of Reference 3 had a different blade root fixity--that is, the blade attachment did not have the flexibility associated with the present rotor mast configuration, and (d) the blade of Reference 3 had bonded to its surface additional pressure transducers and bending gages. The addition of these pressure transducers and bending gages necessitated the use of

25

signal-carrying wires which ran along the trailing edge of the blade to the various stations at which these gages were located. Thus, the geometry of the trailing edge was altered from a sharp to a blunted trailing edge. For the tests in hand, these pressure transducers and bending gages and the corresponding wiring were removed and the trailing edge returned to its original sharp configuration.

All of the data collected and noted in Table IV were reduced and the results analyzed. These results generally confirmed the trends and results found in Reference 3. Hence, only typical results are presented herein. The results selected for presentation were those obtained for the reference blade located at an azimuthal position of 255 degrees. One of the reasons for presenting the data from this azimuthal position was that instabilities were encountered during the tests of Reference 3 and reported in greater detail in Reference 11.

Further, because of the differences in the two rotor configurations noted previously, the only data which could conveniently and directly be compared were those of flatwise bending moment, edgewise bending moments, blade torsional moments, and the chordwise distribution of the measured differential pressures at their various spanwise stations. Presented in Figures 34 and 35 are typical flatwise and edgewise bending moment distributions at two values of the blade collective angle. No unusual characteristics were noted.

Figure 36 presents a cross plot of the variation of the 15 percent span flatwise bending moment with the collective angle. A smooth variation is noted with an indication that a maximum value has been reached at approximately -1.5 degrees of collective angle. It is conjectured that a large portion of the outer span of the blade was stalled. Even though the aerodynamic angle of attack distribution was not known, it is believed that these outboard sections were stalled due to the fact that the sharp leading edge was into the wind and that geometric angles of attack from approximately 8 to 11 degrees existed over these outboard stations. The results of the torsional moment distribution vs. collective angle presented in Figure 37 tend to substantiate this supposition. Both the 15 percent span and the 50 percent span torsional moments indicate a minimum at approximately -1 to -1.5 degrees of collective angle. The relatively large torsional moments are generated by the positive lift effectively acting at the 3/4 chord of each station. Since the 3/4 chord is considerably aft of the elastic axis position, large negative torsional moments are generated on the blade.

Typical differential pressure distributions at several spanwise stations are presented in Figure 38 for two values of the collective angle. These pressure distributions at each spanwise station indicate the large expected suction at the trailing edge of the blade (now acting as the leading edge). Note that the 85 percent span data indicate a distinct peculiarity at chordwise stations between 5 and 20 percent. This peculiarity was observed at all azimuthal positions and all collective angles. It was also noted in the flight test data of Reference 2 as well as the data

of Reference 3. This peculiarity has been attributed to the leading edge cap strip which extends to slightly past 85 percent span. The lack of a sufficient number of pressure transducers in the region outboard of 85 percent does not permit further substantiation of the "cap strip" hypothesis.

Presented in Figure 39 are comparisons between stopped rotor flatwise bending moment distributions obtained during current tests and those obtained in Reference 3. The flatwise moment distributions of Reference 3 indicate lower moments at all values of azimuthal positions compared. While the magnitude of the flatwise bending moment is lower for Reference 3, the distributions at each of the azimuthal positions (90, 120 and 255 degrees) are the same. The lower moments obtained in Reference 3 (particularly for 120 degrees and 255 degrees) can be attributed in part to the fact that the rotor of Reference 3 had no coning angle and in part to the effects of its blunted trailing edge. Also contributing to the lack of agreement was the fact that for the current tests the azimuthal position was not known precisely. The estimated error was ±10 degrees.

The comparison of the pressure data presented in Figure 40 for azimuthal positions of 90 degrees and 225 degrees exhibits the expected differences in amplitude for the reasons noted above. However, of more significance is the close agreement of the distribution found for the forward 60 percent of the chord, including the characteristics previously noted over the 5 to 20 percent chord, region at the 85 percent span. Of equal significance are the considerable differences in the characteristic distribution (as well as magnitude) of the pressure differentials measured over the aft 40 percent of the airfoil chord. This peculiar behavior is attributed to the blunted trailing edge which existed on the reference blade of the rotor of Reference 3.

The instability encountered in Reference 3, and reported in more detail in Reference 11, was not encountered during any of these tests. Even though blade collective angles were tested well within the indicated instability region of Reference 11, no indications of the previously reported instabilities were noted. All of the blade bending moments and torsional moments were relatively constant and did not exhibit any indication of the large intermittent oscillatory motions reported in Reference 11. It should be noted, however, that any difference, or combination of differences, between the two test configurations (discussed previously) could account for the fact that no instability was encountered during the current rotor test program.

27

CONCLUSIONS

The following conclusions were based upon the analysis of a limited amount of the extensive body of experimental data collected during this program.

CONCLUSIONS REACHED FOR THE STEADY-STATE OPERATION OF THE ROTOR AT HIGH ADVANCE RATIOS

1. The mean shaft bending moments measured were found to be relatively insensitive to variations in the collective or shaft angles for a given combination of freestream velocity and rotor speed.

2. It was found that for these tests, as advance ratio was increased, autorotative operation of the rotor was encountered for any fixed positive collective angle.

3. Further, for a fixed advance ratio above 1.0, it was found that autorotation was encountered by increasing the collective angle in a positive direction.

4. For advance ratios above 1.0, autorotation could be encountered by either increasing or decreasing the shaft angle sufficiently beyond zero.

5. Very large oscillatory shaft loads and moments were generated by collective changes at advance ratios much greater than 0.5. The 1-per-rev variations were magnified as the advance ratio increased due to the influence of the reversed flow region.

6. It was found that the shaft angle and the sine component of the blade cyclic angle are interchangeable at the very high advance ratios.

7. The correlation between experiment and the existing theory was found to be very poor for all the high-advance-ratio cases calculated.

CONCLUSIONS DRAWN FOR THE STARTING AND/OR STOPPING OPERATION OF THE ROTOR

1. It was found that no aerodynamic or structural response phenomena of an unusual nature occurred during either the starting or the stopping of the rotor during this study.

2. For the rotor employed in these tests and for the starting and stopping conditions of these tests, the transient oscillations observed in all of the blade and mast bending moments never exceeded twice the steady-state oscillatory moments observed for corresponding operating conditions.

3. The oscillatory characteristics of the loads and moments on a rotor being stopped are very similar to those experienced by the rotor being started.

4. For the range of accelerations tested, acceleration has no measurable effect on the aerodynamics of the blade, and did not play a significant role in the starting or stopping of the rotor.

CONCLUSIONS REACHED FOR THE STOPPED-ROTOR OPERATIONS

1. The trends and nominal values obtained during the previous stopped-rotor tests employing these blades (recorded in Reference 3) were generally verified.

2. The instabilities reported for the previous stopped-rotor tests were not encountered in the present stopped-rotor tests.

RECOMMENDATIONS

   The following recommendations are made to aid in the continued development of stowable rotor vehicles.

1. It is recommended that the large body of experimental data gathered for the steady-state operation of the rigid two-bladed rotor of these tests be studied in more detail. In particular, the pressure information obtained during these tests should be more critically analyzed and utilized.

2. The pressure data collected during the starting and stopping tests should be reduced and analyzed to indicate more conclusively whether the starting/stopping sequences are as similar as they appear to be.

3. Further attempts should be made to correlate the experimental data obtained with existing theory.

4. Additional tests should be conducted at high advance ratios and during starting/stopping sequences on a rigid two-bladed rotor system at much higher rotor speeds than those used in the current tests.

5. Tests should be conducted at high advance ratios and during starting/stopping sequences on a series of rotors for which variations are allowed of the number of blades, the blade fixity, and the hub configuration.

	% SPAN					
% CHORD	40	55	75	85	90	95
2		±15 psi	±15 psi	±15 psi	±15 psi	±15 psi
4	±8 psi			±15 psi		
9		±15 psi		±15 psi	±15 psi	±15 psi
13				±15 psi		
17	±8 psi	±8 psi		±15 psi	±15 psi	±15 psi
23		±8 psi	±8 psi	±15 psi	±15 psi	±15 psi
34	±4 psi					
47.7				±4 psi		
63		±2 psi	±2 psi	±2 psi	±4 psi	
77				±2 psi		
88	±1 psi					
90		±1 psi		±2 psi	±2 psi	±2 psi

Table I. PRESSURE TRANSDUCER LOCATIONS AND RANGES

Table II. TEST CONFIGURATIONS WITH NOMINAL VALUES INDICATED								
CASE NUMBER (RUN-POINT)	ROTOR SPEED (rpm)	TUNNEL VELOCITY (fps)	SHAFT ANGLE (deg)	BLADE ROOT COLLECTIVE (deg)	COSINE BLADE CYCLIC (deg)	SINE BLADE CYCLIC (deg)	TIP ADVANCE RATIO (μ)	FIGURE NO. VOLUME II
2.16	70	80	0	7.5	0	0	0.50	8
2.19	↓	↓	↓	10.5	↓	↓	↓	9
2.20	↓	↓	↓	5.0	↓	↓	↓	10
4.1	70	100	0	7.5	0	0	0.62	11
4.3				10.0				12
4.6	↓	↓	↓	5.0	↓	↓	↓	13
7.1	4	120	0	7.5	0	0	13.03	14
7.2				9.0				15
7.3				10.0				16
7.4				11.0				17
7.5				6.0				18
7.6				5.0	↓			19
7.7				7.5	0	+2.0		20
7.8						+3.0		21
7.9						+4.0		22
7.10						-2.0		23
7.11				↓		-4.0		24
7.13					↓	-6.0		25
7.14				7.5	+2.0	0		26
7.15					+4.0			27
7.16					-2.0			28
7.17				↓	-4.0	↓		29
7.18			+1.9	7.5	0	0		30
7.19			+3.9					31
7.20			-2.0					32
7.21	↓	↓	-4.0	↓	↓	↓	↓	33
8.24	20	120	0	7.5	0	0	2.60	34
8.25				7.5	+1.0			35
8.26				7.5	+2.0			36
8.27				7.5	-1.0			37
8.28				7.5	-2.0			38
8.29				7.5	0	+1.0		39
8.30	↓	↓	↓	7.5	0	-1.0	↓	40
5.29	70	120	0	7.5	0	+1.5	0.74	41
5.30						-0.5		42
5.31						-1.0		43
5.32					↓	-1.5		44
5.33					+1.0	0		45
5.34					+2.0			46
5.35					+3.0			47
5.36					-1.0			48
5.37					-2.0			49
5.38	↓	↓	↓	↓	-3.0	↓	↓	50

CASE NUMBER (RUN-POINT)	ROTOR SPEED (rpm)	TUNNEL VELOCITY (fps)	SHAFT ANGLE (deg)	BLADE ROOT COLLECTIVE (deg)	COSINE BLADE CYCLIC (deg)	SINE BLADE CYCLIC (deg)	TIP ADVANCE RATIO (μ)	FIGURE NO. VOLUME II
8.40	70	120	0	7.5	0	0	0.74	51
8.41	↓	↓	+1.0	7.5	0	-1.0	↓	52
8.42	↓	↓	+1.0	7.5	0	-2.0	↓	53
7.22	70	120	+0.9	7.5	0	0	0.74	54
7.23			+1.9					55
7.24			-1.0					56
7.25	↓	↓	-2.0	↓	↓	↓	↓	57
8.21	7	140	0	7.5	0	0	8.69	58
8.22	↓	↓	↓	9.0				59
8.23	↓	↓	↓	6.0	↓	↓	↓	60
8.14	20	140	0	7.5	0	0	3.04	61
8.15				9.0				62
8.16				10.0				63
8.17				5.0				64
8.18				7.5		↓		65
8.19				7.5		+1.5		66
8.20	↓	↓	↓	7.5	↓	-1.5	↓	67
8.7	50	140	0	7.5	0	0	1.22	68
8.8				8.5				69
8.9				9.0				70
8.10				6.0				71
8.11				5.5		↓		72
8.12				7.5		1.0		73
8.13	↓	↓	↓	7.5	↓	-1.0	↓	74
8.1	70	140	0	7.5	0	0	0.87	75
8.2				8.5				76
8.3				9.0				77
8.4				6.C		↓		78
8.5				7.5		+1.0		79
8.6	↓	↓	↓	7.5	↓	-1.0	↓	80
10.25	5	160	0	7.5	0	0	13.90	81
10.26				8.0				82
10.27				7.0				83
10.28	↓			6.0			↓	84
10.29	70			7.0			0.99	85
10.30				8.0				86
10.31	↓	↓	↓	5.7	↓	↓	↓	87

Table II - Continued

	Table III.	ROTOR START/STOP TEST CONFIGURATIONS (NOMINAL VALUES)					
CASE NUMBER (RUN-POINT)	ROTOR SPEED (rpm)	TUNNEL VELOCITY (fps)	SHAFT ANGLE (deg)	BLADE ROOT COLLECTIVE (deg)	COSINE BLADE CYCLIC (deg)	SINE BLADE CYCLIC (deg)	BRAKE PRESSURE (psi)
8.34	0 → 70	120	0	7.5	0	0	150
8.35	70 → 0	↓					200
8.36	0 → 70	140					150
8.37	70 → 0						150
8.38	70 → 0						200
8.39	70 → 0	↓	↓	↓	↓	↓	225
8.43	70 → 0	120	+1.0	7.5	0	-1.0	200
10.32	70 → 0	160	0	7.0	0	0	225

Table IV. STOPPED-ROTOR TEST CONFIGURATIONS (NOMINAL VALUES)						
CASE NUMBER (RUN-POINT)	TUNNEL SPEED (fps)	AZIMUTHAL POSITION OF REF. BLADE (deg)	SHAFT ANGLE (deg)	BLADE ROOT COLLECTIVE (deg)	COSINE BLADE CYCLIC (deg)	SINE BLADE CYCLIC (deg)
9.1	158	30	0	7.5	0	0
9.2						+1.0
9.3						+2.0
9.4						+3.0
9.5						+4.0
9.6						+5.0
9.7	158	90	0	7.5	0	0
9.8						+1.0
9.9						-1.0
10.1	158	90	0	7.5	0	0
10.2						+1.0
10.3						+2.0
10.4						+3.0
10.5						+4.0
10.6						-1.0
10.7	158	120	0	7.5	0	0
10.8						+1.0
10.9						+1.5
10.10						+2.0
10.11						+2.5
10.12						+3.0
10.13						-3.0
10.14	158	255	0	7.5	0	0
10.15						+1.0
10.16						+2.0
1C.17						+3.0
10.18						+4.0
10.19						+5.0
10.20						+6.0
10.21						+7.0
10.22						+2.0	+7.0
10.23						0	+8.0
10.24						0	+9.0

Table V. STATIC PRESSURE CALIBRATION RESULTS
PSI/INCH TRACE DEFLECTION
(AMPLIFIER ATTENUATION : 1)

% CHORD	% SPAN					
	40%	55%	75%	85%	90%	95%
2%		0.67878	0.69575	0.41477	0.47282	0.40504
4%	0.51347			0.55820		
9%		0.65931		0.43624	0.46955	0.54078
13%				0.55789		
17%	0.92993	0.42771		0.69623	0.35215	0.79868
23%		0.36109	0.52429	0.54764	0.36311	0.35632
34%	0.58477					
47.7%				0.18546		
63%		0.087238	0.11951	0.14164	0.18766	
77%				0.12699		
88%	0.12537					
90%		0.086019		0.26419	0.24454	0.11133

Table VI. BLADE MOMENT CALIBRATION CONSTANTS		
FT-LB/INCH TRACE DEFLECTION		
(AMPLIFIER ATTENUATION: 1)		

DESCRIPTION		CALIBRATION CONSTANT
FLATWISE BENDING	15% SPAN	102.20
FLATWISE BENDING	28% SPAN	30.00
FLATWISE BENDING	36% SPAN	34.89
FLATWISE BENDING	45% SPAN	32.91
FLATWISE BENDING	60% SPAN	34.57
FLATWISE BENDING	65% SPAN	37.13
FLATWISE BENDING	80% SPAN	39.81
FLATWISE BENDING	92.5% SPAN	35.50
EDGEWISE BENDING	15% SPAN	408.30
EDGEWISE BENDING	28% SPAN	277.30
EDGEWISE BENDING	60% SPAN	191.60
EDGEWISE BENDING	80% SPAN	208.00
TORSION	15% SPAN	263.00
TORSION	50% SPAN	45.43

37

Table VII.	CALIBRATION CONSTANTS FOR ROTOR YOKE, MAST, DRAG AND PITCH LINKS AND BOOST TUBES
DESCRIPTION	CALIBRATION CONSTANT
PARALLEL MAST BENDING - LOWER	91.62 ft-lb/in.
PARALLEL MAST BENDING - UPPER	59.10 ft-lb/in.
PERPENDICULAR MAST BENDING - LOWER	73.39 ft-lb/in.
PERPENDICULAR MAST BENDING - UPPER	51.14 ft-lb/in.
SHAFT TORQUE	52.01 ft-lb/in.
YOKE CHORDWISE BENDING	101.40 ft-lb/in.
YOKE FLATWISE BENDING	284.70 ft-lb/in.
PITCH LINK	152.9 lb/in.
DRAG BRACE	429.7 lb/in.
RIGHT FRONT BOOST TUBE	159.6 lb/in.
LEFT FRONT BOOST TUBE	179.5 lb/in.
REAR FRONT BOOST TUBE	185.4 lb/in.
(AMPLIFIER ATTENUATION : 1)	

Table VIII.   CALIBRATION CONSTANTS FOR BLADE COLLECTIVE, CYCLIC AND FEATHERING ANGLES

$$\text{COLLECTIVE ANGLE, deg} = -8.8608 \, (\Delta) +7.943$$
$$\text{SINE COMPONENT ANGLE, deg} = -36.538 \, (\Delta) +0.500$$
$$\text{COSINE COMPONENT ANGLE, deg} = -29.630 \, (\Delta)$$
$$\text{FEATHERING ANGLE, deg} = -4.857 \, (\Delta) +7.842$$

$(\Delta = $ INCHES OF TRACE DEFLECTION AT AMPLIFIER ATTENUATION : 1)
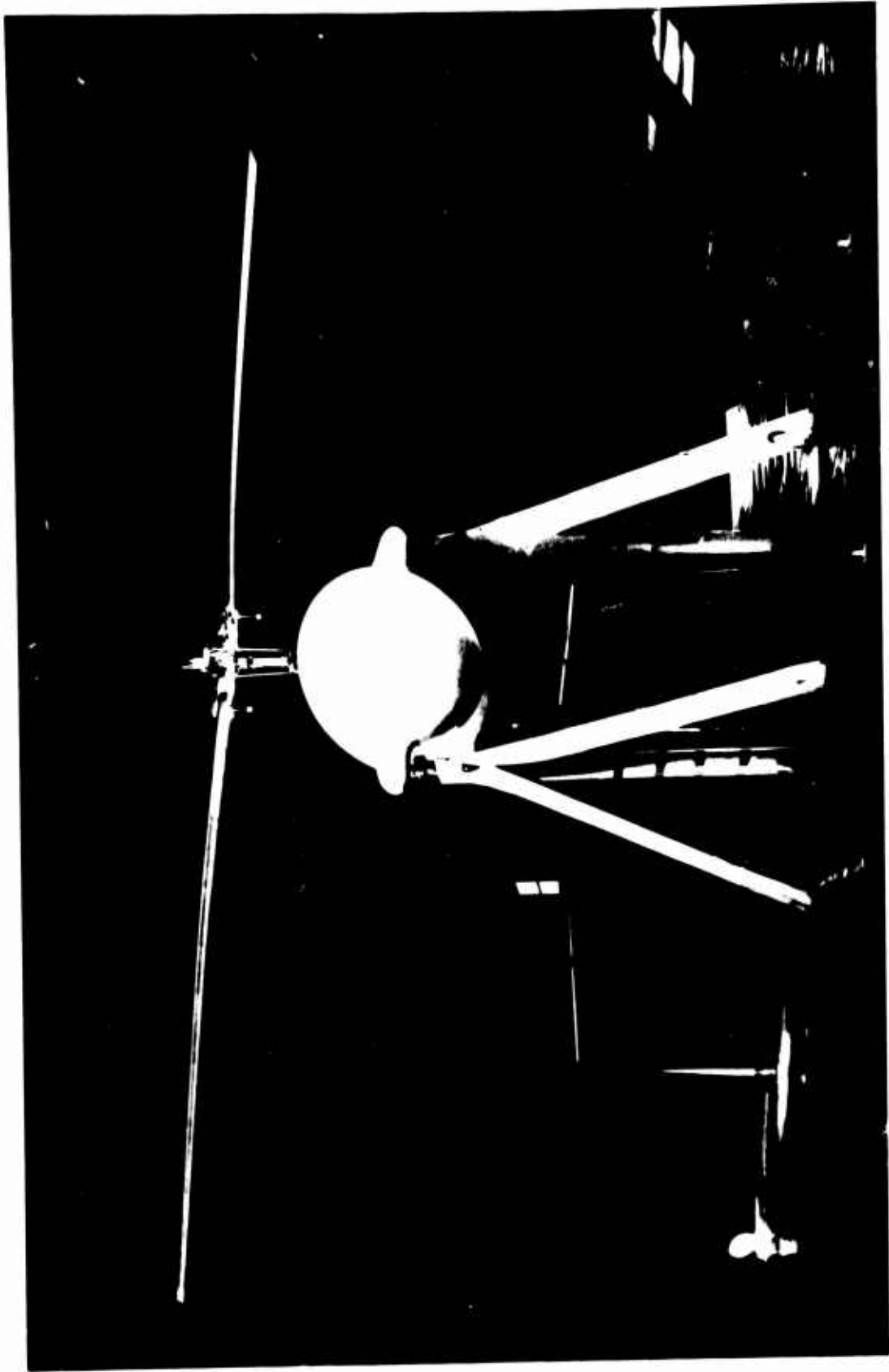
Figure 1. TEST ROTOR IN NASA-AMES 40-FOOT x 80-FOOT WIND TUNNEL.

SLIPRING ASSEMBLY (164 RINGS)

ROTOR HUB

ROTOR MAST

MIXING ARMS

SWASHPLATE

BRAKE ASSEMBLY

TRANSMISSION (1:0.0491 SPEED DECREASER)

2 - UH1A PRESSURE & STRAIN INSTRUMENTED BLADES
(22 FT DIA.; 15¼ IN. CHORD; NACA 0012 A/F SERIES SECTION)

1500 hp A/C VARIABLE-SPEED MOTOR (H₂O COOLED)

CONNECTING SHAFTS

GEARBOX (1:1.085 SPEED INCREASER)

AERODYNAMIC FAIRING
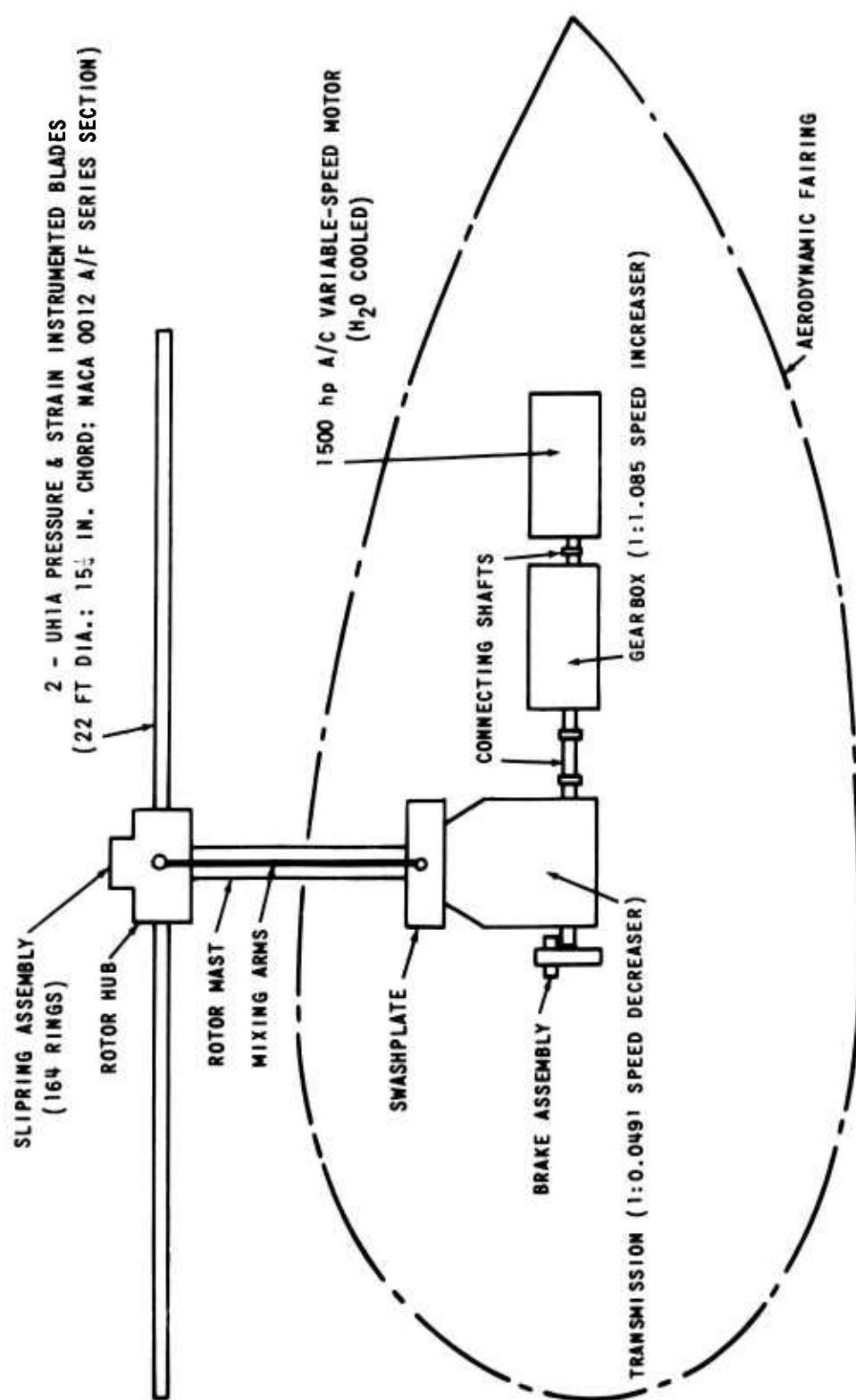
Figure 2. GRAPHICAL DESCRIPTION OF MODEL ASSEMBLY.

40
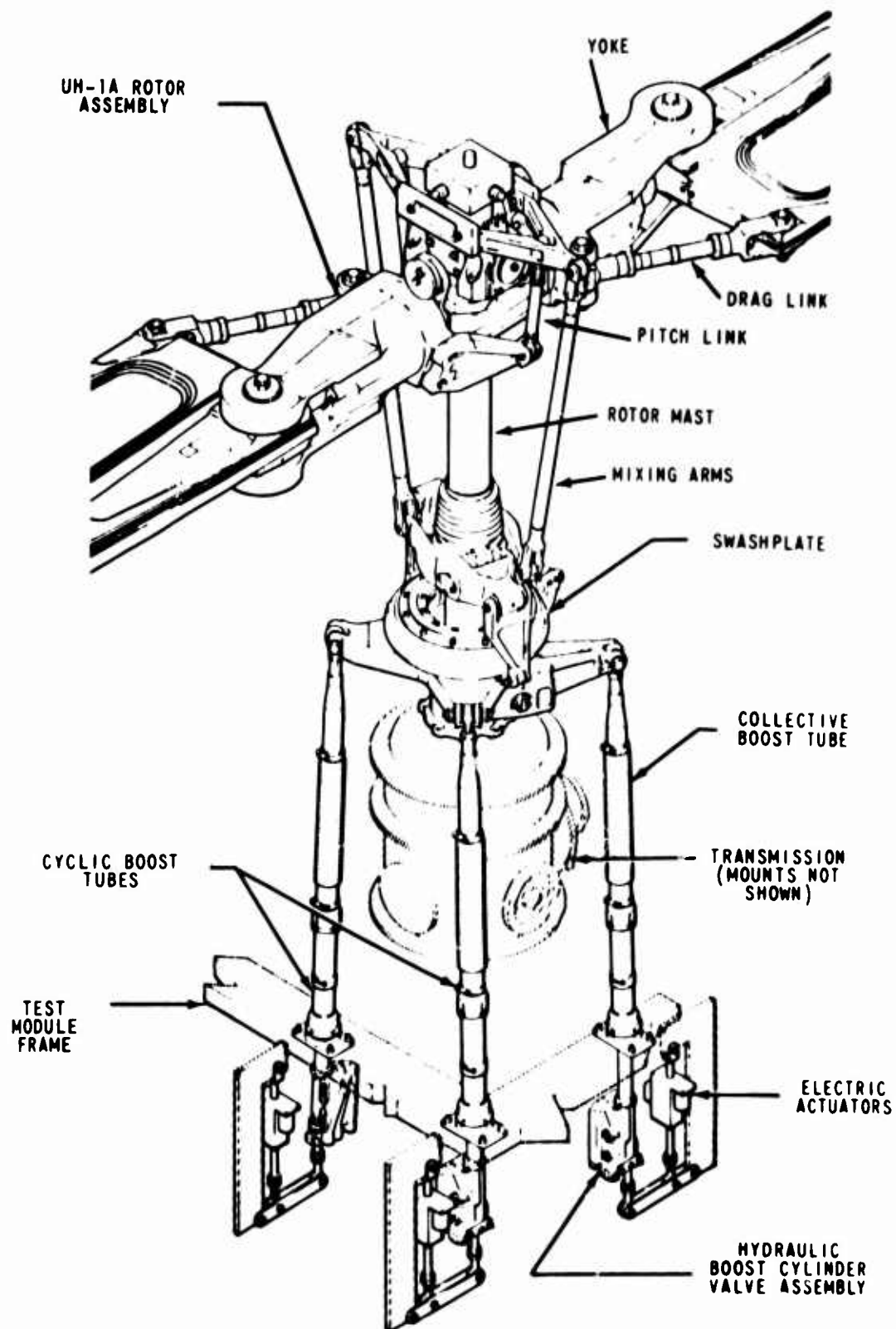
Figure 3. CONTROL SYSTEM ARRANGEMENT.

41
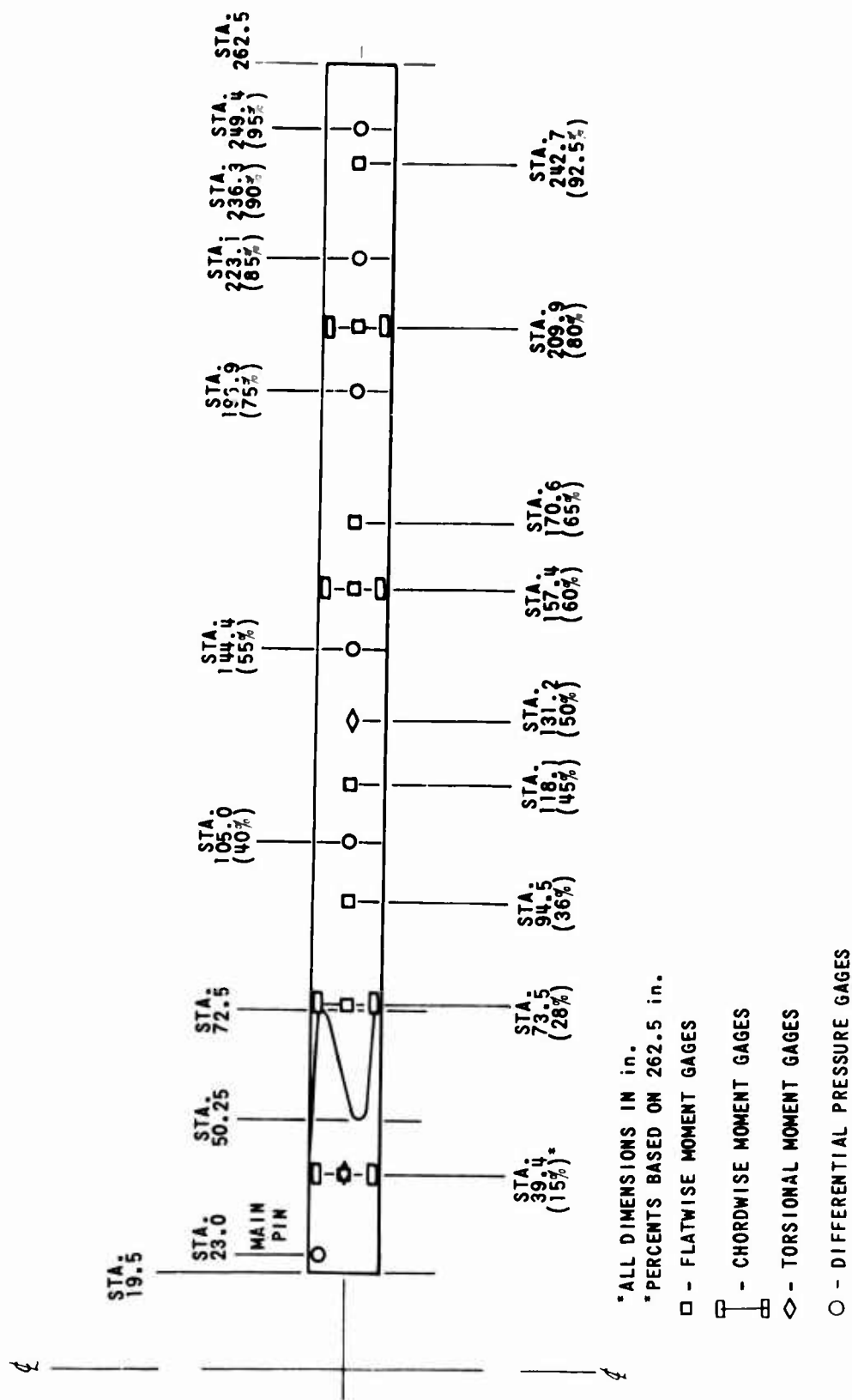
Figure 4. BLADE PLANFORM, INDICATING LOCATION OF BLADE MOMENT AND PRESSURE MEASURING GAGES.

*ALL DIMENSIONS IN in.
*PERCENTS BASED ON 262.5 in.

□ - FLATWISE MOMENT GAGES
⊓—⊐ - CHORDWISE MOMENT GAGES
◇ - TORSIONAL MOMENT GAGES
○ - DIFFERENTIAL PRESSURE GAGES

42
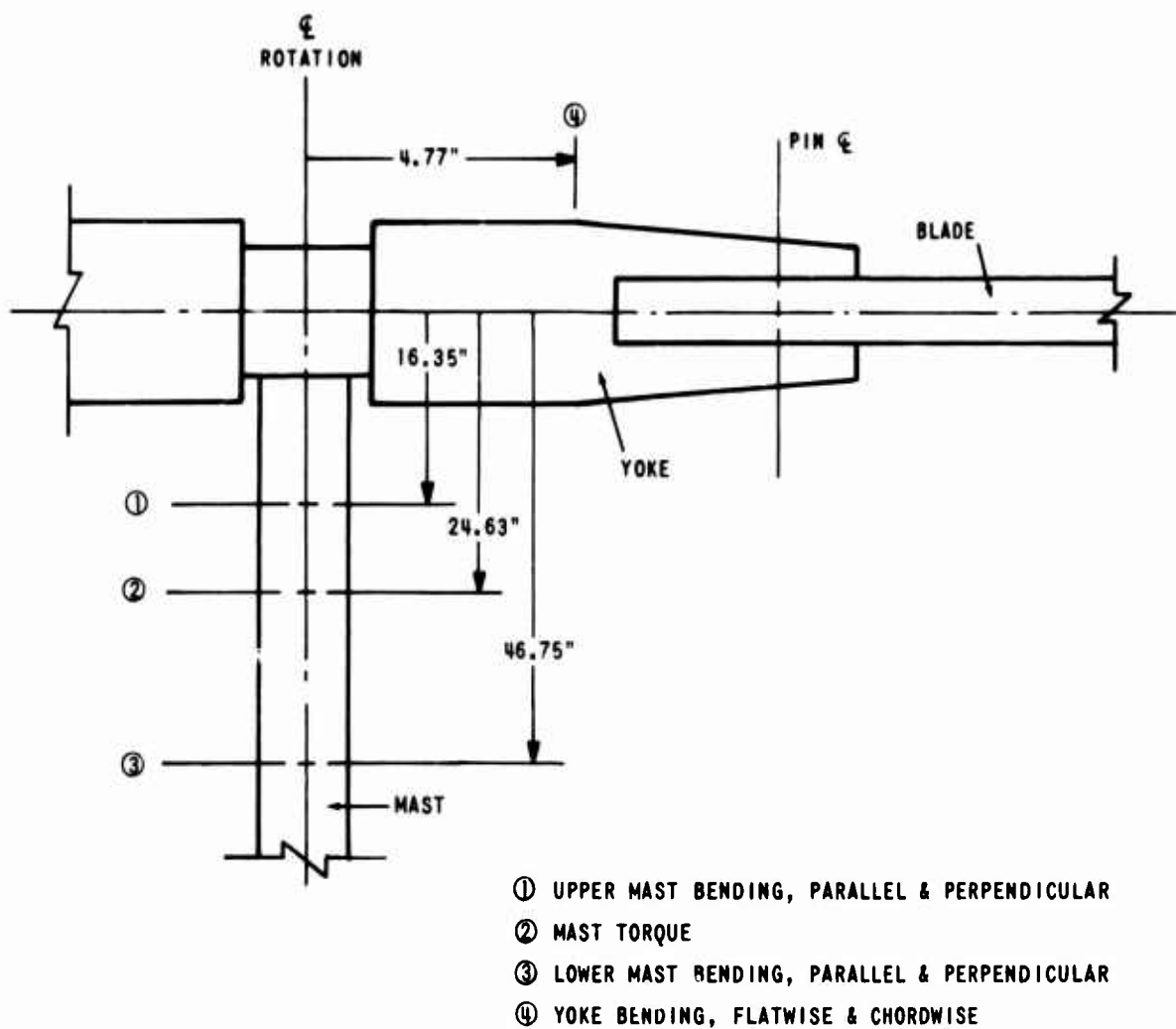
Figure 5.   SCHEMATIC OF MAST AND YOKE, INDICATING LOCATION OF MOMENT GAGES.

43
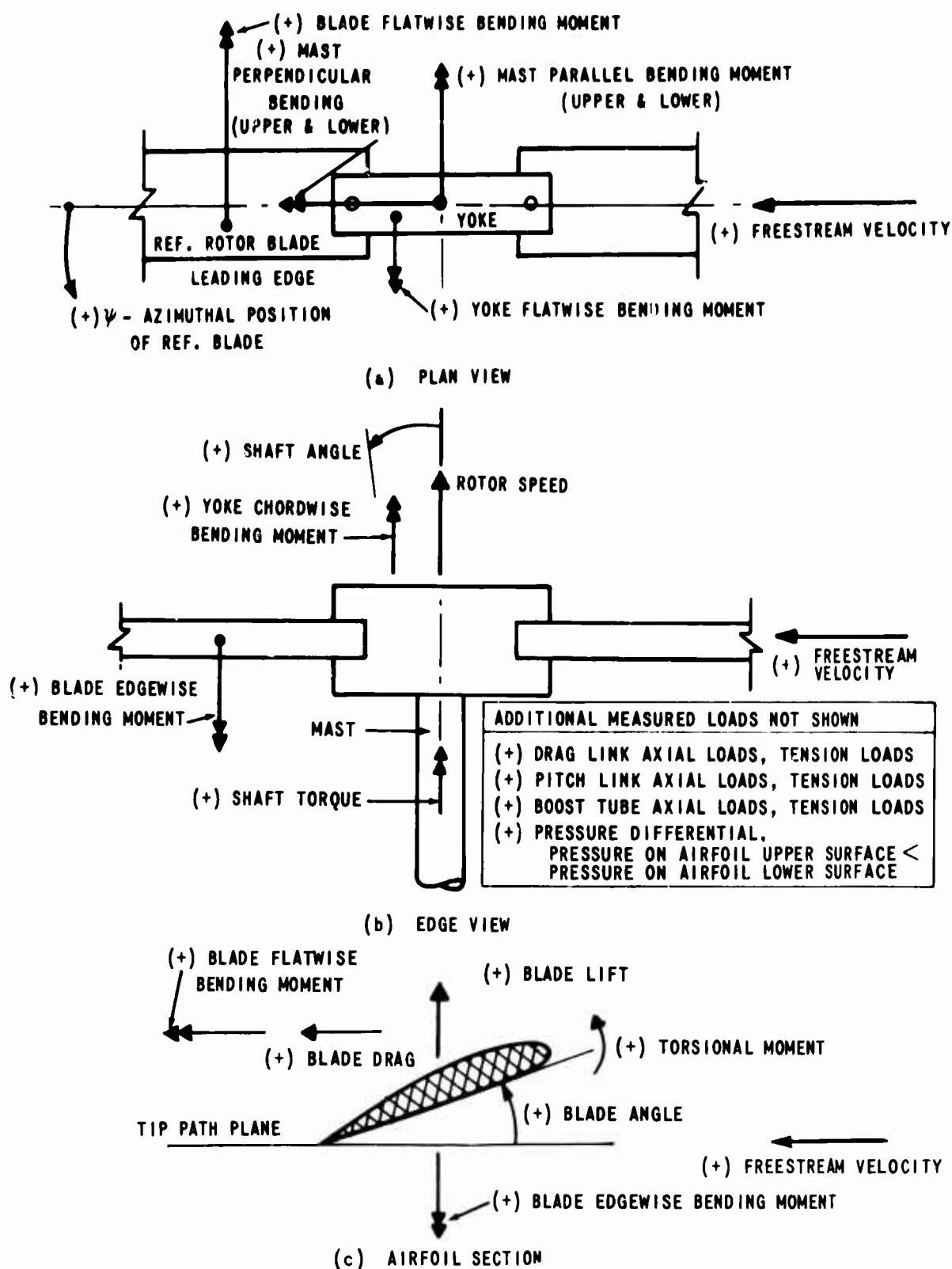
Figure 6. PICTORIAL, INDICATING SIGN CONVENTION FOR LOADS,
MOMENTS AND PRESSURES MEASURED.

44
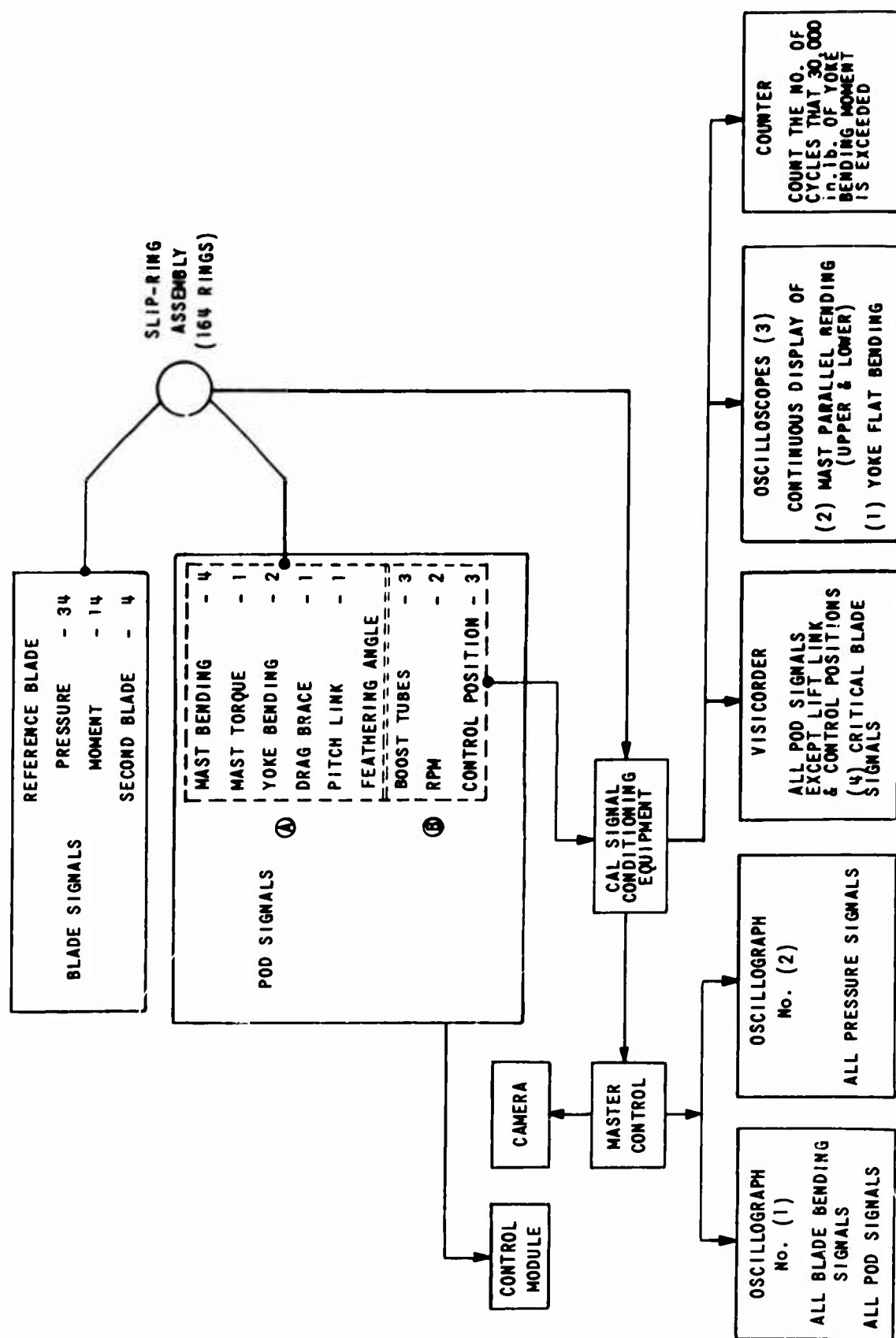
Figure 7. BLOCK DIAGRAM OF ELECTRICAL RECORDING SYSTEM.

45
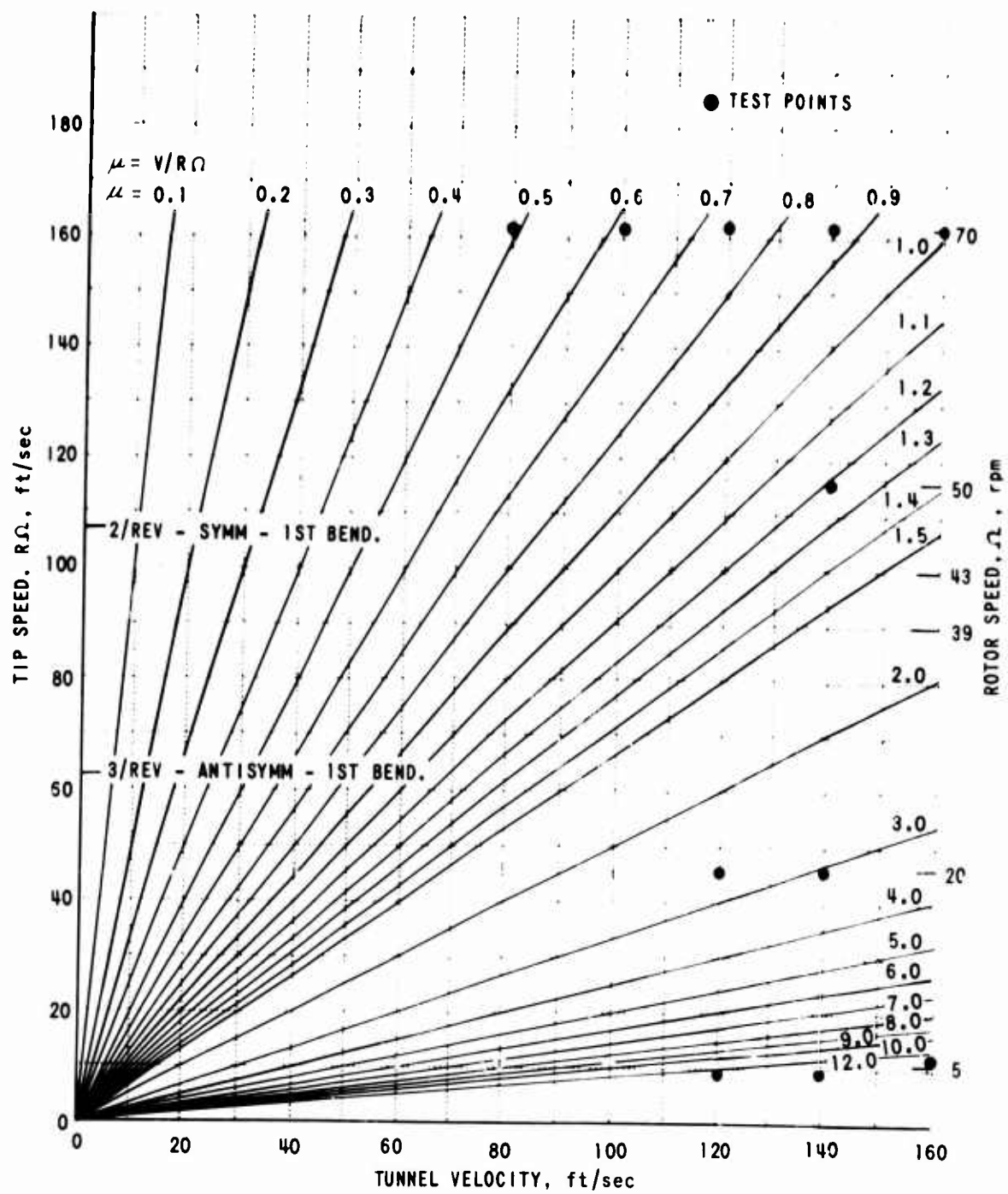
Figure 8.   ROTOR TIP SPEED VS. TUNNEL VELOCITY FOR UH-1A, WITH
EXPERIMENTAL POINTS NOTED.

46
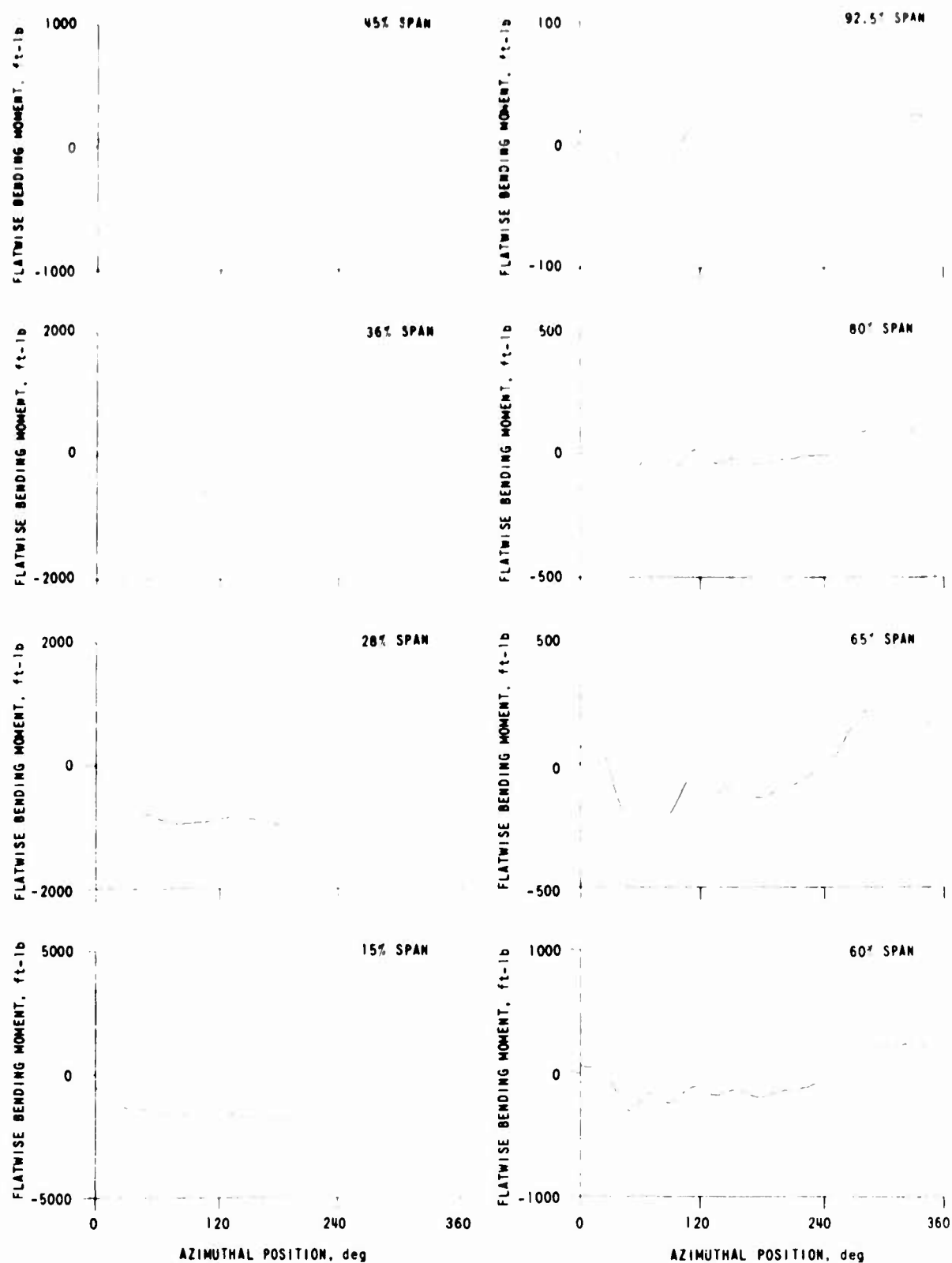
Figure 9. TYPICAL TIME HISTORY OF DATA COLLECTED FROM ROTOR
OPERATING AT V_f = 78 FPS, Ω = 71 RPM AND θ_R = 4.88 DEG.
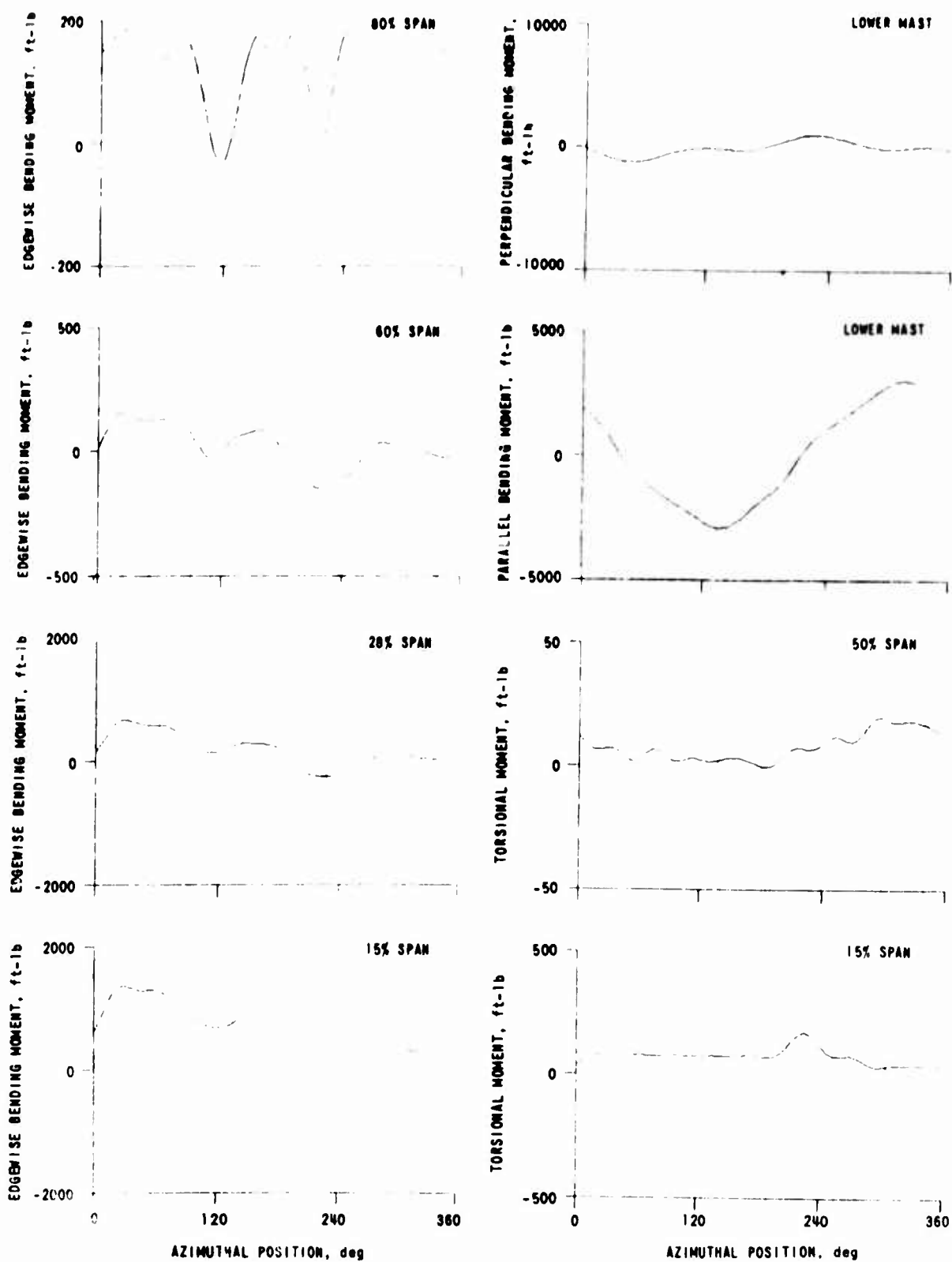
Figure 9. (Continued)
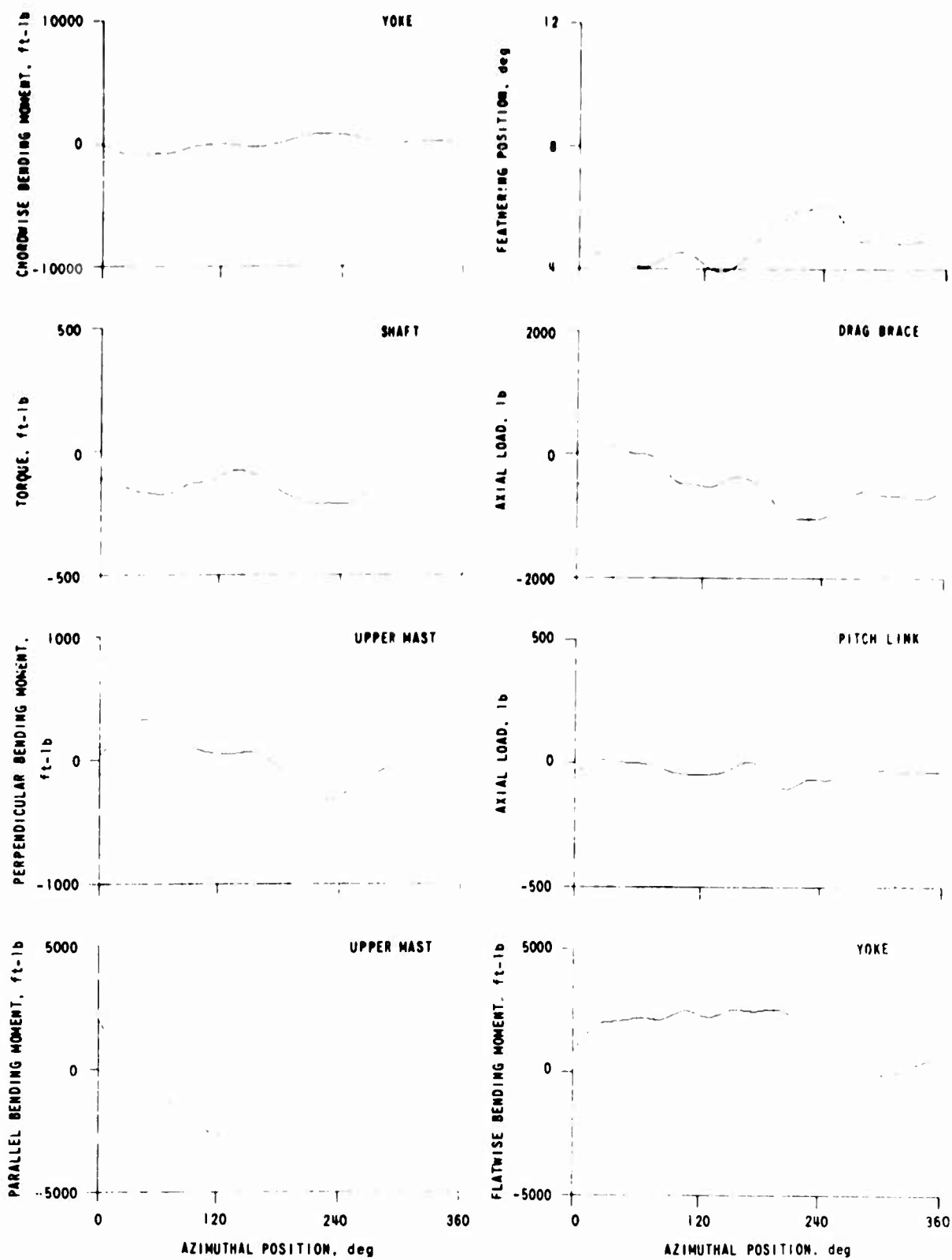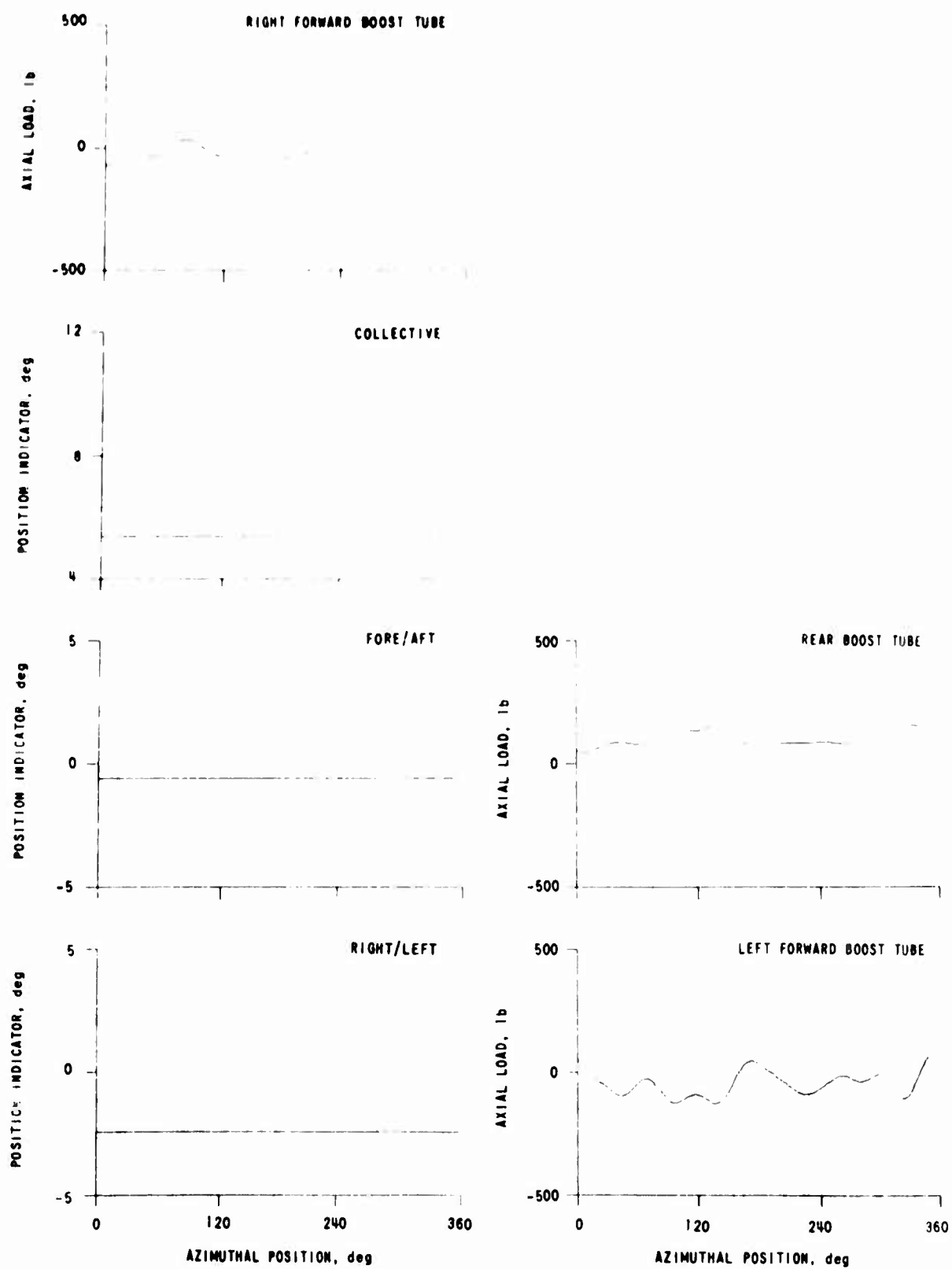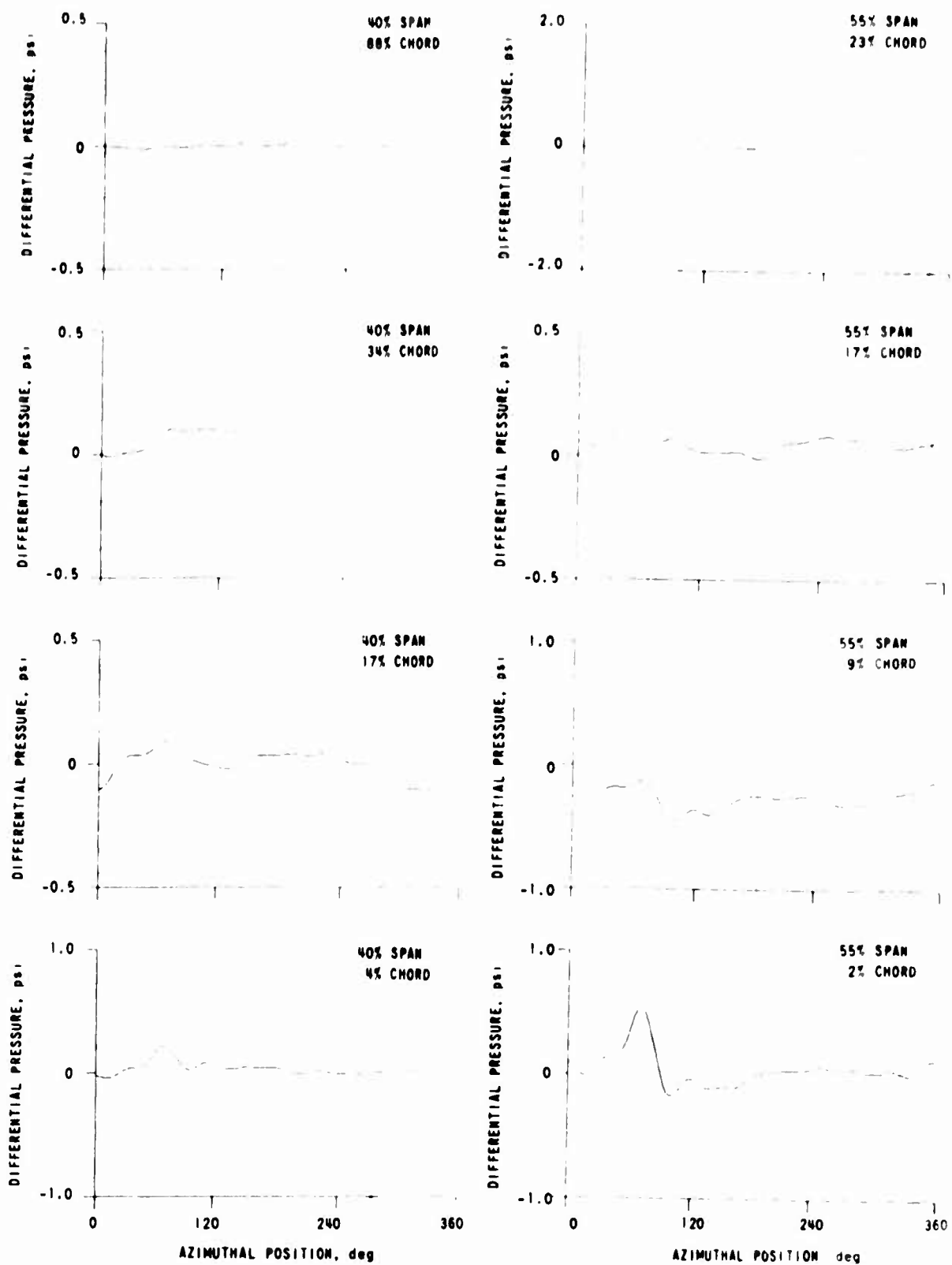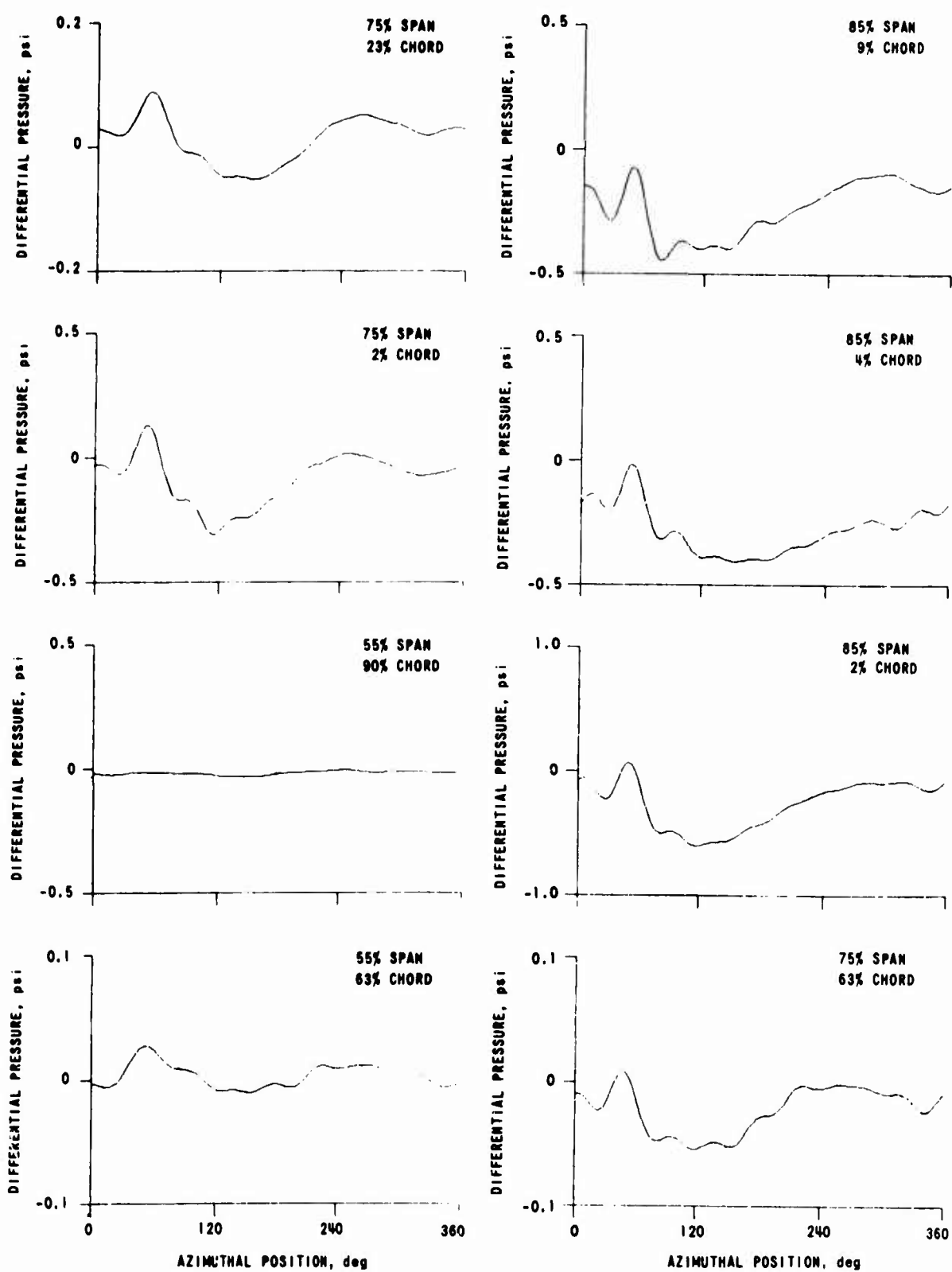
48

Figure 9. (Continued)

49

Figure 9. (Continued)

50

Figure 9. (Continued)

51

Figure 9. (Continued)

52

Figure 9. (Continued)

53

Figure 9. (Continued)

54

Figure 9. (Continued)

55
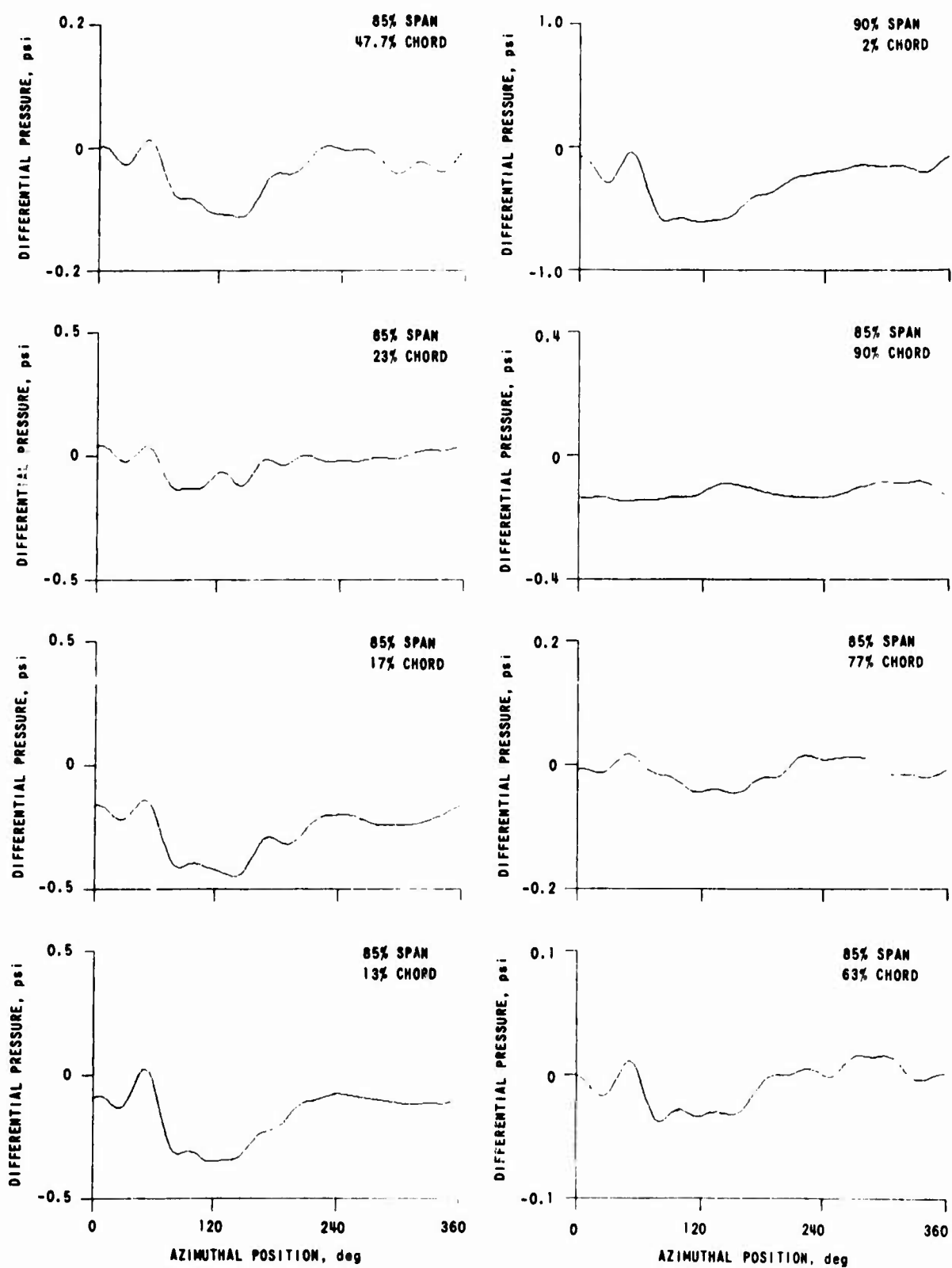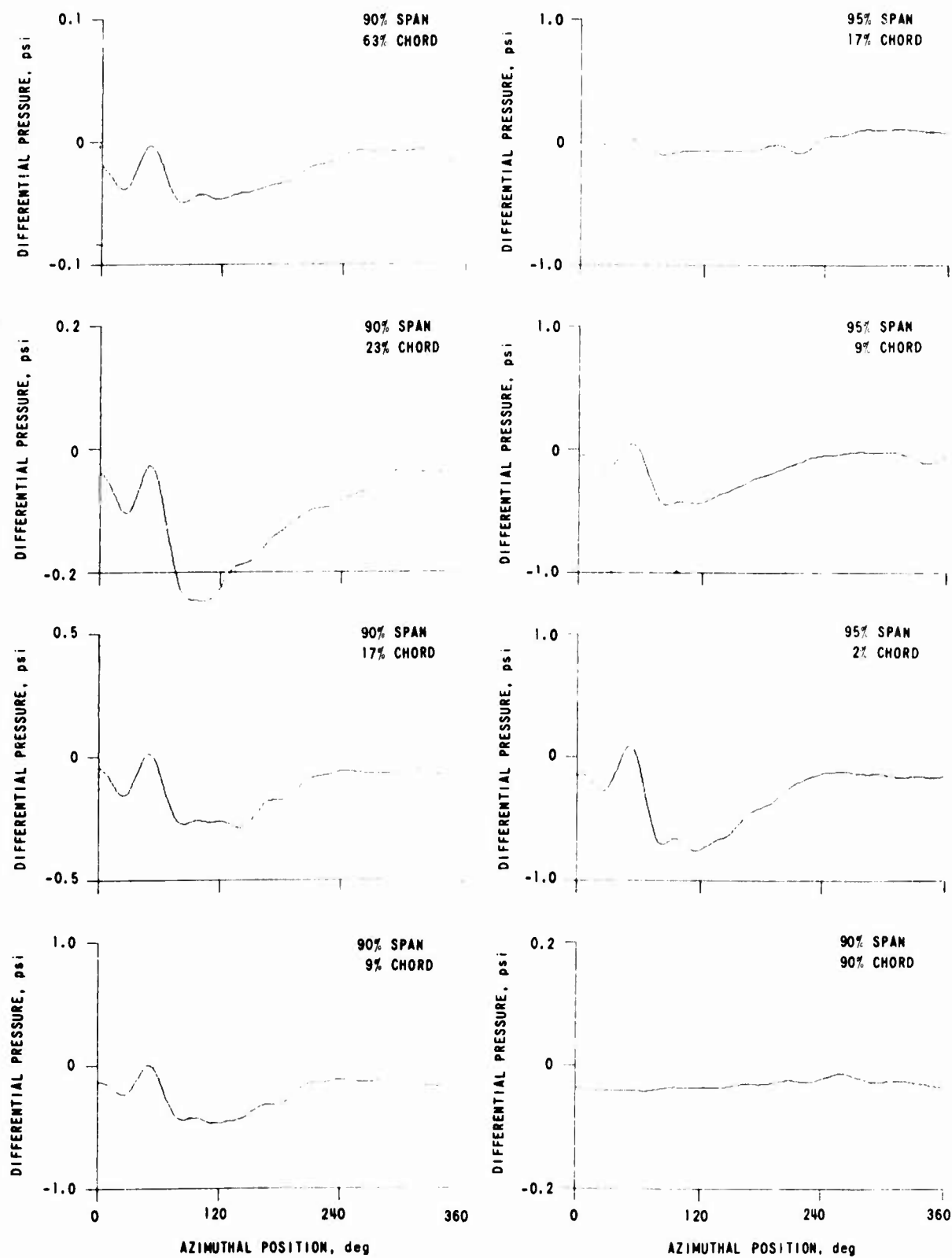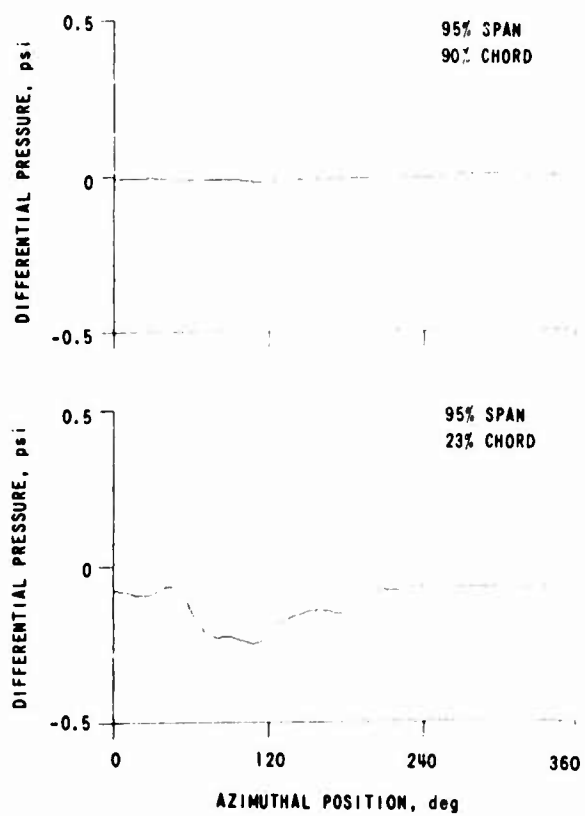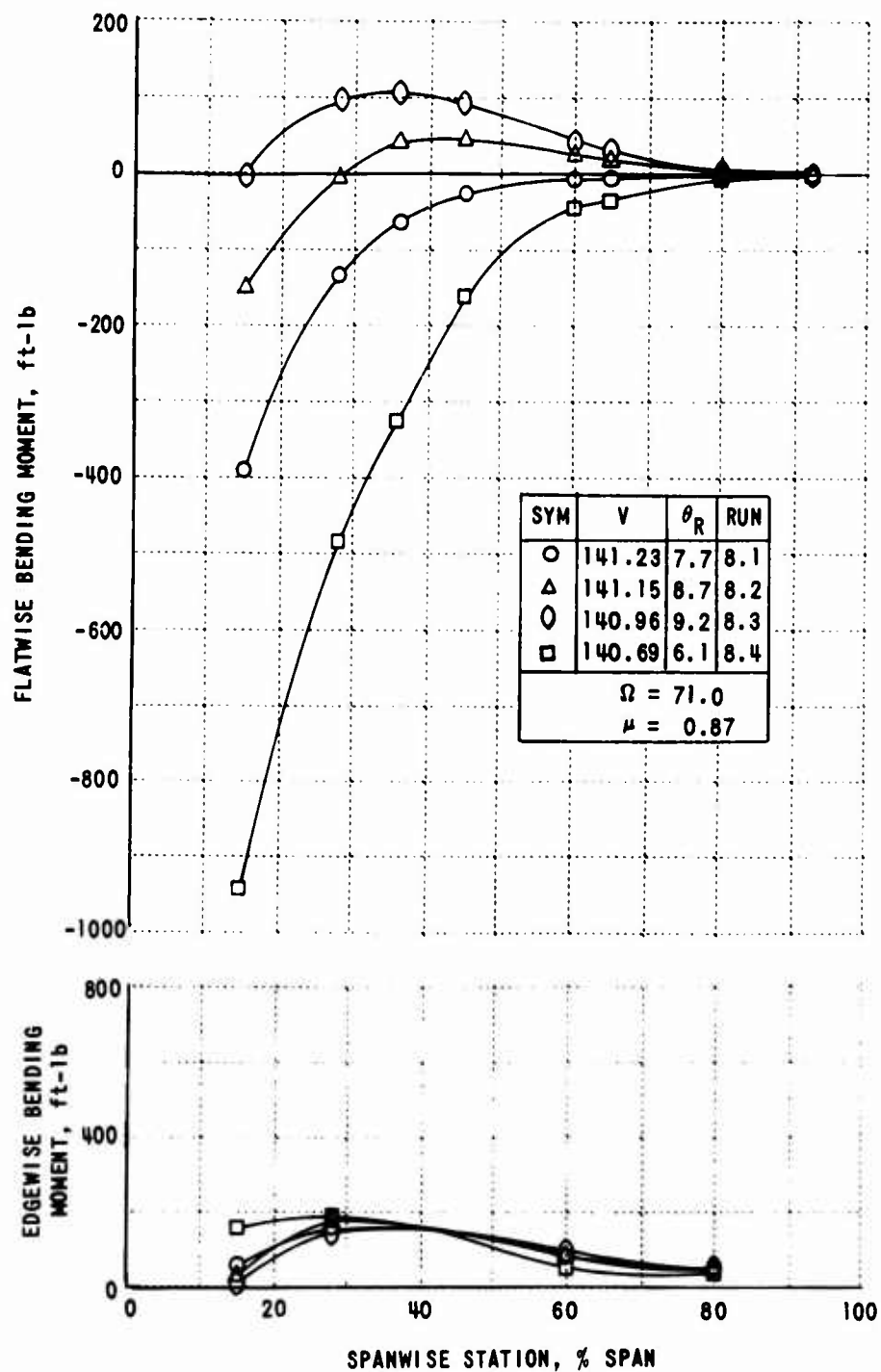
(a)

Figure 10. THE MEAN VALUES OF THE LOADS AND MOMENTS MEASURED ON THE
ROTOR OPERATING AT V_f = 141 FPS AND Ω = 71 RPM –
COLLECTIVE ANGLE VARIATION.

56
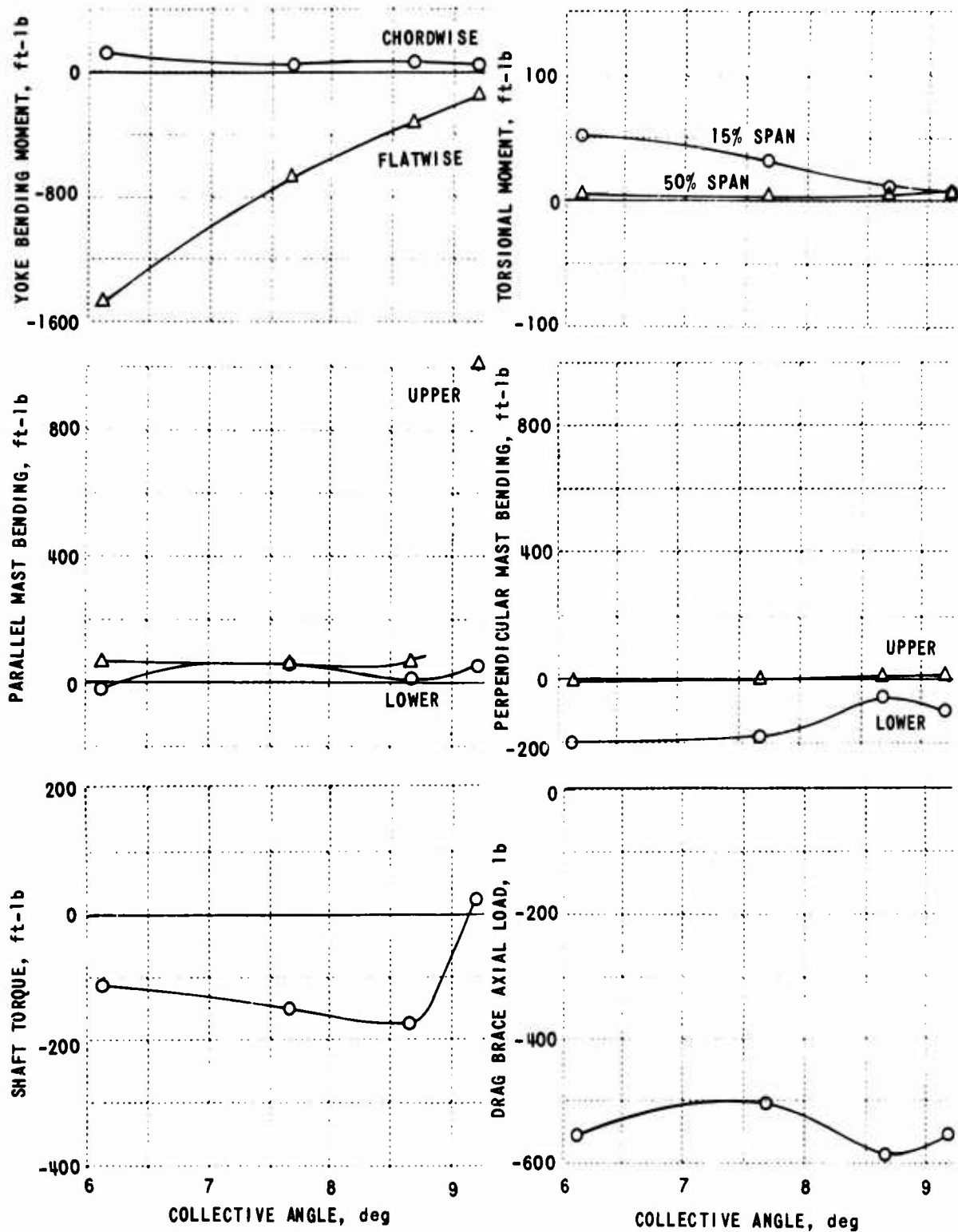
Figure 10. (Continued)
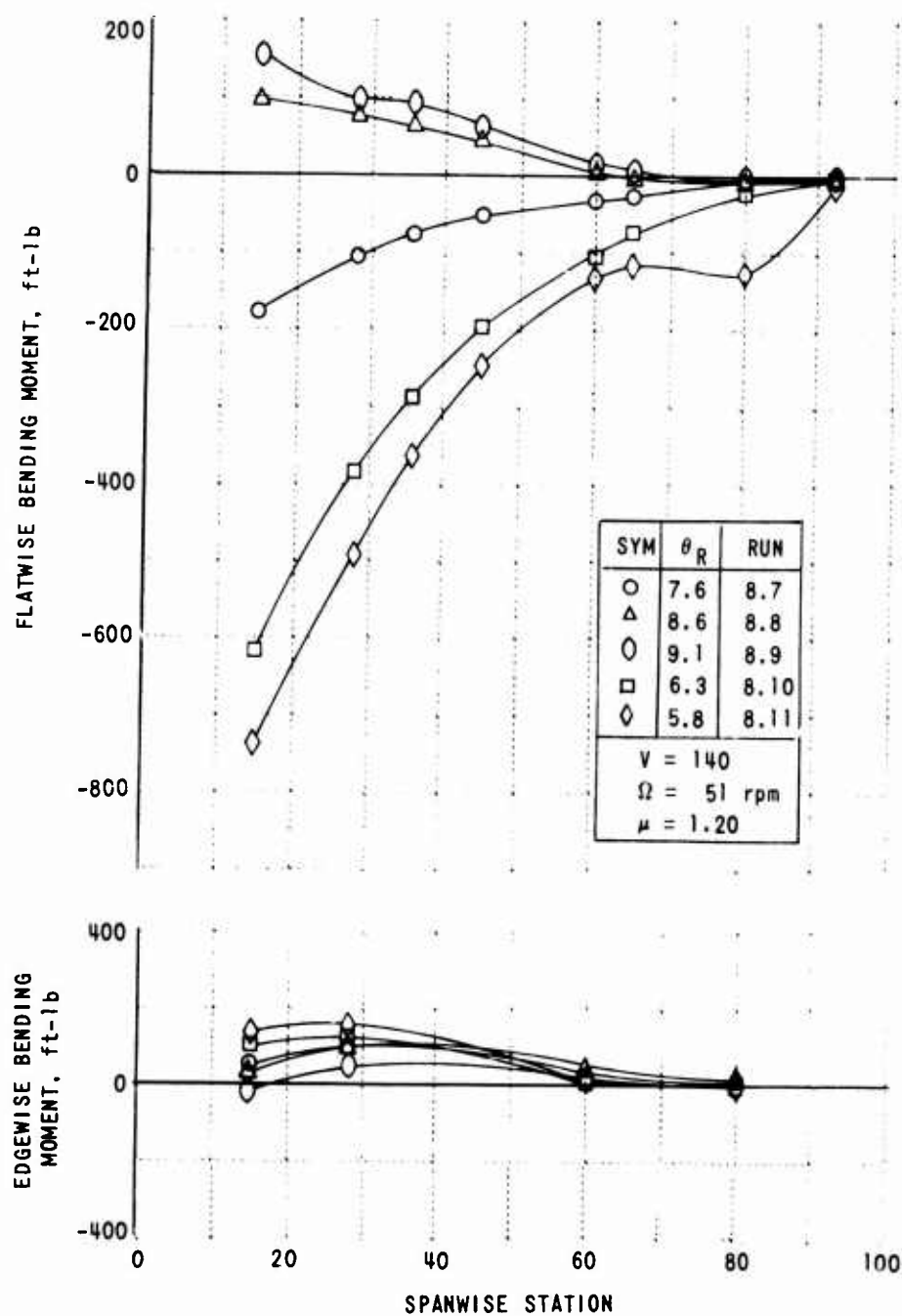
(a)

Figure 11. THE MEAN VALUES OF THE LOADS AND MOMENTS MEASURED ON THE
ROTOR OPERATING AT V_f = 140 FPS AND Ω = 51 RPM –
COLLECTIVE ANGLE VARIATION.

58
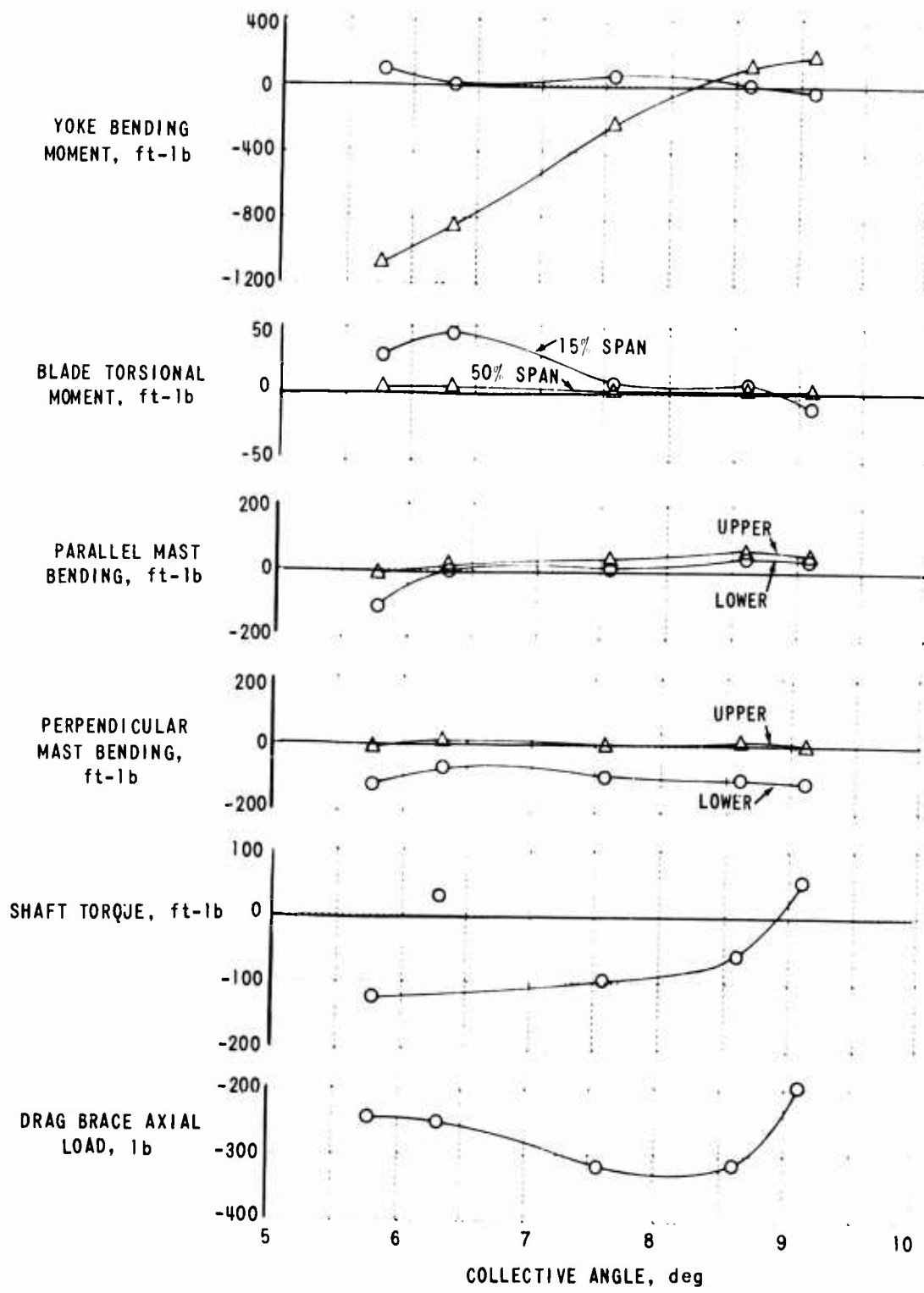
(b)

Figure 11. (Continued)

59
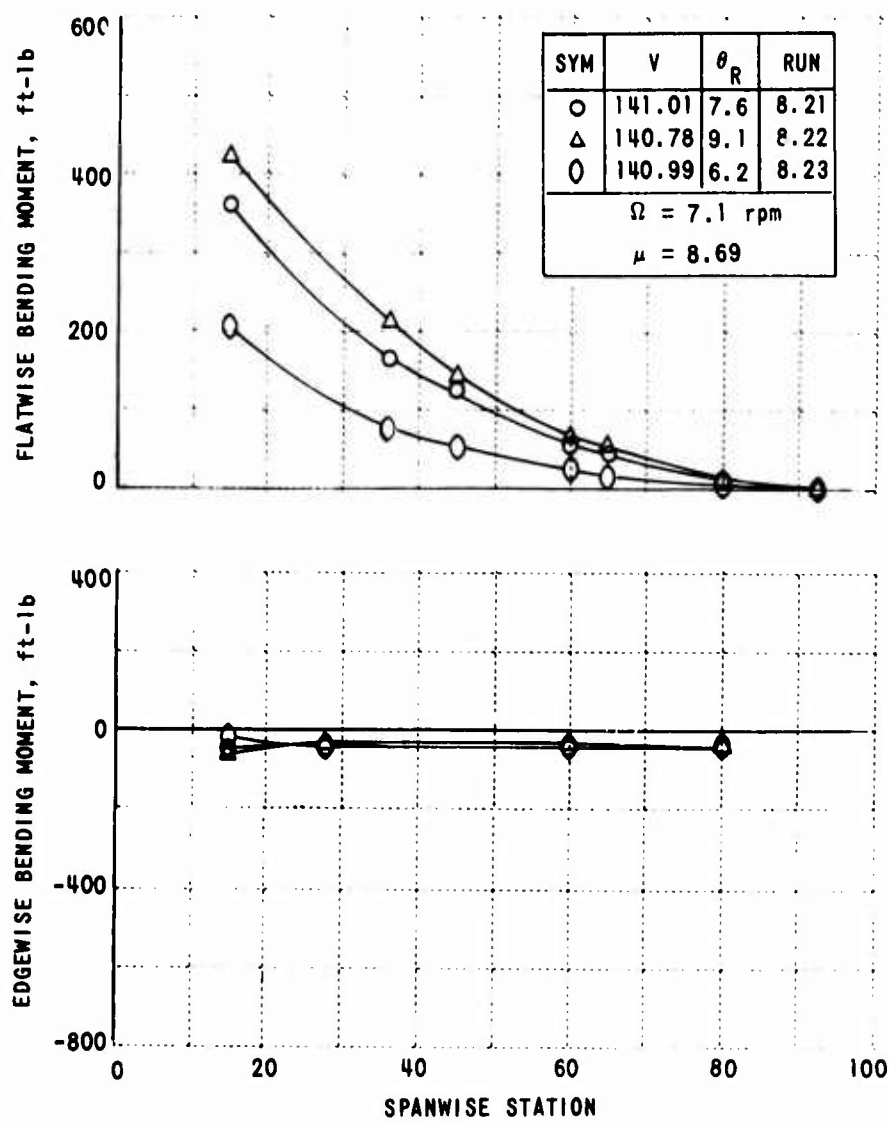
(a)

Figure 12. THE MEAN VALUES OF THE LOADS AND MOMENTS MEASURED ON THE ROTOR OPERATING AT V_f = 141.0 FPS AND Ω = 7.1 RPM – COLLECTIVE ANGLE VARIATION.

60
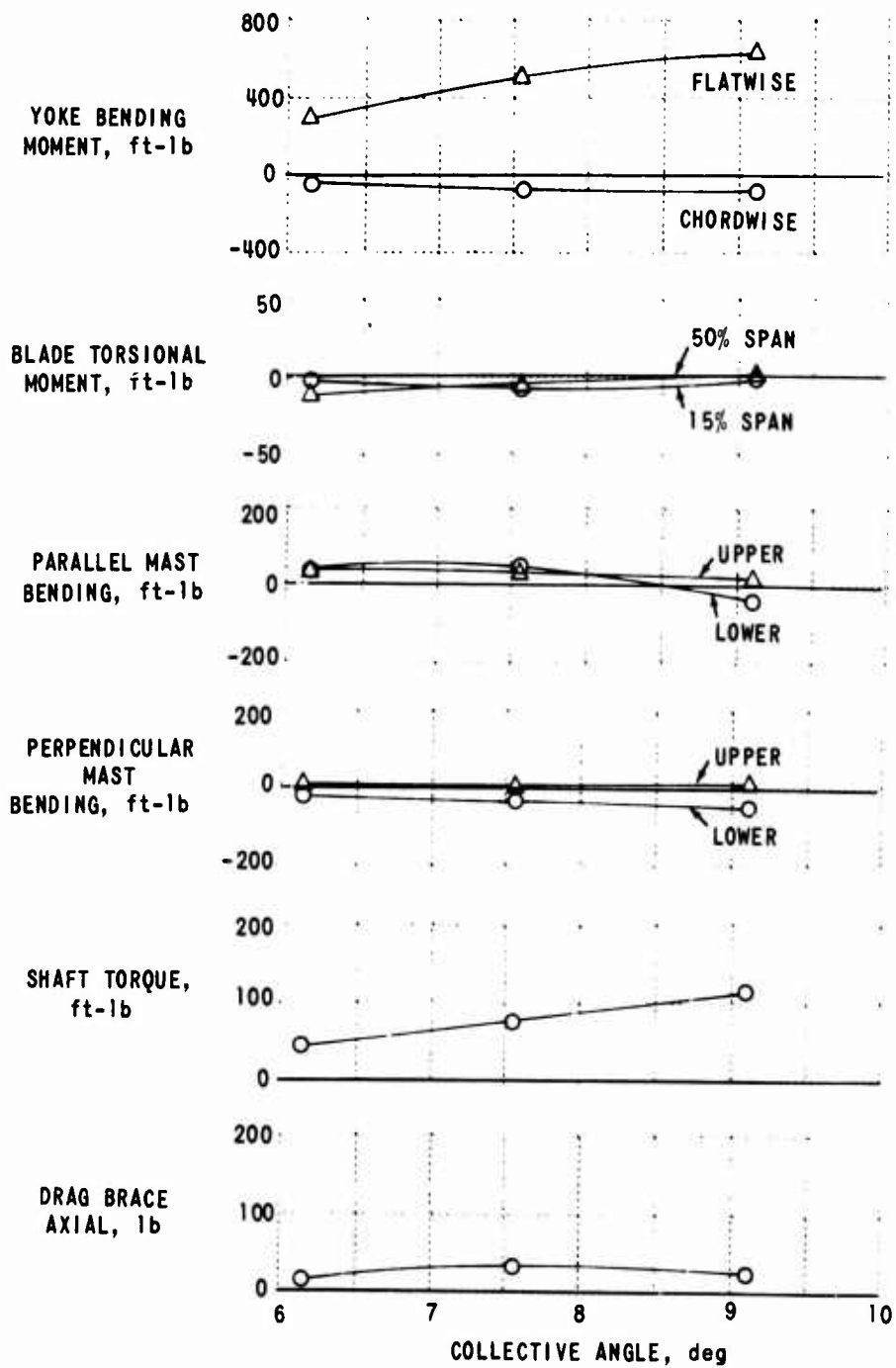
(b)

Figure 12. (Continued)
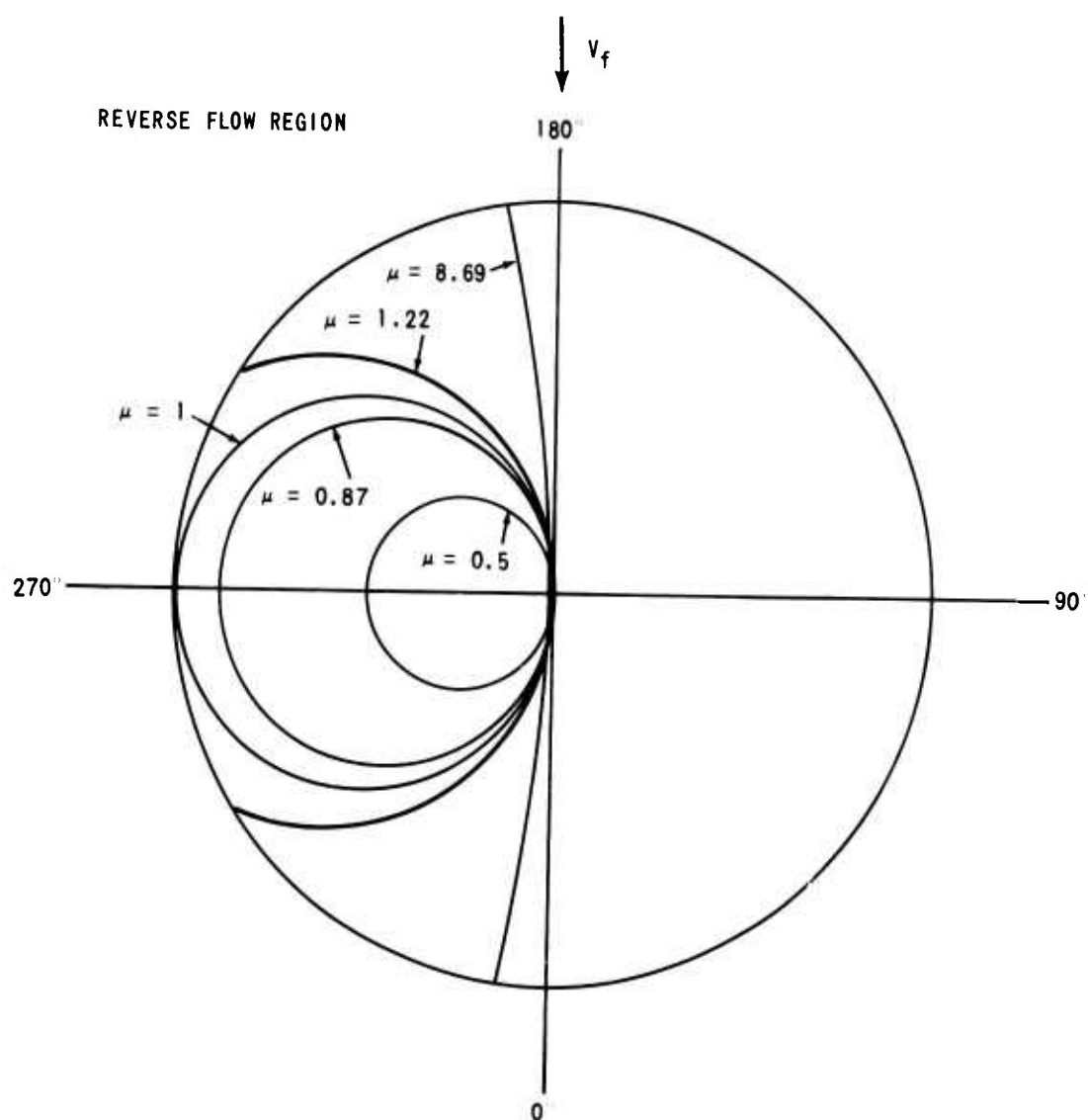
Figure 13. REGIONS OF ROTOR DISK IN REVERSE
FLOW FOR VARIOUS ADVANCE RATIOS.
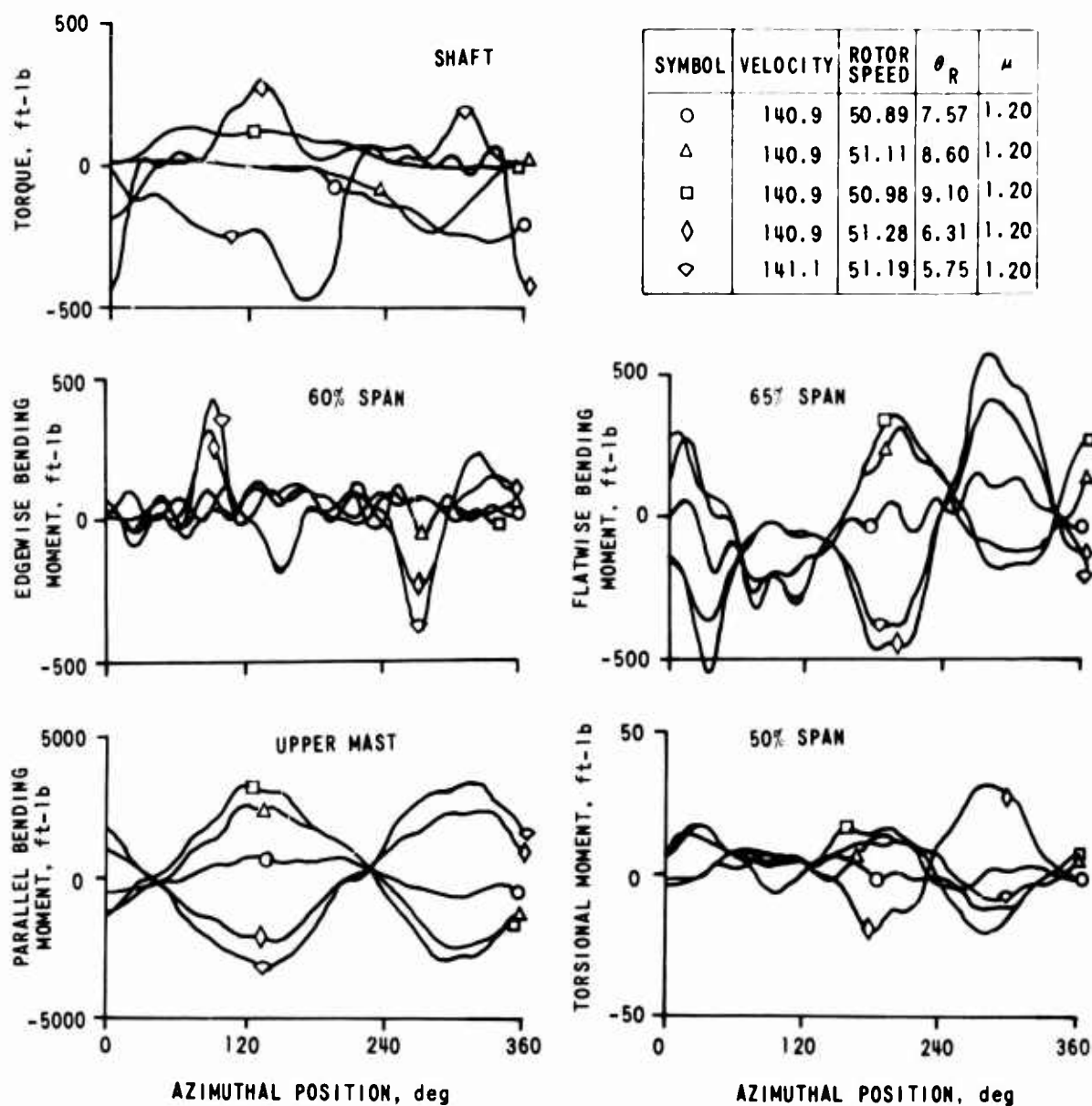
Figure 14. AZIMUTHAL VARIATION OF SELECTED MOMENTS MEASURED ON THE ROTOR OPERATING AT V_f = 141 FPS AND Ω = 51 RPM - COLLECTIVE ANGLE VARIATION.
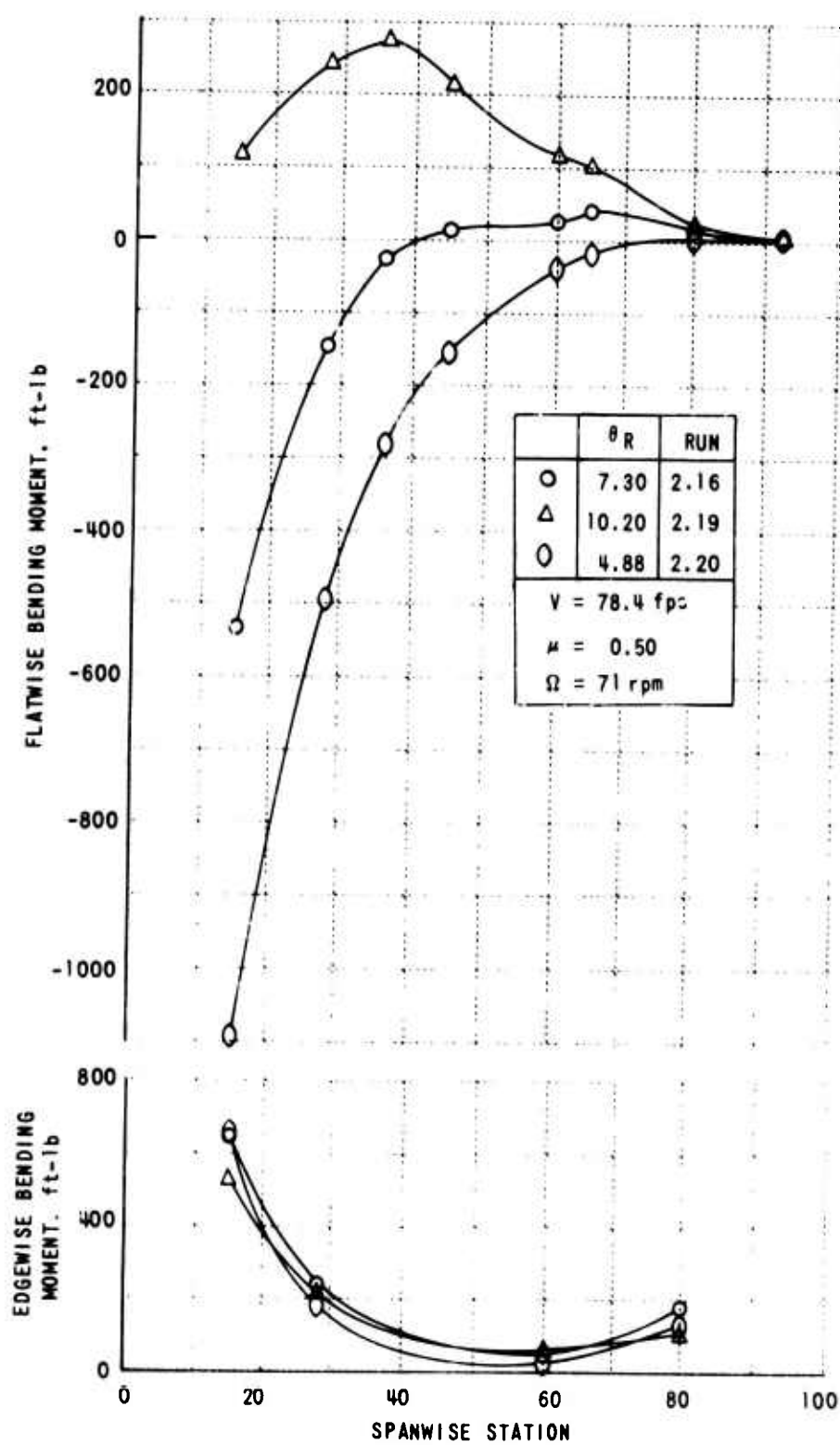
Figure 15. THE MEAN VALUES OF THE LOADS AND MOMENTS MEASURED ON THE ROTOR OPERATING AT V_f = 78.4 FPS AND Ω = 71 RPM - COLLECTIVE ANGLE VARIATION.
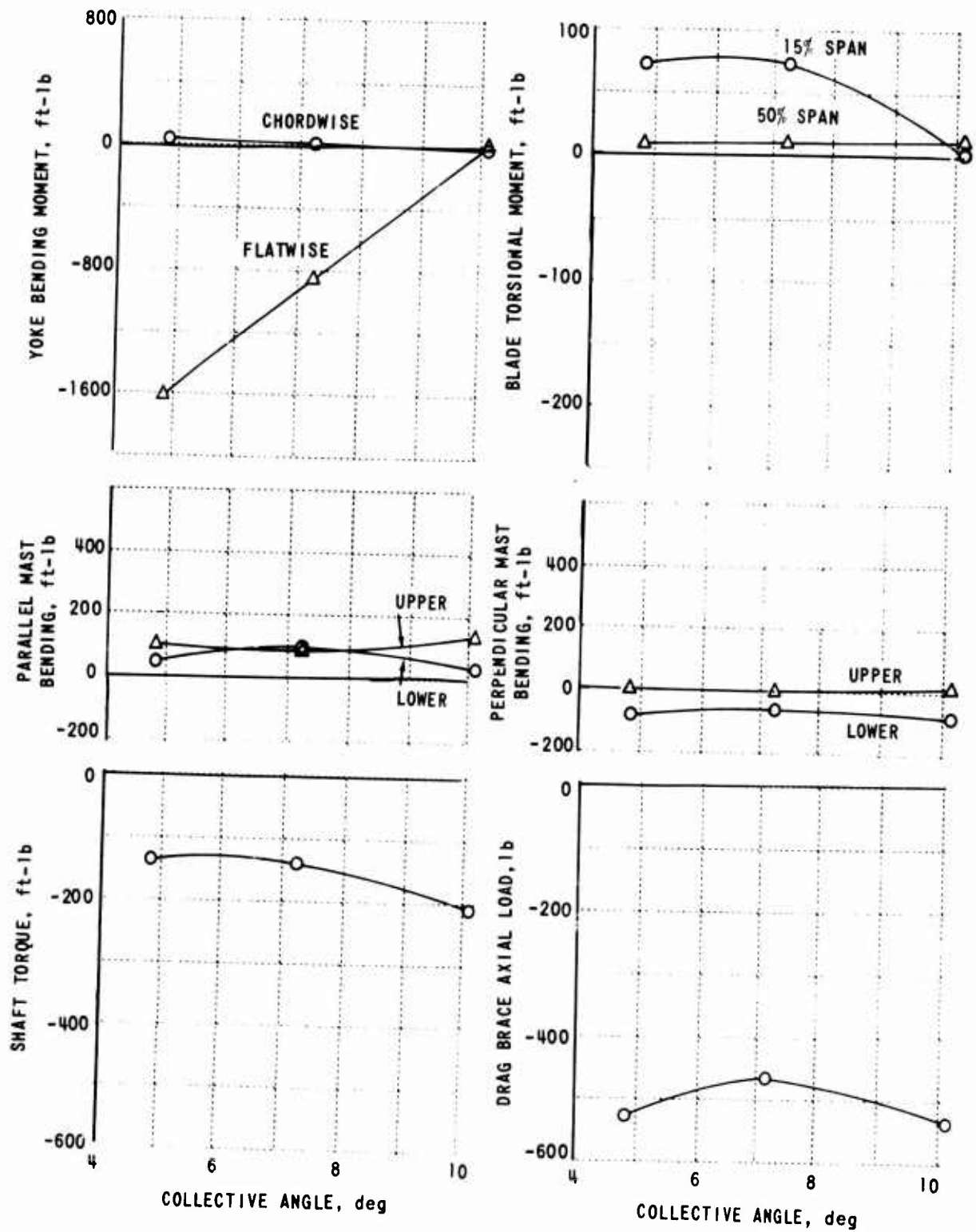
Figure 15. (Continued)
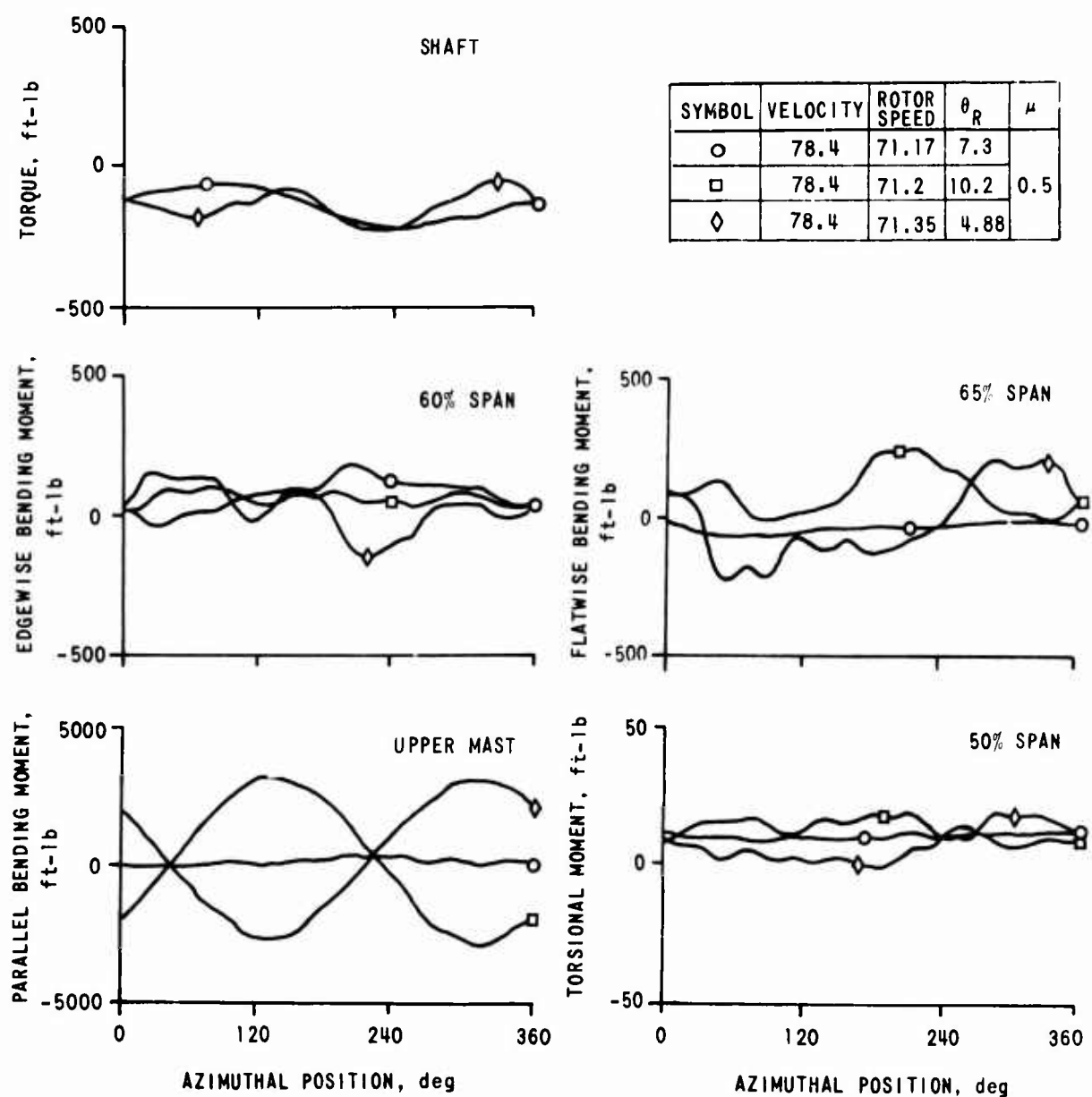
Figure 16. AZIMUTHAL VARIATION OF SELECTED MOMENTS MEASURED ON THE
ROTOR OPERATING AT V_f = 78.4 FPS AND Ω = 71.2 RPM -
COLLECTIVE ANGLE VARIATION.

66
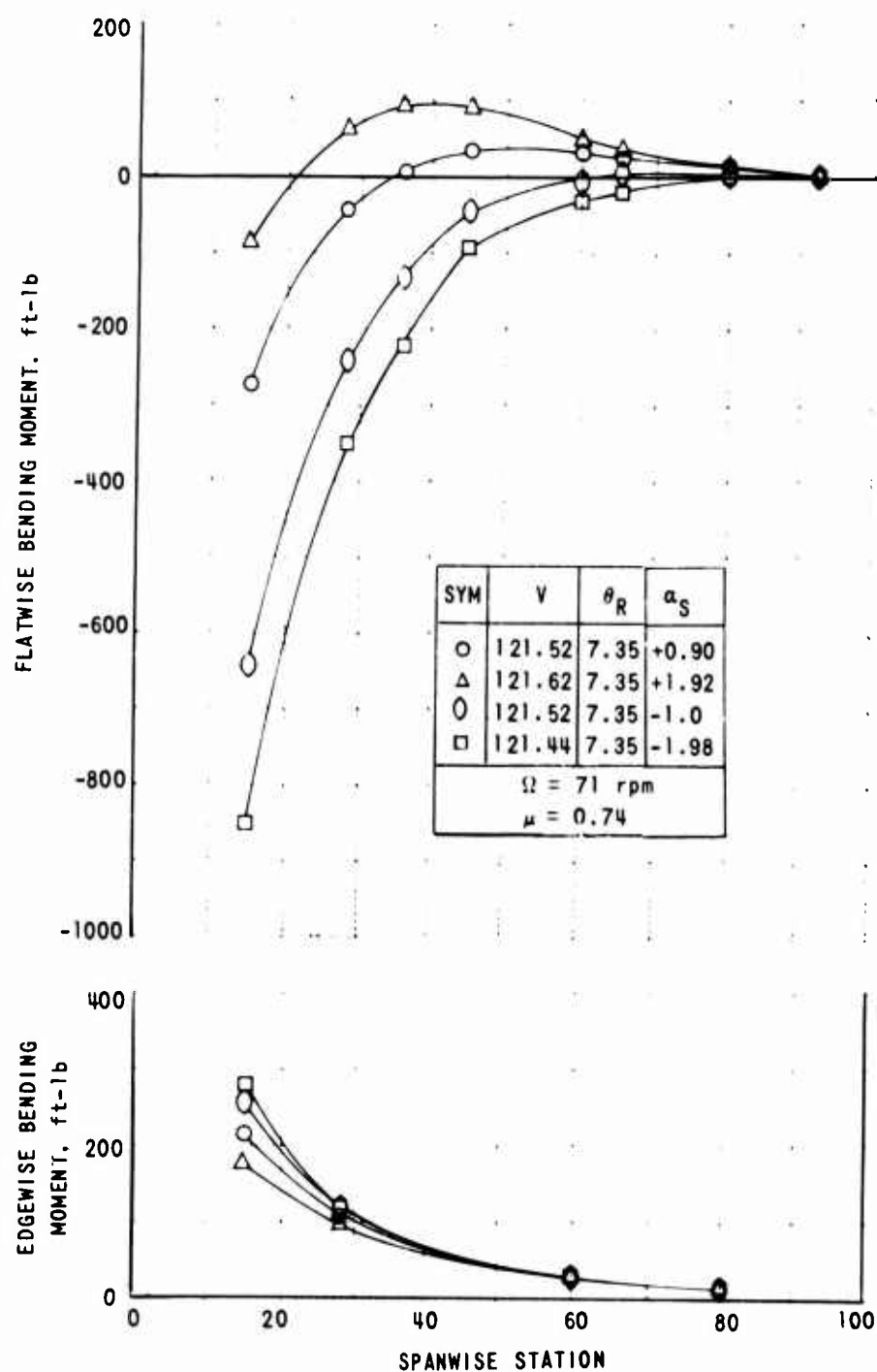
Figure 17. THE MEAN VALUES OF THE LOADS AND MOMENTS MEASURED ON THE ROTOR OPERATING AT V_f = 121.5 FPS AND Ω = 71 RPM — SHAFT ANGLE VARIATION.

67
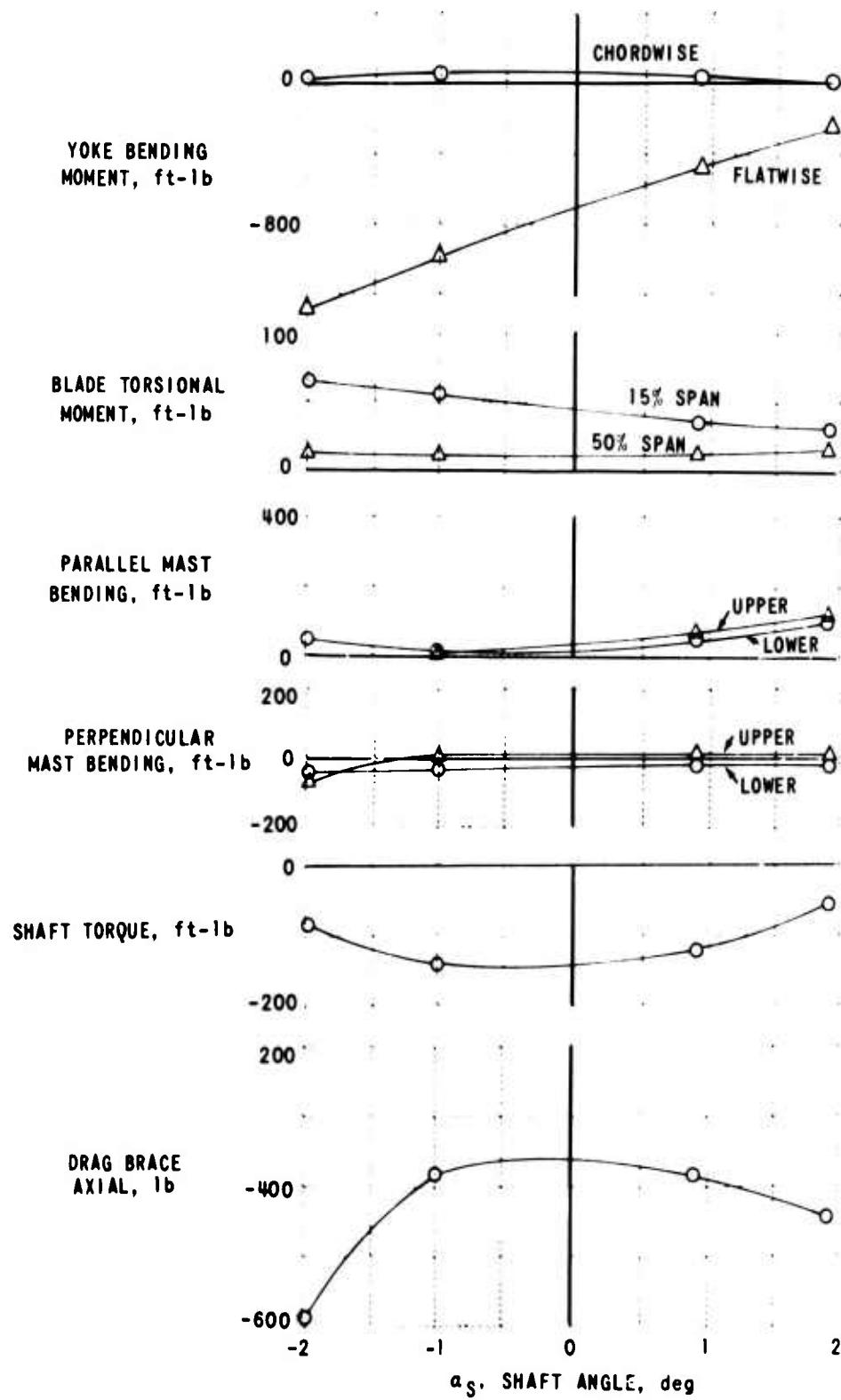
Figure 17. (Continued)

68
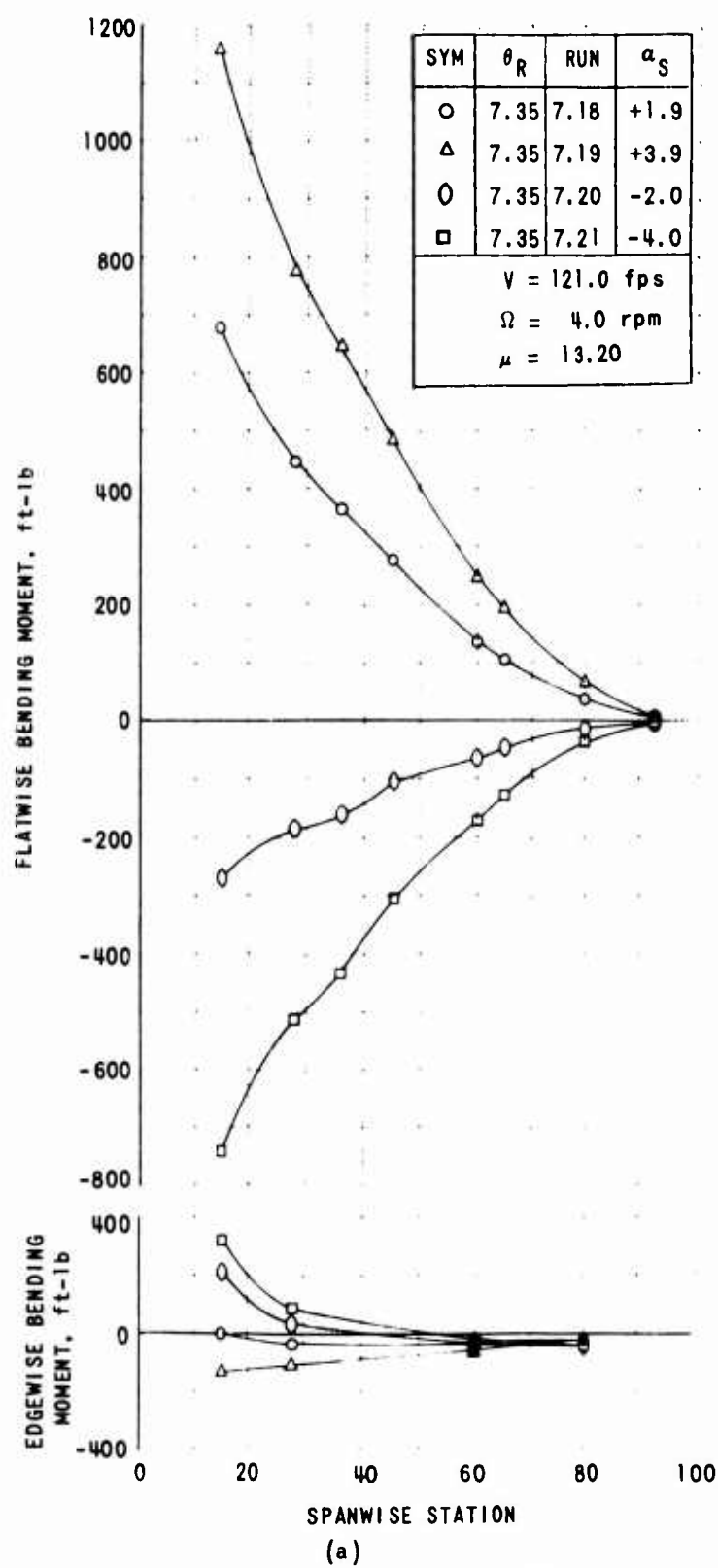
Figure 18. THE MEAN VALUES OF THE LOADS AND MOMENTS MEASURED ON THE
ROTOR OPERATING AT V_f = 121 FPS AND Ω = 4 RPM –
SHAFT ANGLE VARIATION.

69
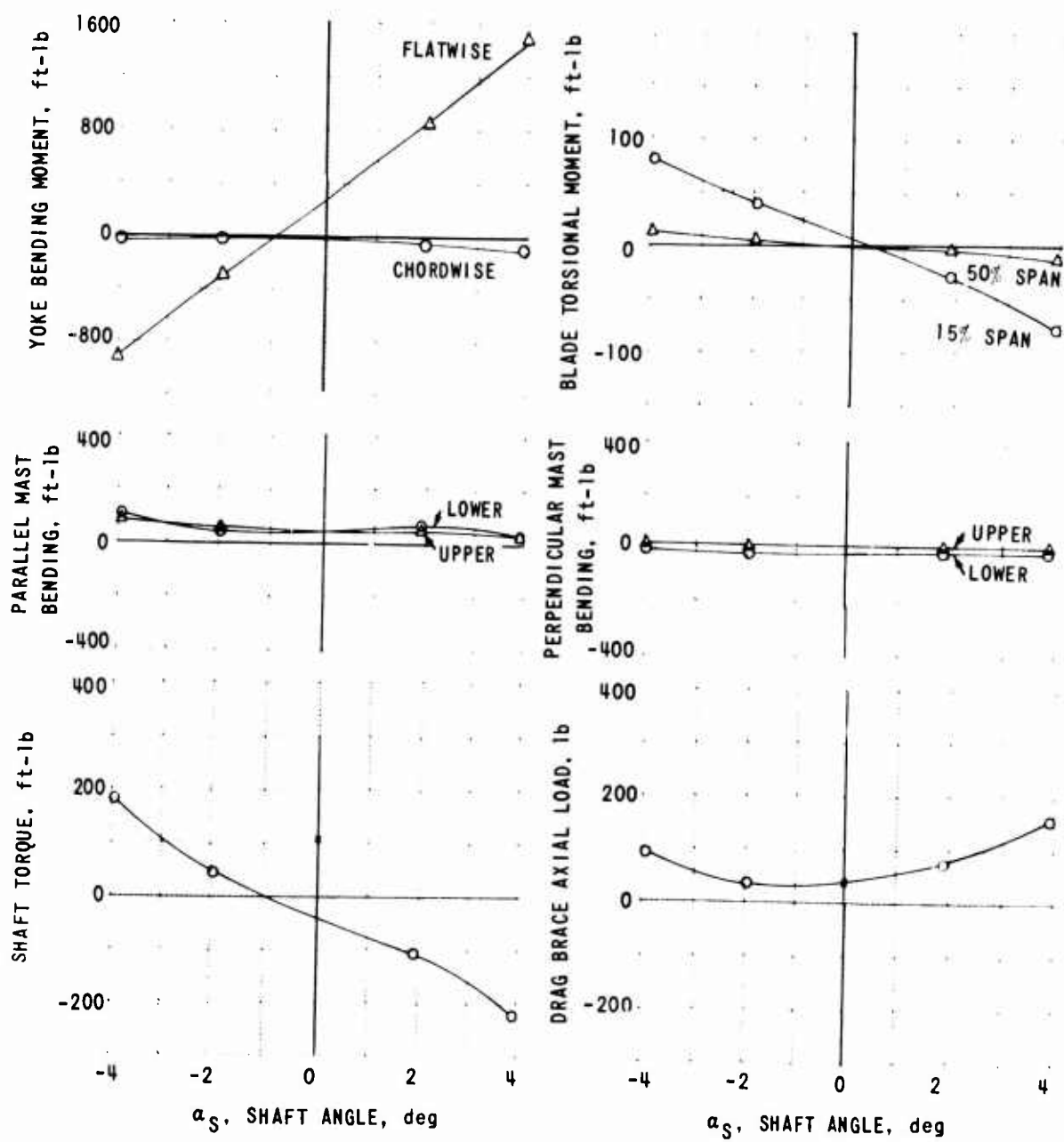
(b)

Figure 18. (Continued)
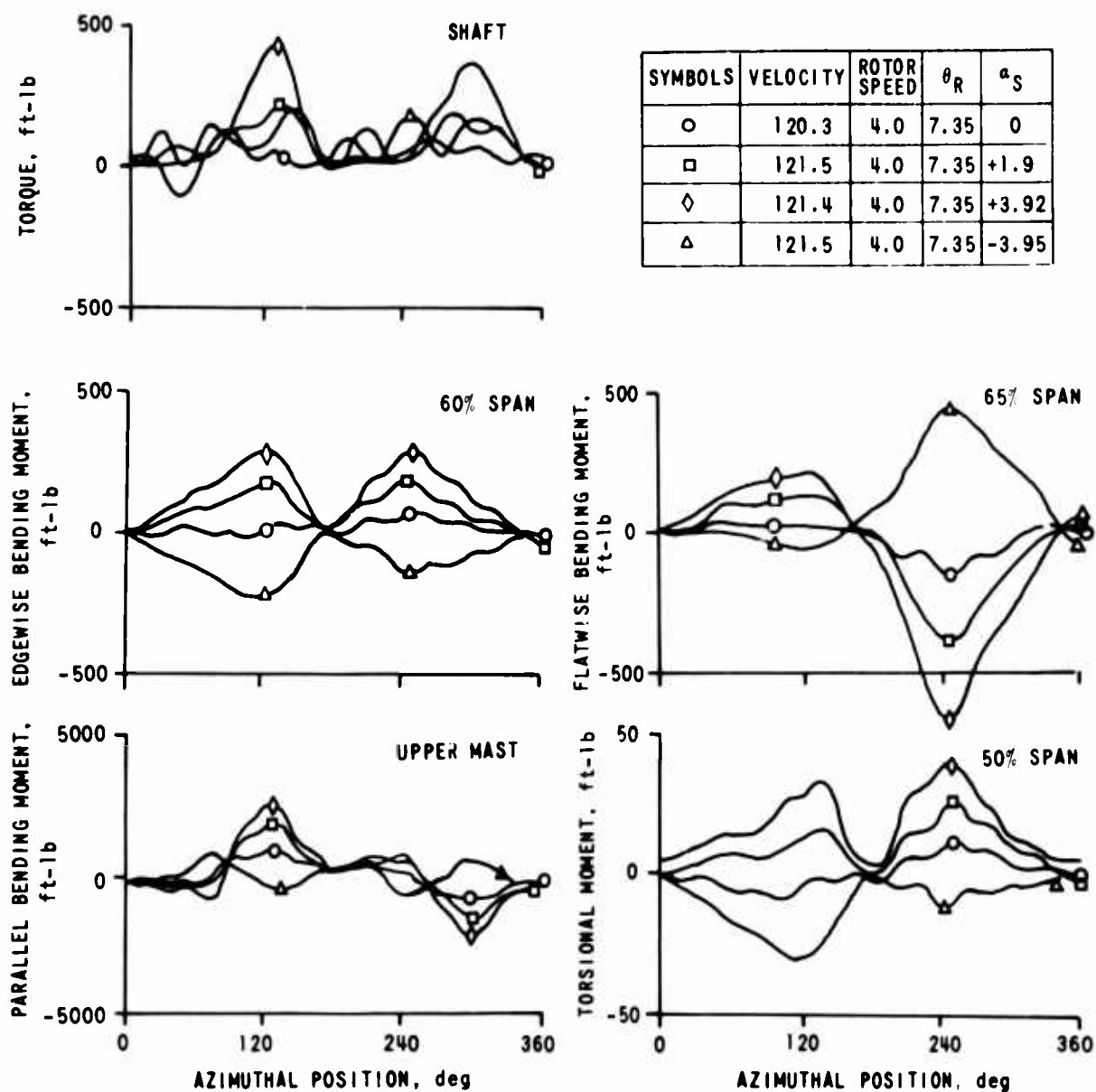
Figure 19. AZIMUTHAL VARIATION OF SELECTED MOMENTS MEASURED ON THE
ROTOR OPERATING AT V_f = 120.3 FPS, Ω = 4.0 RPM, θ_R = 7.35 DEG -
SHAFT ANGLE VARIATION.

71

SYMBOLS	VELOCITY	ROTOR SPEED	θ_R
O	120.29	4.0	7.35°
△	120.29	4.0	8.85°
◊	120.29	4.0	9.85°
□	120.29	4.0	10.90°
⌂	120.29	4.0	5.85°
◊	120.29	4.0	4.90°
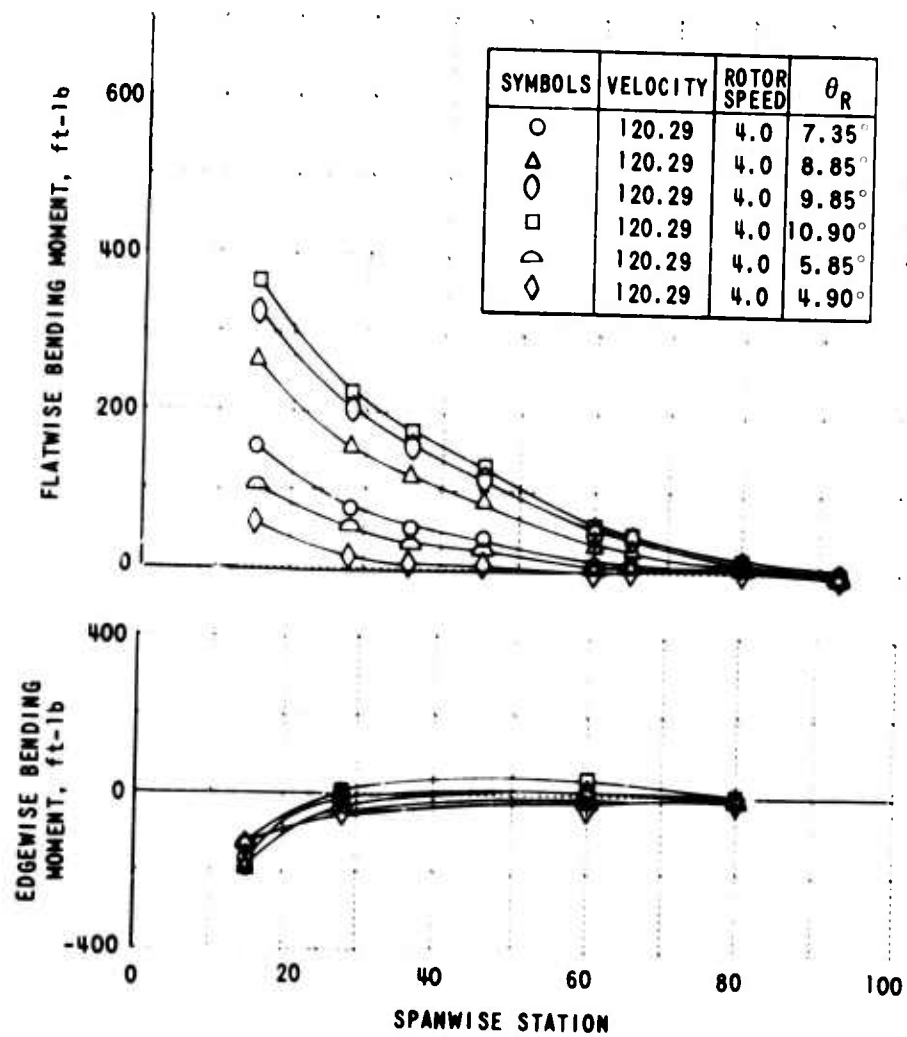
(a)

Figure 20. THE MEAN VALUES OF THE LOADS AND MOMENTS MEASURED ON THE ROTOR OPERATING AT V_f = 120.3 FPS AND Ω = 4.0 RPM – COLLECTIVE ANGLE VARIATION.

72
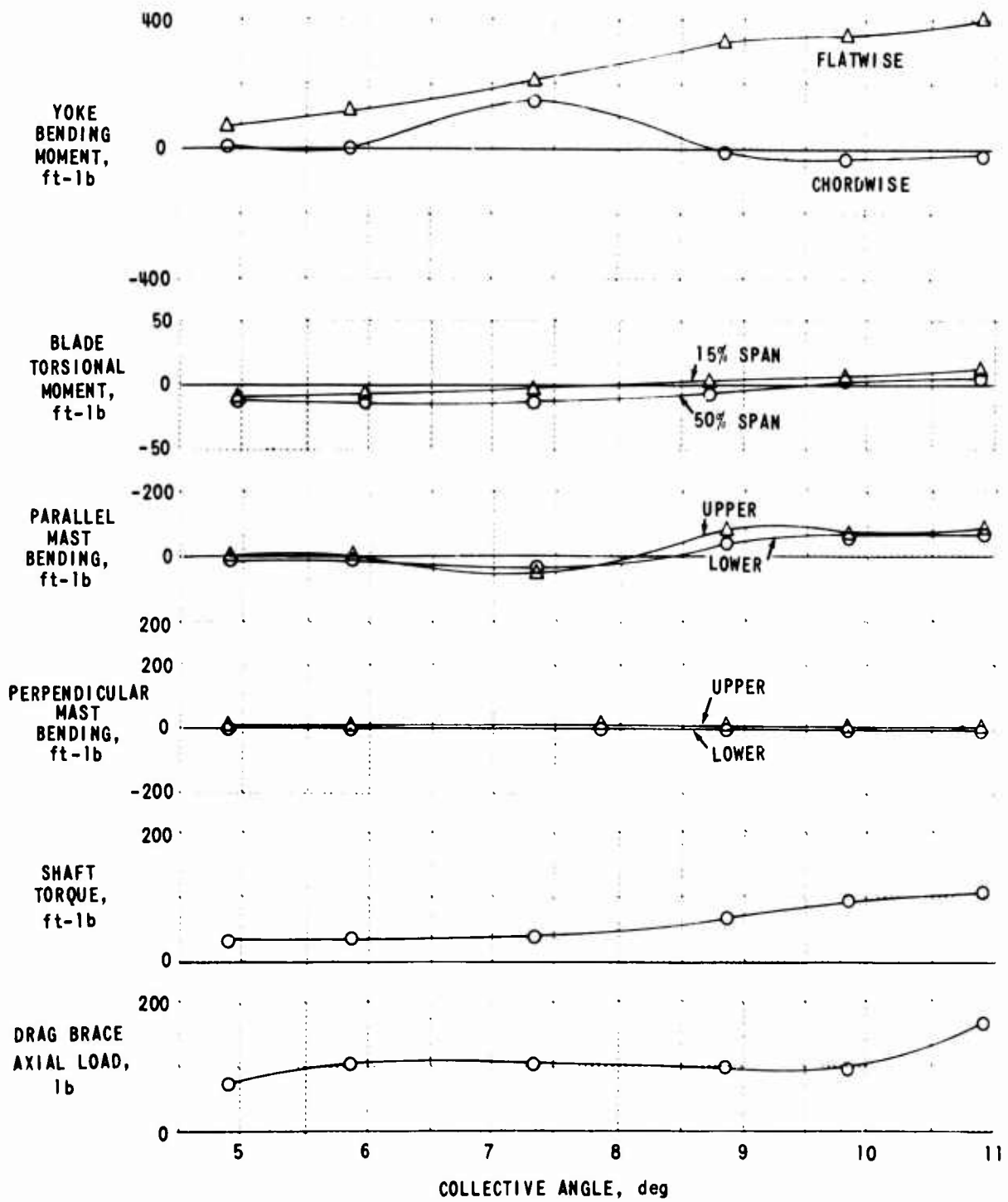
(b)

Figure 20. (Continued)

73
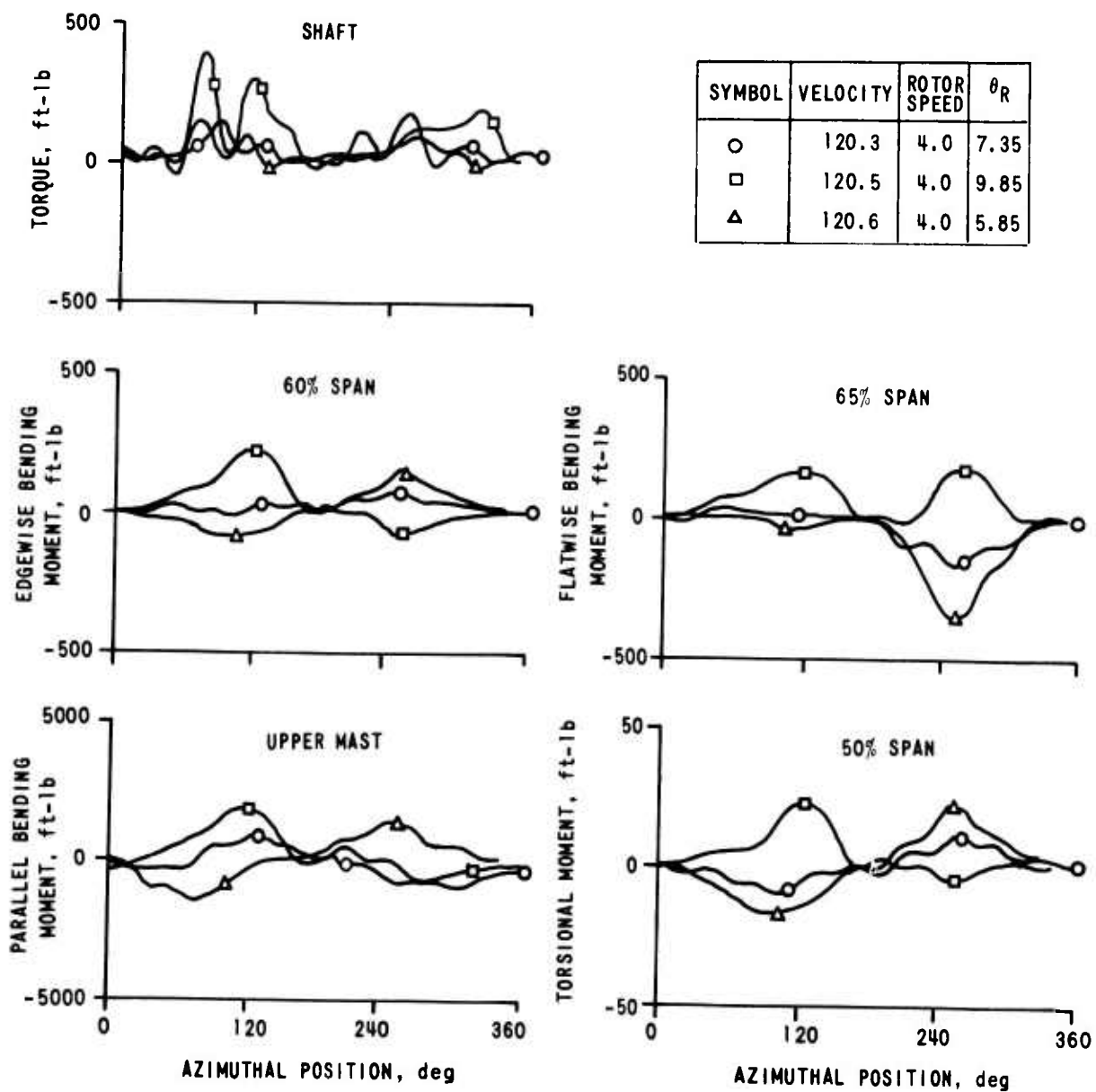
Figure 21. AZIMUTHAL VARIATION OF SELECTED MOMENTS MEASURED ON
THE ROTOR OPERATING AT V_f = 120.3 FPS, Ω = 4.0 RPM -
COLLECTIVE ANGLE VARIATION.

SYMBOL	VELOCITY	ROTOR SPEED	θ_R	α_S	θ_{1S}
○	121.1	4.0	7.35	0	-4.25
□	121.5	4.0	7.35	-3.95	0
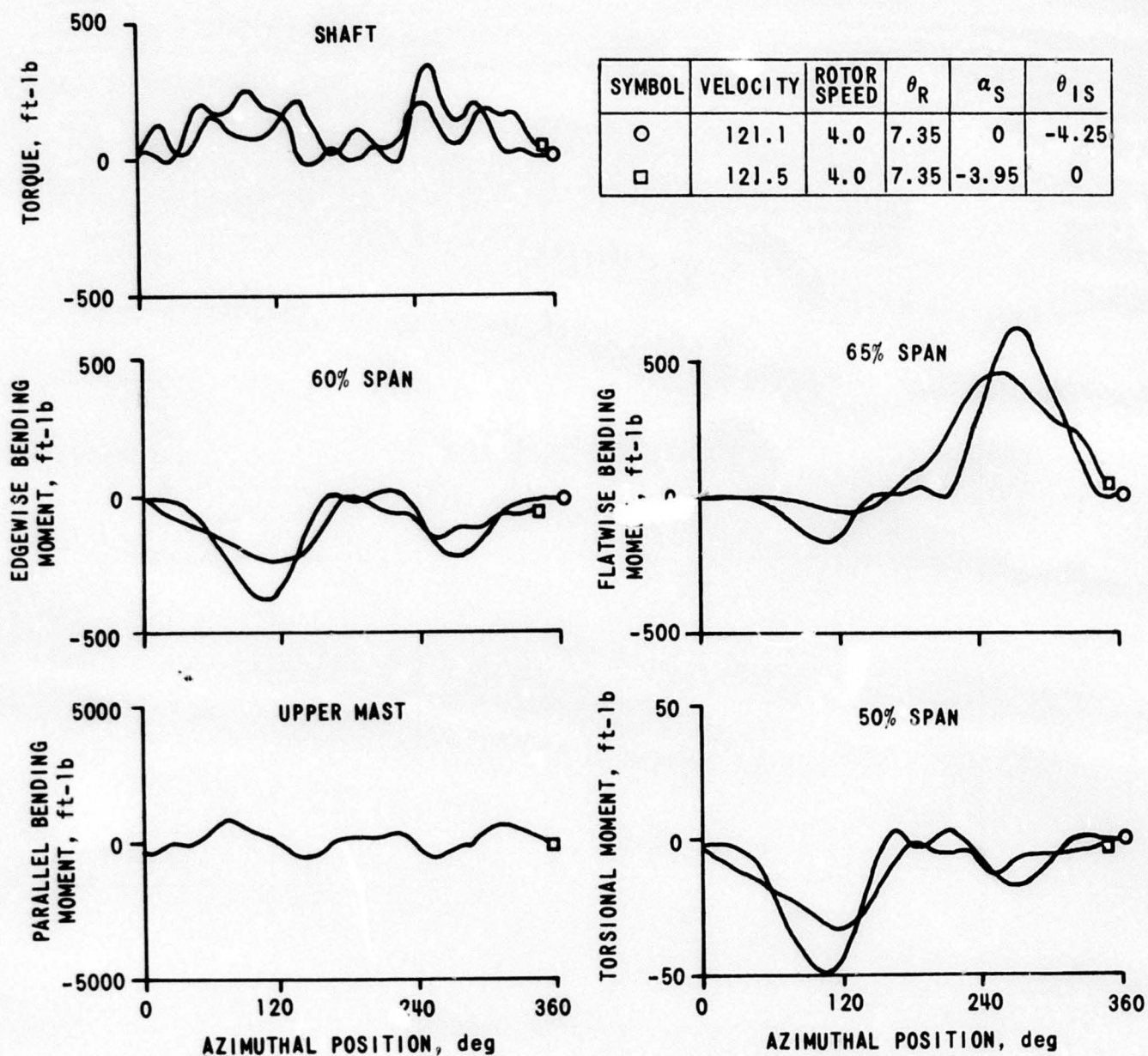
Figure 22. COMPARISON OF THE AZIMUTHAL VARIATION OF SELECTED MOMENTS MEASURED ON THE ROTOR OPERATING AT V_f = 121.5 FPS AND Ω = 4.0 RPM FOR TWO VALUES OF α_S AND TWO VALUES OF θ_{1S}.
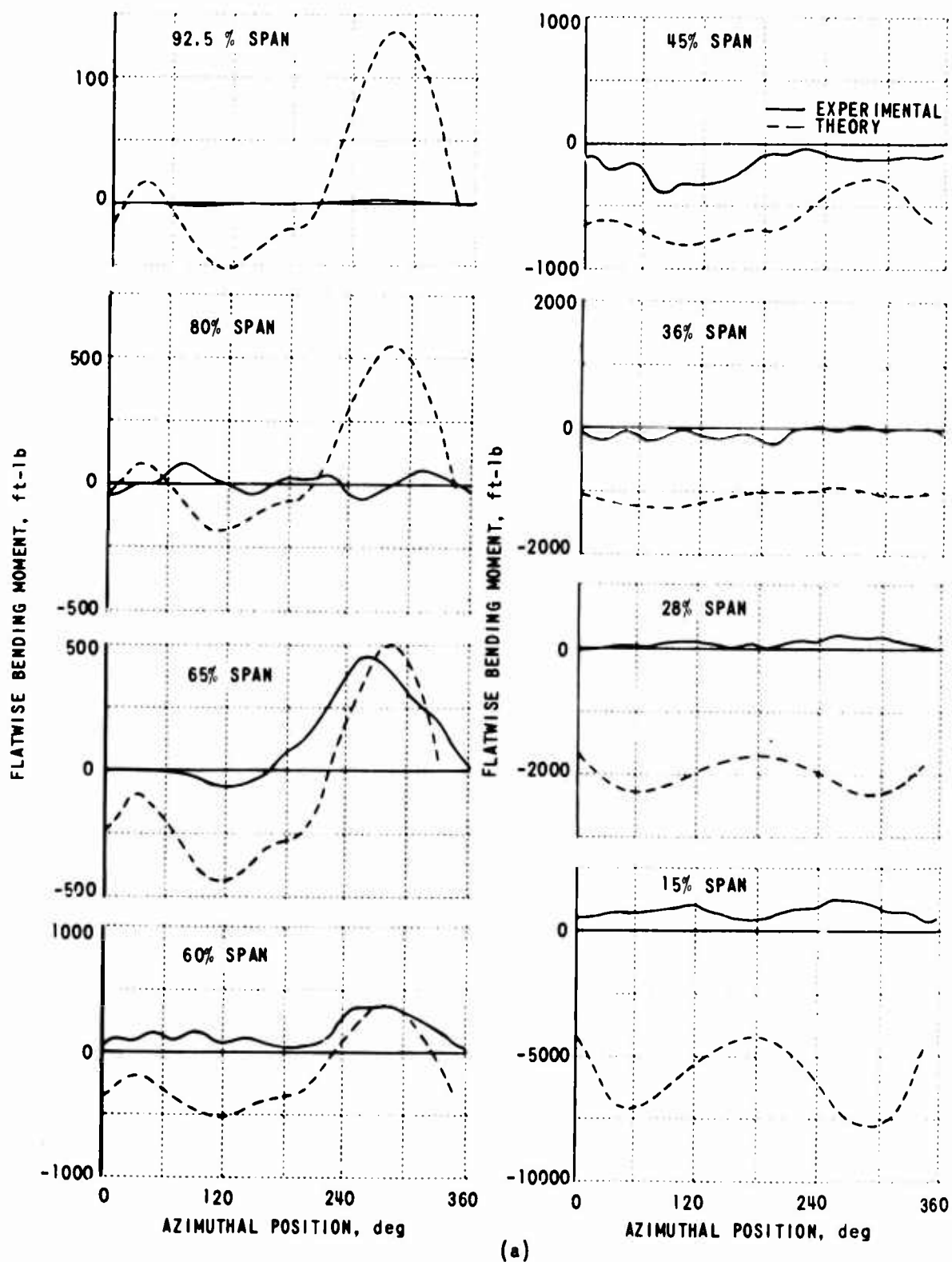
Figure 23. COMPARISON OF THEORY AND EXPERIMENT FOR A ROTOR
OPERATING AT V_f = 121.5 FPS, Ω = 7.35 RPM,
θ_R = 7.35 DEG, α_S = -3.95 DEG, AND θ_{1C} = θ_{1S} = 0.

76
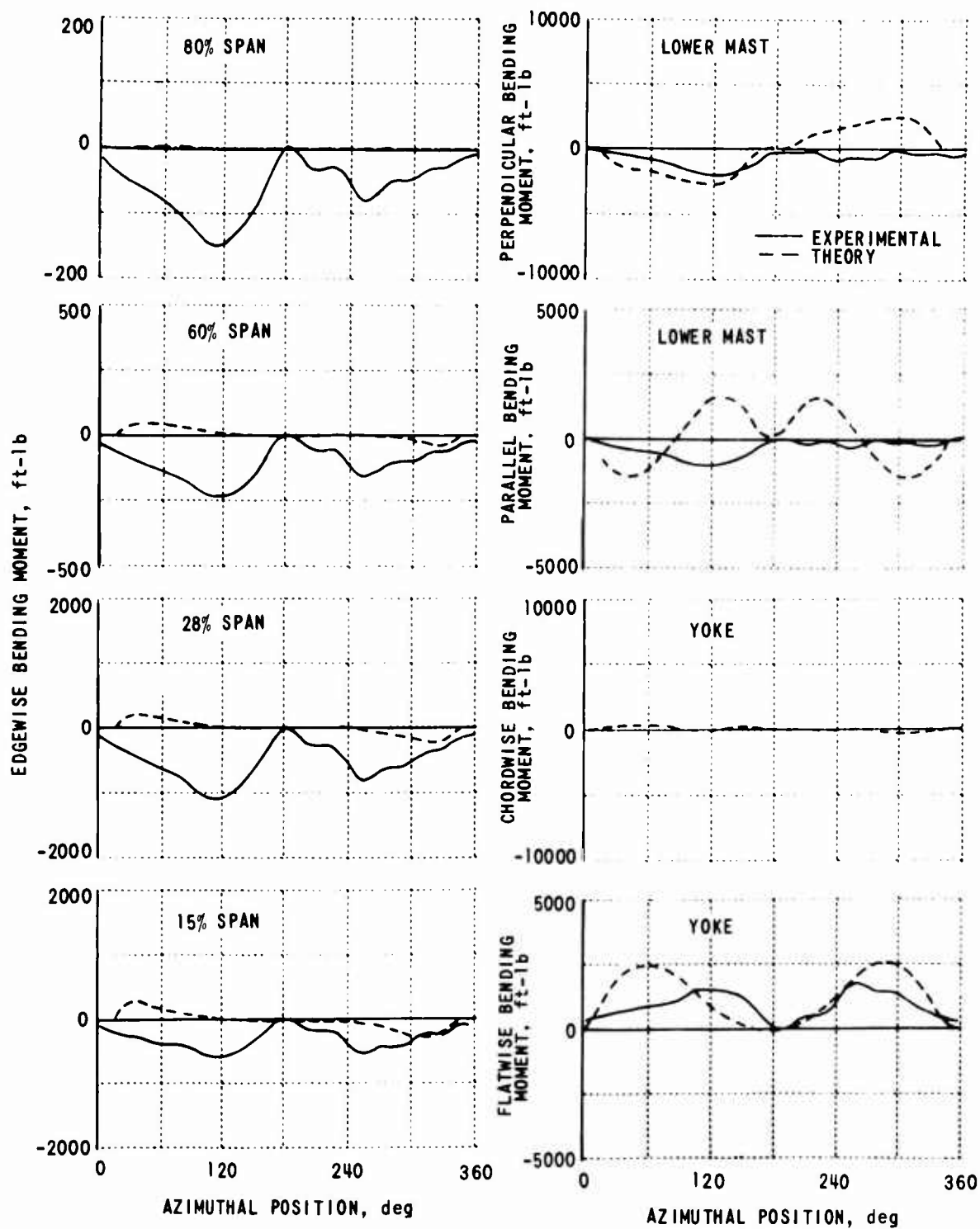
Figure 23. (Continued)
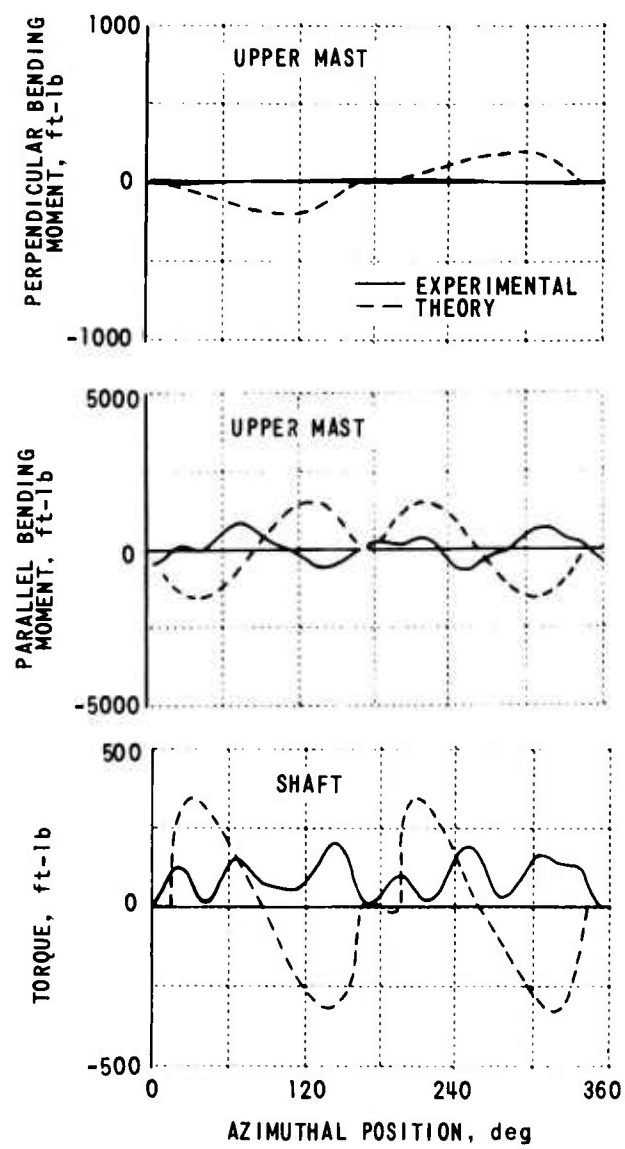
(c)

Figure 23. (Continued)

78
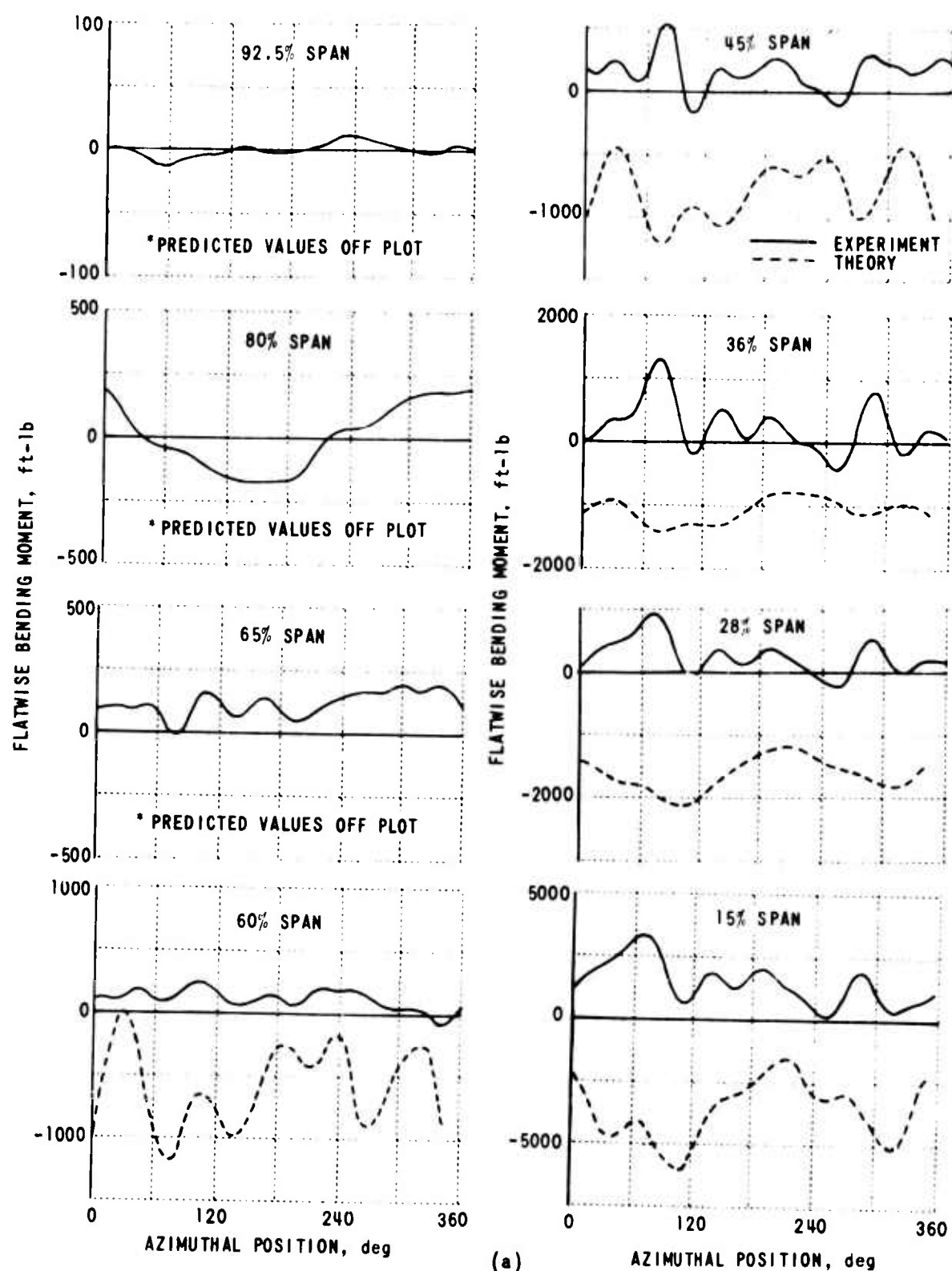
Figure 24. COMPARISON OF THEORY AND EXPERIMENT FOR A ROTOR OPERATING AT V_f = 121.4 FPS, Ω = 71.1 RPM, θ_R = 7.35 DEG, α_S = -1.98 DEG, AND θ_{1C} = θ_{1S} = 0.

79
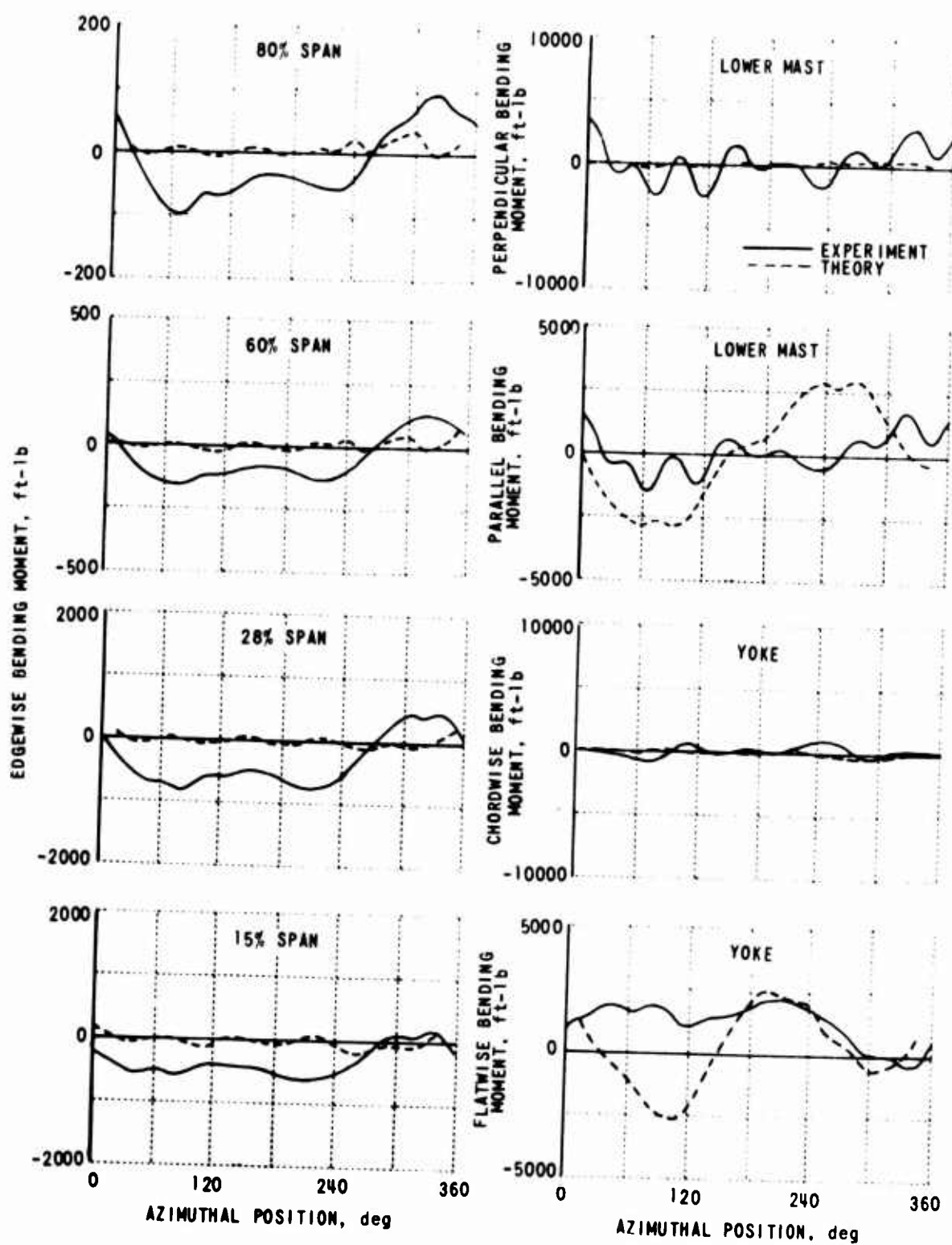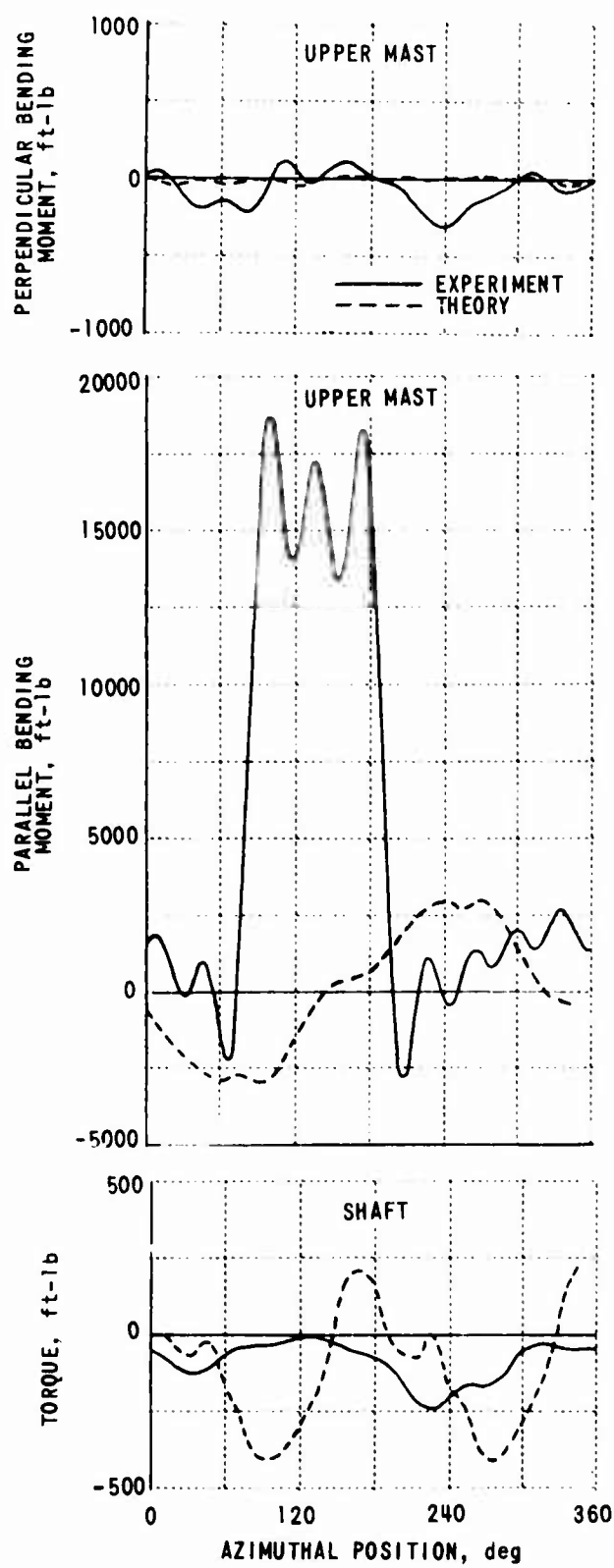
Figure 24. (Continued)

Figure 24. (Continued)

81
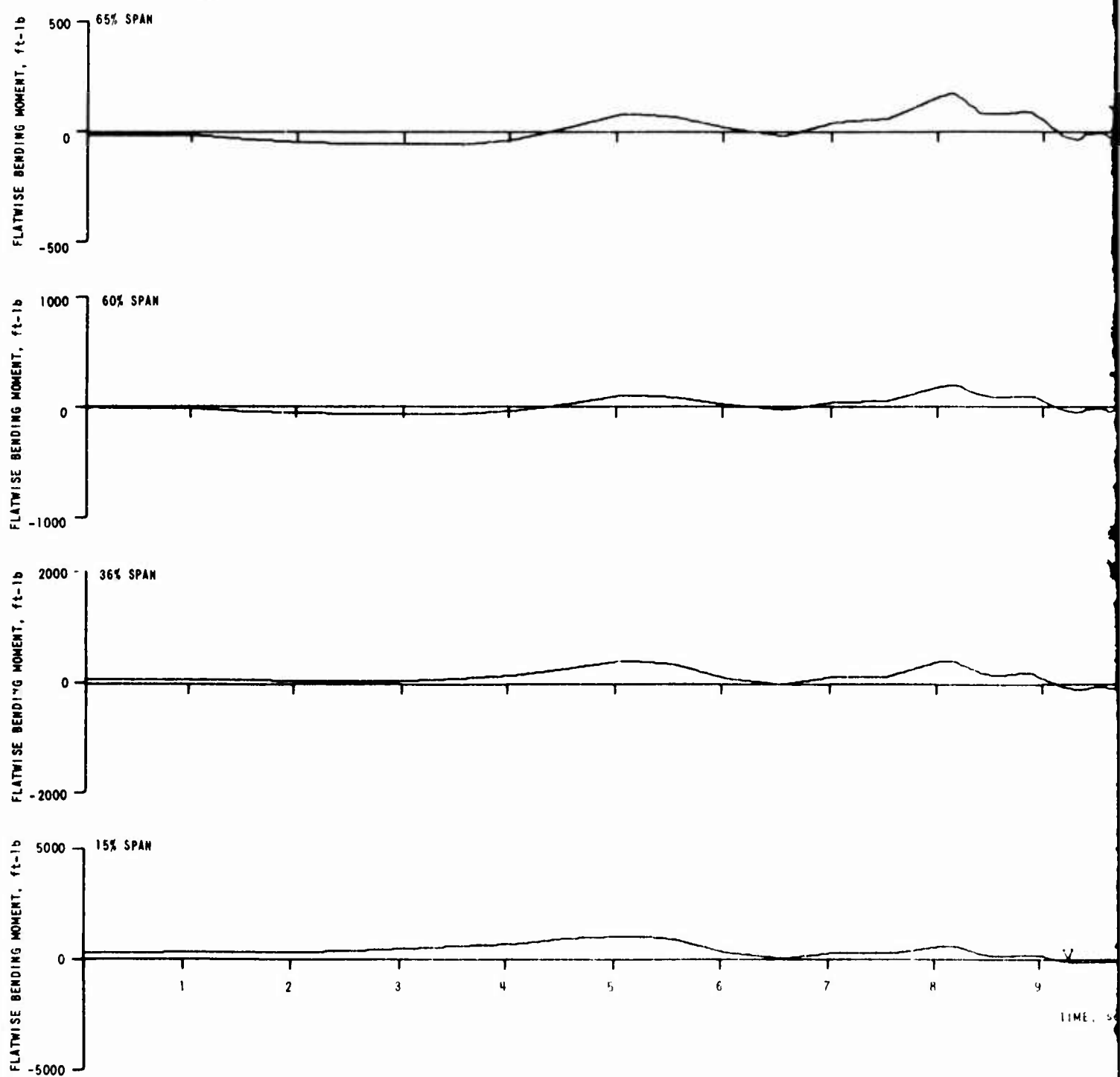
Figure 25. TIME HISTORY OF DATA COLLECTED FROM A ROTOR BEING ACCELERATED TO THE FOLLOWING OPERATING CONDITIONS: VF = 140.6, OMEGA = 71.07, THETR = 7.35, THETIC = 0.00, THETIS = 0.00, ALPHS = 0.00.
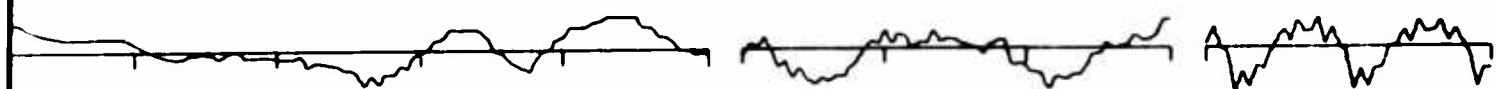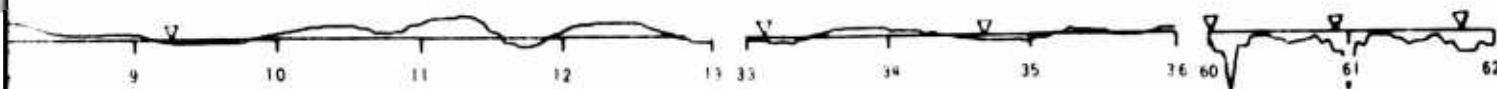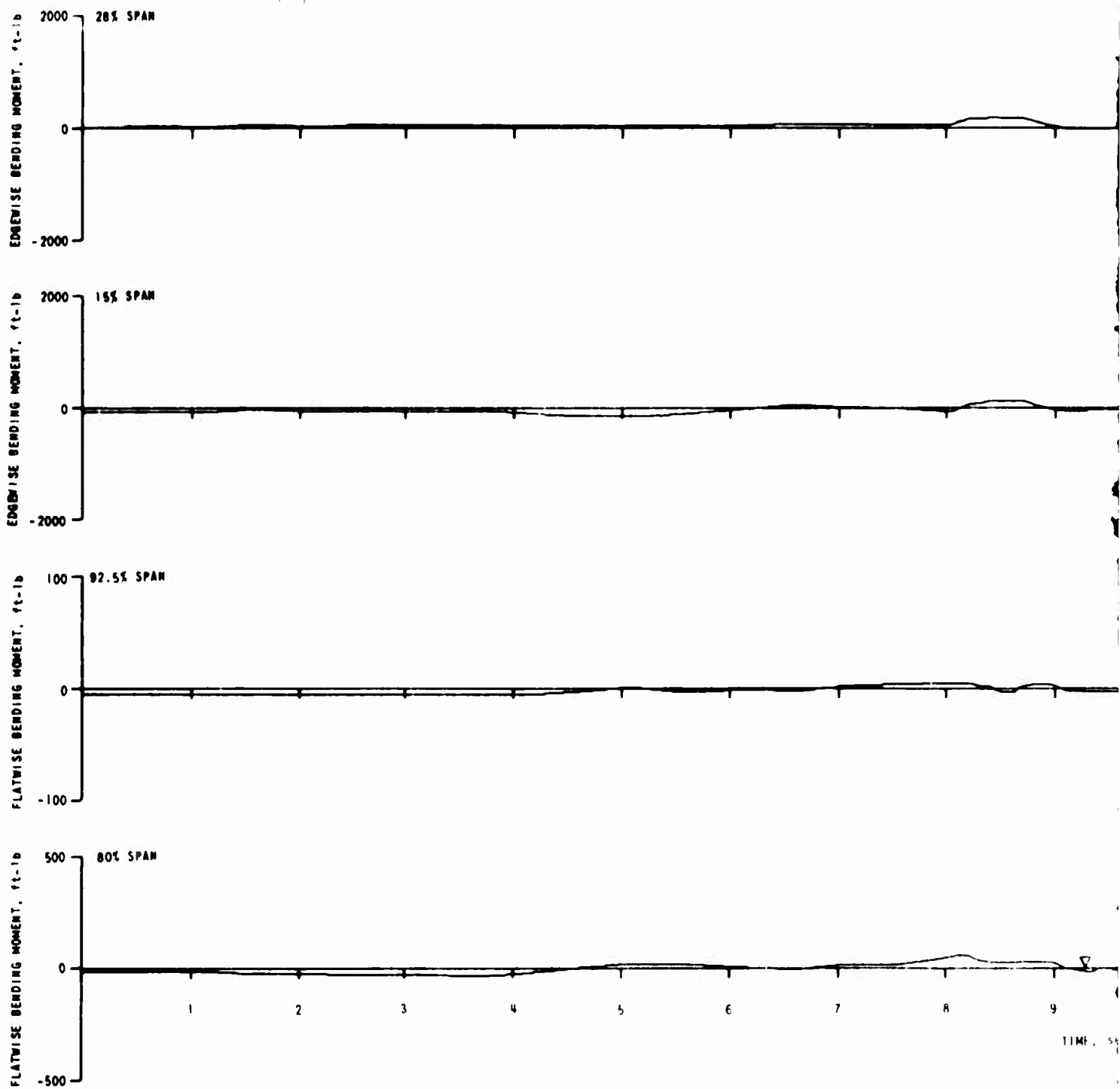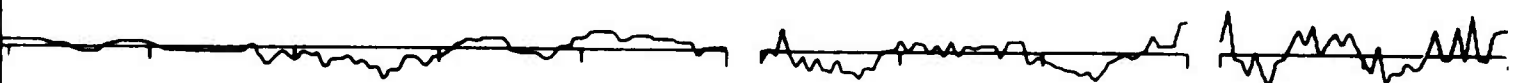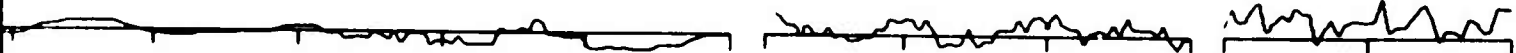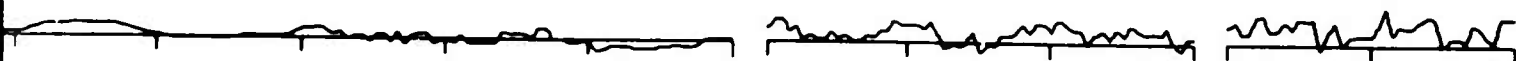
83

∇ RPM INDICATOR

TIME, sec

Figure 25. (Continued)

85

∇ RPM INDICATOR

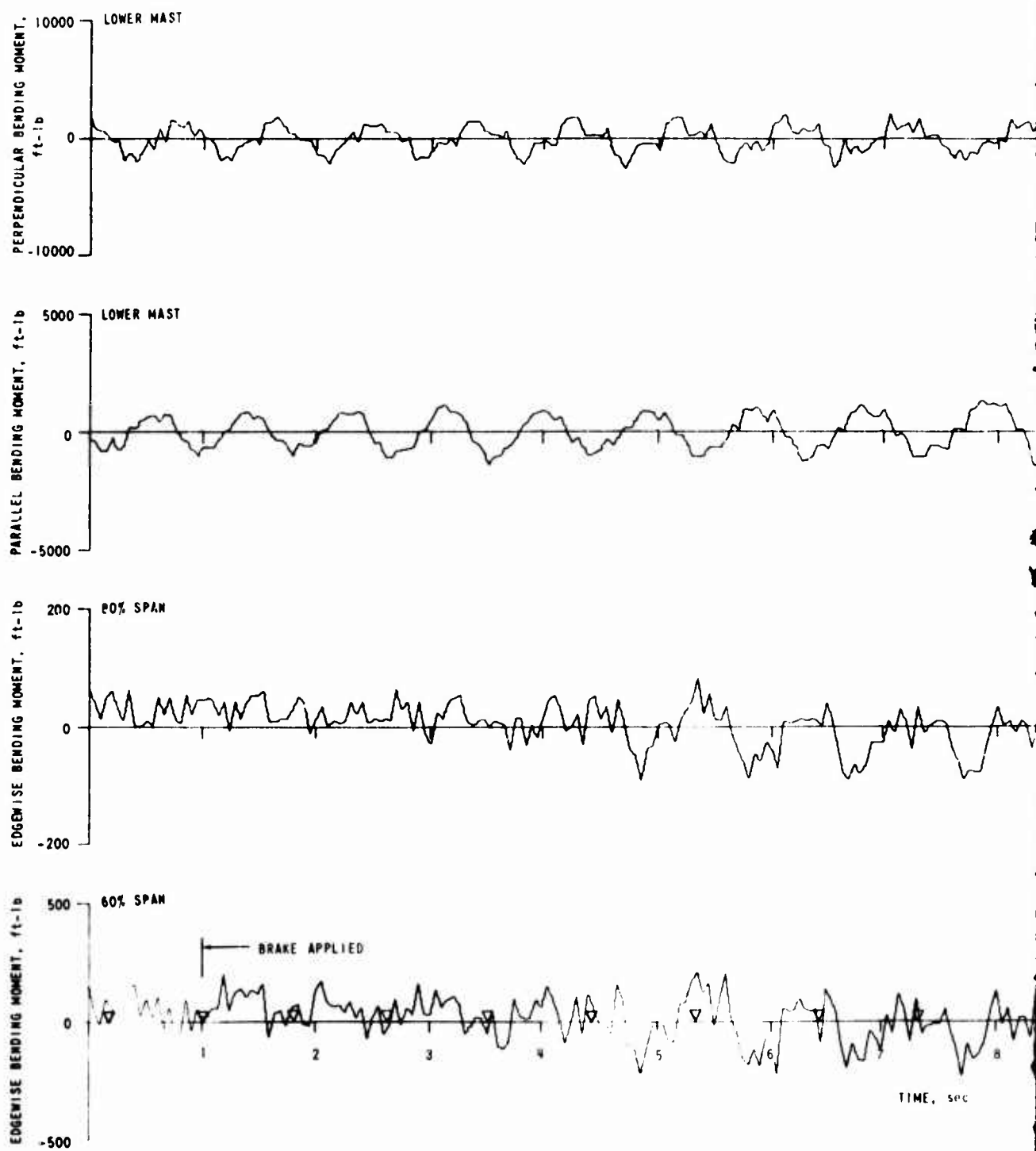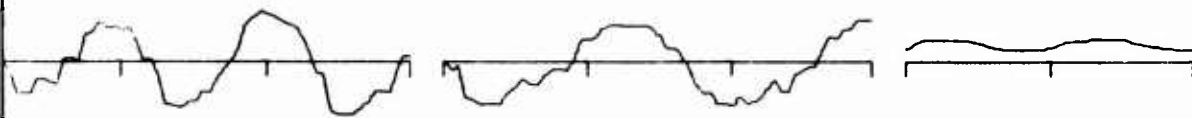9   10   11   12   13 33   34   35   36 60   61   62
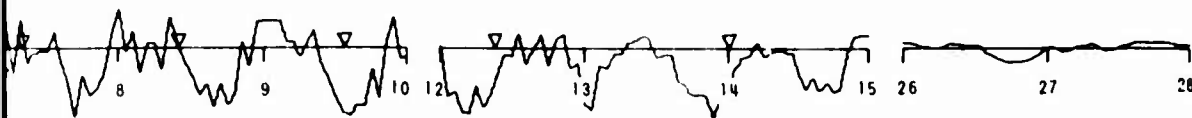
TIME, sec

Figure 25. (Continued)

87

∇ RPM INDICATOR

TIME, sec

Figure 25. (Continued)
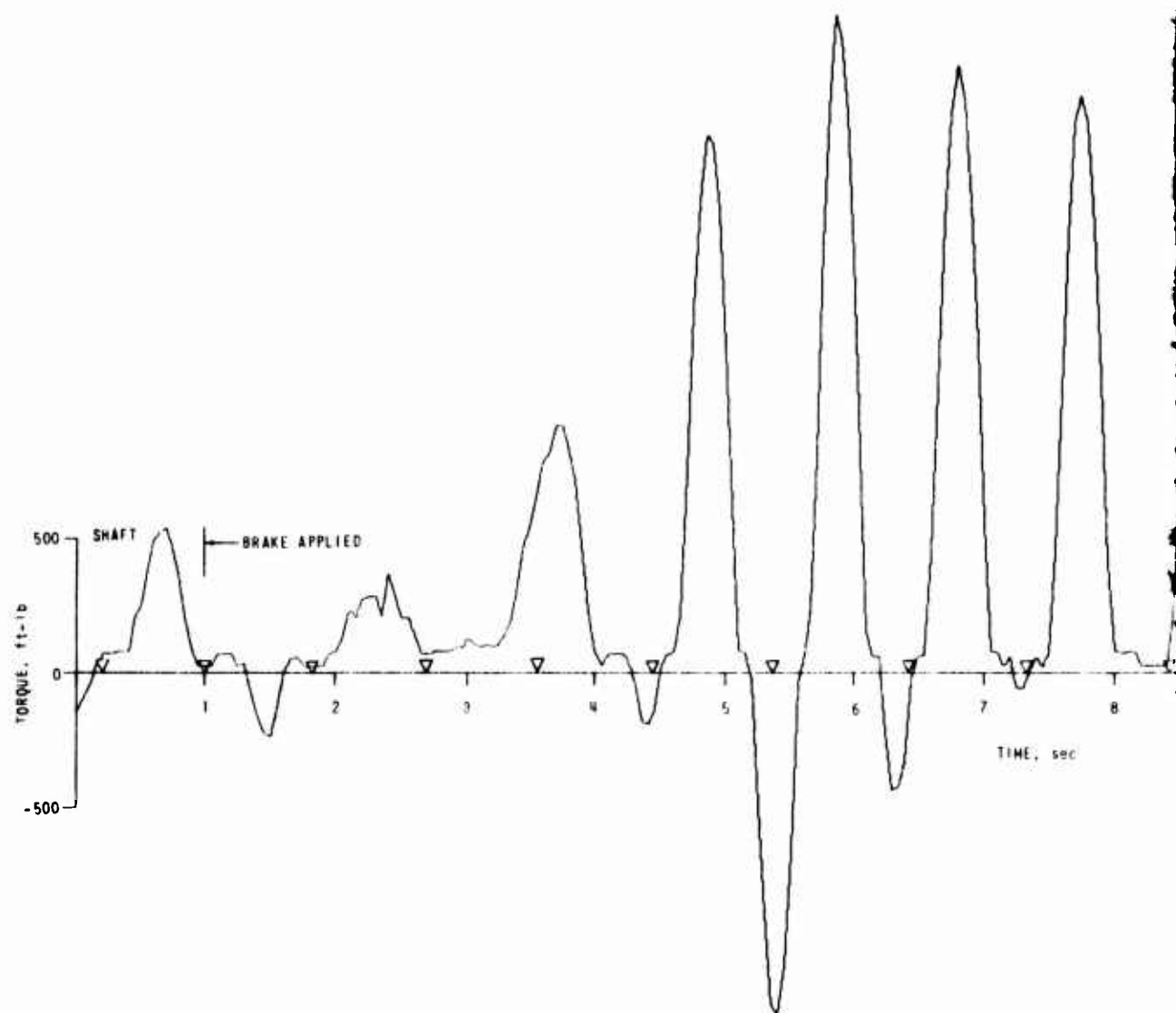
89

∇ RPM INDICATOR

TIME, sec

Figure 25. (Continued)

91

∇ RPM INDICATOR

TIME, sec

Figure 25. (Continued)

93

∇ RPM INDICATOR

TIME, sec

Figure 25. (Continued)

95
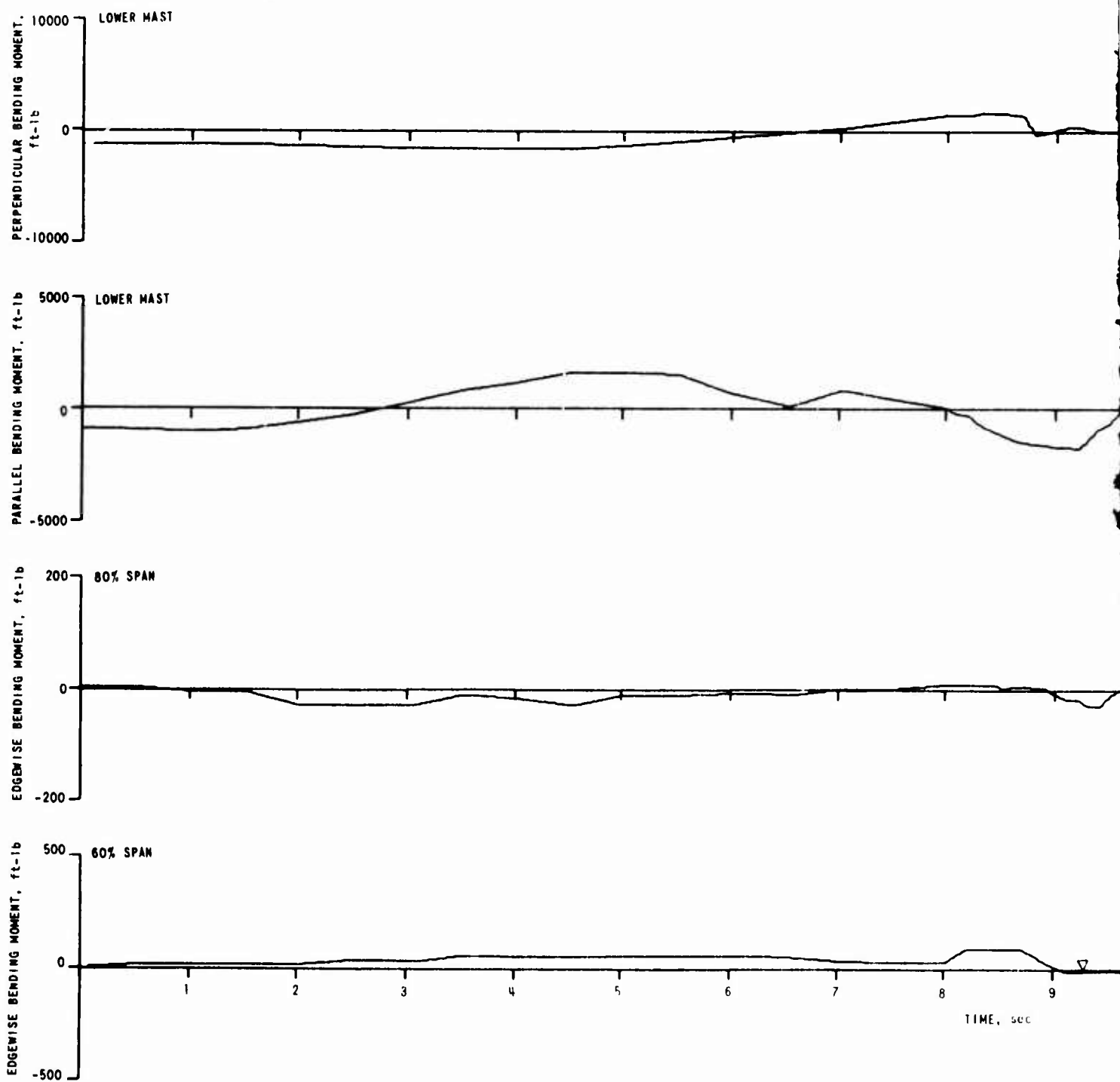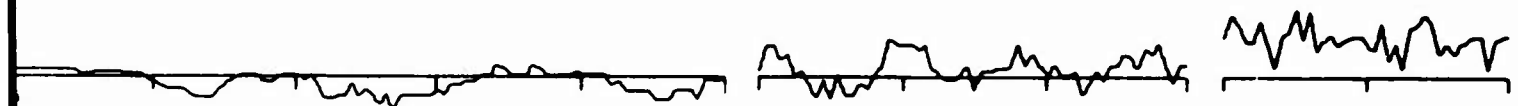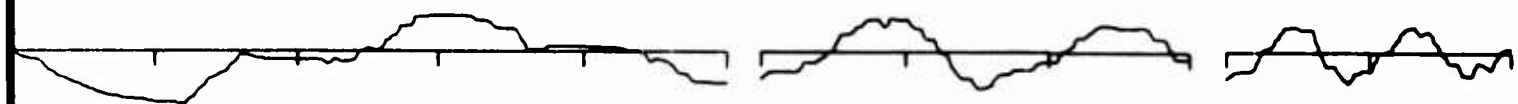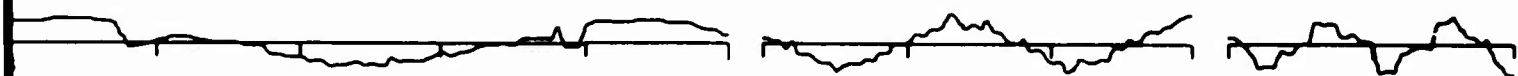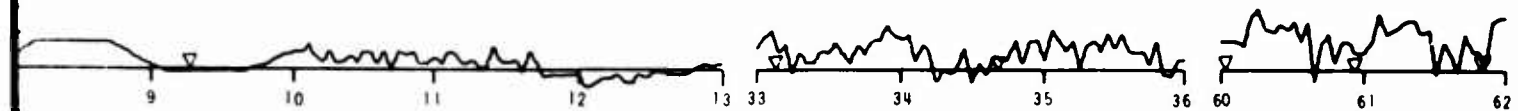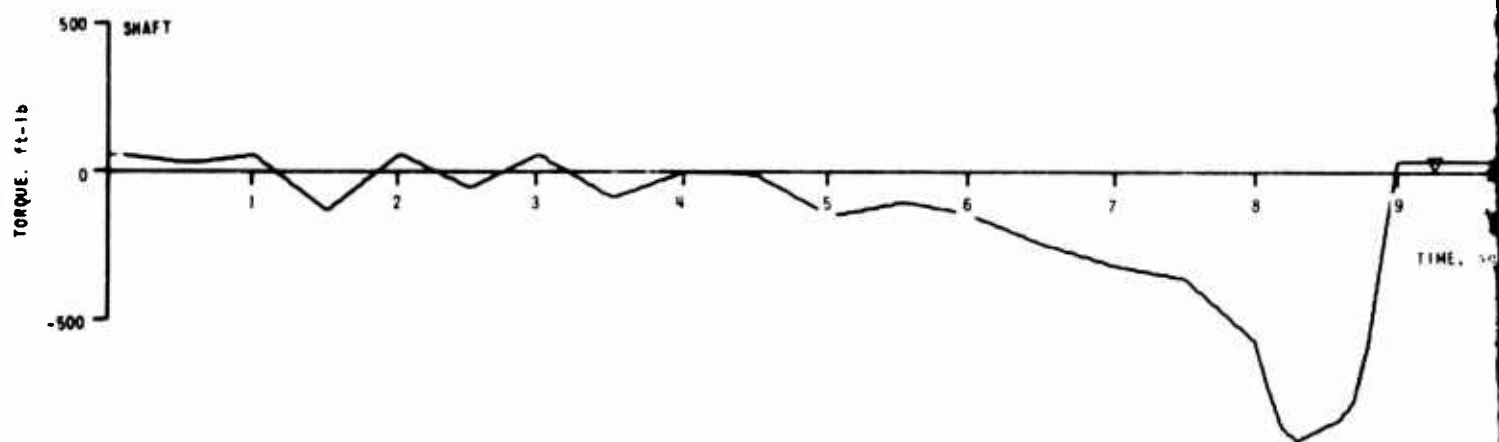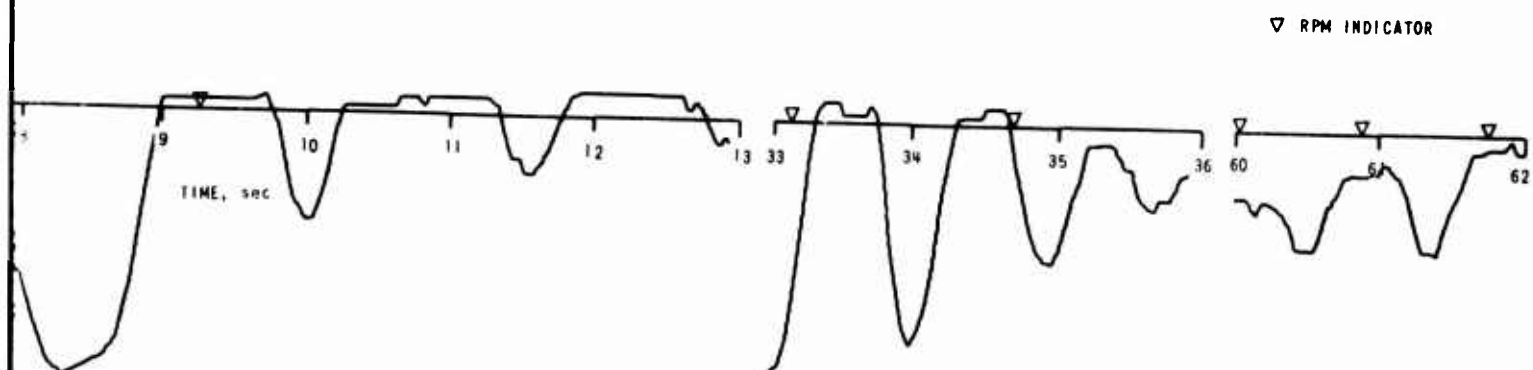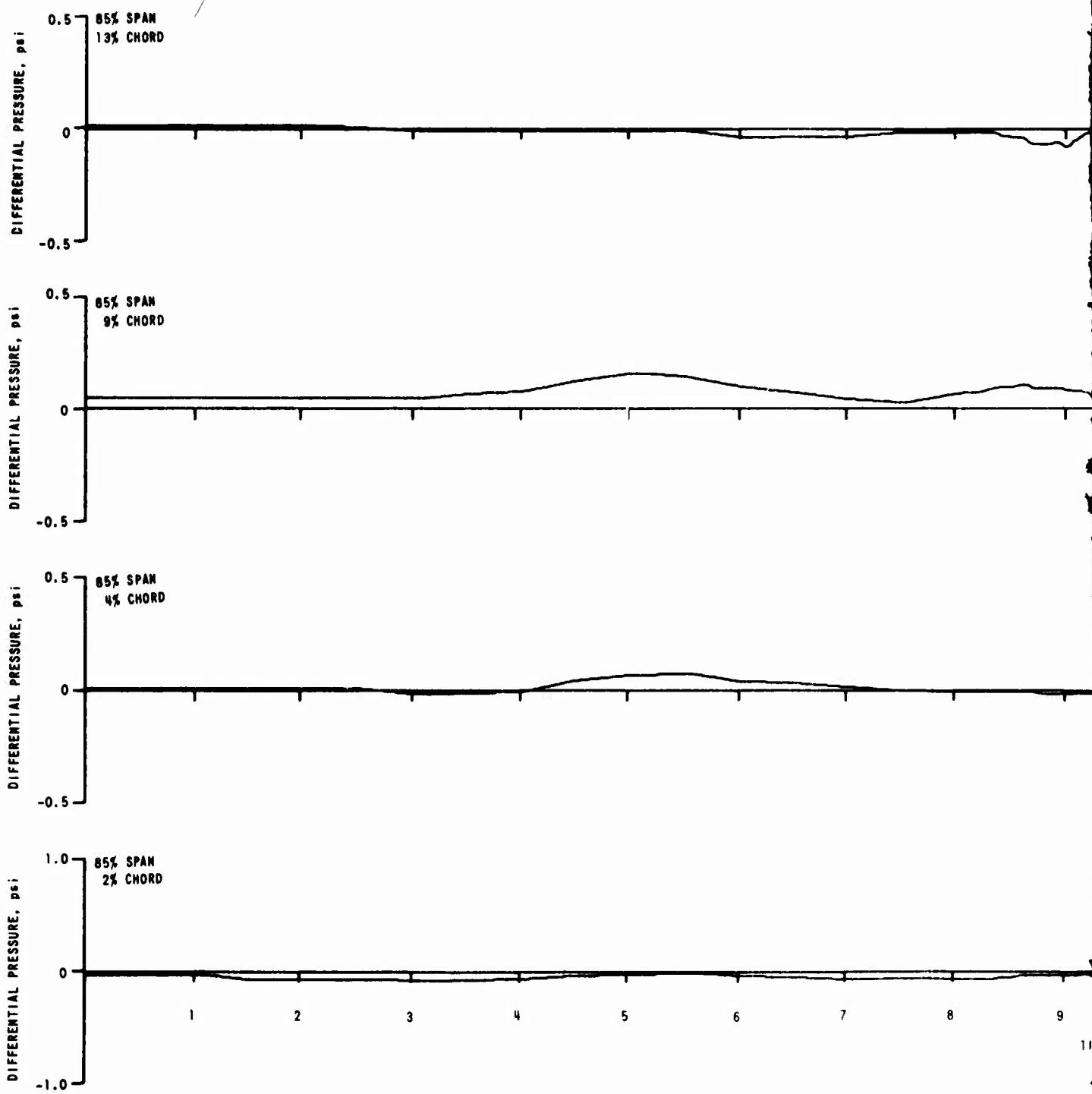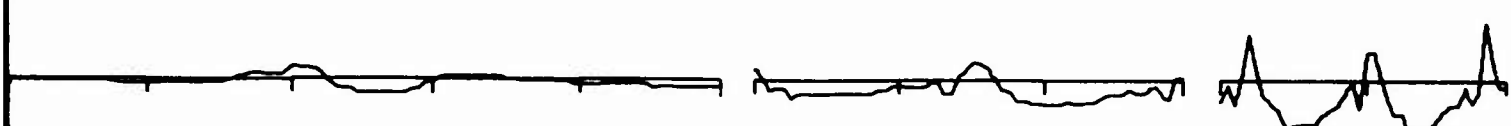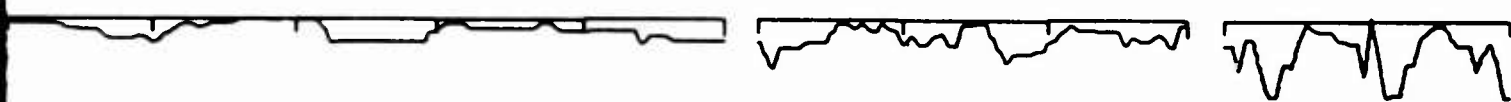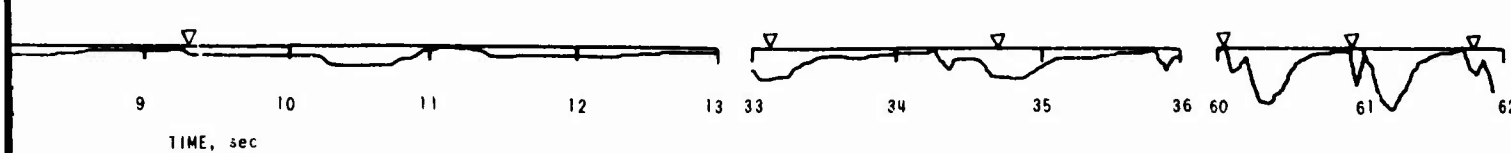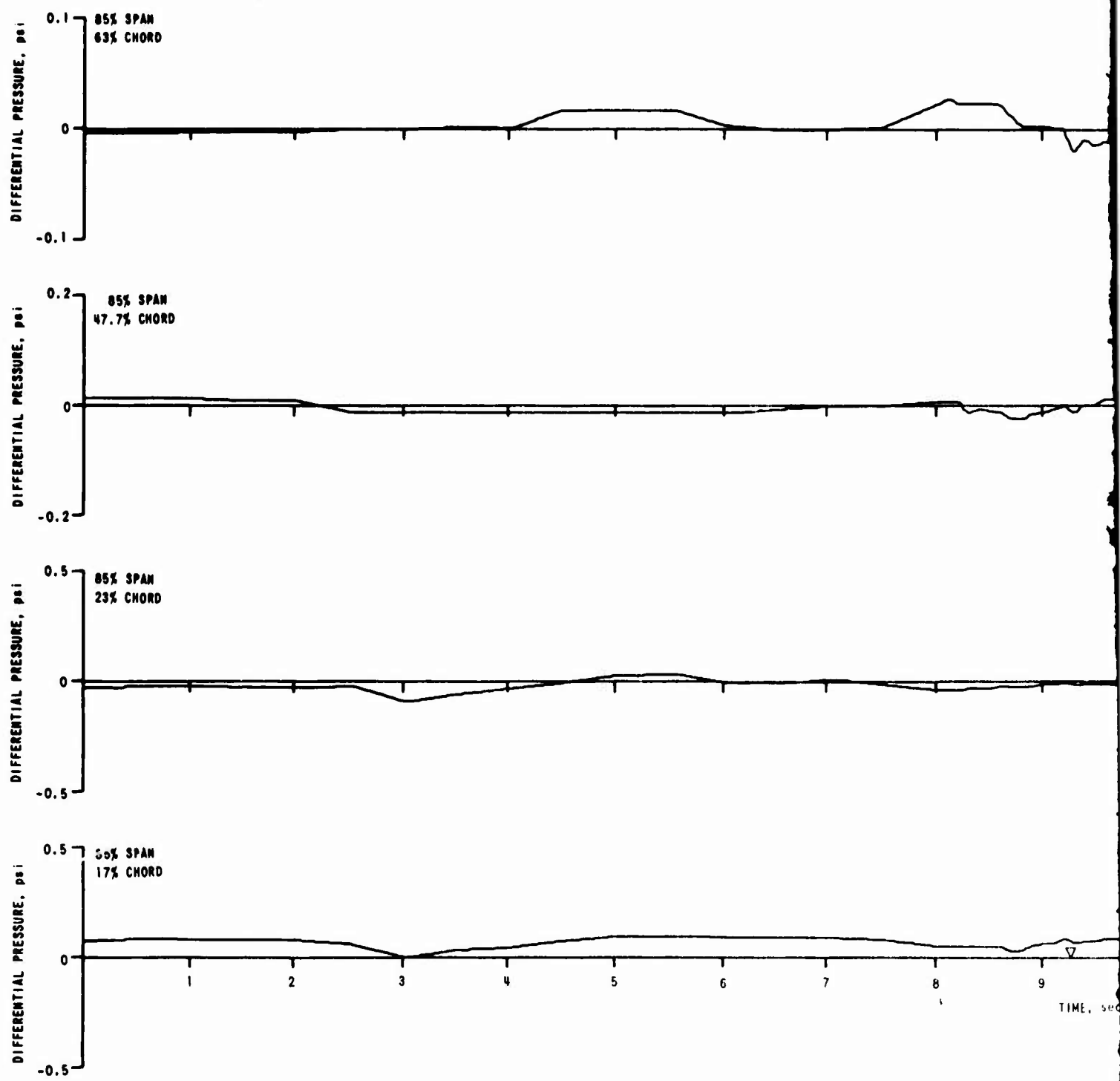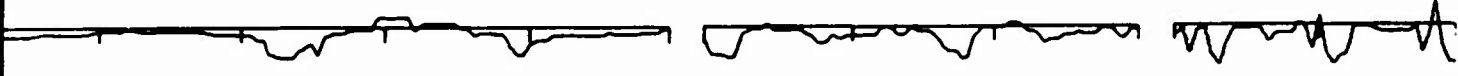
∇ RPM INDICATOR

TIME, sec

9   10   11   12   13   33   34   35   36   60   61   62
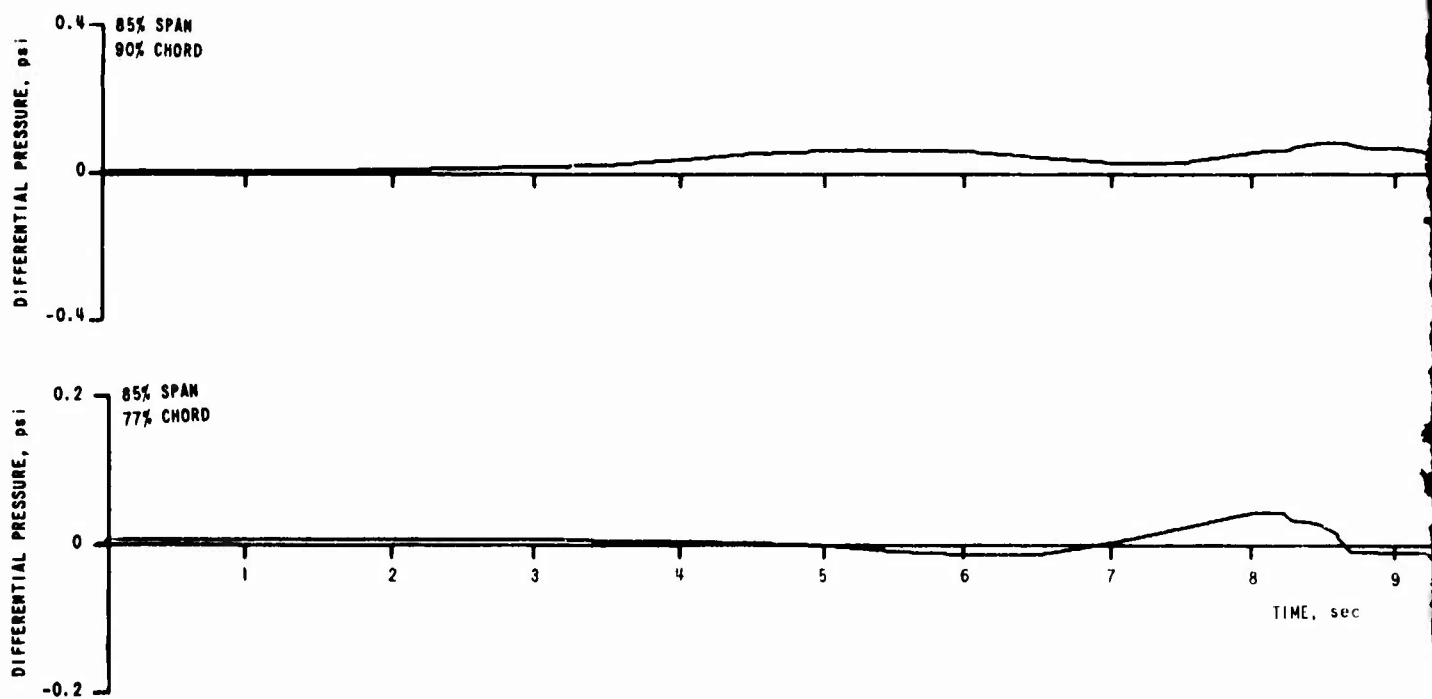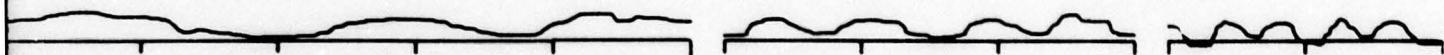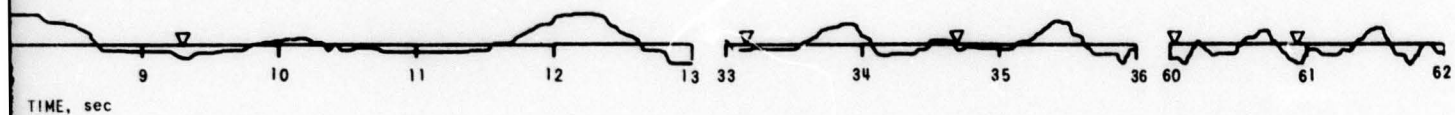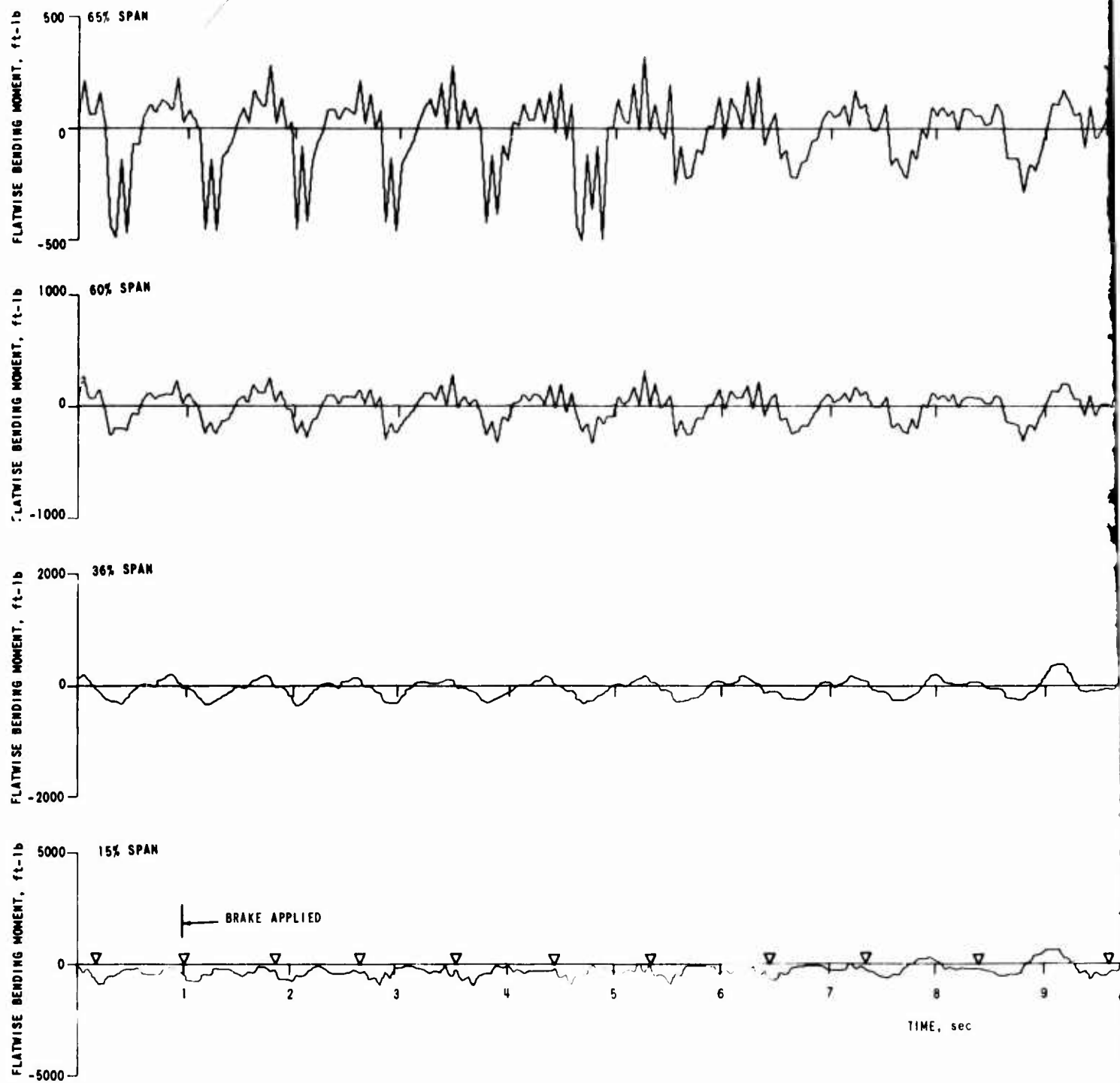
Figure 26. TIME HISTORY OF DATA COLLECTED FROM A ROTOR BEING STOPPED FROM
THE FOLLOWING OPERATING CONDITIONS: VF = 140.5, OMEGA = 71.35,
THETR = 7.35, THETIC = 0.00, THETIS = 0.00, ALPHS = 0.00.

97

∇ RPM INDICATOR

9   10 12   13   14   15 26   27   28

sec

Figure 26. (Continued)

99
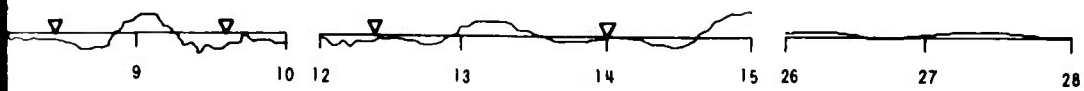
∇ RPM INDICATOR
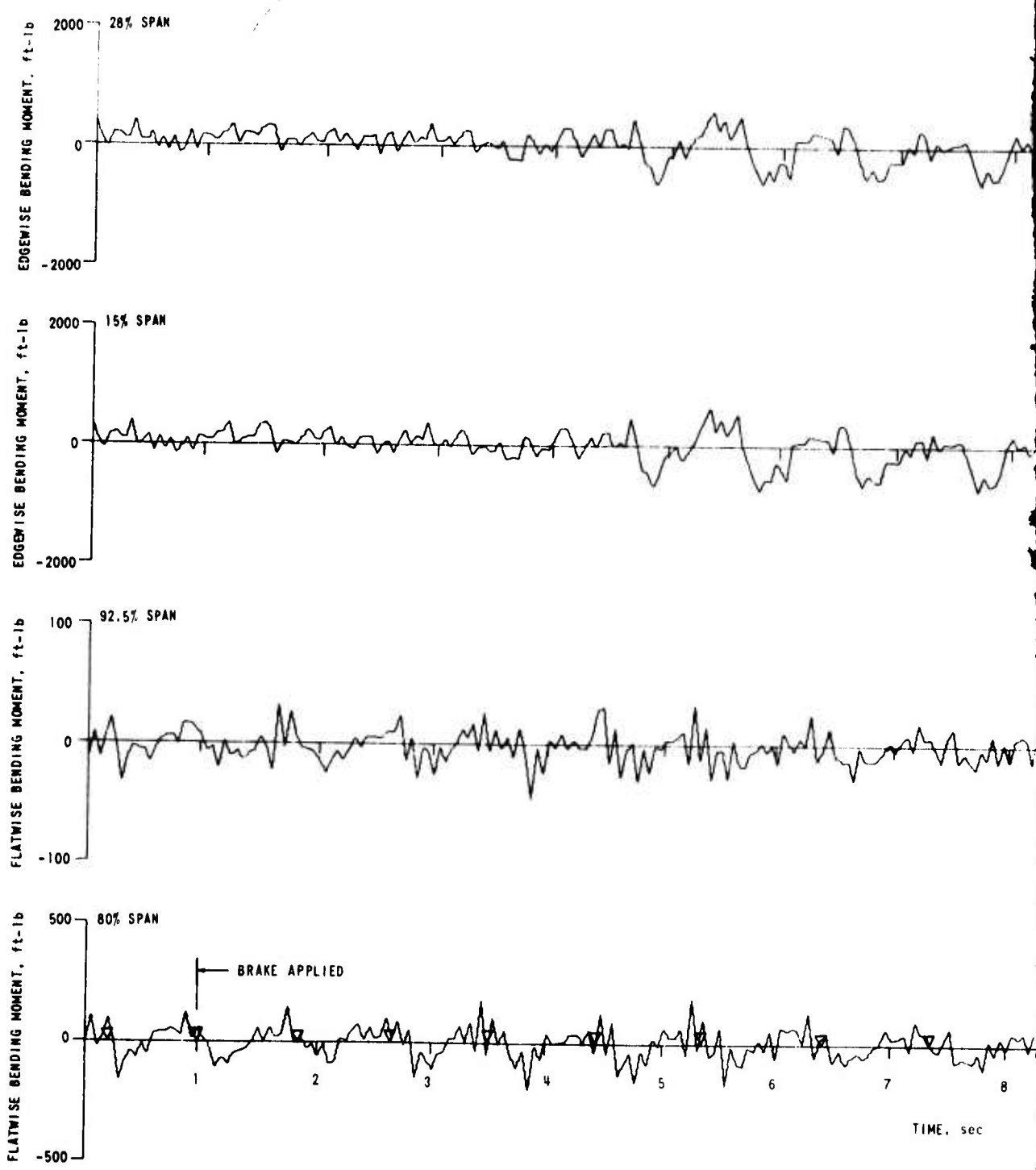
TIME, sec

Figure 26. (Continued)
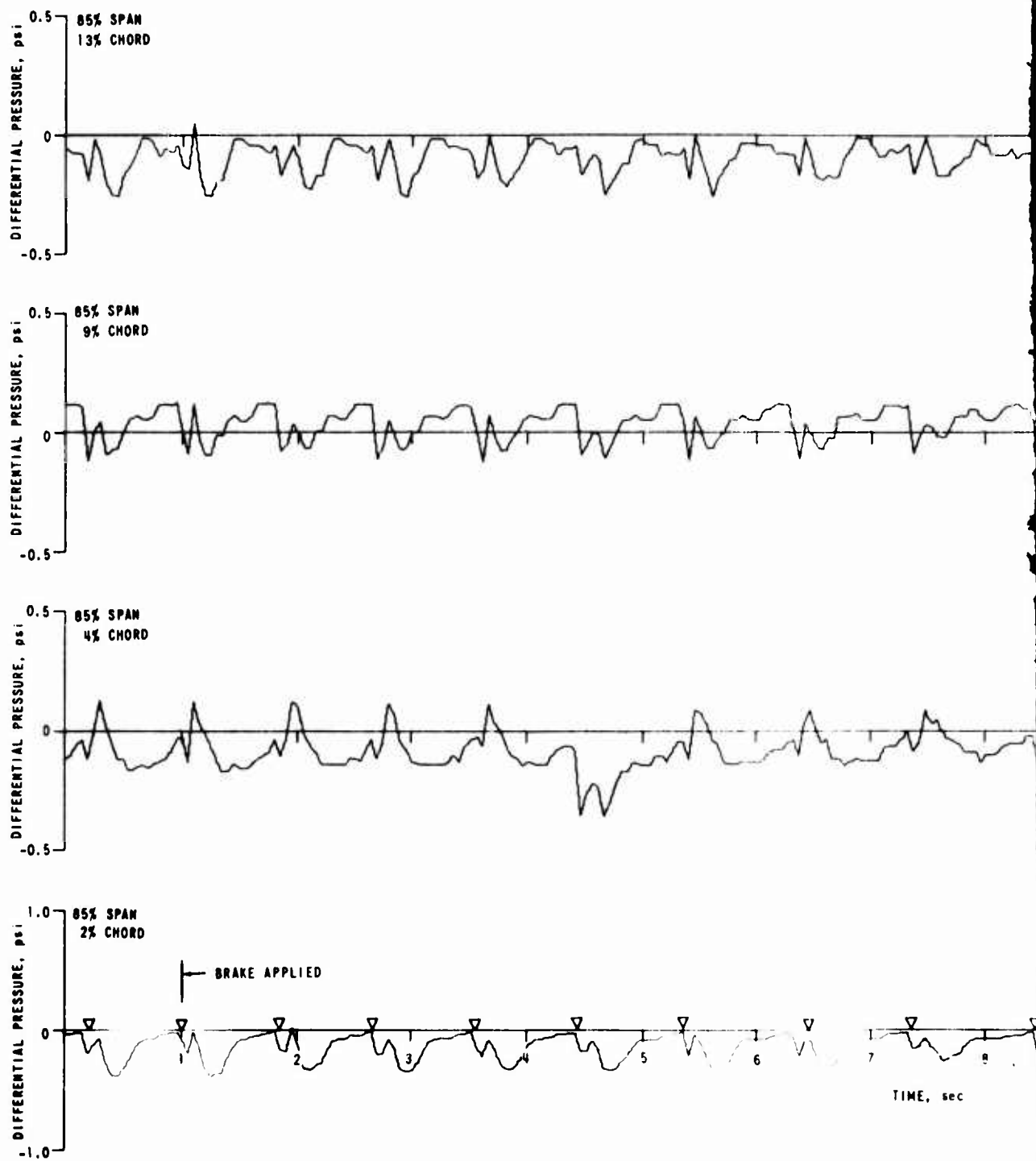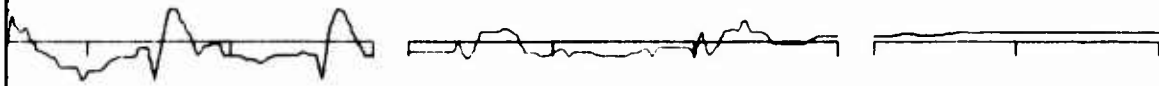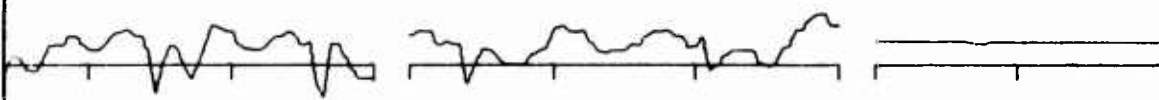
∇ RPM INDICATOR

TIME, sec

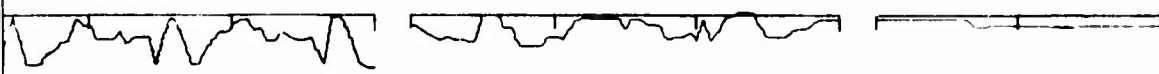Figure 26. (Continued)

103

∇ RPM INDICATOR

TIME, sec
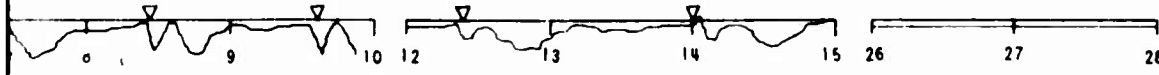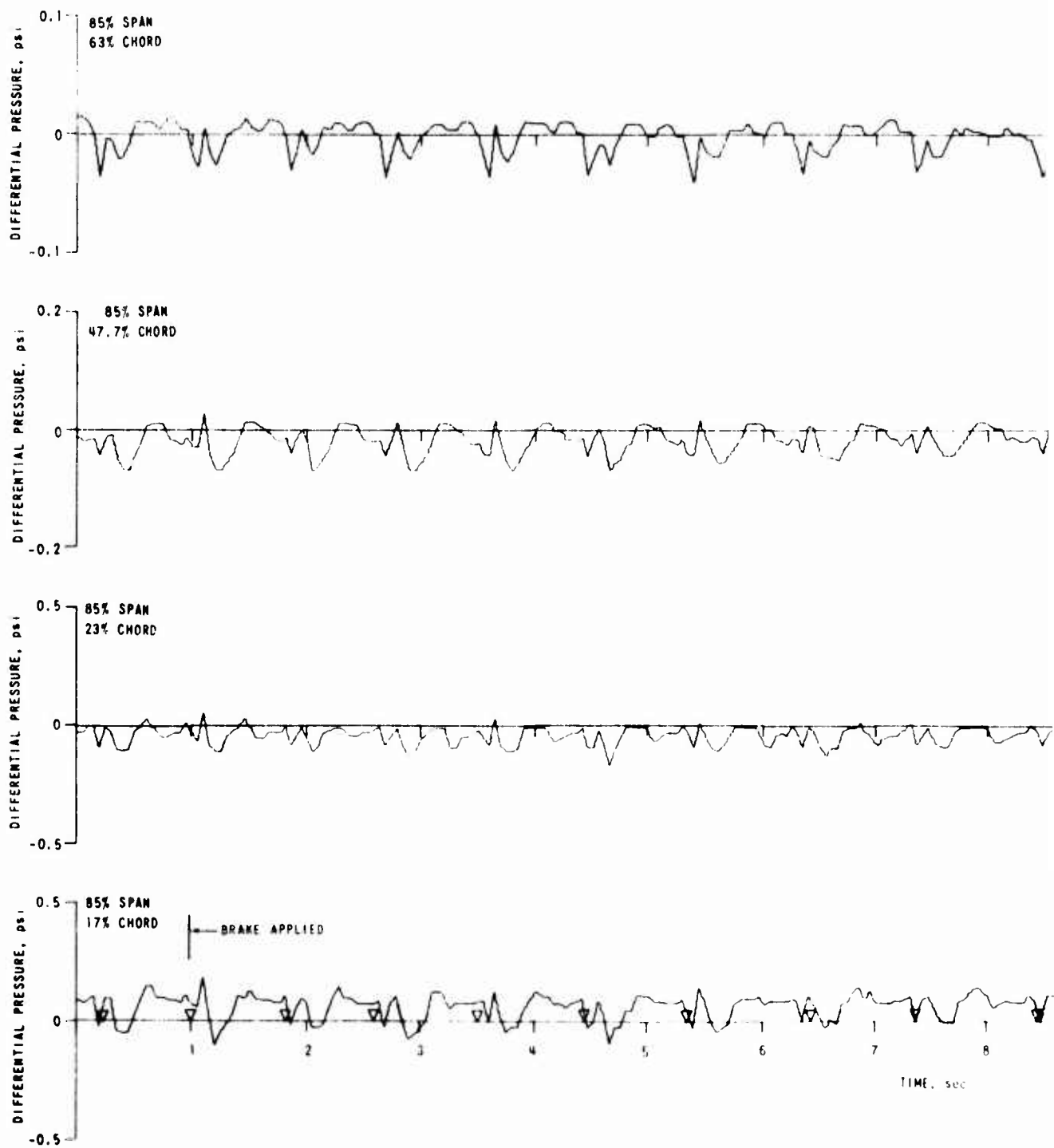
Figure 26. (Continued)

∇ RPM INDICATOR

sec

Figure 26. (Continued)

∇ RPM INDICATOR

8   9   10 12   13   14   15 26   27   28

TIME, sec

Figure 26. (Continued)

109

∇ RPM INDICATOR

7   8   9   10 12   13   14   15 26   27   28

TIME, sec

0.0   1.0   TIME, sec   2.0

↳ BRAKE APPLIED IN HERE
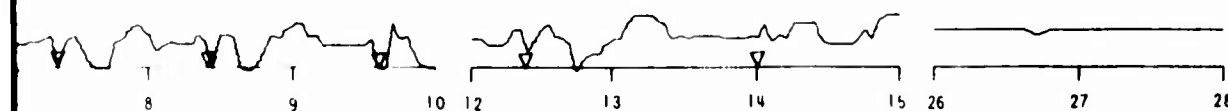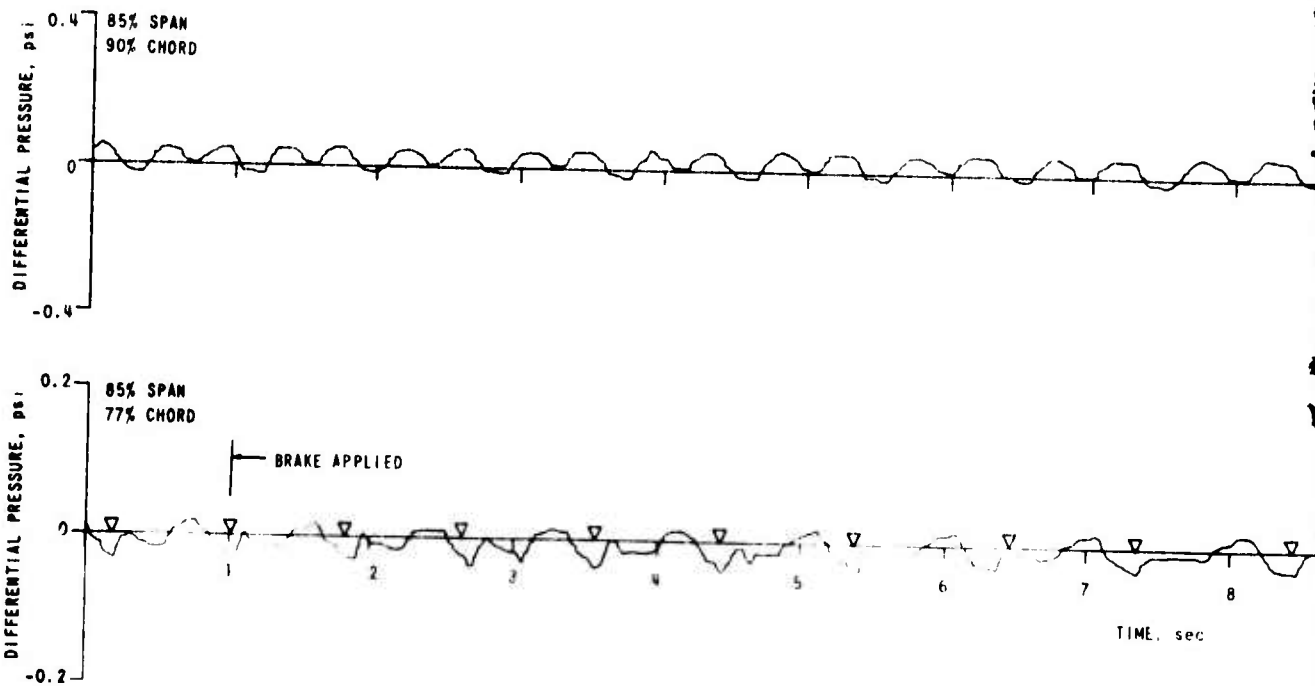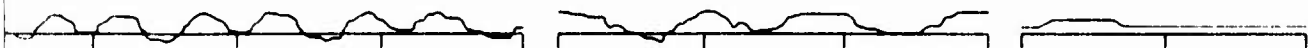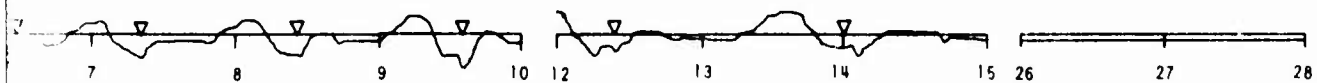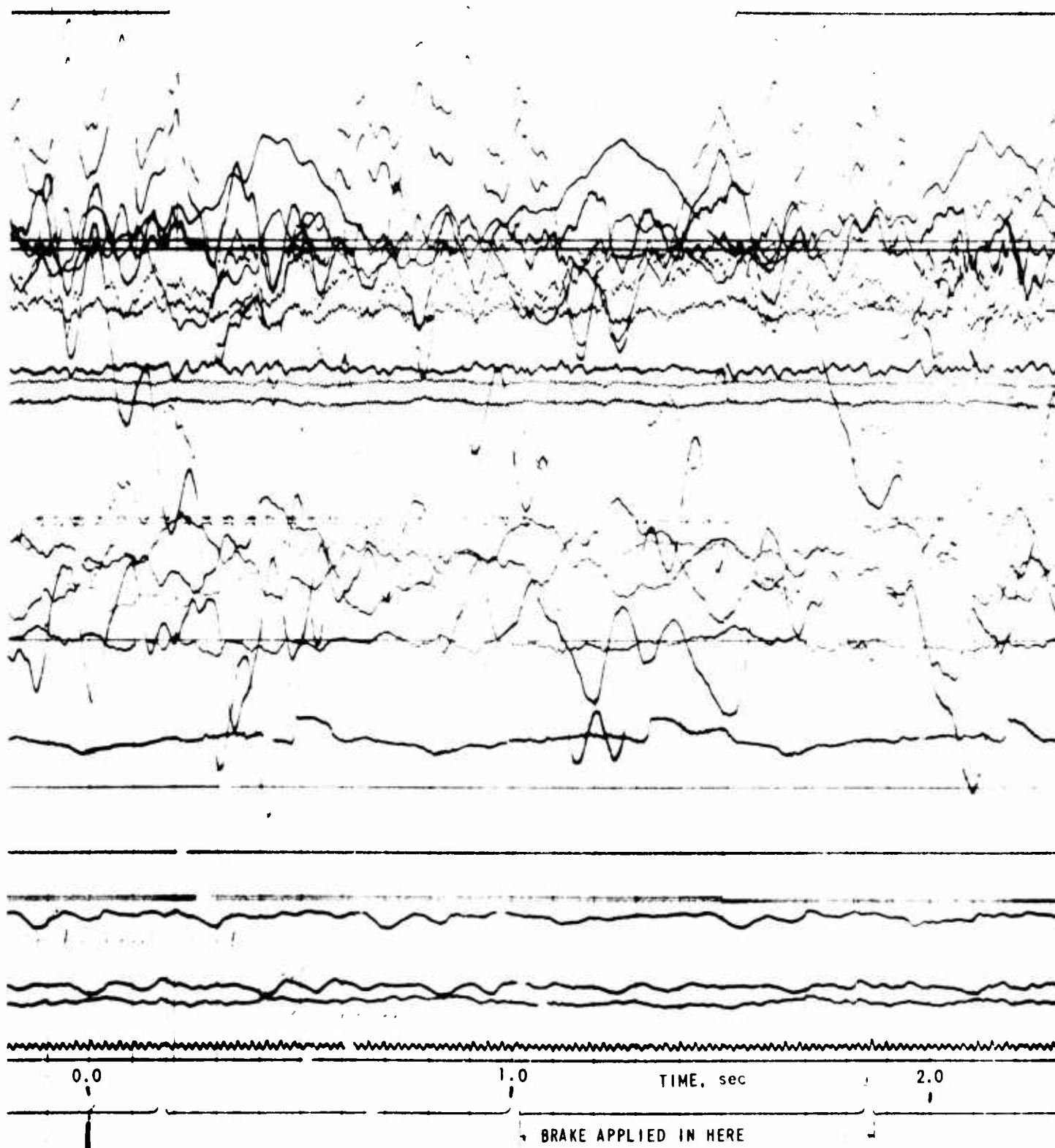
Figure 27. TYPICAL STOPPING OSCILLOGRAPH RECORD
OF BLADE AND MAST SIGNALS.

1	FLATWISE BENDING MOMENT AT 15 SPAN
2	FLATWISE BENDING MOMENT AT 24 SPAN
3	FLATWISE BENDING MOMENT AT 15 SPAN
4	FLATWISE BENDING MOMENT AT 45 SPAN
5	FLATWISE BENDING MOMENT AT 50 SPAN
6	FLATWISE BENDING MOMENT AT 55 SPAN
7	FLATWISE BENDING MOMENT AT 40 SPAN
8	FLATWISE BENDING MOMENT AT 92.5 SPAN
9	CHORDWISE BENDING MOMENT AT 15 SPAN
10	CHORDWISE BENDING MOMENT AT 15 SPAN
11	CHORDWISE BENDING MOMENT AT 50 SPAN
12	CHORDWISE BENDING MOMENT AT 40 SPAN
13	TORSIONAL MOMENT AT 15 SPAN
14	TORSIONAL MOMENT AT 40 SPAN
15	PARALLEL MAST BENDING - LOWER
16	PERPENDICULAR MAST BENDING - LOWER
17	PARALLEL MAST BENDING - UPPER
18	PERPENDICULAR MAST BENDING - UPPER
19	TORQUE
20	CHORDWISE YOKE BENDING
21	BEAMWISE YOKE BENDING
22	PITCH LINK AXIAL LOAD
23	DRAG BRACE AXIAL LOAD
24	FEATHERING POSITION

20.0   21.0   22.0
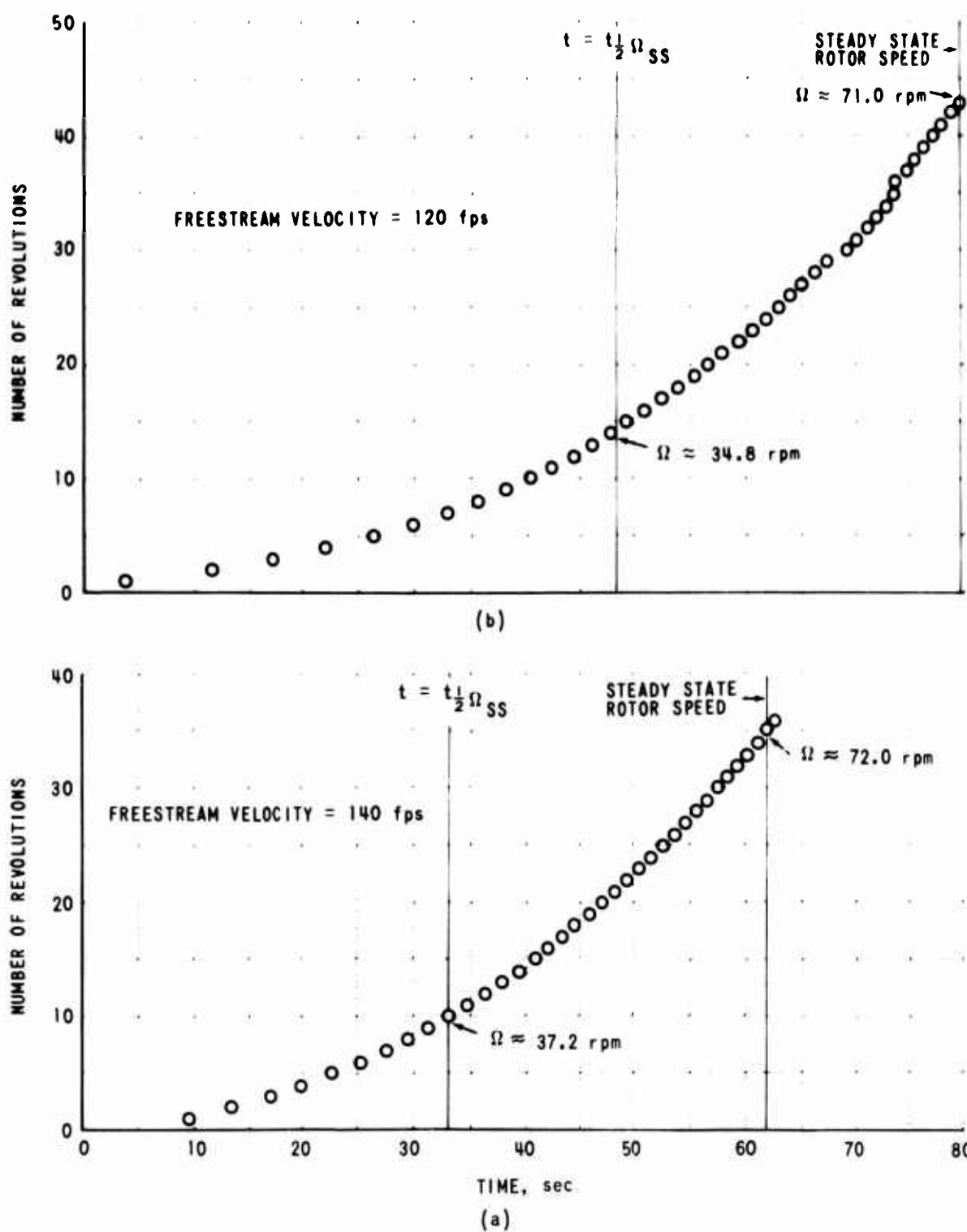
RPM INDICATOR

Figure 28. TIME HISTORIES OF NUMBER OF ROTOR REVOLUTIONS FROM INSTANT OF POWER APPLICATION TO STEADY ROTOR SPEED OF 71 RPM – ROTOR STARTED FOR TWO FREESTREAM VELOCITIES.
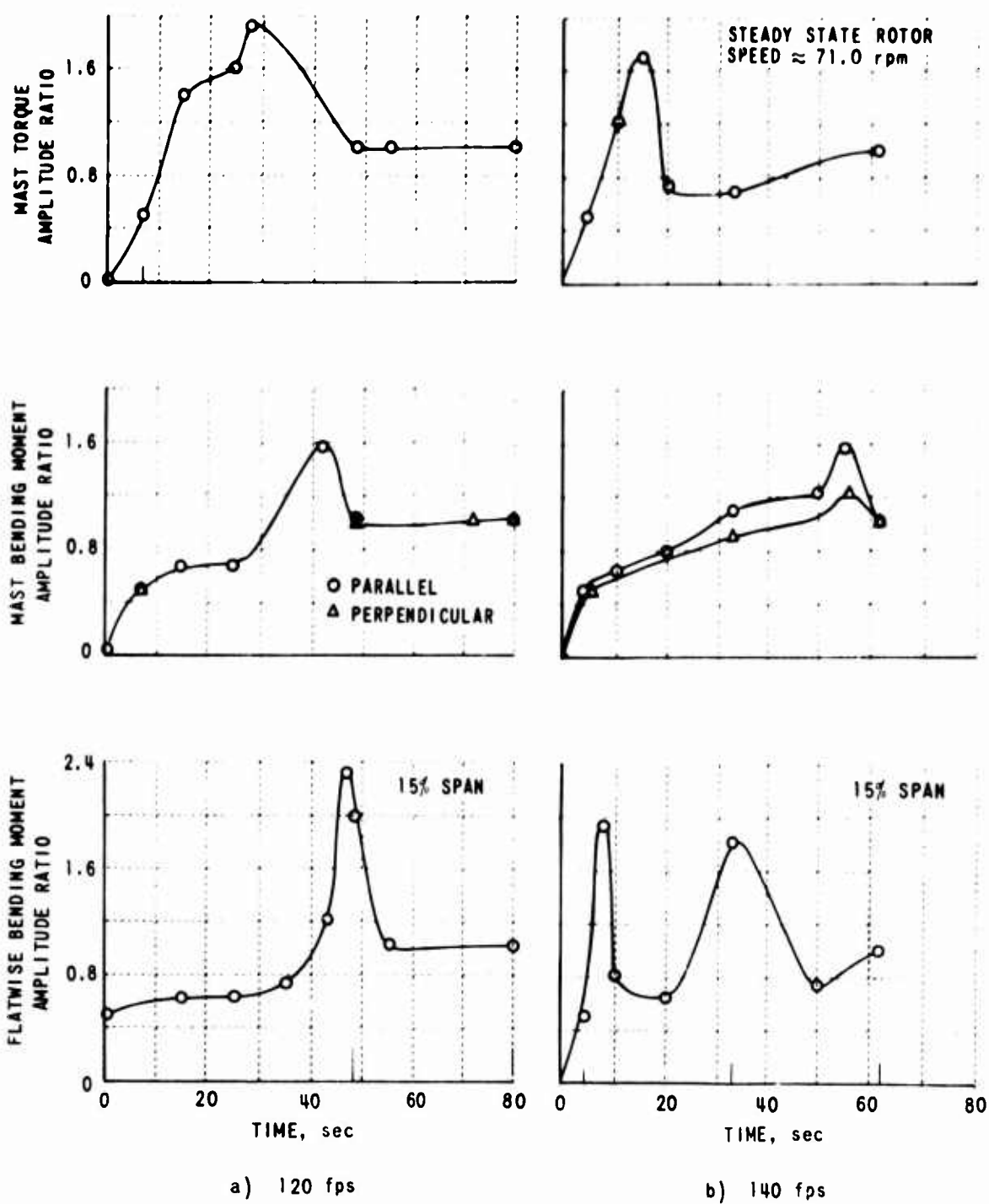
113

Figure 29. PLOT OF SEVERAL BLADE AND MAST MOMENT AMPLITUDE RATIOS
OBSERVED DURING START-UP AT TWO DIFFERENT
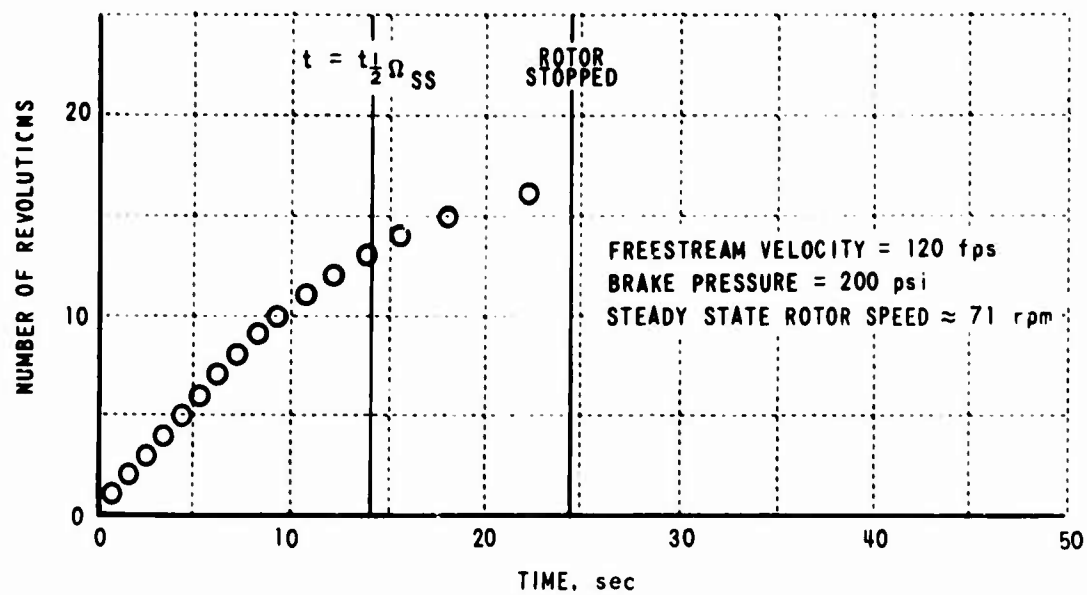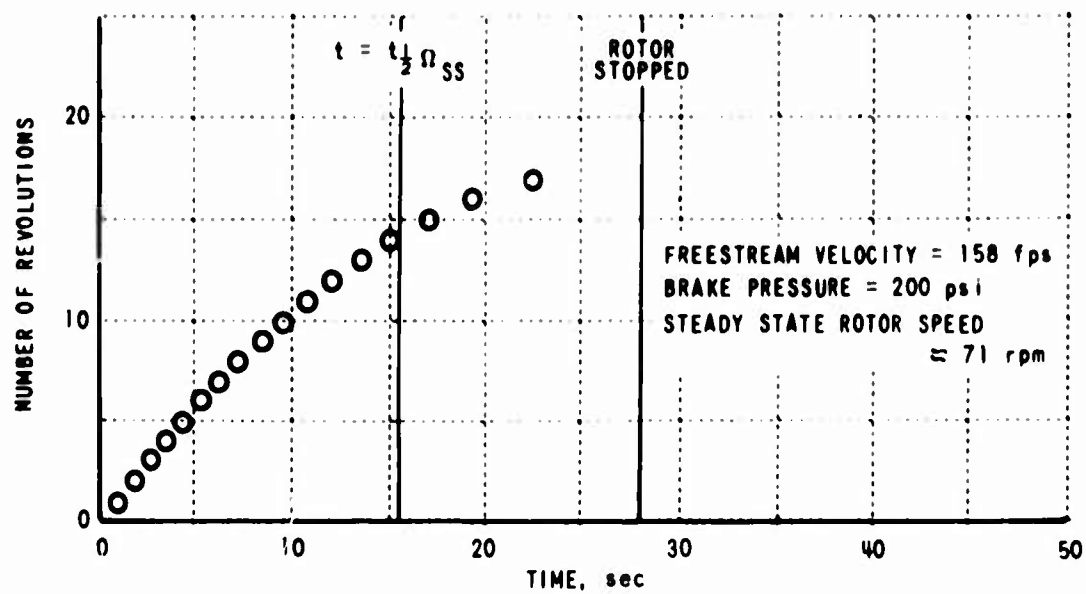FREESTREAM VELOCITIES.

114

Figure 30. TIME HISTORIES OF NUMBER OF ROTOR REVOLUTIONS FROM BRAKE
APPLICATION TO STOP FOR TWO FREESTREAM VELOCITIES.

115
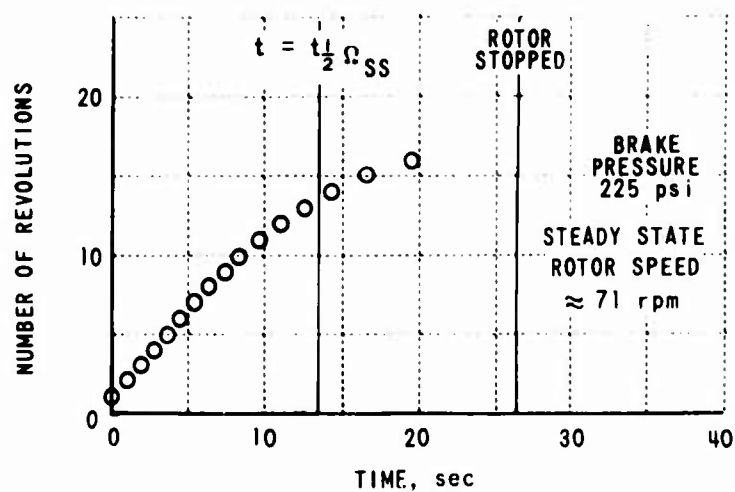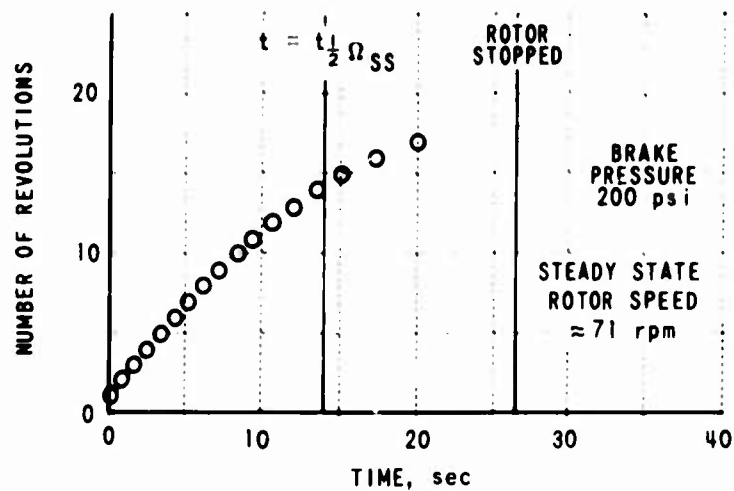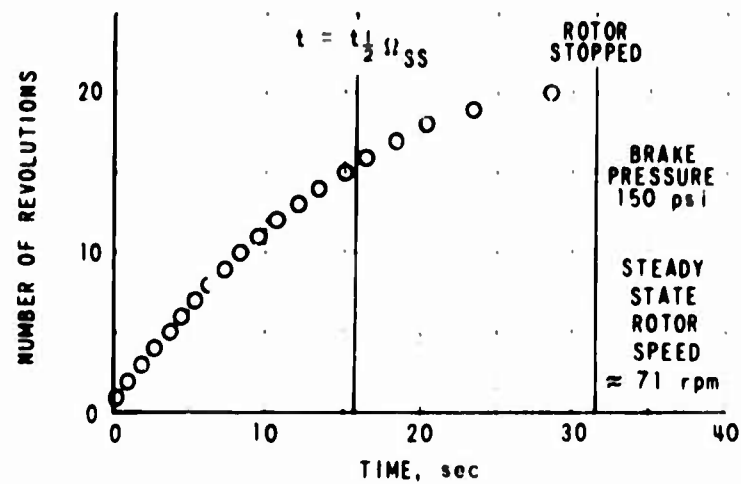
Figure 31. TIME HISTORIES OF NUMBER OF ROTOR REVOLUTIONS FROM BRAKE
APPLICATION TO STOP AT A FREESTREAM VELOCITY OF 140 FPS
EMPLOYING SEVERAL DIFFERENT BRAKE PRESSURES.

116
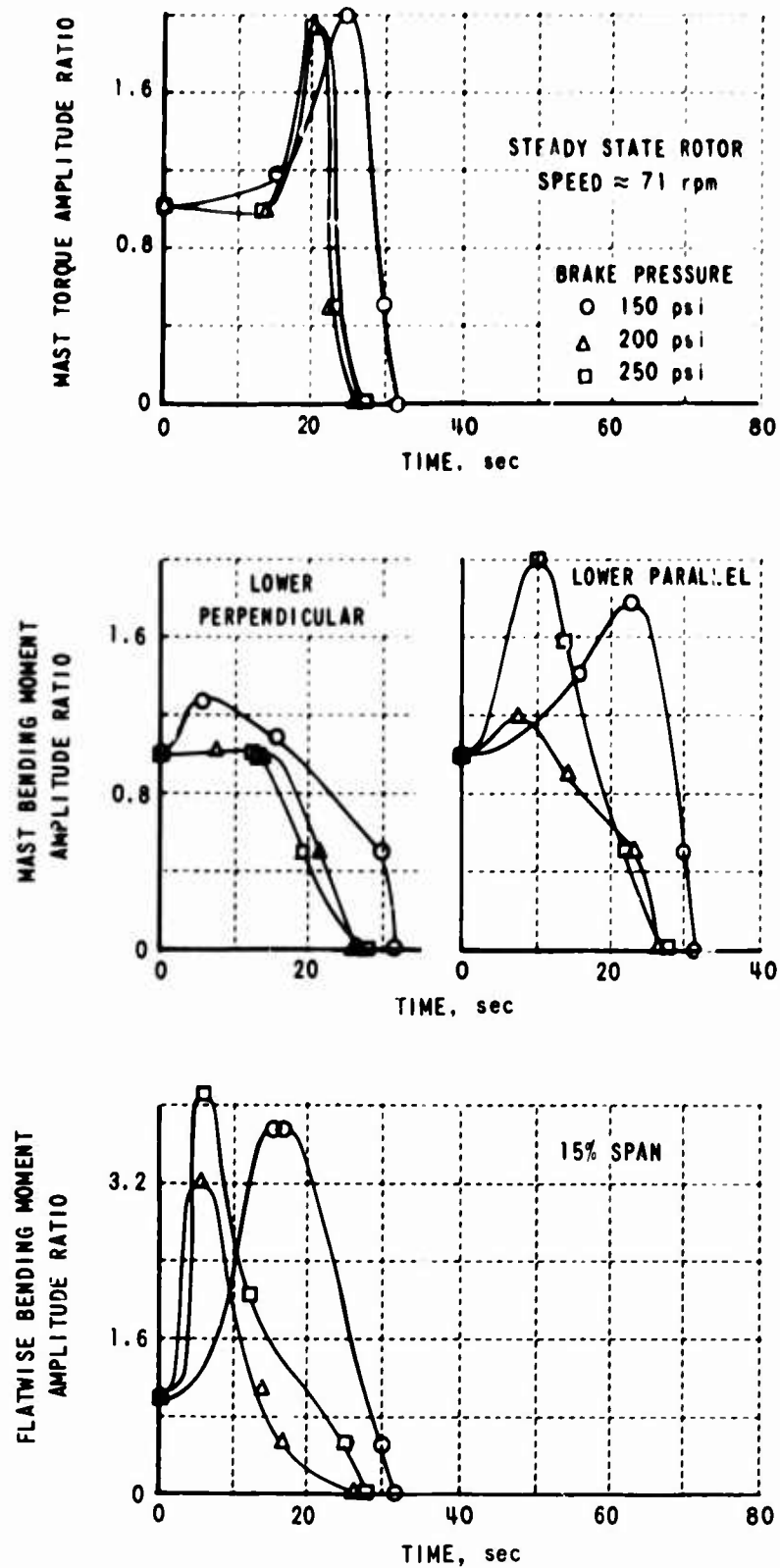
Figure 32. PLOT OF SEVERAL BLADE AND MAST MOMENT AMPLITUDE RATIOS OBSERVED
DURING STOPS AT 140 FPS USING DIFFERENT BRAKING PRESSURES.

117
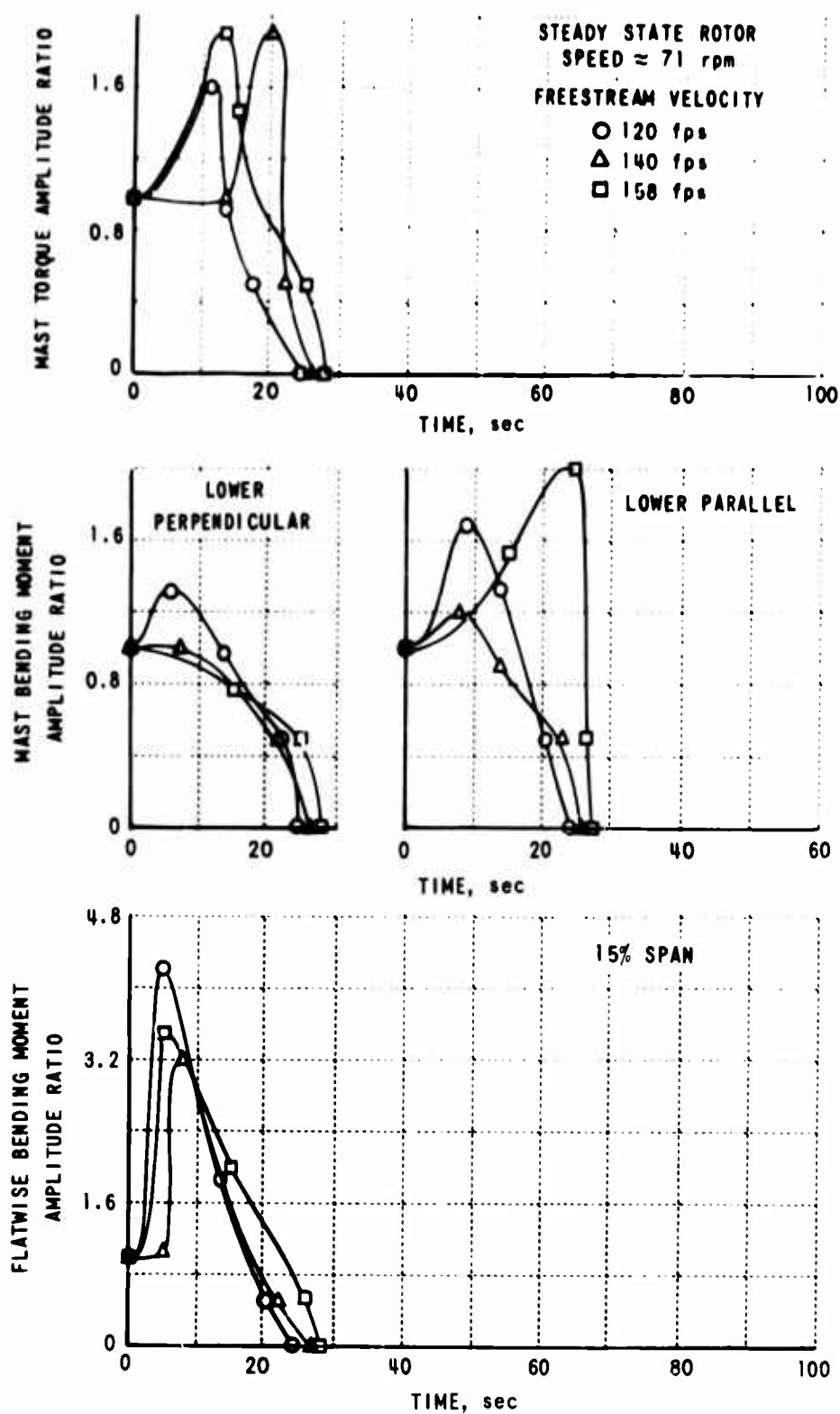
Figure 33. PLOT OF SEVERAL BLADE AND MAST MOMENT AMPLITUDE RATIOS OBSERVED DURING STOPS AT SEVERAL DIFFERENT FREESTREAM VELOCITIES.

118
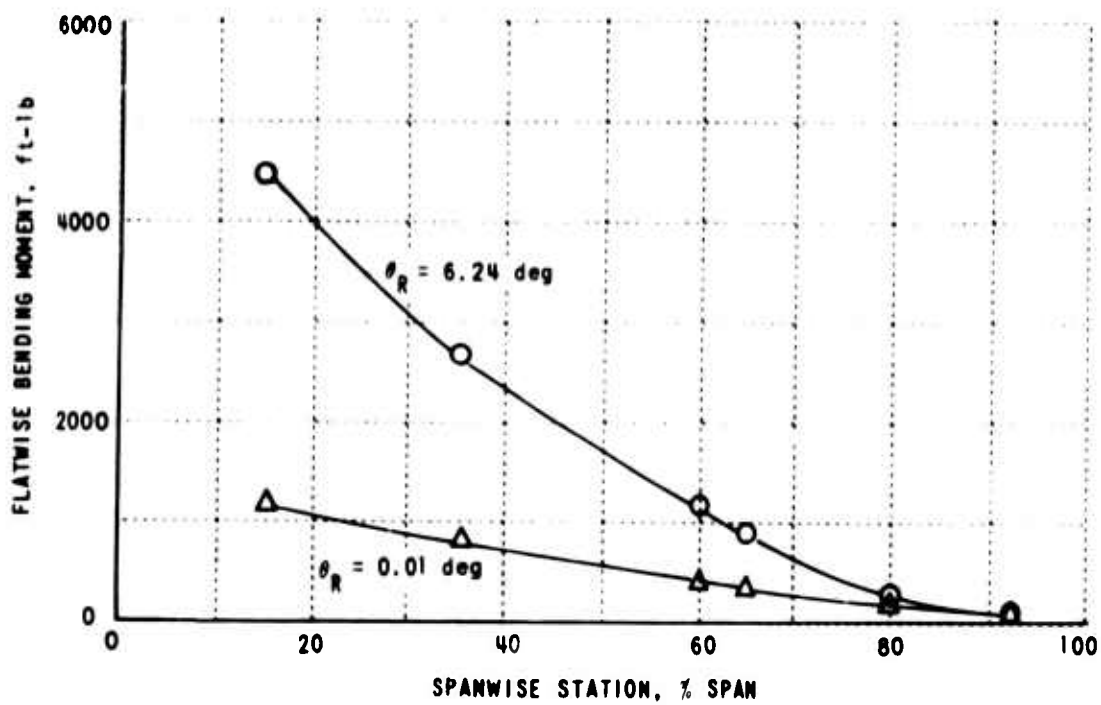
Figure 34. TYPICAL FLATWISE BENDING MOMENT DISTRIBUTION FOR THE ROTOR STOPPED AT AN AZIMUTHAL POSITION OF 255° AT V_f = 160 FPS FOR TWO VALUES OF THE COLLECTIVE ANGLE.
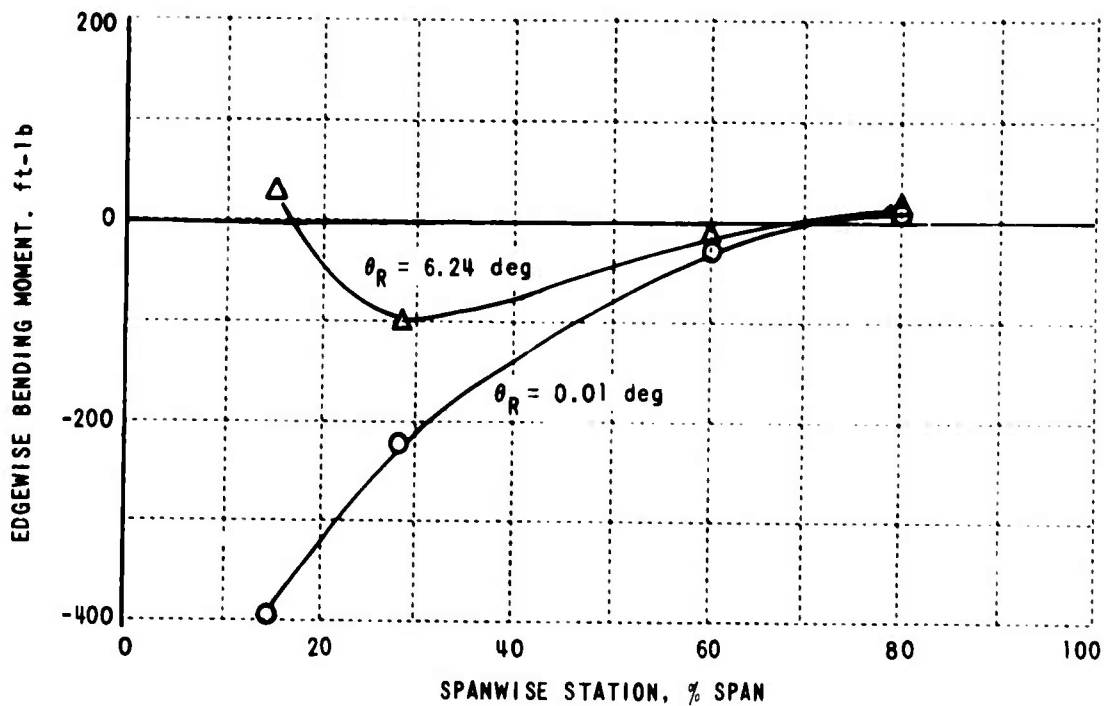
Figure 35. TYPICAL EDGEWISE BENDING MOMENT DISTRIBUTION FOR THE ROTOR STOPPED AT AN AZIMUTHAL POSITION OF 255° AT V_f = 160 FPS FOR TWO VALUES OF THE COLLECTIVE ANGLE.

119
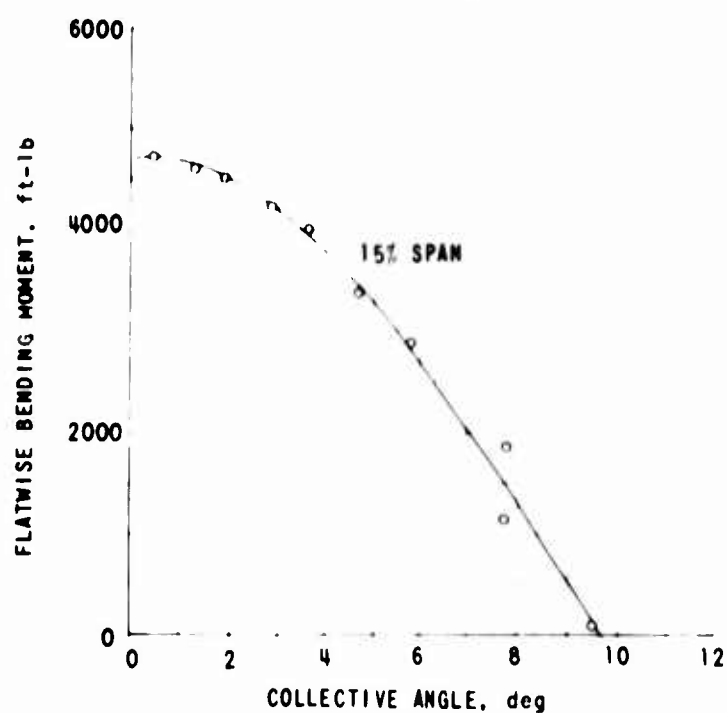
Figure 36. VARIATION OF 15% SPAN FLATWISE BENDING MOMENT WITH
THE COLLECTIVE ANGLE FOR THE ROTOR STOPPED AT AN
AZIMUTHAL POSITION OF 255 AT V_f = 160 FPS.
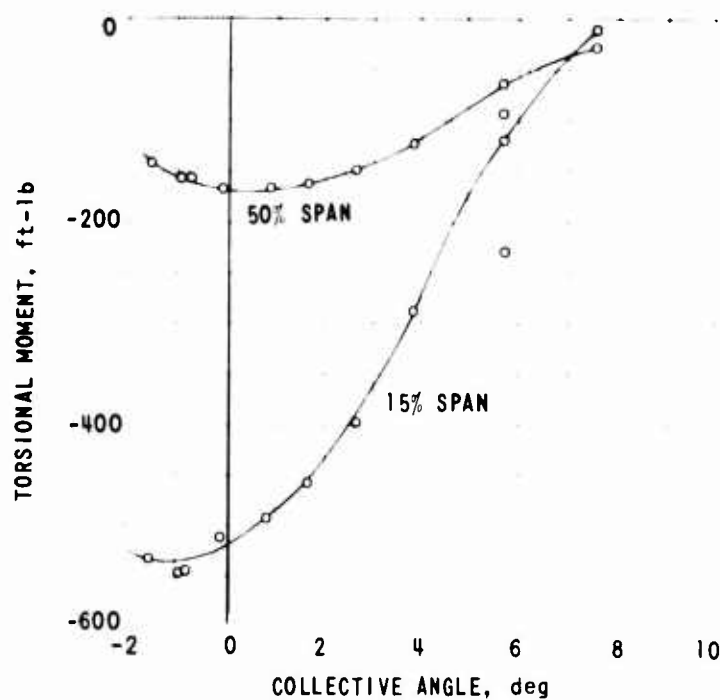
Figure 37. VARIATION OF TORSIONAL MOMENT WITH THE COLLECTIVE ANGLE FOR THE
ROTOR STOPPED AT AN AZIMUTHAL POSITION OF 255 AT V_f = 160 FPS.

120
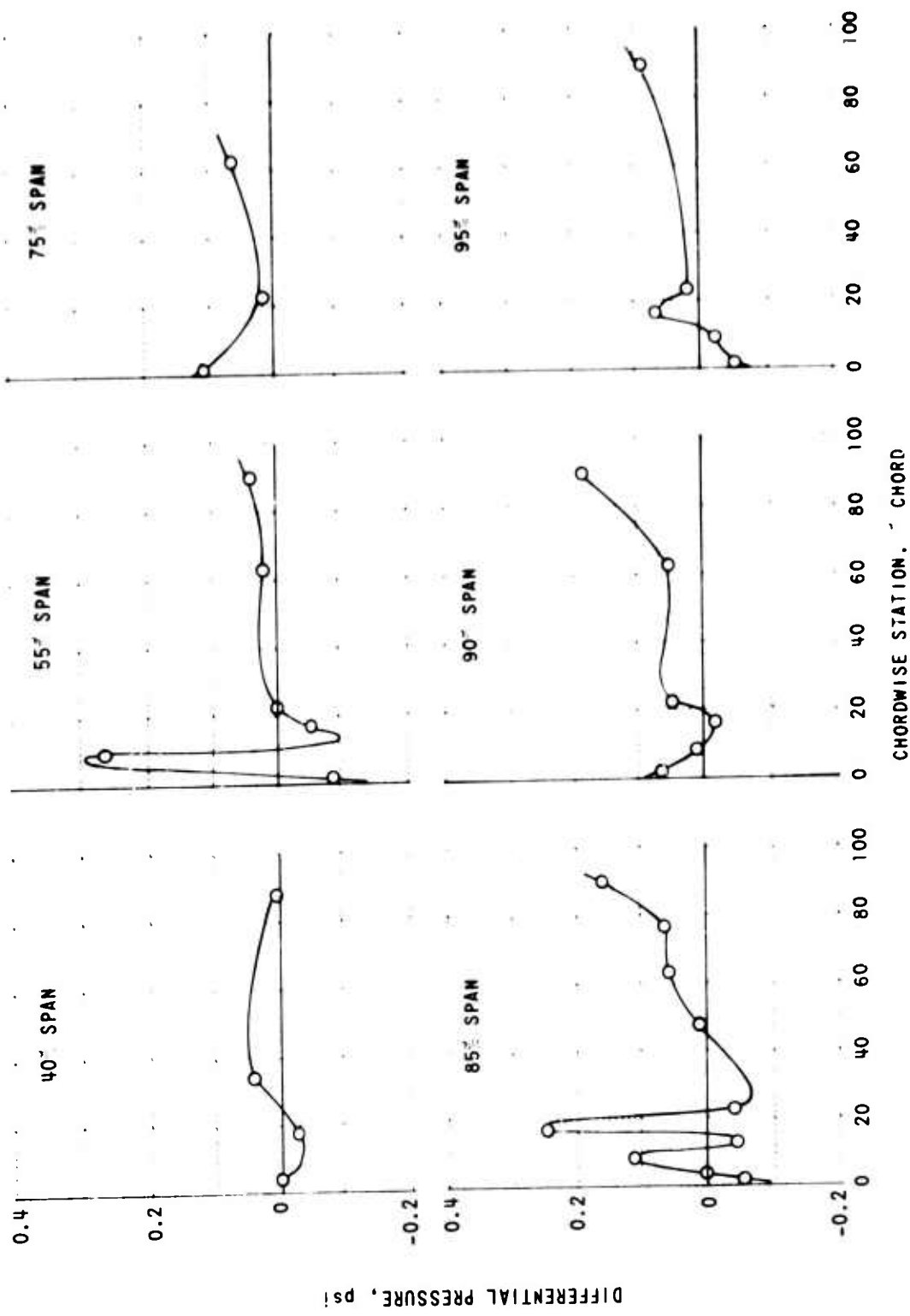
Figure 38. TYPICAL DIFFERENTIAL PRESSURE DISTRIBUTIONS AT SEVERAL SPANWISE STATIONS FOR THE ROTOR STOPPED AT AN AZIMUTHAL POSITION OF 255° AT V_f = 160 FPS FOR TWO VALUES OF THE COLLECTIVE ANGLE.

(a) COLLECTIVE ANGLE = 6.24°

121
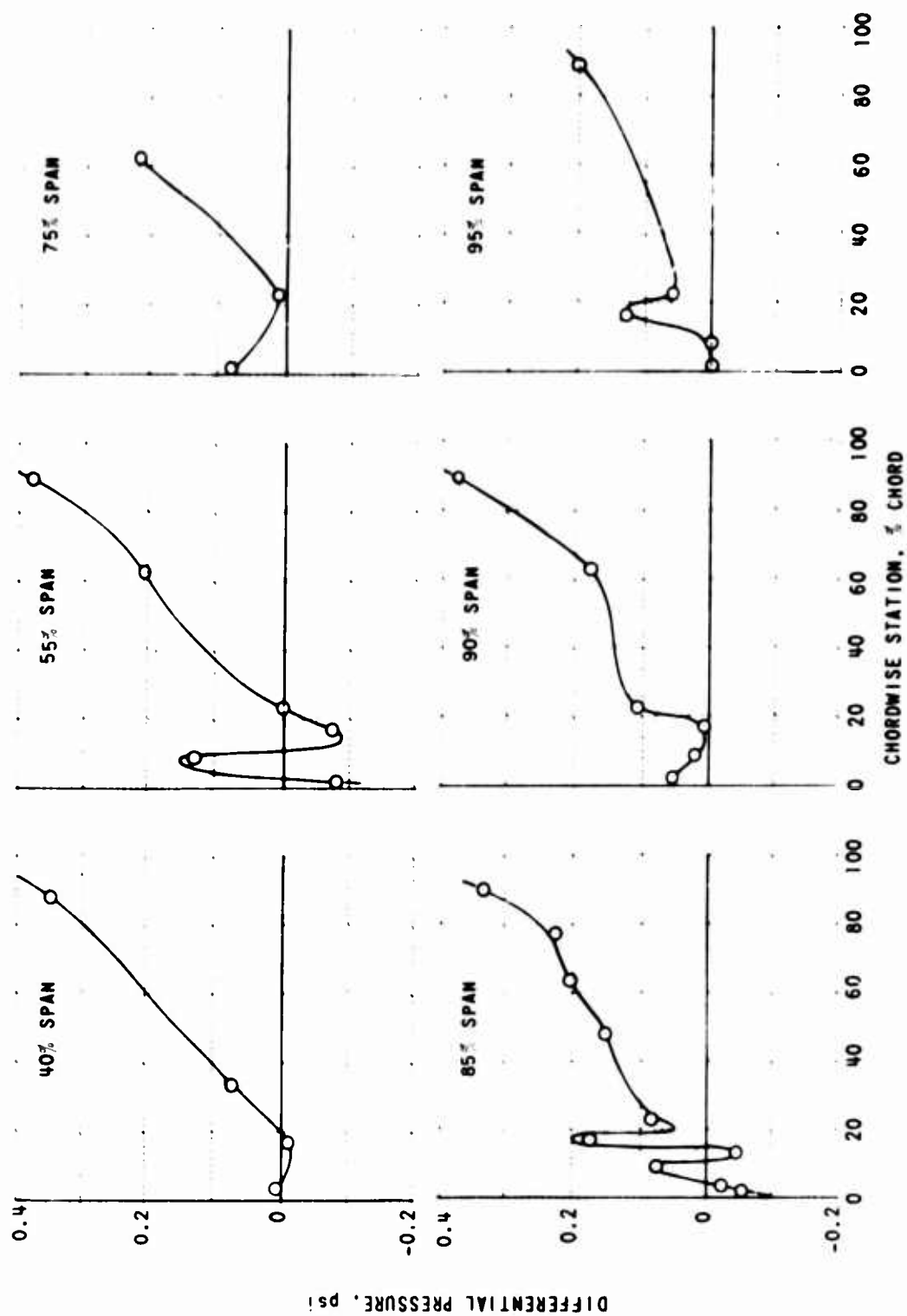
(b) COLLECTIVE ANGLE = 0.01°

Figure 38. (Continued)
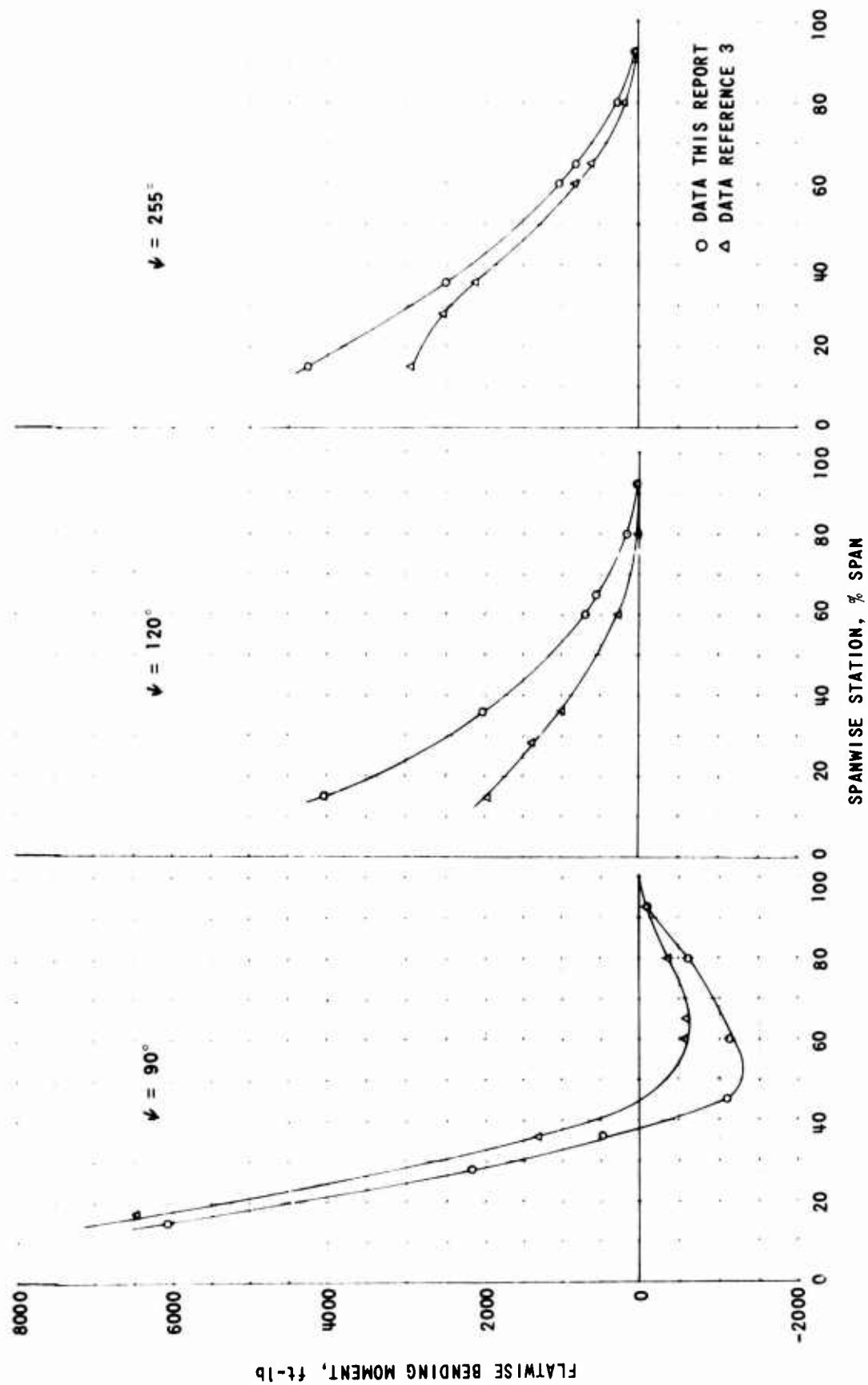
Figure 39. COMPARISON OF STOPPED-ROTOR FLATWISE BENDING MOMENT DISTRIBUTIONS OBTAINED DURING TEST REPORTED HEREIN WITH THOSE OBTAINED IN REFERENCE 3 FOR V_f = 160 FPS.

123
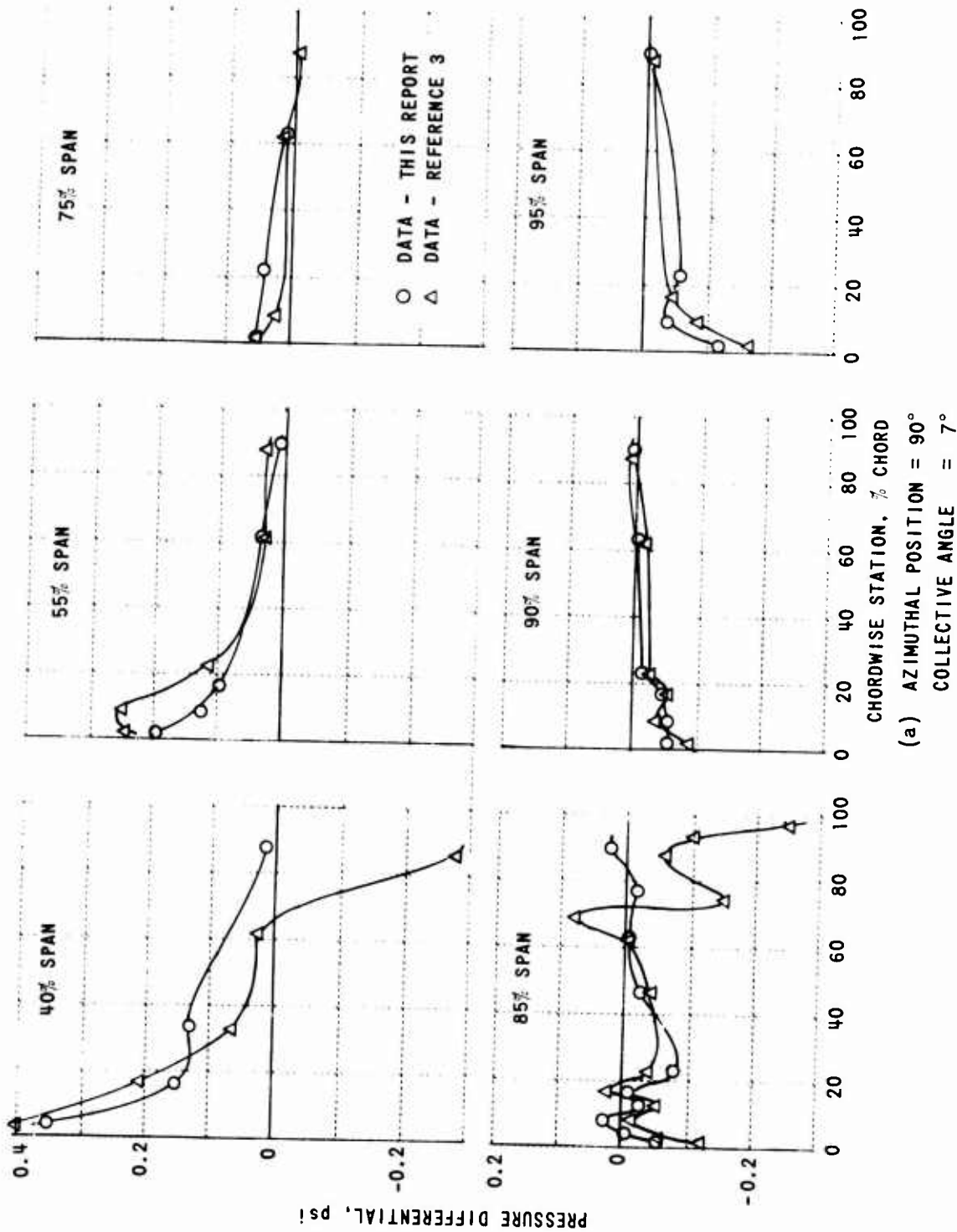
Figure 40. COMPARISON OF STOPPED-ROTOR PRESSURE DISTRIBUTION RESULTS OBTAINED DURING TEST REPORTED HEREIN WITH THOSE OBTAINED IN REFERENCE 3 FOR V_f = 160 FPS.

124
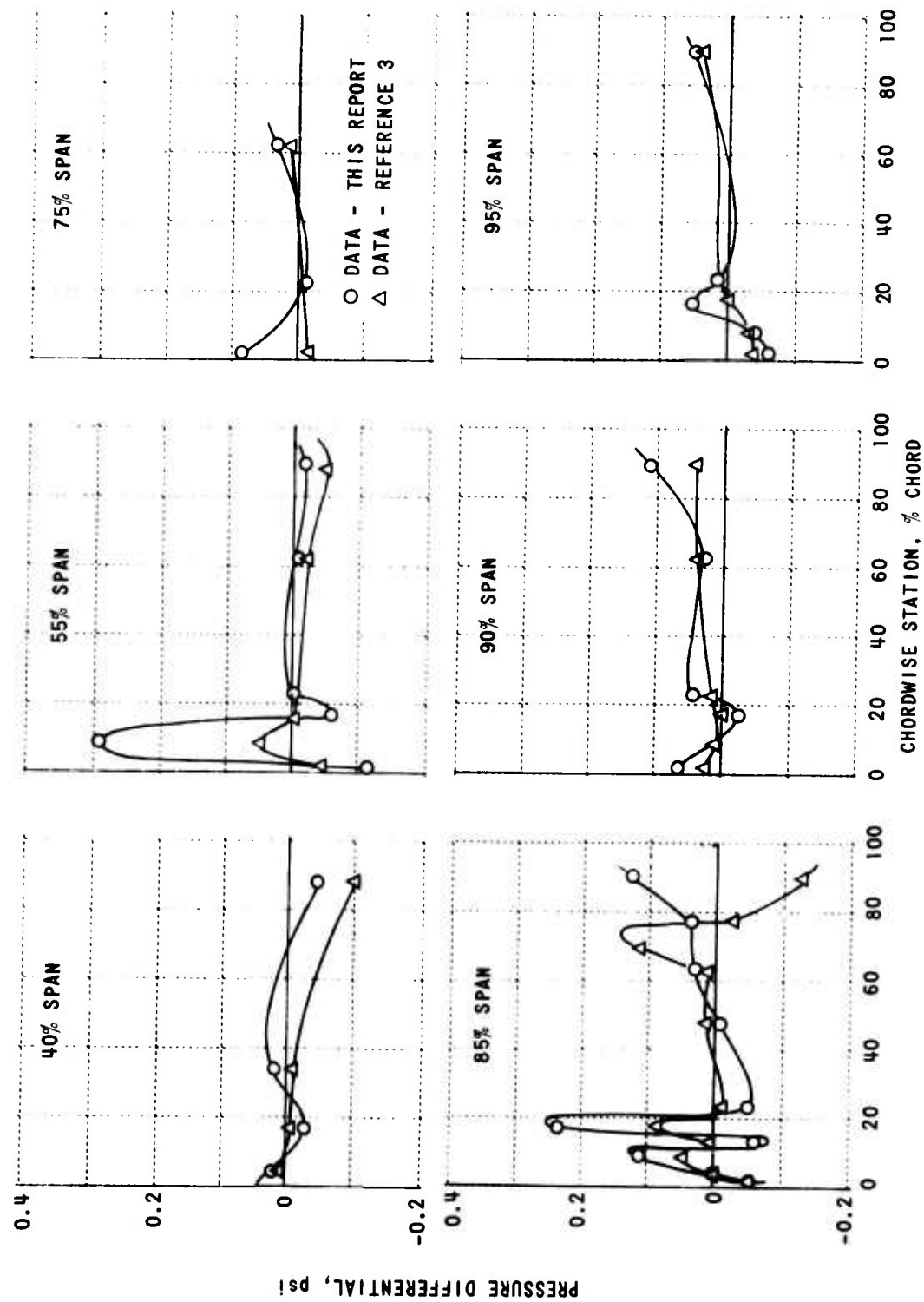
(b) AZIMUTHAL POSITION = 255°
     COLLECTIVE ANGLE = 7.5°

Figure 40. (Continued)

125
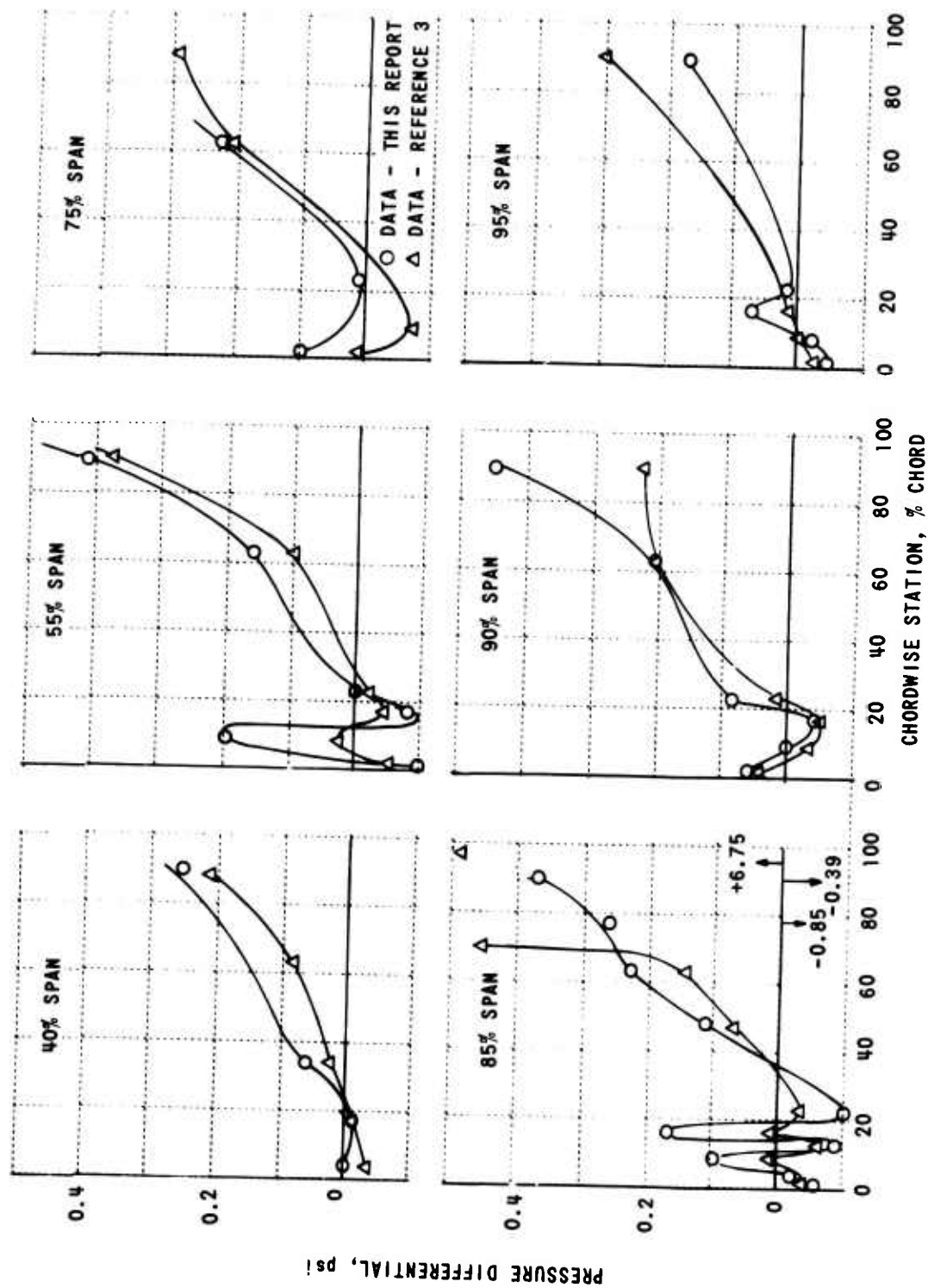
(c) AZIMUTHAL POSITION = 255°
COLLECTIVE ANGLE = 1.61°

Figure 40. (Continued)

ROTOR
FLAPPING
AXIS

WIND

83.23

126.75

155.90
+ 43.37
- 26.08

166.57

STRUT PIVOT

48.5

124.89

97.0

ALL DIMENSIONS ARE IN INCHES.
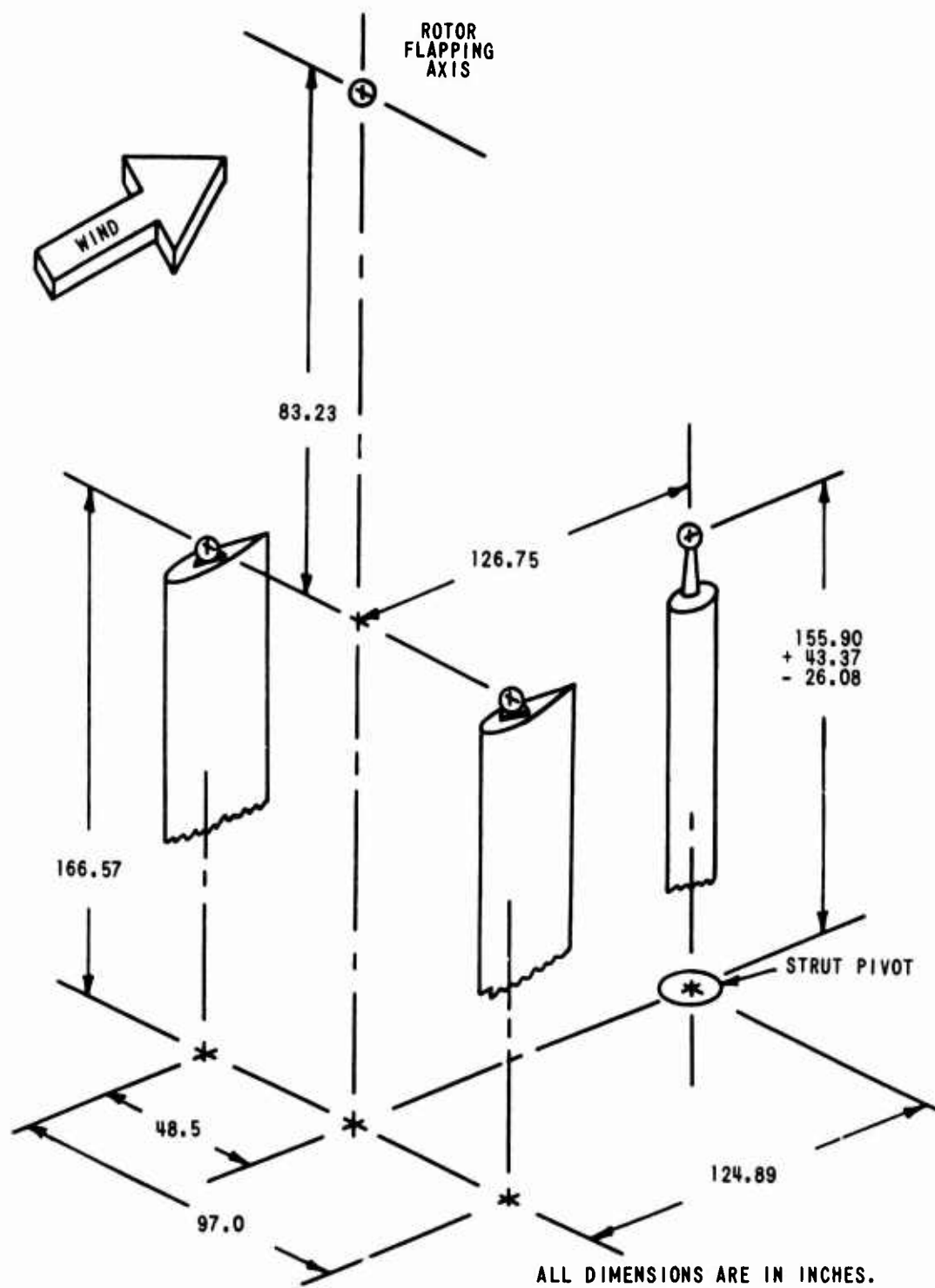
Figure 41. WIND TUNNEL STRUT ARRANGEMENT.

Figure 42. TEST MODULE ON TRANSPORT DOLLY.

128
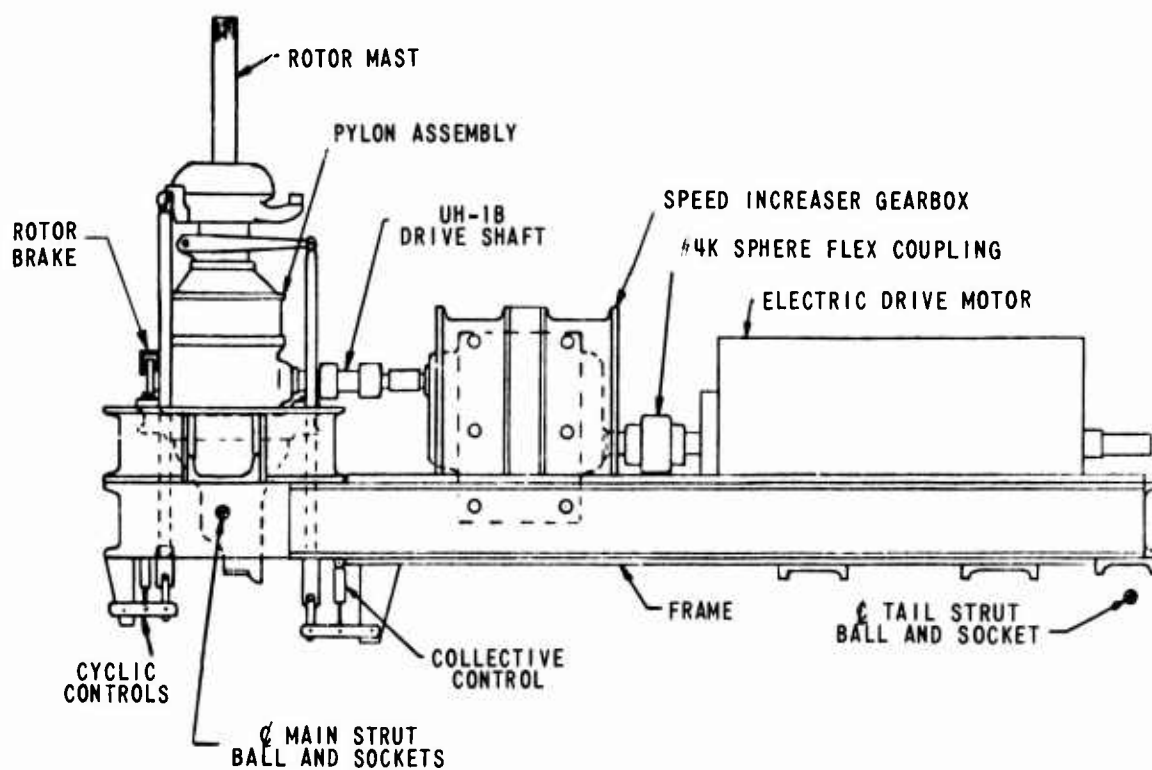
Figure 43. SIDE VIEW OF TEST MODULE.
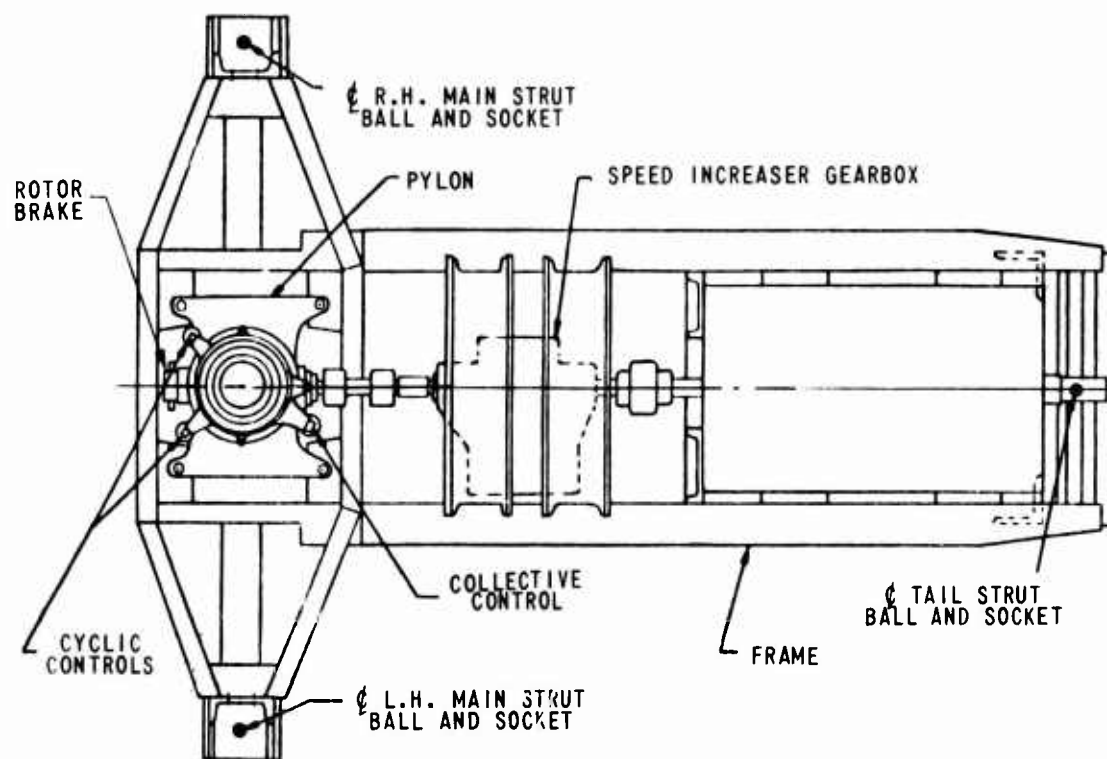
Figure 44. PLAN VIEW OF TEST MODULE.

130
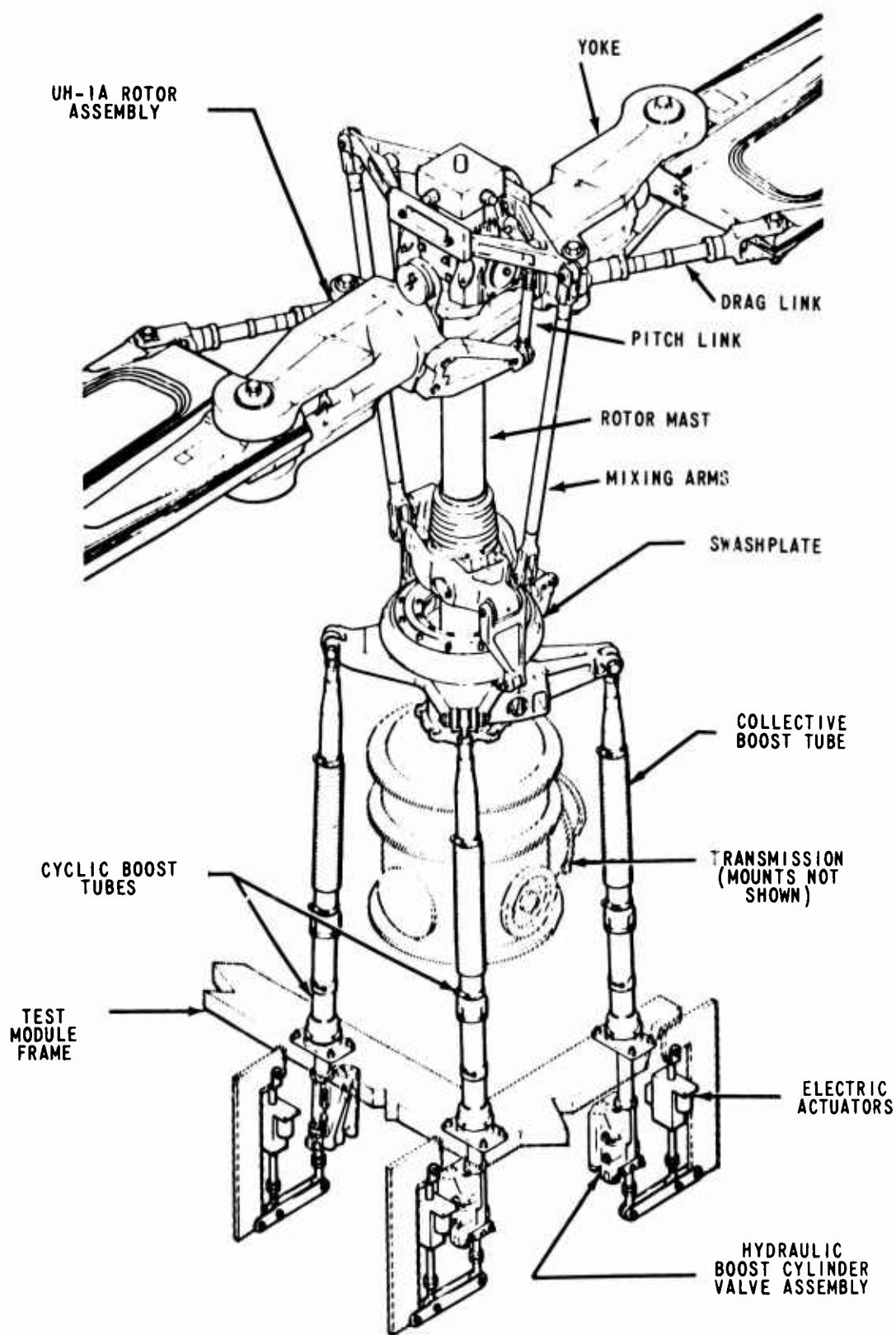
Figure 45. CONTROL SYSTEM ARRANGEMENT.

131

1°	EQUALS
0.123	PITCH LINK
0.221	SCISSORS TUBE
0.124	SCISSORS LINK
0.121	CYCLIC INPUT
0.079	COLLECTIVE LINK
0.230	COLLECTIVE INPUT

PITCH
CHANGE
AXIS

11.76
5.23   6.53
7.00

5.00   SCISSORS
8.90

7.78   SWASHPLATE
7.95

6.82
19.82

COLLECTIVE INPUT
0.230 INPUT
PRODUCES ONE
DEGREE PITCH
CHANGE

CYCLIC INPUT
0.121 INPUT
PRODUCES ONE
DEGREE PITCH
CHANGE
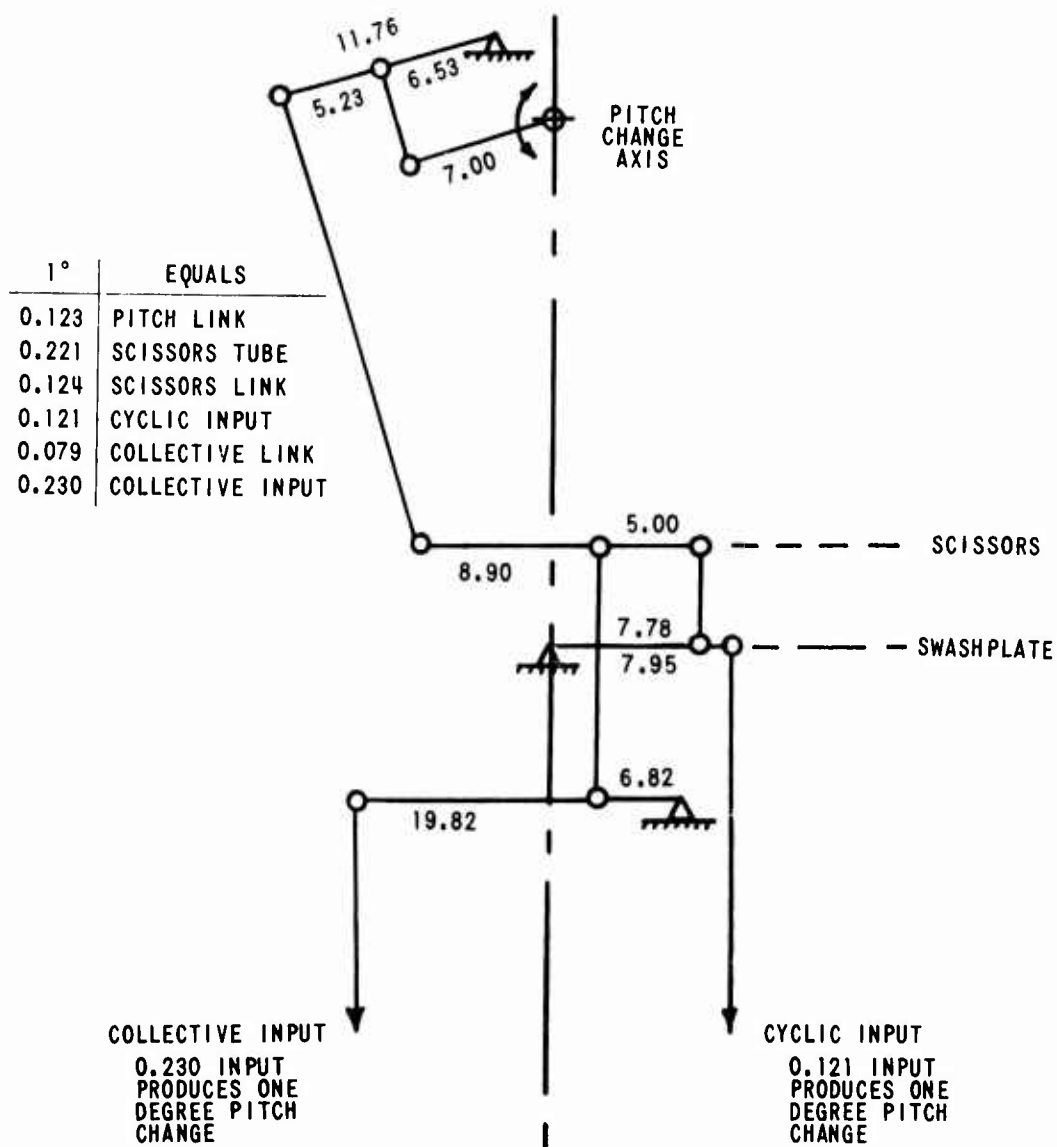
ALL DIMENSIONS ARE IN INCHES.

Figure 46. ROTOR CONTROL MOTIONS.

132

Figure 47. ROTOR BRAKE ASSEMBLY.

133
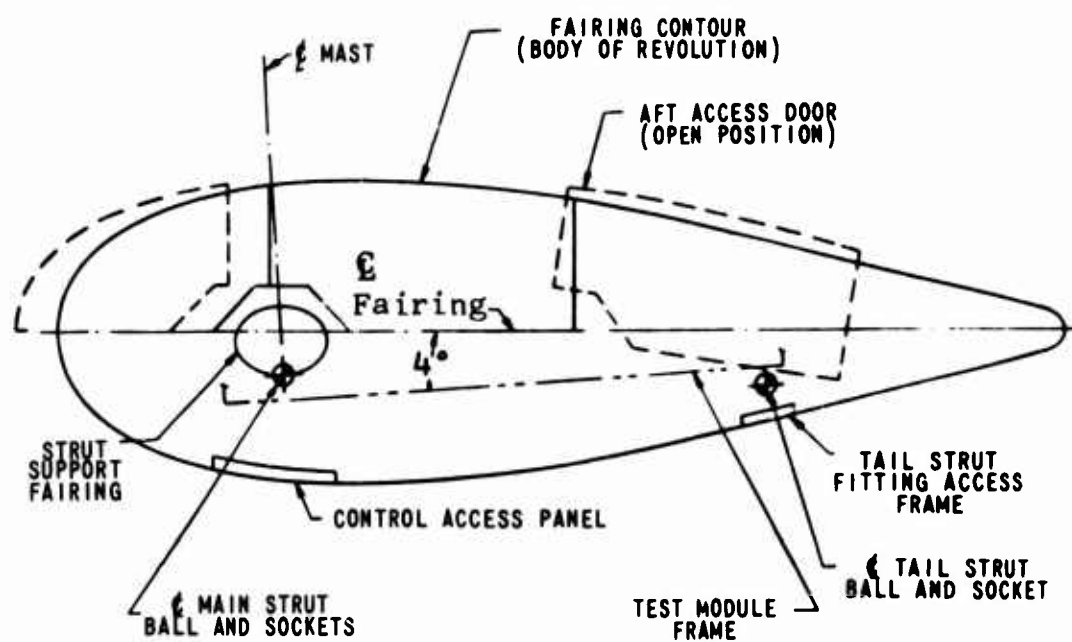
Figure 48. PROFILE VIEW OF FAIRING.

Figure 49. TEST MODULE MOUNTED ON STRUTS IN WIND TUNNEL.
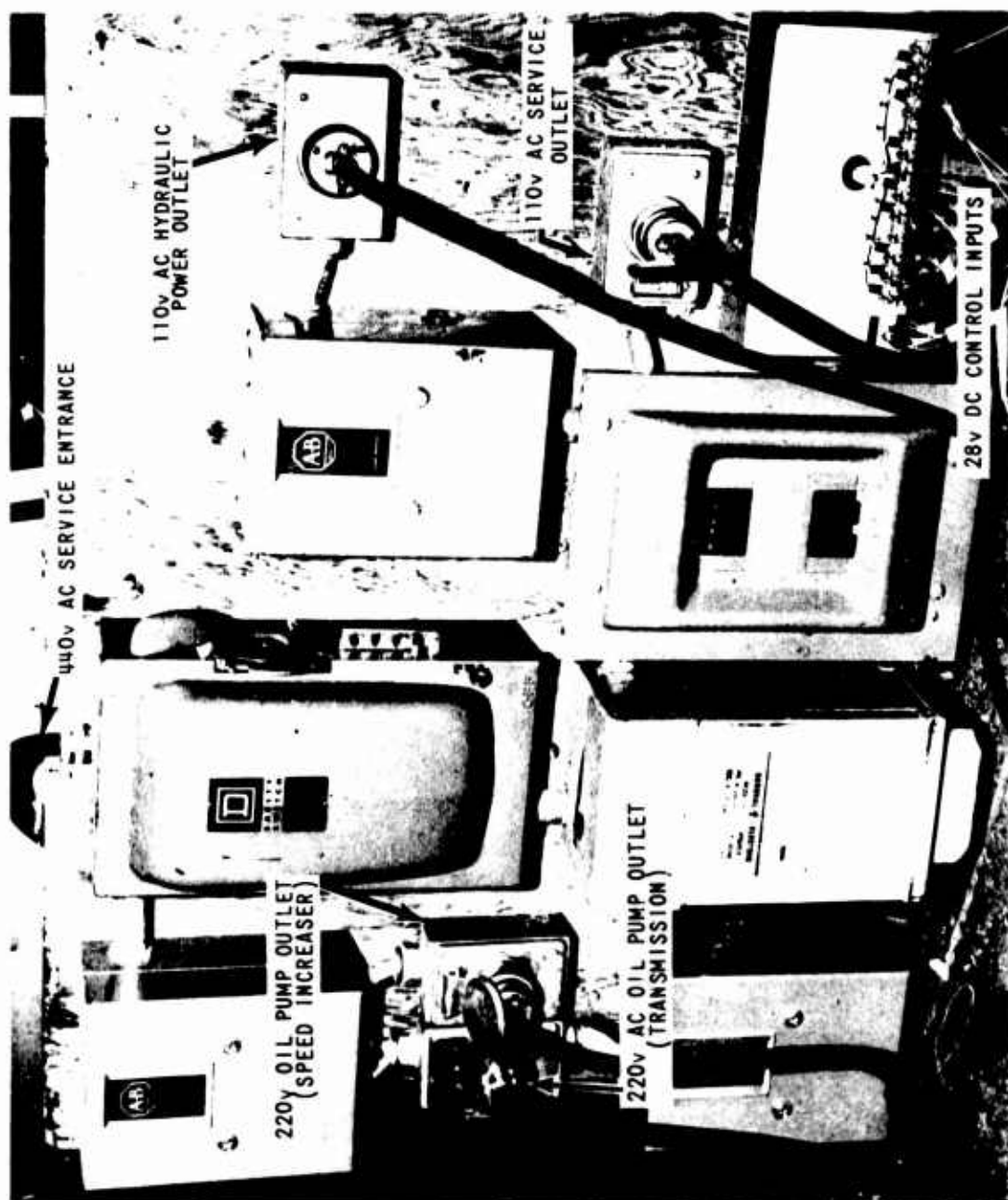
Figure 50. POWER DISTRIBUTION PANEL.
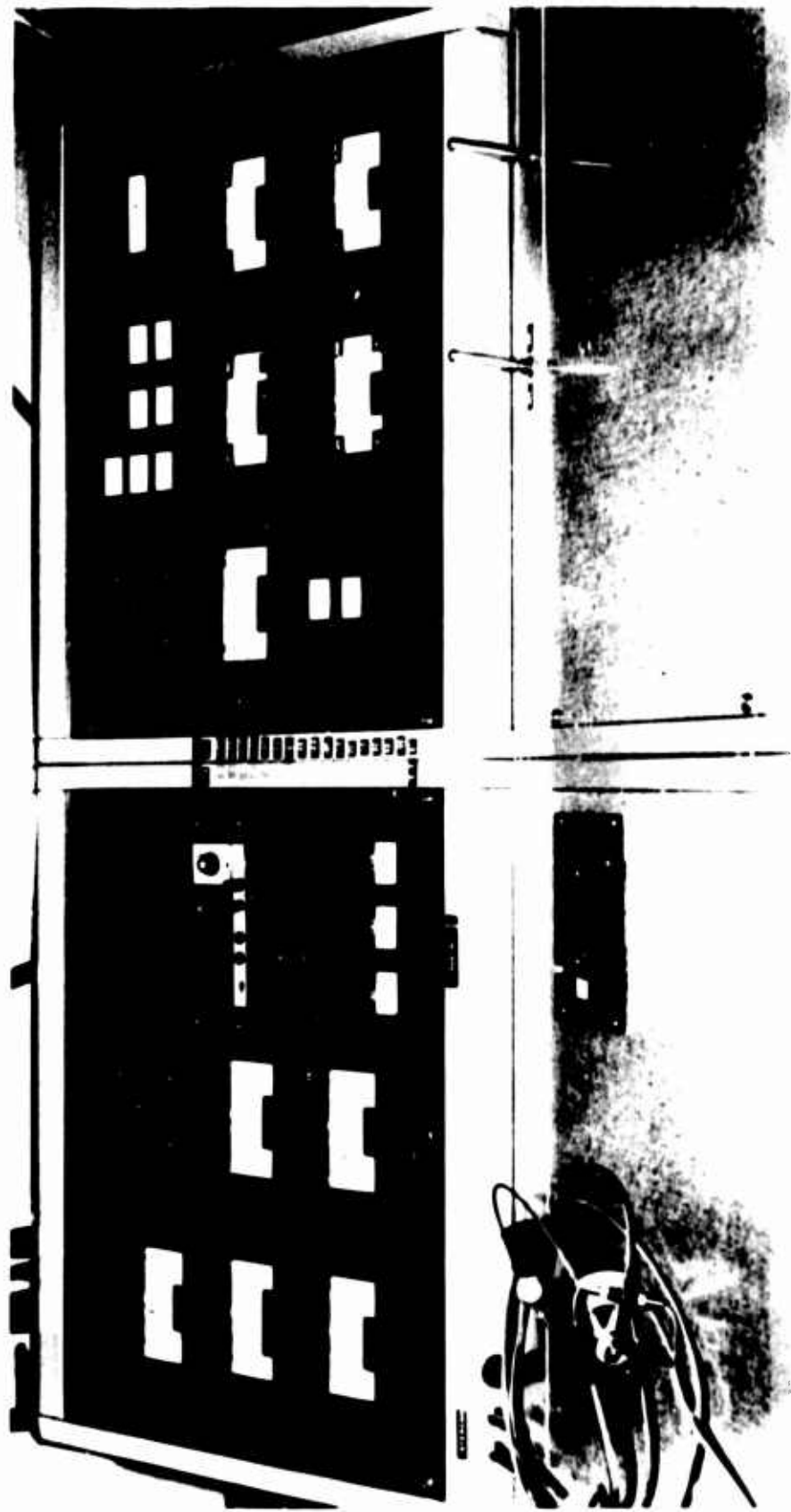
Figure 51. CONTROL MODULE.
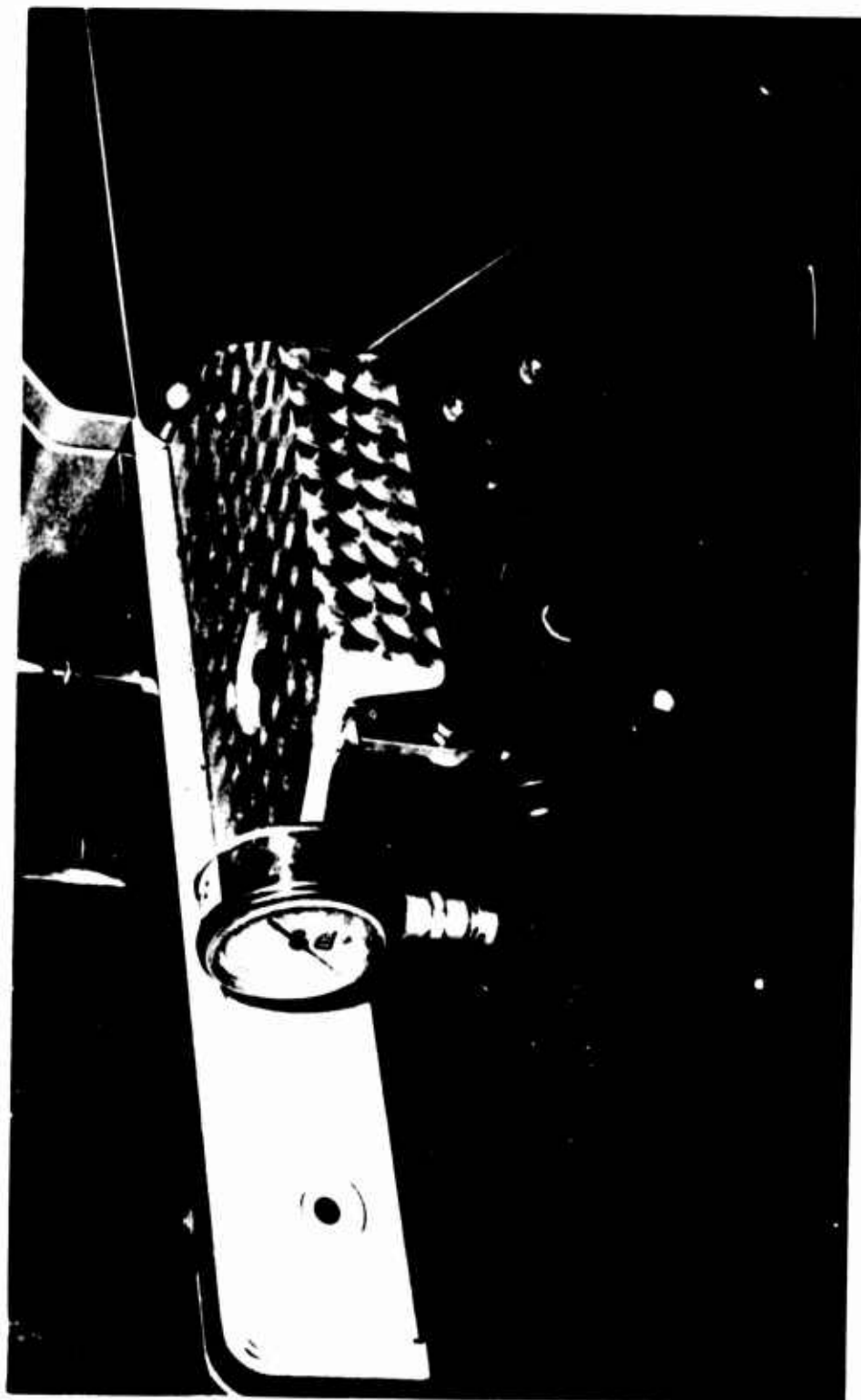
Figure 52. ROTOR BRAKE ACTUATOR ON CONTROL MODULE.
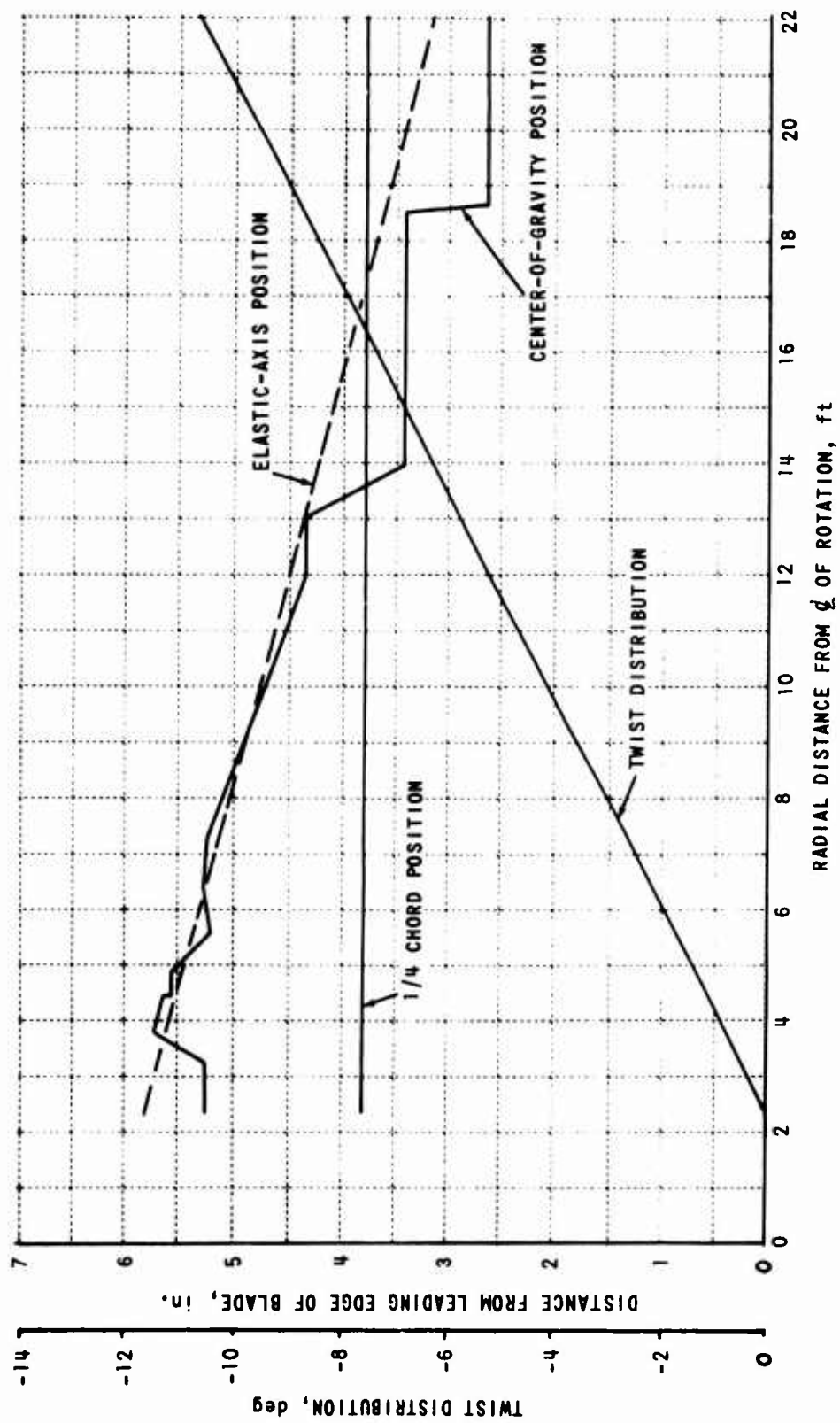
Figure 53. GEOMETRIC PROPERTIES OF THE TEST BLADE.

139
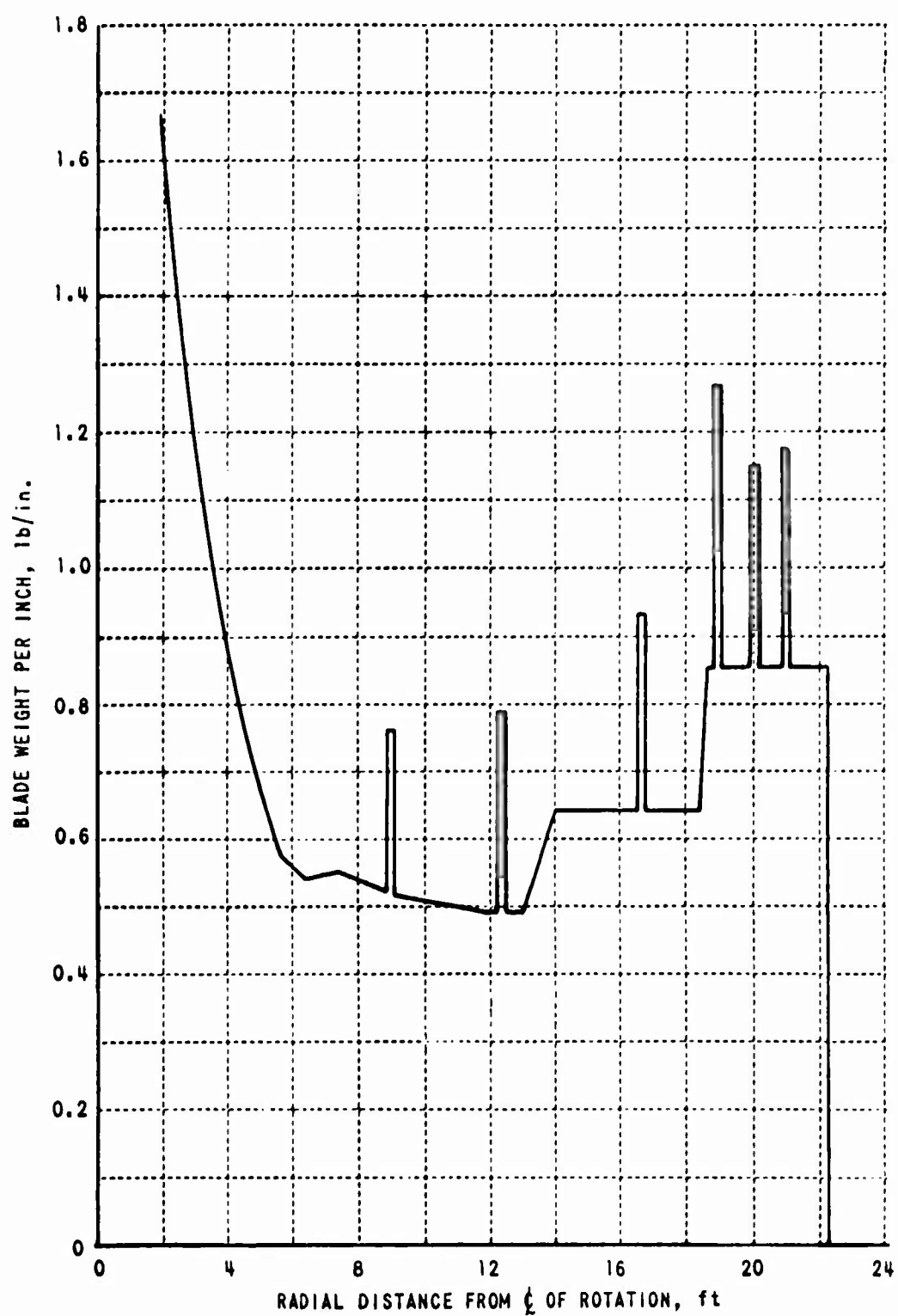
Figure 54. BLADE WEIGHT DISTRIBUTION.
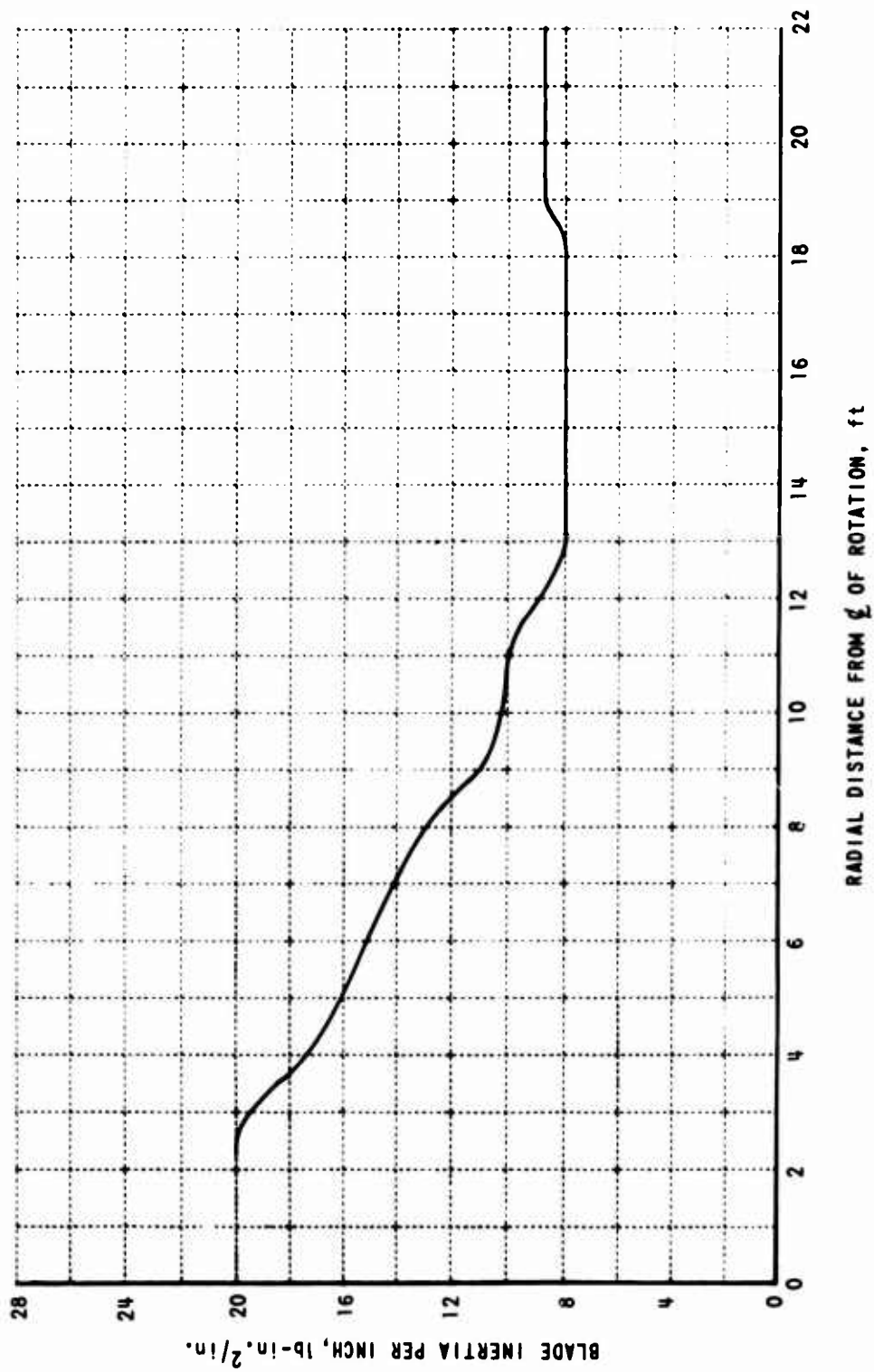
Figure 55. BLADE INERTIA DISTRIBUTION.

141
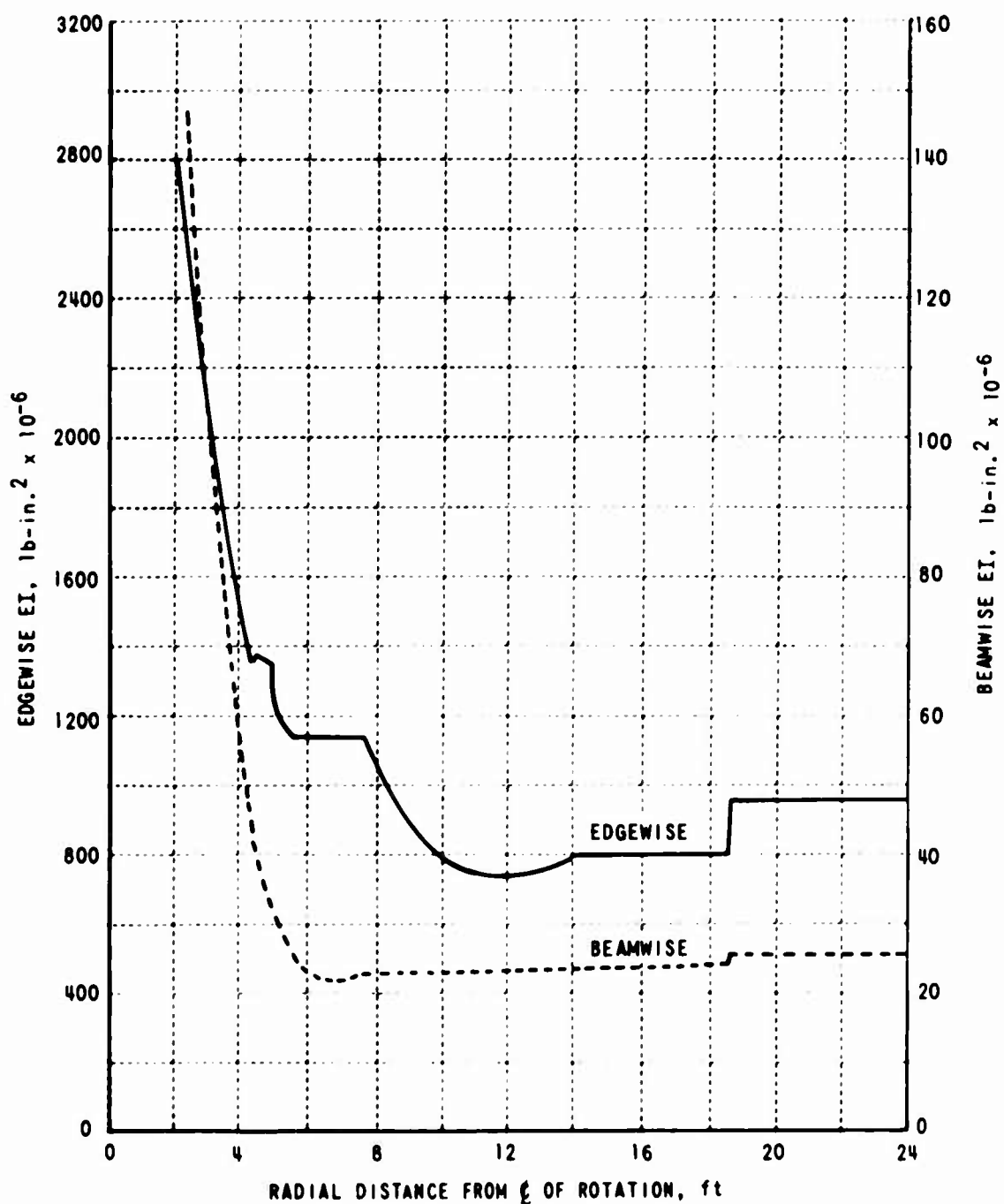
Figure 56. BLADE BENDING STIFFNESS DISTRIBUTION.
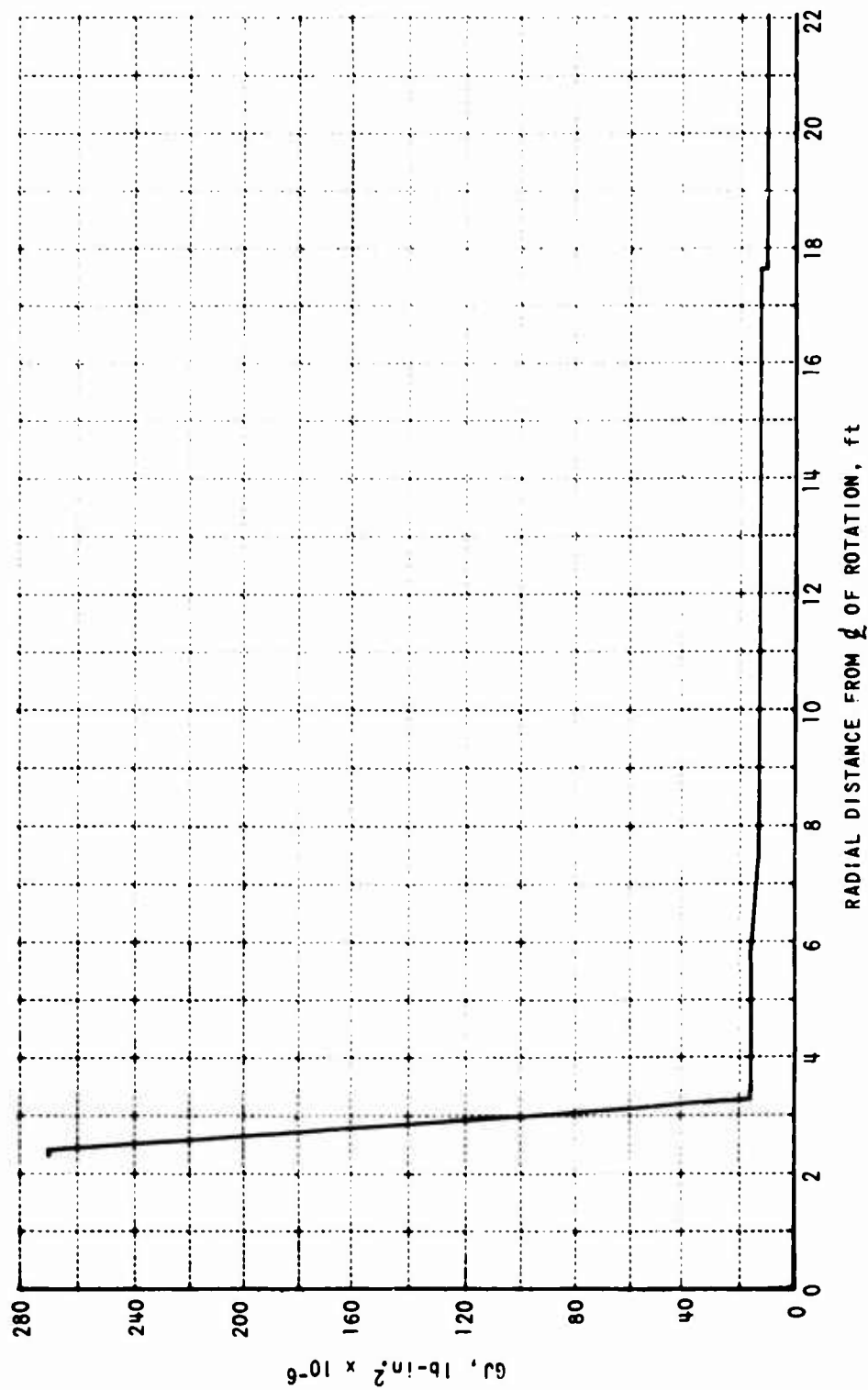
Figure 57. BLADE TORSIONAL STIFFNESS DISTRIBUTION.

143
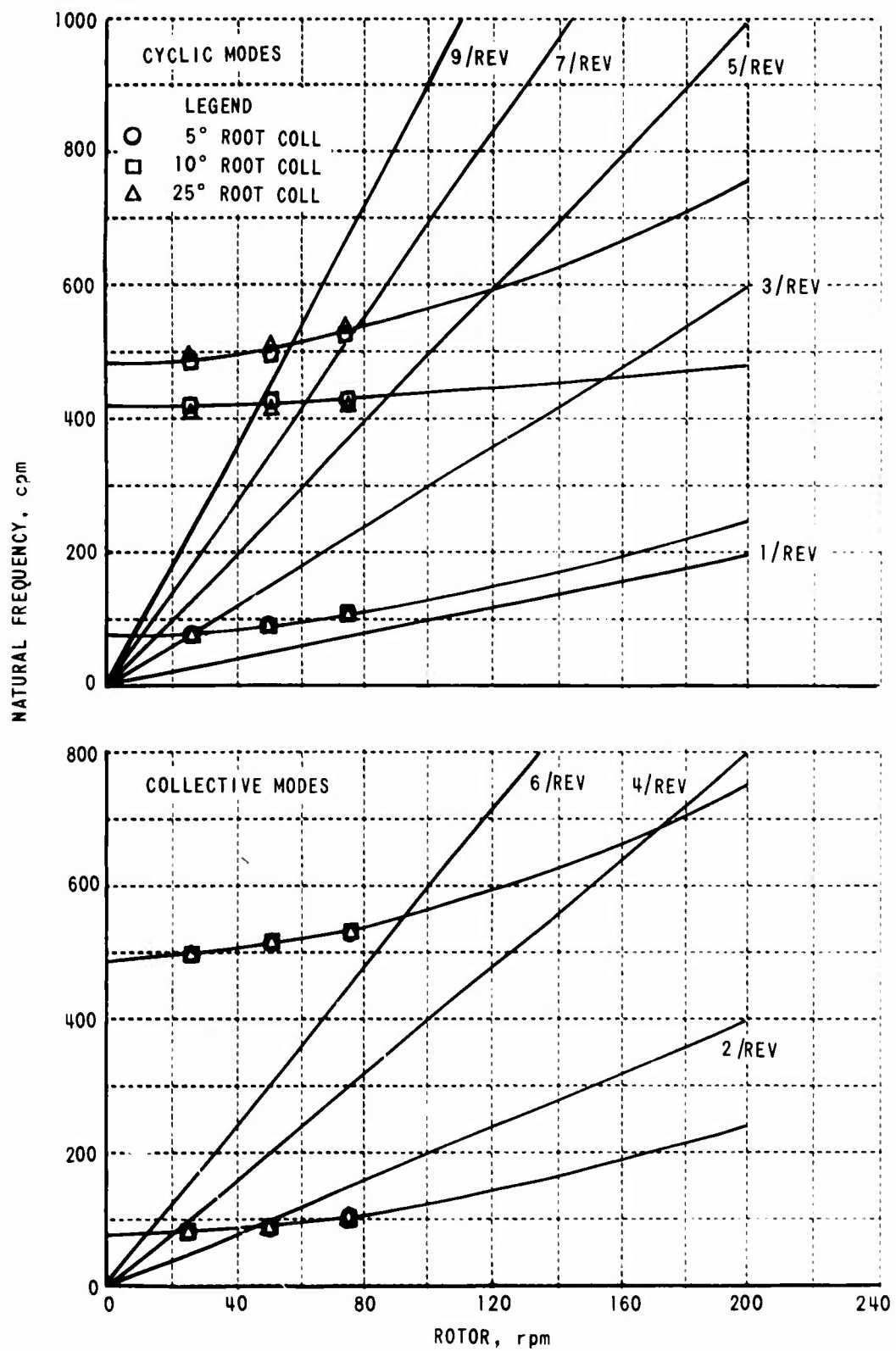
Figure 58. MAIN ROTOR NATURAL FREQUENCIES.

Figure 59. ELECTRICAL RECORDING SYSTEM.

Figure 60. ELECTRICAL RECORDING SYSTEM CONTROL PANEL.

146
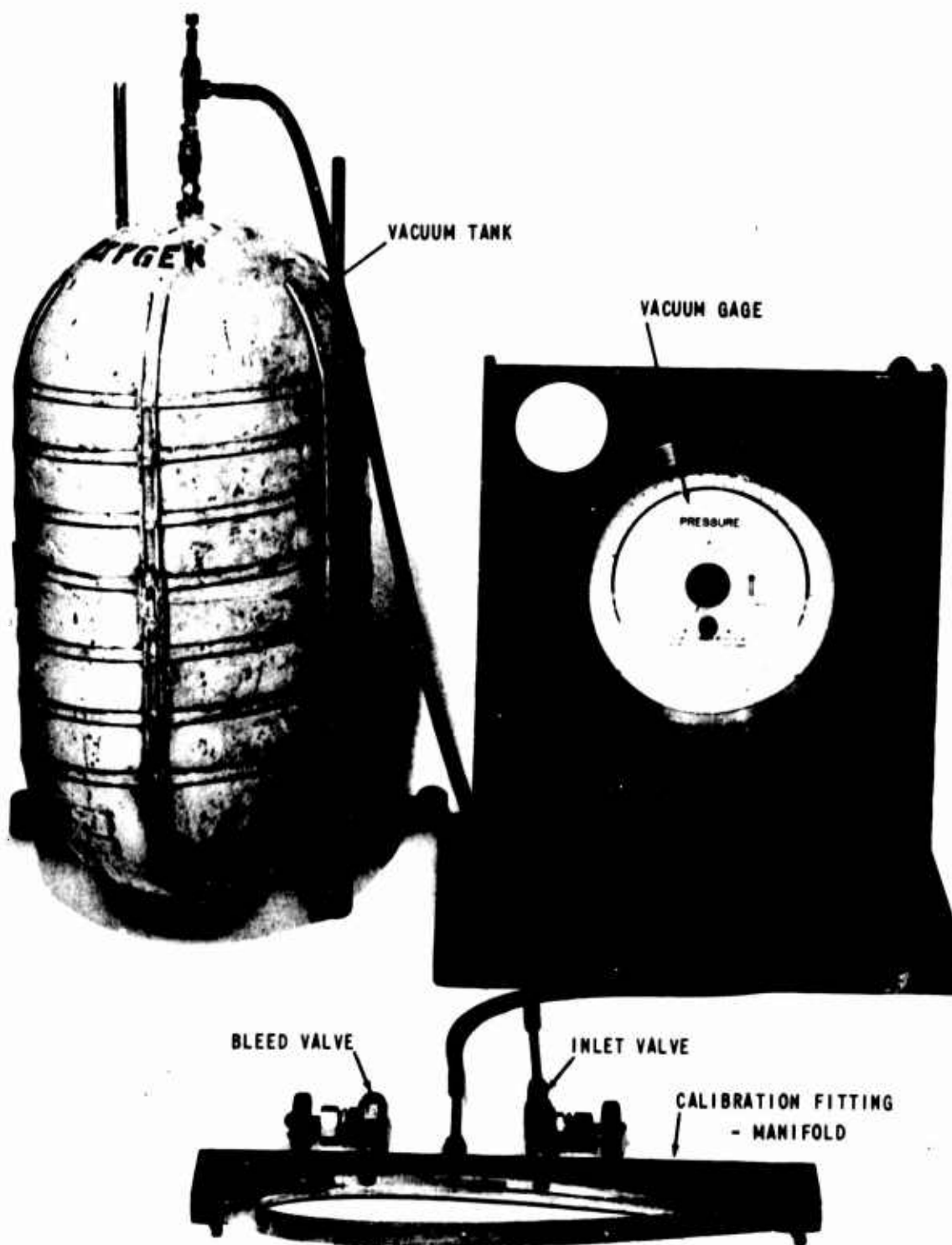
Figure 61. PRESSURE GAGE CALIBRATION EQUIPMENT.

147
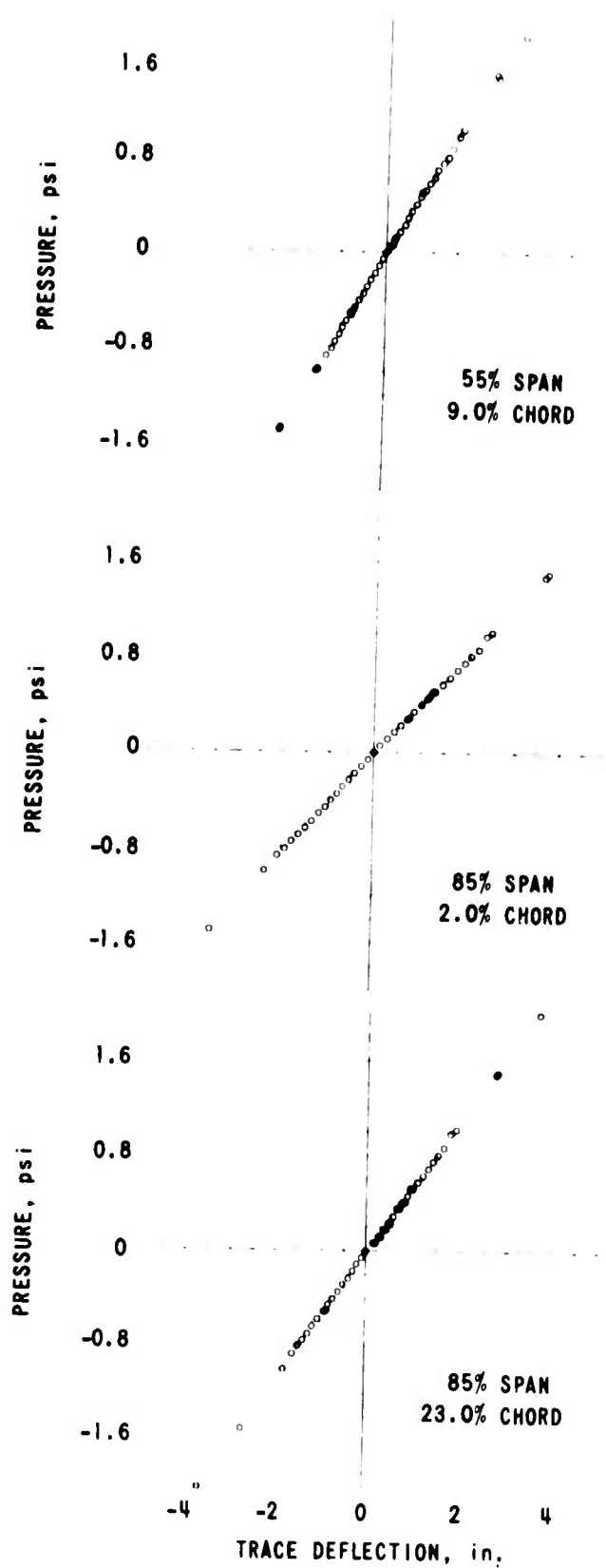
Figure 62. PLOT OF PRESSURE TRANSDUCER OUTPUT VS. APPLIED PRESSURE.
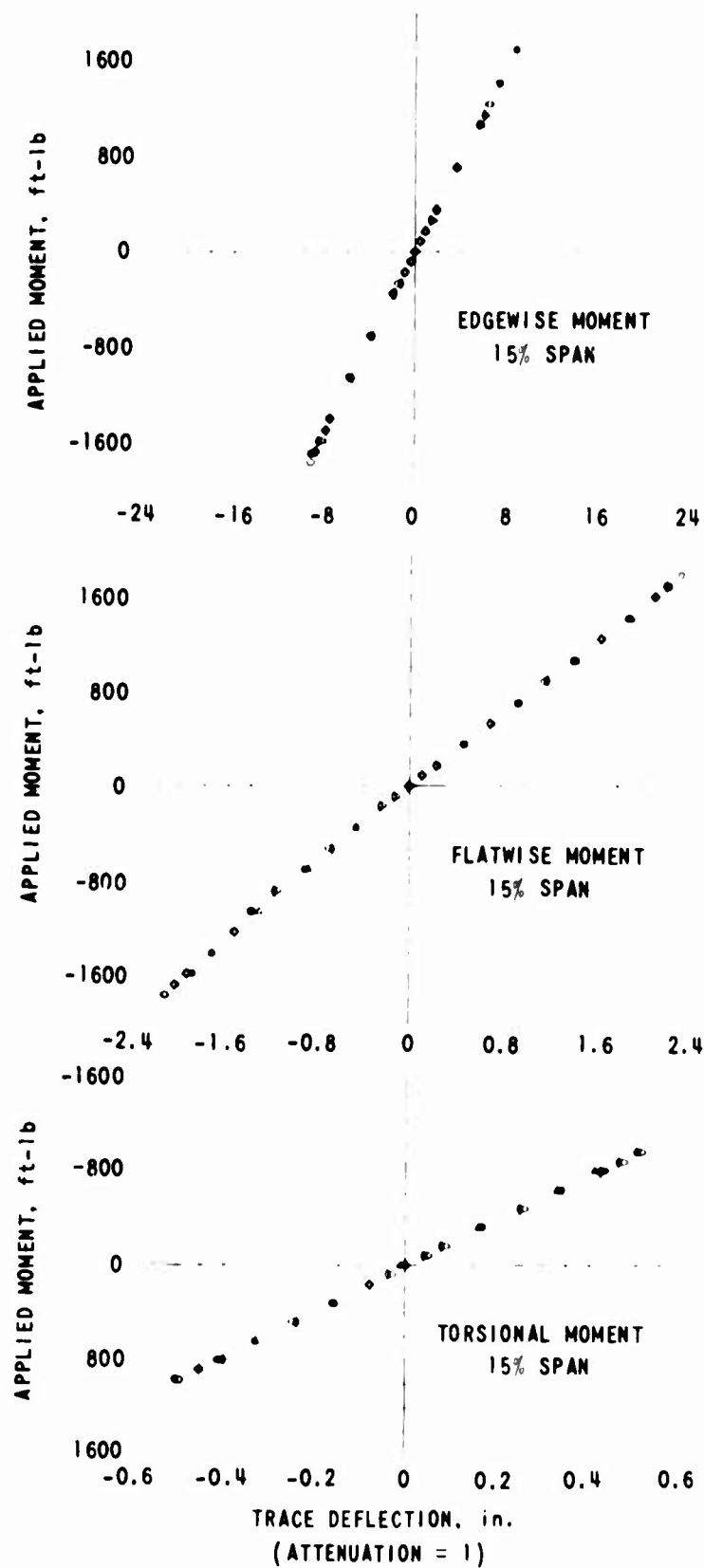
Figure 63. TYPICAL BLADE MOMENT CALIBRATION RESULTS.
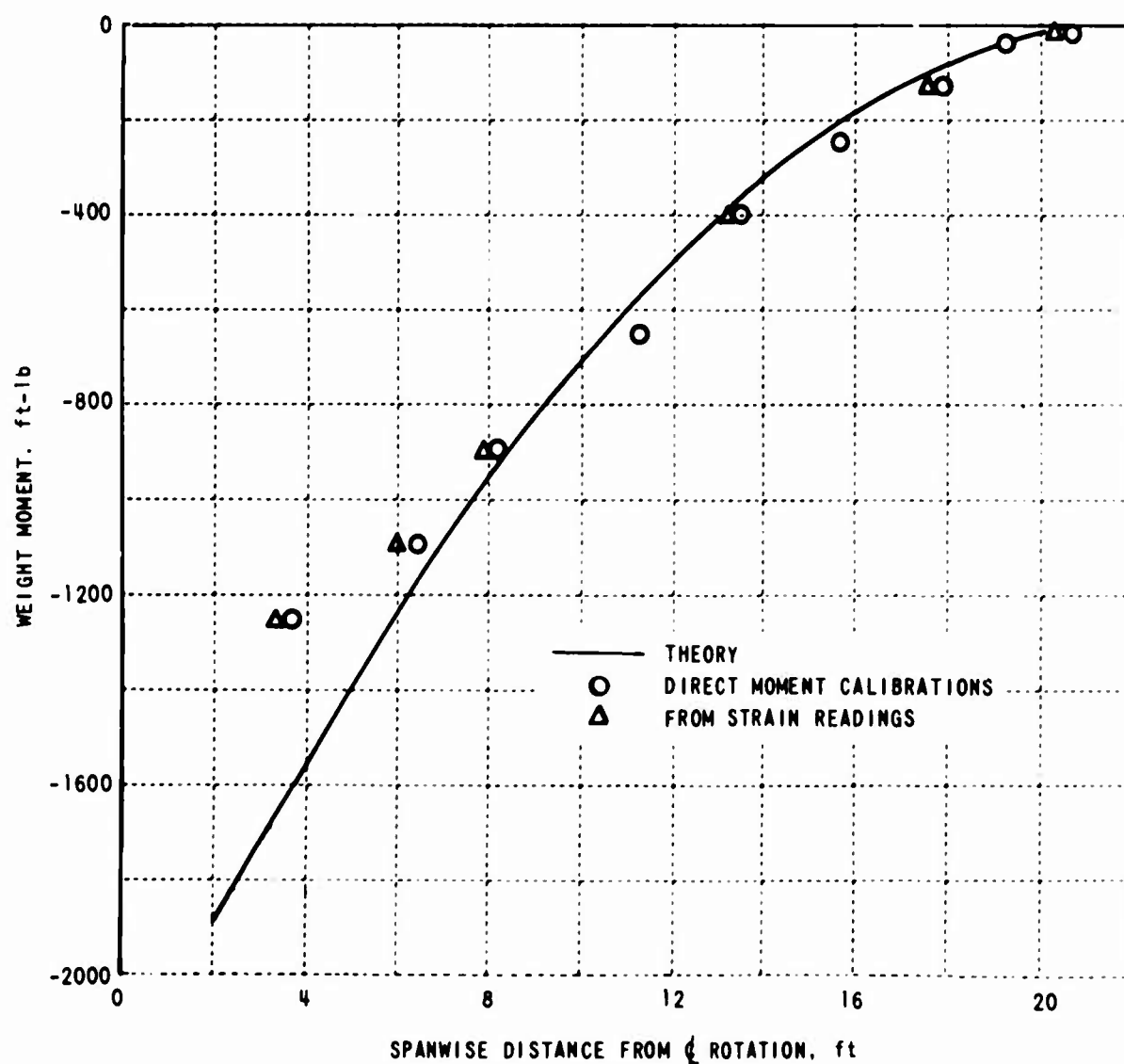
Figure 64. PLOT OF BLADE MOMENT DISTRIBUTION DUE TO WEIGHT.
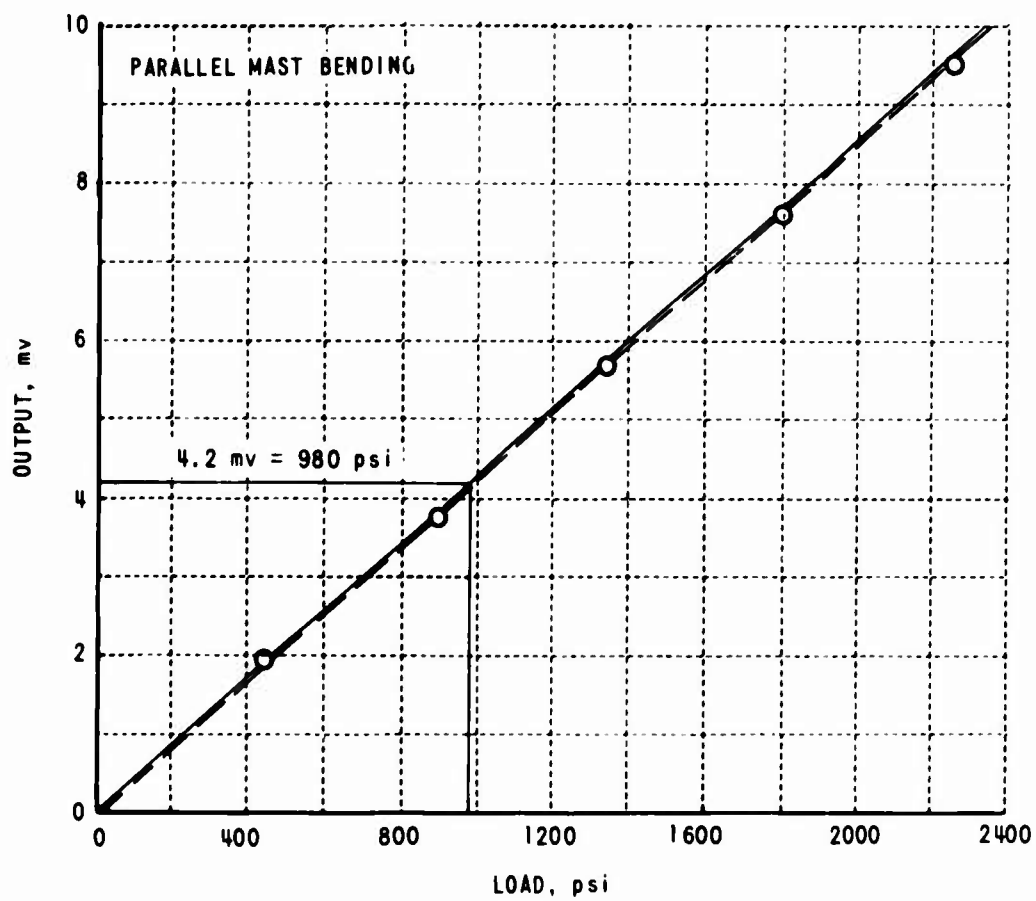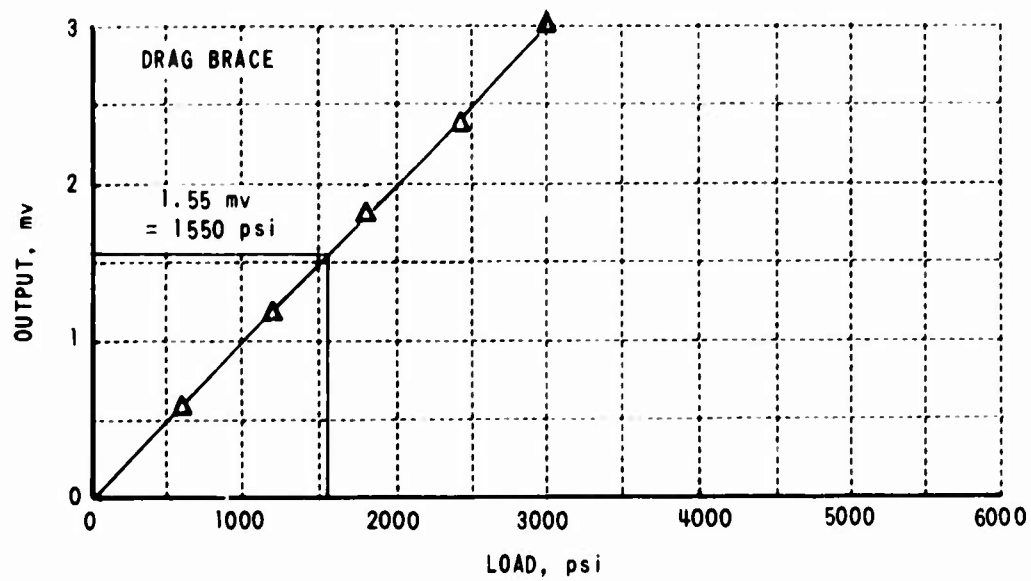
Figure 65. TYPICAL CALIBRATION RESULTS FOR ROTOR MAST AND YOKE.
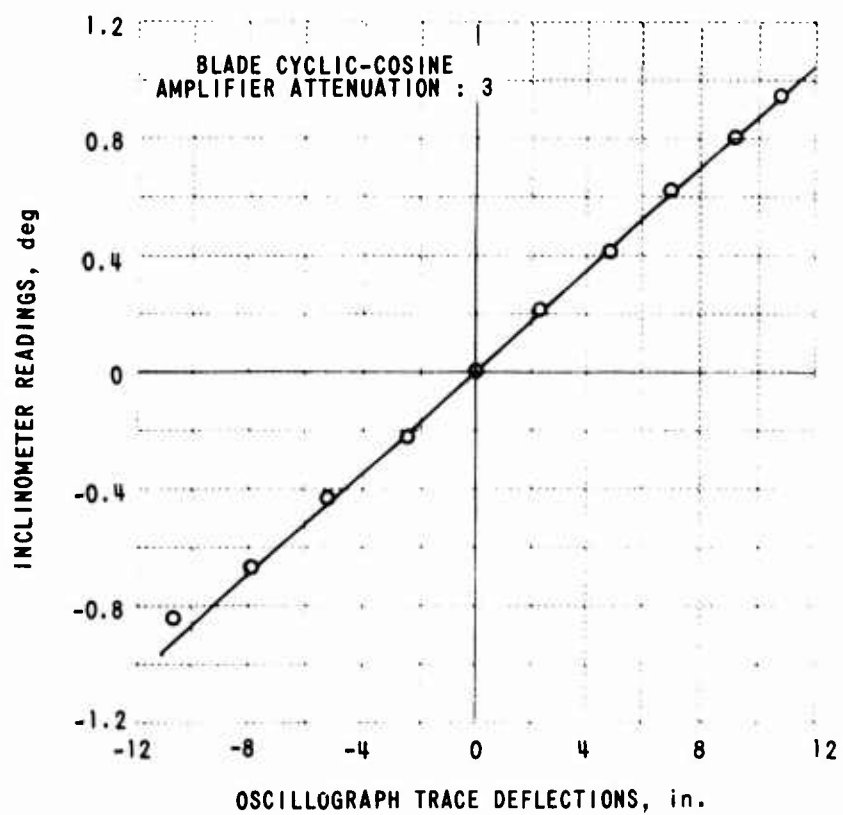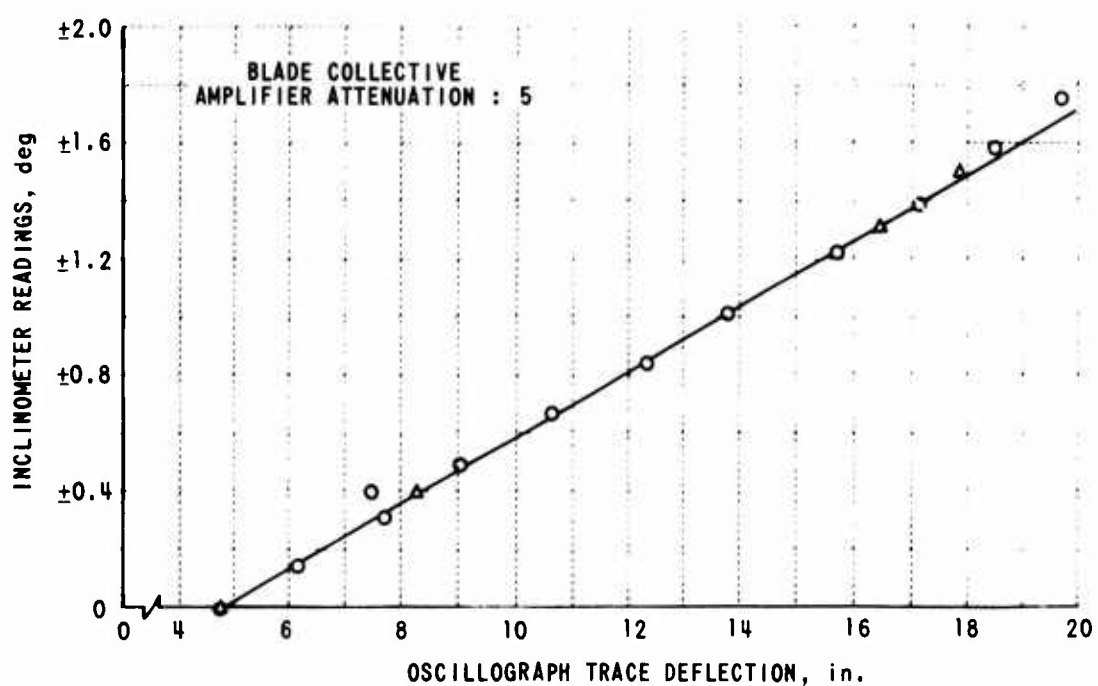
Figure 66. TYPICAL CALIBRATION RESULTS FOR BLADE
COLLECTIVE AND CYCLIC ANGLES.
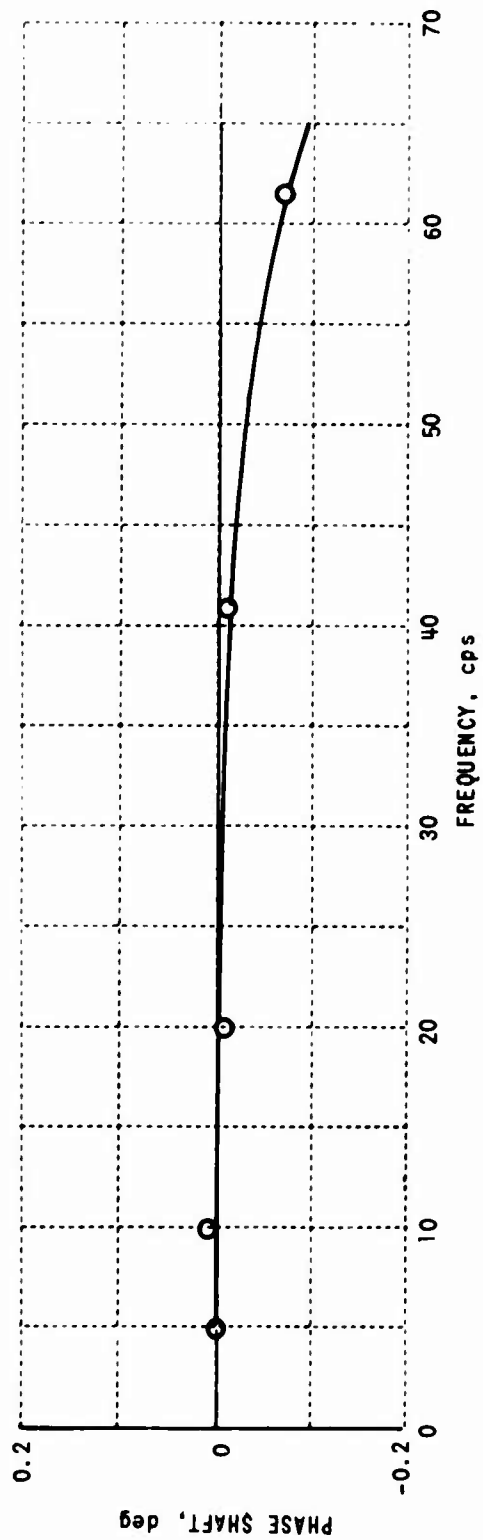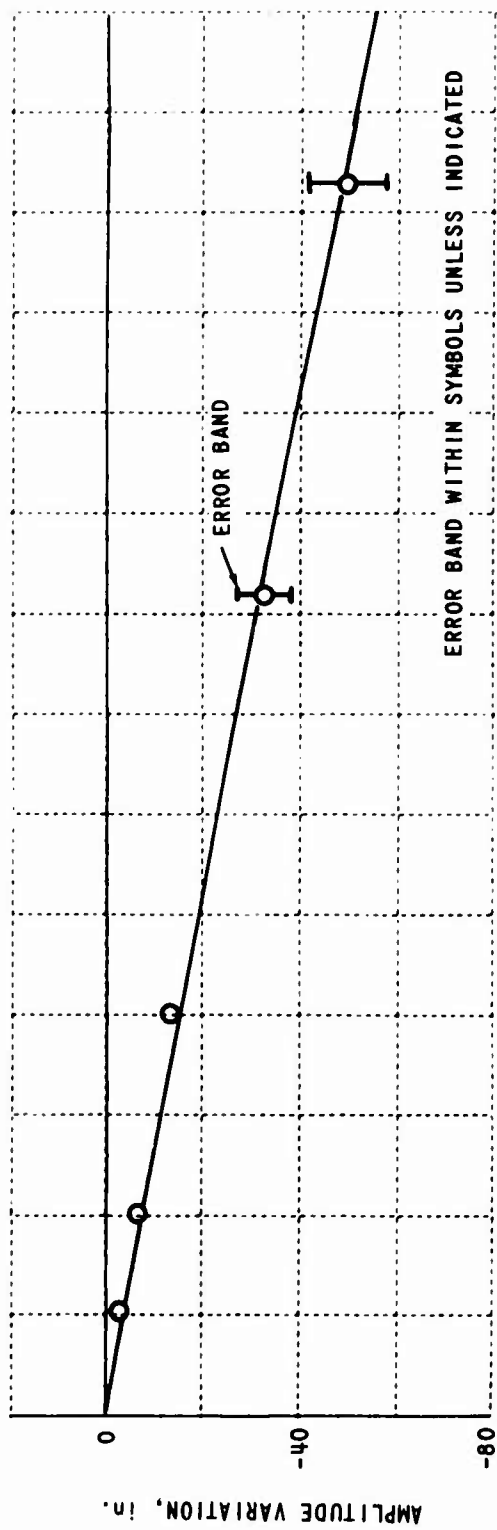
Figure 67. TYPICAL AMPLITUDE AND PHASE RESPONSE OF RECORDING EQUIPMENT.

153

LITERATURE CITED

1. GUIDE FOR PLANNING INVESTIGATIONS IN THE AMES 40-BY-80-FOOT WIND TUNNEL OPERATED BY THE LARGE-SCALE AERODYNAMIC BRANCH, Ames Research Center, NASA, Moffett Field, California, February 1967.

2. Bell Helicopter Company, MEASUREMENT OF DYNAMIC AIR LOADS ON A FULL-SCALE SEMIRIGID ROTOR, TCREC TR 62-42, U. S. Army Transportation Research Command, Fort Eustis, Virginia, December 1962.

3. White, Richard P., Jr., THE AERODYNAMIC AND AEROELASTIC CHARACTERISTICS OF A FULL-SCALE ROTOR BLADE STOPPED IN FLIGHT, USAAVLABS TR 69-7, U. S. Army Aviation Materiel Laboratories, Fort Eustis, Virginia, April 1969.

4. Dimeff, J., and Oswald, A. G., A PENDULOUS ANGLE SENSOR, NASA TM X-1235, May 1966.

5. McCloud, J. L., III, Biggers, J. C., and Stroub, R. H., AN INVESTIGATION OF FULL-SCALE HELICOPTER ROTORS AT HIGH ADVANCE RATIOS AND ADVANCING TIP MACH NUMBERS, NASA TN D-4632, July 1968.

6. Tanner, W. H., and VanWyckhouse, J. F., WIND TUNNEL TESTS OF FULL-SCALE ROTORS OPERATING AT HIGH ADVANCING TIP MACH NUMBERS AND ADVANCE RATIOS, USAAVLABS TR 68-44, July 1968.

7. Paglino, V. M., and Logan, A. H., AN EXPERIMENTAL STUDY OF THE PERFORMANCE AND STRUCTURAL LOADS OF A FULL-SCALE ROTOR AT EXTREME OPERATING CONDITIONS, USAAVLABS TR 68-3, July 1968.

8. Segel, L., ROTOR AIRLOADS, BLADE MOTION AND STRESS CAUSED BY TRANSIENT INPUTS OF SHAFT TORQUE AS RELATED TO STOPPABLE ROTOR OPERATION, USAAVLABS TR 67-18, May 1967.

9. Balcerak, J. C., and Erickson, J. C., SUPPRESSION OF TRANSMITTED HARMONIC VERTICAL AND INPLANE ROTOR LOADS BY BLADE PITCH CONTROL, Cornell Aeronautical Laboratory, Inc., USAAVLABS Technical Report 69-39, July 1969.

10. Piziali, R. A., A METHOD FOR PREDICTING THE AERODYNAMIC LOADS AND DYNAMIC RESPONSE OF ROTOR BLADES, Cornell Aeronautical Laboratory, Inc., USAAVLABS Technical Report 65-74, January 1966.

11. White, Richard P., Jr., INSTABILITIES ASSOCIATED WITH A ROTOR BLADE STOPPED IN FLIGHT, Journal of the American Helicopter Society, Vol. 14, No. 2, April 1969.

APPENDIX I

A DESCRIPTION OF THE TEST MODULE AND BLADES

The test equipment consisted of the rotor test module, power distribution panel, and control console designed and fabricated under USAAVLABS Contracts DA 44-177-AMC-291(T) and DAAJ02-67-C-0018 and modified under the subject program to accommodate a UH-1A rotor. The equipment is described in the following paragraphs.

ROTOR TEST MODULE

The rotor test module included a mounting frame, a rotor pylon, a drive system, and an aerodynamic fairing. The module was designed for mounting on the primary support system in the NASA-Ames 40- x 80-Foot Wind Tunnel. The mounting geometry is shown by Figure 41. The module was supported in the tunnel by two fixed struts and a gimbal-mounted tail strut. The struts were attached to the test module through ball and socket joints. The tail strut was extended (or retracted) by an electrically driven jack screw to provide the desired angle-of-attack range. A three-wheeled dolly was provided for transport and storage of the test module when it was not installed in the tunnel test section. Figure 42 shows the test module installed on the transport dolly.

The test module frame mounted the pylon, the speed increaser gearbox, and the drive motor as shown in Figures 43 and 44. The pylon installation consisted of a UH-1B transmission and mast assembly and modified rotor controls. The mounting arrangement and the suspension configuration were the same as those of the helicopter installation. The control system arrangement is shown in Figure 45. Except for the control input linkages, the basic control geometry was the same as that of the helicopter installation. Dimensional data for the control system are given in Figure 46.

Cyclic control was provided by two electric linear actuators connected through independent linkages to the servo control valves of the right- and left-hand cyclic control boost tubes. The amplitude and the phasing of the cyclic input to the rotor were controlled by the relative extension and/or retraction of these two actuators. The actuators were remotely controlled by the switching circuits at the control console.

The rotor collective control was provided by a single electric actuator remotely controlled from the control console connected through a linkage to the servo control valve of the collective control boost tube. The collective or steady value of rotor blade pitch was controlled by the extension or retraction of the actuator.

156

Hydraulic control power was supplied from two independent systems on the test module. One system was supplied by a transmission-mounted pump and operated only when the rotor was turning. The second system was supplied by an electric motor-driven pump. The electrically driven system was connected through the power distribution panel and was controlled by the main power switch in the control console. This system provided hydraulic power for control system checkout and calibration in addition to rotor operation.

The rotor drive system consisted of a UH-1B transmission, a speed increaser gearbox, and an electric drive motor. The drive motor was provided by NASA-Ames and was rated for 1500 hp at 3000 rpm. The motor speed was controlled by NASA personnel during the tests and was continuously variable from approximately 100 to maximum rpm. To provide the proper power and speed match between the drive rotor and helicopter transmission for the rotor operating speed envelope for these tests, a 1.085:1 ratio gear set was employed. With this gear set the overall speed change from drive rotor to rotor shaft was a 1:0.0532735 reduction.

Cooling and lubrication for the speed increaser gearbox were provided by an oil-to-water heat exchanger and an electrically driven oil pump and reservoir mounted below the gearbox. The drive motor and gearbox were connected by a commercial flexible coupling. The gearbox and transmission were coupled by a standard UH-1B input drive shaft. Minor modifications of the standard UH-1B transmission were accomplished to meet the requirements of the tests. An external lubrication system, consisting of electric-motor-driven pump and a reservoir, was installed to provide adequate lubrication at the low test speeds. A standard UH-1 rotor brake was installed on the forward accessory pad to allow stopped-rotor investigations and to maintain rotor azimuth positions during nonrotating tests (see Figure 47). An adapter was designed and fabricated to allow installation of the UH-1A rotor to the UH-1B mast. A split cone was designed and fabricated to engage the rotor flapping stop to constrain the rotor from flapping.

The mounting frame, pylon, and drive system were enclosed by an aerodynamic fairing. The fairing, shown in Figure 48, was a "teardrop" shaped body of revolution with two local protuberances at the lift strut attachment points. The maximum diameter of the fairing body was 6.66 feet, and the overall length was 22 feet. The forward sections (approximately 16 feet) were of molded sandwich construction with fiberglass inner and outer skins, paper honeycomb cores, and aluminum alloy bulkheads and stiffeners. The tail section of the fairing was a monocoque design with aluminum alloy skins. The fairing was provided with flush panels for access to the struts and also to the controls and fluid connectors located on the underside of the mounting frame. The upper nose section of the fairing opened upward and pivoted forward for access to the transmission, controls, and instrumentation. The upper section of the fairing aft of the mast opened upward and slid aft to provide access to the drive

157

system. The upper access doors were fitted with flush "quick release" latches; all other panels were fitted with flush screw-type fasteners. These features are shown in Figure 49.

POWER DISTRIBUTION PANEL

The test module required 24 volts DC and 110/120 volts AC power for operation and servicing. The AC power was supplied through a 35-foot-long umbilical cable which connected to the power distribution panel as shown by Figure 50. For the wind tunnel tests, the umbilical cable was routed through the left-hand main strut fairing to the distribution panel. The panel was located below the test section floor. The distribution panel had four coded receptacles which were mated to corresponding plugs on the umbilical. The four connections were for the service outlet, hydraulic pump motor, and oil pump motors on the test module. Power for the three circuits was obtained through the transformer, master switch, and external power cable installed on the panel. The power cable was provided with a connector for attachment to a 440-volt, 60-cycle, 3-phase, AC external power receptacle. The common outlet was "live" whenever the panel master switch was closed and provided power for the tools, lights, etc., for servicing and maintenance of the test module. Power for the pump motor circuits was controlled by two "normally open" 24-volt DC relays mounted on the distribution panel. The hydraulic pump motor relay was series-connected with the master DC power switch on the control module. This arrangement provided hydraulic pressure for control boost whenever DC power was available for control system actuation. The oil pump motor relays were series-connected with a "normally open" pressure-actuated switch in the transmission-driven hydraulic system and the master DC power switch on the control module. Power was supplied to the oil pump motor circuits for lubrication of the speed increaser gearbox and transmission whenever the rotor was operating and DC power was available for control system actuation.

CONTROL MODULE

The rotor speed (NASA drive motor) and the module pitch (tail strut actuator) controls were provided by the NASA test facility. All other rotor control and monitoring functions were provided on the desk-type control module shown in Figure 51. The control and monitoring functions were arranged in two major panel groups: an operator station and a test engineer station.

The operator's station was on the right-hand section of the control module and included the controls, rotor brake actuator, and indicators required for operation of the test module. On the upper section of the operator's panel were mounted a rotor tachometer, the hydraulic and oil systems' warning indicator lights, and the DC power switch. The DC power switch, through its associated relays, controlled all the power (except the NASA motor and instrumentation circuits) required for operation of the test module. The system warning indicator lights were

158

series-connected with individual pressure and temperature switches in the two hydraulic systems, the transmission oil system, and the speed increaser gearbox oil system. The warning lights incorporated a "press to test" circuit and were normally "off" unless there was a loss in pressure or excessive temperature rise in their respective systems. The rotor tachometer was used to monitor rotor rpm and to provide an indication of rapid power changes such as power failure, inadvertent autorotation entry, or a high range of control input.

Three control position indicators were mounted in a horizontal row along the center of the panel. The indicators displayed, from left to right, positions of collective pitch, longitudinal cyclic control, and lateral cyclic control. The collective pitch was controlled by two push-button switches mounted below the collective position indicator. The operator set the collective pitch by depressing and holding either the "UP" or the "DOWN" switch until the desired setting was obtained on the collective pitch indicators. The longitudinal and lateral cyclic pitch was controlled by two spring-centered lever-type switches which were located just below the operator's panel and in line with the respective position indicators. The operator moved the switches off-center to the left or right to obtain the desired setting on either of the control position indicators.

The rotor brake actuator (see Figure 52) was mounted on the right-hand side of the control module and consisted of a hydraulic master cylinder/reservoir brake pressure indicator and a manual actuating lever. The operator set the brake by applying a pumping action to the lever until the desired brake pressure was obtained. An internal relief valve permitted excessive pressure from being developed in the system.

The test engineer's station was at the left side of the control module. A remote control unit for operating the data acquisition system was installed in the lower panel. The upper panel mounted five load meters for monitoring loads during testing, an airspeed indicator, and a switch-selected digital control position readout used to permit the pre-cise setting or recording of the control positions during test. The load meters provided a continuous on-line display of the load levels for critical components. The oscillatory, mean, or peak load values could be selected for readout by a three-position selector switch on the back panel of the console.

The load meter arrangement for this particular test included a mean load readout for mast torsion and oscillatory load readouts for the main rotor yoke flapwise and chordwise bending moments and the rotor shaft parallel bending moments near the critical stations at the upper and lower ends of the shaft. A single digital readout was installed on the right-hand side of the panel and was switch selectable for display of the collective, F/A cyclic, or lateral cyclic control positions. The switch was normally positioned to display the control position of interest, and final control settings were based on the digital readout. The digital readout was also used for all control system calibrations.

159

ROTOR

The test rotor was a rigid configuration of the normally semi-rigid two-bladed UH-1A underslung hub. The rotor was installed on the rotor shaft using the existing trunnion, pillow block, and flapping bearings. A split cone installed around the rotor shaft and against the rotor flapping stops was employed to prohibit flapping. The rotor blades that were used for these tests were the instrumented UH-1A blades used to obtain the blade airload data presented in References 2 and 3. A complete and detailed description of the rotor blades can be found in Reference 2. The blade geometric properties are presented in Figure 53, the blade weight distribution is presented in Figure 54, the blade mass inertia distribution is presented in Figure 55, the blade-bending stiffness distributions are presented in Figure 56, and the blade torsional stiffness distribution is presented in Figure 57.

The rotor frequency plot for this rotor with the hub rigid is presented in Figure 58. Some additional data for the rotor are summarized below:

Airfoil Designation	NACA 0015
Chord	1.26 ft
Diameter	43.75 ft
Twist (Total Aerodynamic)	-11.9 deg
Disc Area	1503 sq ft
Solidity	.0369

APPENDIX II

A DESCRIPTION OF THE DATA RECORDING EQUIPMENT

      A block diagram of the instrumentation and data recording system is presented in Figure 7. The link between the instrumentation in the rotating frame and the data recording system in the fixed frame was a slipring assembly consisting of 164 rings. Of the 164 rings, 14 rings carried the power required to the instrumentation gages, and the remaining rings were used for data signals. A description of the various components of the instrumentation and recording equipment is presented below.

COMPONENTS OF INSTRUMENTATION

Pressure Transducers

      The pressure transducers used during these tests were NACA-developed miniature pressure transducers. These pressure transducers were designed to measure the pressure differential between the upper and lower surfaces of the rotor blade. The basic pressure transducer is described in NACA Technical Note 2659. The location and pressure range of each transducer used in these tests is presented in Table I.

Blade and Mast Strain Gage Instrumentation

      Strain gages having a resistance of 350 ohms and a gage factor of 2.10 + 0.5% were used to measure the moments applied to the blade in the flatwise, edgewise, and torsional directions. Their locations are presented in Figure 4 . Similar type gages were employed to measure the loads and moments in the mast, yoke, drag brace and boost tubes. Their locations are presented in Figure 5 .

Feathering Angle Transducer

      The feathering angle of the reference blade was measured with a rotary transducer mounted to the shaft and connected to the blade yoke through a rigid two-armed linkage.

Shaft Angle Transducer

      The shaft inclination of the rotor was measured with a pendulous angle sensor (dangleometer). This device was developed by NASA and is reported in NASA TN X-12-1235.

RPM Indicator

      The rotor rpm was determined with a standard magnetic pickup and a steel arm attached to the rotor swash plate. A signal was

generated in the magnetic pickup once per revolution as the steel arm interrupted the magnetic field created by the pickup.

SIGNAL CONDITIONING AND AMPLIFYING EQUIPMENT

The signal conditioning and amplifying equipment consisted of three main sections:

1. The amplifying section consisted of seven banks of CEC System L 3KC carrier equipment. Each bank contained one power supply, (an oscillatory, type 2-105A), along with 12 amplifiers CEC type 113B.

2. Galvanometer matching networks were required to match the amplifier output impedance to the galvanometers used. Since several different types of galvanometers were used, individual galvo matching networks were required.

3. A switching network which consisted of relays, precision resistors, potentiometers and transformers constituted the third section of the conditioning equipment. The relays provided for selection of any one of three circuits. The first circuit was the data signal circuit, and it provided the necessary link between the blade instrumentation and the recording equipment. The second circuit consisted of the dummy load resistor (DLR) circuit which placed a known resistor across one leg of the pressure or strain bridge to allow electrical calibration of that given data channel. This capability was provided for all data channels. The third circuit was the automatic gain set check (GSC) circuit which allowed the automatic recording of the amplifier attentuation settings. The three main sections described above are shown in Figure 59.

MASTER CONTROL

Shown in Figure 60 is the panel from which all recording devices were remotely actuated. This panel allowed actuation of the recording oscillographs as well as the recording movie camera equipment. In addition to the recording control switch, the panel had two counters which displayed the record numbers and the event numbers being recorded on the oscillograph for correlation between the two oscillographs, the test conditions and the test engineer's log. Also located on the master control was the counter designed to count the number of times a given signal level was exceeded on a predetermined component (in this case, yoke flatwise bending). This was incorporated

162

as an additional safety check to maintain continuous count of the number of critical cycles encountered.

OSCILLOGRAPHS

Two 50-channel CEC recording oscillographs, model 5-119-P3-50, were employed to record all of the data signals. Type 7-312, 7-315 and 7-323 galvanometers were installed in the recorders. One oscillograph was used to record primarily the blade and mast moments and loads, and the second oscillograph was used to record primarily the pressure data. One channel on each oscillograph was provided to allow correlation in time between the two oscillographs. Also provided was a 100 cycle per second timing trace.

VISICORDER AND OSCILLOSCOPES

One 36-channel visicorder was provided by NASA-Ames to allow on-line monitoring of selective data channels. In addition to the visicorder, three oscilloscopes were provided to allow visual display of the signals from the structural components considered most critical. This equipment is shown in Figure 60. Also shown in the figure is the readout for the shaft inclination (dangleometer).

APPENDIX III

RESULTS OF THE CALIBRATION OF THE DATA
INSTRUMENTATION AND RECORDING EQUIPMENT

During the course of this program, various component tests were conducted to establish the equipment performance. The results of these tests are summarized below.

PRESSURE TRANSDUCER CALIBRATION

A brief study was conducted to find the maximum and minimum differential pressures which might be expected at the various spanwise stations of the blade for the flight conditions to be run during this program. The data obtained during the test programs reported in References 2 and 3 were surveyed. It was found that during a large portion of the stopped-rotor tests reported in Reference 3, the pressure transducers were operated in a range which was approximately 0.1 of their design range. During the full-scale flight test of this rotor system, reported in Reference 2, with only a few exceptions, these pressure transducers were operating in a range which was approximately 0.5 of their design range. Since the full-scale steady-state flight tests were conducted at approximately 160 feet per second and a rotor speed of 314 rpm and since the current tests were to be limited to 70 rpm, it was felt that the pressure data measured during the full-scale flight test provided an upper bound on the magnitude of the pressures to be expected. The lower bound on the expected pressures to be measured were established by the stopped-rotor tests.

Pressure data were taken at each of the six spanwise pressure stations by connecting a vacuum tank and gage to a manifold mounted on the blade as shown in Figure 61. The output of each transducer was recorded on the CEC oscillograph through the CEC System D amplifiers. Four sets of pressure data at each station were taken. One set with the pressure manifold attached to the upper surface of the airfoil was taken over a range 0 to 1.0 psi in increments of approximately 0.06 psi. During these tests an alcohol manometer having a reading accuracy of approximately 0.00087 psi was used. With the manifold in the same position, the tests were repeated with a pressure range 0 to 2.0 psi in increments of approximately 0.5 psi. The measuring instrument used in these tests was the dial pressure gage shown in Figure 61. In all cases, a vacuum was applied to the manifold by venting the manifold through the inlet valve into the vacuum tank shown in Figure 61. An identical sequence of tests was conducted for the lower surface. All of the data measured were plotted on a single plot for each transducer. All subsequent check calibrations were also plotted on the same graphs; thus, linearity, hysteresis and repeatability were checked.

164

Typical plots of the results obtained for several pressure transducers are presented in Figure 62. Presented in Table V are the calibration constants which relate the pressure transducer output to the oscillograph trace deflection (adjusted for an amplifier attenuation setting of 1).

CALIBRATIONS OF THE ROTOR BLADE BENDING MOMENTS AND TORSIONAL MOMENTS

A simple loading rig was constructed to facilitate calibration of the flatwise, edgewise and torsional moment gages on the blade. Two calibrations of each type of moment were made. The first consisted of small incremental loadings and the second of much larger incremental loadings. The corresponding results were plotted on the same graph paper to determine sensitivity, repeatability and accuracy of measurements. Subsequently, calibrations made during pretest, test and post test were also plotted on the initial calibration results. Typical blade moment calibration results for the 15% spanwise station are presented in Figure 63.

All calibrations were conducted with the blade hanging under its own weight. Hence, the reference position of the blade was its deflected position. This deflected shape caused couplings between the various blade moments. For instance, application of a pure drag load at a given station induced a torsional deflection, due to the torsional moment produced by the drag load acting through the static deflection at the given station. In addition to couplings introduced by the deflected shape of the blade, couplings were also introduced by the fact that the blade is twisted as well as the fact that the elastic axis varies along the span. These coupling effects varied from station to station and in many instances were found to be nonlinear. To account at least partially for these coupling terms, each term was linearized and the approximate slope used in computation of the overall moments applied to the blade.

Shown in Table VI are the main calibration constants required to convert observed oscillograph trace deflections into the applied moments at a given station.

BLADE MOMENT DISTRIBUTION DUE TO ITS OWN WEIGHT

During the calibration tests, as well as the tunnel tests, the zero reference position for all moment calibrations was chosen as that of the blade deformed under its own weight. Since it was necessary to account for these weight moments in the determination of the applied aerodynamic moments, it was necessary to determine the moment distribution of the blade due to its weight.

To determine the moments introduced by the blade weight, the blade was supported in a horizontal position at several spanwise stations, thereby effectively removing the weight moments. This position was used as the zero reference. The moments due to the blade weight were then

165

measured with respect to this "no load" reference position. In addition to the moment measurements, strain measurements were also made during these tests. The measured weight moment distribution obtained is shown in Figure 64. Also shown is the weight moment distribution calculated from the estimated weight distribution and stiffness distribution given in Figures 54 and 56. Also presented are the corresponding moments calculated from the measured strains from the formula

$$M = \frac{\sigma I}{12 c}$$

From the agreement shown, it can be inferred that (1) the blade geometry is well known, i. e. , the estimated weight distribution and the thickness and stiffness distributions are fairly accurate; (2) simple engineering beam theory yields good correlation with the experimental results.

ROTOR MAST ASSEMBLY CALIBRATION

Calibrations of the rotor pylon, rotor yoke, drag and pitch links, and boost tubes were done by the Bell Helicopter Company. The results of these calibrations are shown in Figure 65. Presented in Table VII are the calibration constants which relate the applied loads to the corresponding oscillograph output.

BLADE AND SHAFT ANGLE CALIBRATIONS

Calibration of the shaft angle transducer (dangleometer) was conducted by NASA-Ames. The calibration was performed so that the shaft angle could be read directly from the shaft angle readout, which is shown in Figure 60.

Calibrations were performed to determine the input vs. output characteristics of the collective and cyclic blade angle position indicators. These calibrations were performed with an inclinometer placed at the 23-inch station on the rotor yoke. The transducer outputs were monitored on the CEC oscillograph as well as on the control module readout equipment. These calibrations were repeated several times during and after the tests. The blade feathering angle transducer was similarly calibrated. The results of these calibrations are presented in Figure 66. Presented in Table VIII are the corresponding calibration constants required to convert the transducer output in terms of oscillograph deflections to the corresponding blade angles.

CALIBRATION OF THE ELECTRICAL RECORDING EQUIPMENT

Tests were conducted on the electrical recording equipment to determine the input to output characteristics of the system to DC and AC inputs. The behavior of the dummy load circuitry and the gain set check

166

circuitry were all carefully examined and their characteristics noted.

The dynamic response characteristics of the system were checked by putting in a known oscillatory signal (known in terms of the amplitude and frequency) and recording the corresponding output on the oscillographs. The corresponding output was then harmonically analyzed to determine the output, amplitude, frequency, and higher harmonic content, if any. Typical results are presented in Figure 67. It was found that (1) the output amplitude was relatively constant out to approximately 20 cycles per second and (2) the phase angle shift varied in a linear fashion with frequency

For purposes of data reduction, no corrections to the recorded amplitudes were made. The correction to the data for the phase angle shift with frequency is noted below:

$$\phi_c = -0.72\,\omega$$

where

ϕ_c = correction to be added to measured phase angle

ω = frequency, Hz

The above discussion is applicable to all channels of the data recording equipment.

167